THE EFFECT OF FIRING TEMPERATURE ON MICRO-STRUCTURAL PROPERTIES OF NON-EXPANSIVE CLAYS IN DEVELOPMENT OF EFFECTIVE INTERNAL CURING CONCRETE AGGREGATE

Manamperi Mudiyanselage Hasitha Wikum Bandara

168022M

Thesis submitted in partial fulfilment of the requirement for the degree
Doctor of Philosophy in Civil Engineering

Department of Civil Engineering

University of Moratuwa

Sri Lanka

May 2020

DECLARATION OF THE CANDIDATE & SUPERVISOR

"I declare that this is my own work and this thesis does not incorporate without acknowledgement any material previously submitted for a Degree or Diploma in any other University or institute of higher learning and to the best of my knowledge and belief, it does not contain any material previously published or written by another person except where the acknowledgement is made in the text.

Also, I hereby grant to University of Moratuwa the non-exclusive right to reproduce and distribute my thesis, in whole or in part in print, electronic or other medium. I retain the right to use this content in whole or part in future works (such as articles or books)."

_____

M.M.H.W Bandara

Department of Civil Engineering

University of Moratuwa

Sri Lanka

The above candidate has carried out research for the PhD thesis under my supervision.

_____

Prof. W. K. Mampearachchi

Department of Civil Engineering

University of Moratuwa

Sri Lanka

ABSTRACT

Internal curing concrete provides number of advantages in the concrete construction industry. It provides adequate water to hydrate all the cement. Moreover, internal curing increases the durability, compressive strength and eliminates the formation of shrinkage cracks. The most popular internal curing materials are the manufactured and natural lightweight aggregates. Those aggregates generally produce using expansive clays. Natural lightweight aggregates and expansive clay mines are not available in most countries limiting the production of internal curing concrete to a few countries. Moreover, those aggregates have various disadvantages in use of internal curing concrete production. Mainly, it reduces the compressive strength of concrete. Furthermore, some aggregates have lower water absorption capacity, and some have lower water desorption capacity. Thus, the main focus of this research is to develop an effective pore structure for internal curing aggregate using non-expansive clays.

Different clay samples were obtained from local mine in Nachchaduwa, Dankotuwa, Metiagoda, and another clay sample was imported from China. Subsequently, those were chemically analyzed, and the percentage of each chemical composition was obtained. Afterwards, selected clay types were identified as bloating and unbolting clays according to the method that was suggested by Charles M. Riley. Nachchaduwa and dankotuwa; Metiagoda and China clay samples were identified as bloating and unbolting clays respectively. After that, the level of expansion was identified based on the bloating coefficient. All the clay samples showed lower bloating coefficient than 2.5. Thus, they were categorized as non expansive clays.

The requirements for effective internal curing aggregates were identified through an extensive literature review and limits of those parameters were defined based on the literature review. Moreover, a aggregate production process was established by considering various effect of clay heating on development of pore structure. The effective range of heating temperature of each clay type was identified according to a simultaneous thermal analysis. Subsequently, clay specimens of equal sizes were prepared using each clay samples and heated at selected range of temperature to produce various pore structures within the clay specimens. Afterwards, heated samples were cooled, crushed, and fine aggregates were produced. Pore size, pore connectivity, pore strength and the pore expansion of each aggregate were identified through an extensive analysis of the pore structure. Afterwards, the aggregates were categorized based on the properties of the pore structure of each aggregate.

The internal curing properties of those pore structures were measured based on water absorption, water desorption and density of the aggregates. Afterwards, performance of those pore structures was identified, and limits of the effective pore structures were defined. Bloted non-expansive clay materials were identified as the most suitable materials to produce effective pore structure within heated clay mass. Conversely, unbloted non-expansive materials were not suitable to produce internal curing aggregate. According to the research findings, the effective pore structure should contain at least 27% of open porosity. The mean pore radius and the pore expansion should range from 0.3 to 0.5μm and from 1.1 to 1.5 mean bloating coefficient respectively. Furthermore, the compressive strength of pore structure should be greater than 10N/mm^2.

Finally, two different aggregates which have the effective pore structure and less effective pore structure were selected for verification process. The selected aggregates were produced in larger scale using industrial facilities of Rajarata and Midaya factories. Subsequently, three different types of grade 30 concrete were prepared from each aggregate type to validate the effectiveness of pore structure. Those concrete types were external curing concrete (ECC), non-

curing concrete (NCC) and internal curing concrete (ICC). Moreover, internal curing concrete with 3 days external curing (ICC/3EC) was prepared to study the combined effect of external and internal curing. ECC specimens were kept under submerged for curing, ECC/3EC samples were kept in submerged only for 3 days. NCC and ICC specimens were kept in open space. During the preparation of concrete specimens, workability of the samples was measured. Afterwards, concrete specimens were tested to obtain the compressive strength values at 7, 14 and 28 days. Subsequently, the drying shrinkage of the internal curing concretes which contain the selected aggregates was measured. According to those results, the aggregates which contain the effective pore structure exhibit effective internal curing properties while other aggregate failed to act as an effective internal curing aggregate.

Keywords: Self-expansion; Poorly expansive clay; Black coring; Porous structure; Water absorption; Sand replacement; Strength

DEDICATION

- To my mother who could not get a better sleep for the last 28 years.
- To my father who went through all the troubles to make me who I am today.
- To my supervisor who believed in me and empowered me to achieve this dream.
- To the people of Sri Lanka whom I owe a debt of gratitude for paying for my education

ACKNOWLEDGEMENTS

First and foremost, I would like to express my sincere gratitude to my supervisor Prof. W.K. Mampearachchi for the continuous support, patience and motivation not only in academic work but also in difficult life situations. His guidance helped me in all the time of research and writing of this thesis. I could not have imagined having a better supervisor and a mentor for my Ph.D. study.

Besides my supervisor, I am also immensely grateful to my progress review committee: Prof. Adikary S.U., Prof. Asoka Perera, and Prof. R. U. Halwatura for their insightful comments and encouragement, but also for the hard questions which incented me to widen my research from various perspectives.

I wish to express my sincere thanks to the laboratory staff of Highway Engineering Laboratory, Structural Engineering Laboratory, Environment Engineering Laboratory and Materials Engineering Laboratory of Department of Civil of Engineering, University of Moratuwa.

I wish to express my sincere thanks to the laboratory staff of Materials Engineering Laboratory of Department of Materials Science and Engineering, University of Moratuwa. I wish to express my special thanks to technical officer Mr. Rathnayake and Mr Mihiranga who have provided tremendous help and support in use of furnace and SEM. They did not allow me to do only research work, but they taught me about those machines and made my confidence.

I extend my gratitude to the staff of Rajarata tiles (Pvt) Ltd and Midaya ceramics (Pvt) Ltd for giving me the opportunity to use their factory premises and machines to carry out my research work. I wish to express my special thanks to Mr.Thusitha who is the chief engineer and Mr.Jude Fernando who is the director of Midaya ceramic.

I thank my fellow research colleagues for the stimulating discussions, for all the support they have given me to successfully complete my experimental work.

Finally, I am profoundly grateful to my parents for their love and support throughout my life. Thank you both for giving me strength to reach for the stars and chase my dreams. My brothers deserve my wholehearted thanks as well. Also, I would like to thank my loving life partner Thathsarani for her understanding and support through thick and thin of my journey.

TABLE OF CONTENTS

Declaration of the Candidate & Supervisor i

Abstract ii

Dedication iv

Acknowledgement v

Table of Contents viii

List of Figures xii

List of Tables xiii

List of Abbreviations xiv

1 Introduction 1
- 1.1 Objectives . . . 2
- 1.2 Scope . . . 3
- 1.3 Structure and overview of the thesis . . . 4

2 Literature Review 5
- 2.1 Introduction . . . 5
- 2.2 Curing of concrete . . . 5
  - 2.2.1 General . . . 5
  - 2.2.2 Problems of conventional curing . . . 7
  - 2.2.3 Internal curing concept . . . 8
  - 2.2.4 Impact of internal curing . . . 9
  - 2.2.5 Problems of internal curing . . . 11
  - 2.2.6 Research need . . . 12
- 2.3 Internal curing theories . . . 12
  - 2.3.1 Chemical shrinkage . . . 13
  - 2.3.2 Autogenous shrinkage . . . 14
  - 2.3.3 Shrinkage cracks . . . 14
  - 2.3.4 Humidity drop . . . 16
  - 2.3.5 Requirement of the EICA . . . 16
  - 2.3.6 Summary of findings . . . 18
- 2.4 Different methods of internal curing . . . 19

2.4.1 Internal curing with materials which can bound water chemically 19
2.4.2 Internal curing with materials which have unbound water . . . 20
2.4.3 Internal curing with materials which can absorb water physically 20
2.4.4 Internal curing with materials which can held water physically 21
2.4.5 Internal sealing with water soluble chemicals 24
2.4.6 Comparison of internal curing methods 25
2.5 Development of the Pore structure for EICA 26
2.5.1 Parameters of pore structure of the EICA 26
2.5.2 Effective pore structure (EPS) 29
2.6 Effect of heating process on development of pore structures 30
2.6.1 Effect on material type 30
2.6.2 Effect on strength development 32
2.6.3 Effect on water absorption and desorption kinetics 38
2.6.4 Summary 41

3 Research Methodology **42**
3.1 Introduction 42
3.2 Raw materials selection 42
3.3 Selection of heating temperature 45
3.4 Preparation of clay specimens 45
3.5 Heating process 46
3.6 Measurement of the level of expansion (Kp) 46
3.7 Produced aggregates with different pore structures 47
3.8 Identification of the pore structure of the aggregates. 50
3.8.1 Measurement of the pore connectivity 50
3.8.2 Measurements of Pore sizes and pore distribution 50
3.8.3 Measurements of the Compressive Strength 51
3.9 Internal curing Properties of the pore structures 52
3.9.1 Measurements of the water absorption 52
3.9.2 Measurements of the water desorption 52
3.9.3 Measurements of the density 53
3.9.4 Summary 54

4 Results and Analysis **55**
4.1 Development of the heating process 55
4.1.1 Simultaneous thermal analysis (STA) 55
4.1.2 Level of Self-expansion 60
4.1.3 Summary 61
4.2 Identification of different pore structures 66
4.2.1 Variation of pore size and pore distribution 66
4.2.2 Variation of pore connectivity 74
4.2.3 Variation of the compressive strength 78
4.3 Summary of the identified pore structures 80
4.4 Measurements of internal curing properties of pore structures 83
4.4.1 Variation of density 83
4.4.2 Variation of water absorption 86

4.4.3 Variation of water desorption 89
4.5 Summary of the internal curing properties of the pore structures 92
4.6 Identification of the effective pore structure (EPS) for internal curing aggregate 95
4.6.1 Relationship among density, expansion and compressive strength 95
4.6.2 Relationship between water absorption and open porosity . . . 97
4.6.3 Relationship between mean pore size and water desorption . . 98
4.6.4 The effective pore structure. 100

5 Result Validation **103**
5.1 Validation of the test results 103
5.1.1 Introduction 103
5.1.2 Aggregate production in industrial facilities 103
5.1.3 Mix design 105
5.1.4 Compressive strength and workability 106
5.1.5 Drying shrinkage 107
5.2 Validation of the test results 107
5.2.1 Water absorption 107
5.2.2 Drying shrinkage 108
5.2.3 Compressive strength and workability 110
5.3 Summary 114

6 Conclusion and Recommendation **115**
6.1 Recommendations and future work 116

Appendix A SEM images and identified pores **129**

Appendix B Real scale work study of calculating the unit cost of internal curing concrete aggregate **151**
B.1 Raw materials extraction 152
B.2 Raw materials transportation 154
B.3 Raw materials preparation 155
B.4 Firing cost 157
B.5 Aggregate preparation cost 158
B.6 Overall supervision cost 159
B.7 Calculation of the unit cost for aggregate 159

LIST OF FIGURES

2.1 Curing methods of concrete 7
2.2 Internal and external drying of concrete 8
2.3 Conventional curing and Internal curing 9
2.4 Self-desiccation of a concrete system 15
2.5 Requirement of ICA to produce effective ICC. 17
2.6 Polymer network of SAP. 21
2.7 Visualization of water transport through pore system 27
2.8 Visualization of water transport and pore isolation 29
2.9 Visualization of the parameters of smart aggregate 29
2.10 Bloating clays 31
2.11 Visualization of gases movements 32
2.12 Variation of strength with firing temperature and staying time 35
2.13 Variation of K_p according to firing temperature and staying time . . . 37
2.14 Control variables of the heating process 41

3.1 Production process of different pore structures 42
3.2 Selected clay mines. 43
3.3 Percentage chemical composition of bloating clays. 44
3.4 preparation of clay specimens. 46
3.5 Heating process 47
3.6 Prepared aggregate from Nachchaduwa clay. 48
3.7 Prepared aggregate from Dankotuwa clay. 48
3.8 Prepared aggregate from Metiagoda clay. 49
3.9 Prepared aggregate from China clay. 49
3.10 Measurement of submerged weight of aggregates 50
3.11 Pore structure analysis 51
3.12 Loading machine 51
3.13 Aggregate soaking process 52
3.14 Humidity chamber 53
3.15 Measuring aggregate weight in Phynometer 54

4.1 STA of Nachchaduwa clay sample 56
4.2 STA of Dankotuwa clay sample 57
4.3 Metiagoda clay sample 58
4.4 STA of China clay sample 59
4.5 level of Self expansion in Nachchaduwa clay 62
4.6 level of Self expansion in Dankotuwa clay 63
4.7 level of Self expansion in Metiagoda clay 64

4.8 level of Self expansion in China clay 65
4.9 SEM images of the different pore structure (Nachchaduwa clay) . . . 68
4.10 Identified boundaries of pores in SEM images (Nachchaduwa clay) . . 68
4.11 SEM images of the different pore structure (Dankotuwa clay) 69
4.12 Identified boundaries of pores in SEM images (Dankotuwa clay) . . . 69
4.13 SEM image of the pore structure of the aggregate (Metiagoda) 70
4.14 SEM images of the different pore structure (Metiagoda clay) 71
4.15 Identified boundaries of pores in SEM images (Metiagoda clay) 71
4.16 SEM images of the different pore structure (China clay) 73
4.17 Identified boundaries of pores in SEM images (China clay) 73
4.18 SEM image of the pore structure of the aggregate (China) 74
4.19 Open porosity variation of Nachchaduwa clay 75
4.20 Open porosity variation of Dankotuwa clay. 76
4.21 Open porosity variation of Metiagoda clay 77
4.22 Open porosity variation of China clay 77
4.23 Variation of the compressive strength in Nachchaduwa clay 78
4.24 Variation of the compressive strength in Dankotuwa clay 79
4.25 Variation of the compressive strength in Metiagoda clay 80
4.26 Variation of the compressive strength in China clay 81
4.27 Variation of density in Nachchaduwa clay 83
4.28 Variation of density in Dankotuwa clay 84
4.29 Variation of density in Metiagoda clay 85
4.30 Variation of density in China clay 85
4.31 Variation of water absorption in Nachchaduwa clay 86
4.32 Variation of water absorption in Dankotuwa clay 87
4.33 Variation of water absorption in Metiagoda clay 88
4.34 Variation of water absorption in China clay 89
4.35 Variation of water desorption in Nachchaduwa clay samples 90
4.36 Variation of water desorption in Dankotuwa clay samples 91
4.37 Variation of water desorption in Metiagoda clay samples 92
4.38 Variation of water desorption in China clay samples 93
4.39 Relationship between density and K_p 96
4.40 Relationship between density and Strength 96
4.41 China clay sample 98
4.42 Relationship between pore size and water desorption 99
4.43 Relationship between pore size and K_p 100
4.44 Aggregates which satisfy the main requirement of EICC 101

5.1 Prepared aggregate from Dankotuwa clay. 104
5.2 Stationary furnace 105
5.3 Crushing and sieving process 105
5.4 Prepared concrete specimens 107
5.5 Tested concrete specimen 107
5.6 Prismatic concrete specimens 108
5.7 Drying shrinkage apparatus 108
5.8 Water absorption rate of C12 aggregate 109

5.9 Water absorption rate of N9 aggregate 109
5.10 Pore structure of C12 aggregate 110
5.11 Pore structure of N9 aggregate 110
5.12 The average drying shrinkage of prepared concrete specimens. 111
5.13 The compressive strength of ICC/N9. 112
5.14 The compressive strength of ICC/C12 113

6.1 Parameters of Effective pore structure. 116

A.1 Pore structure of the aggregate prepared at 800°C (Nachchaduwa clay) 130
A.2 Identified pore boundaries of the aggregate prepared at 800°C (Nachchaduwa clay) 130
A.3 Pore structure of the aggregate prepared at 900°C (Nachchaduwa clay) 131
A.4 Identified pore boundaries of the aggregate prepared at 900°C (Nachchaduwa clay) 131
A.5 Pore structure of the aggregate prepared at 1000°C (Nachchaduwa clay) 132
A.6 Identified pore boundaries of the aggregate prepared at 1000°C (Nachchaduwa clay) 132
A.7 Pore structure of the aggregate prepared at 1100°C (Nachchaduwa clay) 133
A.8 Identified pore boundaries of the aggregate prepared at 1100°C (Nachchaduwa clay) 133
A.9 Pore structure of the aggregate prepared at 1200°C (Nachchaduwa clay) 134
A.10 Identified pore boundaries of the aggregate prepared at 1200°C (Nachchaduwa clay) 134
A.11 Pore structure of the aggregate prepared at 1300°C (Nachchaduwa clay) 135
A.12 Identified pore boundaries of the aggregate prepared at 1300°C (Nachchaduwa clay) 135
A.13 Pore structure of the aggregate prepared at 800°C (Metiagoda clay) . . 136
A.14 Identified pore boundaries of the aggregate prepared at 800°C (Metiagoda clay) 136
A.15 Pore structure of the aggregate prepared at 900°C (Metiagoda clay) . . 137
A.16 Identified pore boundaries of the aggregate prepared at 900°C (Metiagoda clay) 137
A.17 Pore structure of the aggregate prepared at 1000°C (Metiagoda clay) . 138
A.18 Identified pore boundaries of the aggregate prepared at 1000°C (Metiagoda clay) 138
A.19 Pore structure of the aggregate prepared at 1100°C (Metiagoda clay) . 139
A.20 Identified pore boundaries of the aggregate prepared at 1100°C (Metiagoda clay) 139
A.21 Pore structure of the aggregate prepared at 1200°C (Metiagoda clay) . 140
A.22 Identified pore boundaries of the aggregate prepared at 1200°C (Metiagoda clay) 140
A.23 Pore structure of the aggregate prepared at 800°C (China clay) 141
A.24 Identified pore boundaries of the aggregate prepared at 800°C (China clay) 141
A.25 Pore structure of the aggregate prepared at 900°C (China clay) 142

A.26 Identified pore boundaries of the aggregate prepared at 900°C (China clay) . . . 142
A.27 Pore structure of the aggregate prepared at 1000°C (China clay) 143
A.28 Identified pore boundaries of the aggregate prepared at 1000°C (China clay) . . . 143
A.29 Pore structure of the aggregate prepared at 1100°C (China clay) 144
A.30 Identified pore boundaries of the aggregate prepared at 1100°C (China clay) . . . 144
A.31 Pore structure of the aggregate prepared at 1200°C (China clay) 145
A.32 Identified pore boundaries of the aggregate prepared at 1200°C (China clay) . . . 145
A.33 Pore structure of the aggregate prepared at 800°C (Dankotuwa clay) . 146
A.34 Identified pore boundaries of the aggregate prepared at 800°C (Dankotuwa clay) . . . 146
A.35 Pore structure of the aggregate prepared at 900°C (Dankotuwa clay) . 147
A.36 Identified pore boundaries of the aggregate prepared at 900°C (Dankotuwa clay) . . . 147
A.37 Pore structure of the aggregate prepared at 1000°C (Dankotuwa clay) . 148
A.38 Identified pore boundaries of the aggregate prepared at 1000°C (Dankotuwa clay) . . . 148
A.39 Pore structure of the aggregate prepared at 1100°C (Dankotuwa clay) . 149
A.40 Identified pore boundaries of the aggregate prepared at 1100°C (Dankotuwa clay) . . . 149
A.41 Pore structure of the aggregate prepared at 1200°C (Dankotuwa clay) . 150
A.42 Identified pore boundaries of the aggregate prepared at 1200°C (Dankotuwa clay) . . . 150

B.1 The manufacturing framework of the aggregates 152
B.2 Extracted raw clay materials 153
B.3 Available equipment at Rajarata tile plant 156
B.4 Decoration (Onglaze) electrical furnace 158

LIST OF TABLES

2.1 Chemical shrinkage of different compounds in cement. 13
2.2 Water storing methods of different materials. 19
2.3 Lightweight aggregates types 23
2.4 Water absorption of different porous materials. 25
2.5 Volume percentage of three types of pores. 28
2.6 The compressive strength variation with heating rates. 38
2.7 Comparison of fast and slow heating processes 39
2.8 Effect on heating rate and temperature on water absorption 40
2.9 Change in water absorption according to heating time and temperature 40

3.1 Chemical composition of the selected clay samples. 44
3.2 Re-calculated chemical composition of the selected clay samples. . . . 45

4.1 Pore size variation of the pore structures of Nachchaduwa clay. 67
4.2 Pore size variation of the pore structures of Dankotuwa clay. 67
4.3 Pore size variation of the pore structures of Metiagoda clay. 72
4.4 Pore size variation of the pore structures of China clay. 74
4.5 Parameters of different pore structures 81
4.6 Internal curing properties of the pore structures 93

5.1 Mix design calculation for grade 30 concrete 106
5.3 The variation of the compressive strength and workability according to the grade of concrete. 114

B.1 Specification of the excavator 153
B.2 Cost for the raw material extraction 154
B.3 Specifications of the loader 154
B.4 Specifications of the tipper 155
B.5 Cost for the raw material transportation 155
B.6 Cost for the raw material preparation 157
B.7 Details of Furnace and firing cost 157
B.8 Cost for aggregate preparation 158
B.9 Cost for management 159

LIST OF ABBREVIATIONS

Abbreviation	**Description**
ICC	Internal Curing Concrete
LWA	Lightweight Aggregate
ICA	Internal Curing Aggregate
K_P	Bloating coefficient
W/C	Water to cement ratio
FM	Fineness Modulus
EICA	Effective Internal Curing Aggregate
SAP	Superabsorbent Polymers
EPS	Effective Pore Structure
BNEC	Bloated-non Expansive Clays
UNEC	Unbloated-non Expansive Clays
SSD	Surface Saturated Dry
STA	Simultaneous Thermal Analysis
DSC	Differential Scanning Calorimetry
TGA	Thermogravimetry Analysis

CHAPTER 1

INTRODUCTION

Conventional concrete is usually cured by external methods such as immersion, ponding, fogging and wet covering. Those external curing methods only avoid drying of the concrete surface. Generally, concrete is cured for fourteen days as a field practice in local construction industry. As a result of that, construction time increases. On the other hand, conventional and high strength concretes may be subjected to early age cracks which affect durability and strength of the concrete [1]. Thus, it is necessary to maintain high relative humidity during the cement hydration process to reduce formation of drying shrinkage cracks. Sometimes, external curing methods cannot maintain a high relative humidity within concrete [2]. Internal curing provides excess water throughout the concrete by using internal water reservoirs and maintains a high relative humidity throughout the concrete [1]. As a result of that, internal curing outperforms more than the external curing.

Lightweight porous aggregates are the most popular material for internal curing concrete production. Sometimes, lightweight porous aggregates reduce the compressive strength of concrete. On the other hand, some aggregates absorb more water but release low amount of water. As a result of that, there are drawbacks in utilization of lightweight porous aggregates for internal curing. Porous aggregates can absorb considerable amount of water due to the capillary forces. Pore size, pore connectivity and strength of the pore structure affect the water absorption and desorption kinetics of the aggregate. The problem is, still researches have not clearly understood about the optimum pore structure for aggregates to use as effective internal curing aggregate. As a result of that, researches focus on developing an effective pore structure for porous aggregate to use as an an effective internal water reservoir.

Heating temperature is a governing factor when developing a micro-structure within clay mass. Hence, it is necessary to study the effect of the firing temperature on mi-

crostructure and physical properties of clay material in the development of internal curing aggregate. Thus, different non-expansive clays were heated at different temperatures and different pore structures were produced. The requirements of effective internal curing aggregates were identified based on theories, specifications and researches of internal curing aggregate. Afterwards, the internal curing properties of different pore structures were analyzed, and the optimum structure were determined considering pore size, pore connectivity, pore expansion and pore strength of aggregate. Finally, the findings were accommodated in a new aggregate and ICC was successfully produced using the aggregate.

1.1 Objectives

In order to achieve the aforementioned research requirement, it is proposed to,

1. determine the properties of effective internal curing porous aggregate.
2. determine the effect of heating temperature in the development of pore structure within the heated clay materials.
3. determine the effect of pore size, pore connectivity, pore expansion and pore strength on properties of internal curing aggregate.
4. develop an effective aggregate for internal curing using non-expansive clay ($K_p < 2.5$).

1.2 Scope

There are number of international investigations on internal curing concrete aggregates. Generally, lightweight aggregate (LWA) is used for the manufacturing of internal curing concrete. Thus, expansive clays which have the K_p value greater than 4 is widely used for manufacturing of LWA. Those type of expansive clay are not available in most countries, but non-expansive clays which have lower Kp value than 2.5, are available in most countries. Moreover, high expansion is not a requirement of the internal curing aggregate. Thus, this research was focused on development of effective pore structure within manufactured clay aggregate to produce effective internal curing concrete. Throughout this study, the effect of heating process on the development of a pore structures was studied and the optimum pore structure was defined based on pore size, pore connectivity, pore expansion and pore strength. If any pore structure can satisfy these requirements, it can be used as an effective internal curing aggregate. Thus, these findings are very important in the development of manufactured internal curing aggregate.

1.3 Structure and overview of the thesis

This thesis is structured in six main chapters.

Chapter 1 summarizes the research background and the research problems and defines the objectives and scope of the research.

Chapter 2 serves as a review of literature which mainly discussed the development of internal curing aggregates. This chapter further discussed the advantages and disadvantages of conventional curing and internal curing processes, the requirement of the internal curing aggregate based on the theories of internal curing, the behavior of different materials as internal curing aggregate. Finally, the development of effective pore structure within selected clay masses was discussed.

Chapter 3 presents the research methodology. It discussed the establishment of heating process to develop pore structure within clay mass and the methodologies that used to develop effective pore structure. Finally, the identification of the pore structures was discussed in this chapter.

Chapter 4 demonstrates the analysis of the prepared pore structures, the effect of heating temperature on the development of different pore structures, characteristics of prepared pore structures, internal curing properties of prepared pore structures. Finally, it provides the limits of pore structures to develop effective internal curing aggregate.

Chapter 5 describes the application of the developed pore structures in production of internal curing concrete. Moreover it analyzed the effectiveness of the optimum pore structure as internal curing aggregate.

Chapter 6 draws conclusions about the key findings and provides recommendations for future work.

CHAPTER 2

LITERATURE REVIEW

2.1 Introduction

This chapter focuses on the properties of internal curing concrete (ICC) and the requirement of porous aggregate to use as an effective internal curing agent. Section 2.2 presents available curing methods and analyses the most effective method to cure concrete. Section 2.3 studies the theoretical background of ICC. Moreover, the required properties of an effective aggregate were quantitatively identified. Subsequently, section 2.4 describes the different types of internal curing methods and analyze the effectiveness of those methods. Section 2.5 describes basic theory behind the development of an effective aggregate for internal curing. Section 2.6 explains effect of the heating process, in the development of an effective pore structure for internal curing aggregates (ICA).

2.2 Curing of concrete

2.2.1 General

Curing plays an important role on strength development and durability of concrete. Curing is defined as the "action taken to maintain moisture and temperature conditions in a freshly placed cementitious mixture, to allow hydraulic cement hydration and (if applicable) pozzolanic reactions to occur so that the potential properties of the mixture may develop"[3]. Curing occurs after the initial setting of concrete. A properly cured concrete has an adequate amount of moisture to continue the cement hydration process. Proper cement hydration process will increase strength of concrete without

leaving unhydrated cement particles within concrete. Thus, an effective curing system is essential in the development of concrete strength.

Concrete curing methods can be divided broadly into two categories: external curing and internal curing, as shown in Figure 2.1. Generally, concrete is cured using external water curing methods such as water ponding, water sprinkling, wet covering. Ponding is a popular method for external curing.

Generally, this method is suitable for curing horizontal surfaces such as roofs, roads, and slabs. After placing concrete, it covers with moist hessian or canvas. Then, it removes after 24 hours. Subsequently, small ponds are built across the concrete surface by using clay or sand. Finally, those ponds are periodically filled with water depending on the atmospheric conditions. This method is very efficient but, the water requirement is very high. On the other hand, those ponds easily break and after the curing process, it is difficult to remove the ponds. Spraying water continuously to the concrete surface provides an efficient curing process. Generally, it is used for curing concrete slabs. Spraying can be done on aligned surfaces to keep the concrete surface continuously wet. The wet covering method also uses to cure both horizontal and vertical surfaces. It is the most popular method of external curing. It can be done by covering the concrete surface with moist hessian, canvas or cover of cement bags. During the curing period, these coverings are periodically wetted.

Internal sealing can be done by using curing membranes. It can be done by covering the concrete by using a layer of waterproof materials. This membrane can build either in solid or liquid form. Wax emulsions, bituminized waterproof papers and plastic films are the common types of membrane used. This method does not require any continuous supervision. On the other hand, this method is very efficient in places where water is not available. Those types of external curing techniques can be done easily without any technical knowledge, but there are some disadvantages.

External water cannot penetrate the concrete system due to the high density and low permeability of concrete. On the other hand, external curing process lengthens project duration consuming more time and money. In that case, the internal curing concept emerged as a new technology for concrete curing, but it is not popular in most countries due to the lack of internal curing materials and technology. Internal curing can be divided into two parts as internal water curing and internal sealing. Internal sealing can be done using chemicals, but it will increase the production cost. Internal water curing can be done using internal curing materials as shown in Figure 2.1. The most popular internal curing method is the internal water curing with lightweight aggregates

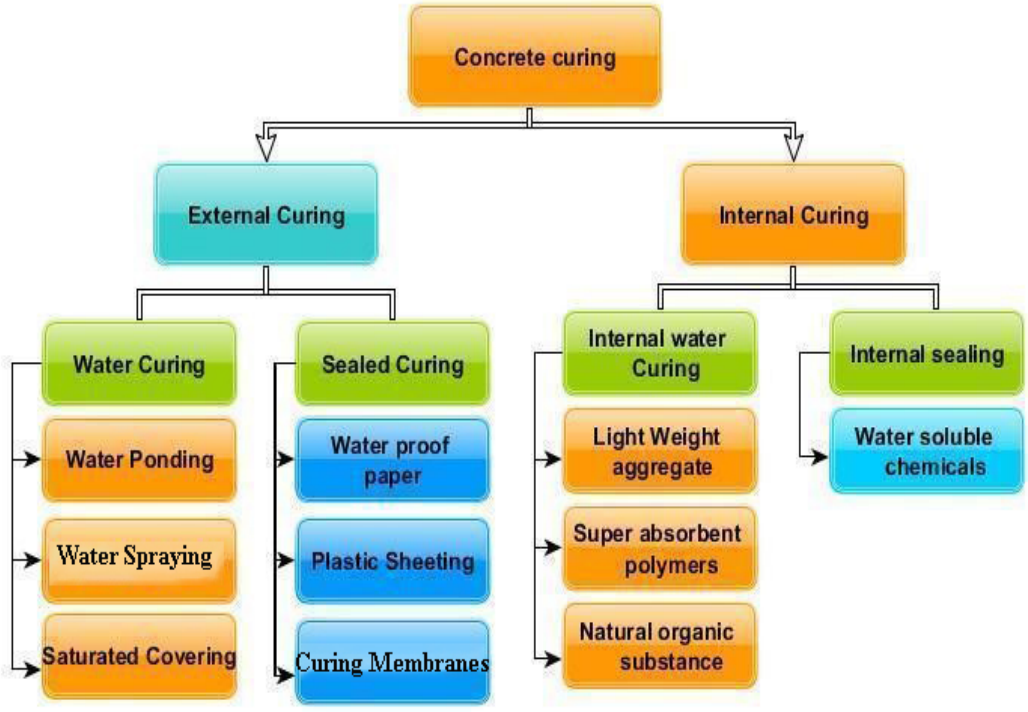


Figure 2.1: Curing methods of concrete

(LWA).

2.2.2 Problems of conventional curing

External curing involves, maintaining the required moisture condition of the freshly placed concrete surface by providing water externally or by sealing the concrete. In conventional external curing, some of the moisture escapes into the air through the concrete surface, some are consumed by the cement hydration process. Thus, an unsealed system can simultaneously undergo both internal and external drying as shown in Figure 2.2(a). In a sealed external curing system, moisture does not evaporate, but gets consumed by the hydration process [4]. Thus, the sealed system also undergoes internal drying as shown in Figure 2.2(b).

During the drying process, water exists inside the capillary pores of concrete is consumed and decreases the relative humidity inside the concrete system. As a result of that, vapor filled pores forms and increases internal stresses of the concrete as shown in Figure 2.2(a) and Figure 2.2(b). Consequently, drying shrinkage and cracking occurs [3]. Internal drying can be avoided providing excess water to the cement system. It reduces the risk of drying shrinkage. External water cannot penetrate the concrete

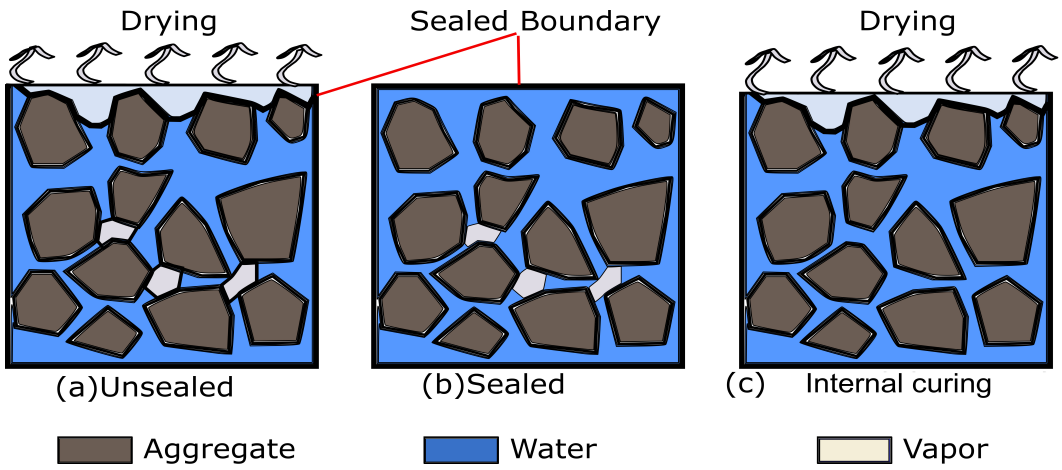


Figure 2.2: Internal and external drying of concrete

system to provide water for cement hydration because, normally concrete has a low permeability which decreases further with the hydration process [5]. External water will only affect several millimeters from surface of concrete [1], but internal curing can provide water for cement hydration as relative humidity reduces inside the concrete system as shown in Figure 2.2 (c) [1]. As a conclusion, external curing methods are not as effective as expected and do not solve the internal drying issue of concretes.

2.2.3 Internal curing concept

Internal curing is a new construction technology that can be adopted as an alternative solution to the problem of external curing. Internal curing provides additional water throughout the concrete by using internal water reservoirs as shown in Figure 2.3. Internal curing was defined by the American Concrete Institute (ACI) as "a process by which the hydration of cement continues because of the availability of internal water that is not part of the mixing water"[3]. It reduces humidity drop inside the concrete and avoids internal drying of the concrete [1]. Consequently, it reduces the risk of cracking.

The dome of the Pantheon was constructed in the Roman era using a lightweight concrete with natural LWA. Man-made LWA was produced in 1919, and the patent of production of LWA was received by Stephen J. Hayde [1]. After that, both natural and man-made LWA was used to produce lightweight concrete. However, the internal curing potential of the pre-wetted lightweight aggregate was identified by the concrete researchers in the 1950s and 1960s [6].

The first publisher of the internal curing potential of lightweight aggregates was Paul

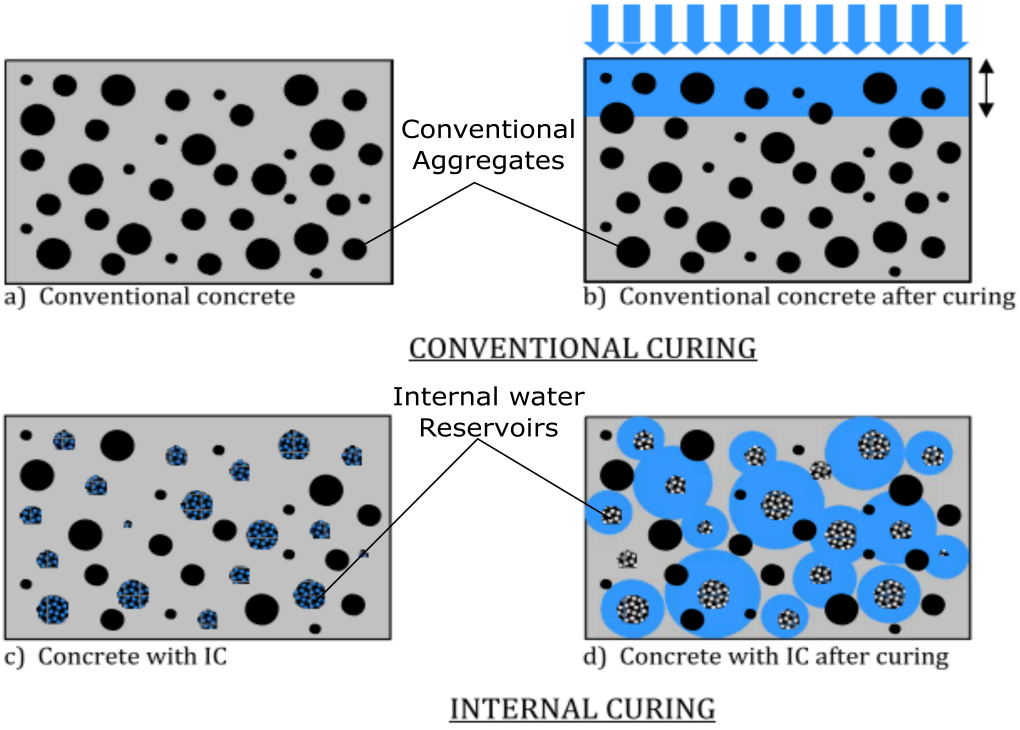


Figure 2.3: Conventional curing and Internal curing

Krieger in 1957, who wrote "Lightweight aggregates absorb a considerable amount of water during the mixing which apparently can transfer to the paste during hydration". Since then, researchers have been investigating different materials such as LWA, fly ash, super absorbent polymers, sawdust and rice husks to produce ICC. The most popular internal curing method is internal water curing using LWA. Thus, some researchers developed internal curing mix-designs successfully using LWA. State Highway 121 North of Dallas in Texas, High Early Strength ICC Off Ramp of I-635 in Mesquite in Texas, and Kansas US 54 Expansion are the existing internally cured concrete pavements [6].

2.2.4 Impact of internal curing

Concrete mixtures that have the w/c ratio lesser than about 0.42, may not complete the hydration process due to the insufficient moisture content [7]. As a result of that, anhydrous cementitious materials will be left inside the concrete system. However, achieving high strength is only possible if the cementitious system is fully hydrated [8].

The compressive and tensile strengths of ICC depend on the nature of curing condi-

tion, mixture proportions and age of specimens. Internal curing concrete may increase strength due to an enhancement in the hydration process and a reduction in early age shrinkage crack formation. Conversely, a reduction in concrete strength can be experienced in some concretes as the internal curing agents are mechanically weaker than conventional aggregates. Typically, ICC increases the compressive strength, flexural strength and splitting tensile strength up to 10%, 5% and 5% respectively [9]. Practically, a variation in concrete strength can be observed due to the variation of aggregate properties.

Raoufi and others [10] studied the internal curing concrete properties with LWA. In this study, samples were cured in a sealed condition, and internal curing was provided by various replacement levels of two different LWAs as internal curing agents. According to the results, the tensile strength of concrete at 7 days was reduced in samples that have 25% of LWA replacement. Further increasing of LWA replacement reduced the strength of concrete. Generally, LWAs are weaker than the conventional aggregates and LWAs are manufactured only to produce lightweight concrete. Thus, increasing the replacement of LWA can reduce the strength of concrete even though the internal curing increases the strength of concrete. Internal curing process often enhances the strength of concrete in later time periods due to the additional water supply for a longer period using internal curing reservoirs [1]. Golias and others [11] found that influence of internal curing water becomes evident at the later age and it was most substantial for the samples stored in a drying environment. Thus, the internal curing concrete showed a comparatively higher strength relative to the concrete specimens that incorporated conventional curing.

The durability of the concrete will depend on the permeability of the reinforced concrete. As self-desiccation occurs, concrete will be susceptible to cracking at the time of placement. Those cracks do not concern in the load-bearing capacity of the concrete structure but, has a significant effect on the durability of concrete structures. Thus, the major durability problems occur when concrete has high permeability due to shrinkage cracks. As a result of that, chlorides from the surrounding (chloride-bearing environment) and acidic gas can penetrate the concrete system and causes corrosion in reinforcements. This is the main durability problem in concrete[1]. Besides these, there are few more factors which do not significantly affect the durability of the concrete [12]. Internal curing reduces the permeability and increases the durability of concrete [13]. According to Raos and Darters [9] study, internal curing concrete shows a 60% and 10% reduction in shrinkage cracks and permeability of concrete respectively. Henkensiefken and others [14] also observed a reduction in plastic shrinkage cracks and crack

widths in internal curing specimens compare to conventional concrete. Subsequently, complete elimination of the plastic shrinkage cracks was observed at conventional environmental exposure conditions when a sufficient amount of LWA was used (18%) as an internal curing agent.

Geiker and others [15] studied about relative humidity and autogenous deformations of internal curing concrete. Internal curing concrete samples had been prepared using LWA in different quantities. Internal curing concrete mixture exhibited the maintenance of a substantially higher internal relative humidity. As a result of that, a significant reduction in autogenous shrinkage was observed (section 2.3.3). In the same time, when there was a 20 % replacement level of LWA, autogenous shrinkage was reduced completely. Those factors prove that plastic shrinkage cracking and autogenous deformations can be reduced using internal curing concrete [16]. Friggle and others, observed a small reduction in unit weight and elastic modulus of internal curing concrete[17]. Subsequently, internal curing concrete reduced the coefficient of thermal expansion [18]. There may be other beneficial effects, but aforementioned are the major ones. Each of these small variations of concrete is potentially beneficial to increase the performance of concrete. However, the combined effects of all variations change the performance of concrete significantly.

2.2.5 Problems of internal curing

Internal curing concrete technology provides number of advantages in construction industry but, internal curing materials are not available in most countries limiting the production of internal curing concrete pavements to a few countries. As a result of that, researchers have been investigating on potential of internal curing capabilities of various materials such as microencapsulated water, superabsorbent polymers, recycled aggregate, naturally occurring lightweight aggregates (pumice, vermiculite, slag, scoria, perlite), manufactured lightweight aggregates (shale, clay, slate), fly ash, volcanic cinders, organic matters etc. On the other hand, those aggregates have various advantages and disadvantages but there is no single material which satisfies all the requirements of effective ICA. Those drawbacks of different materials and their usages are discussed in detail under section 2.4.

2.2.6 Research need

The effective aggregates that used to produce ICC, should absorb and a store considerable amount of water. Subsequently, it should release stored water for cement hydration without compensating the strength of concrete. Kovler [2] had conducted a review of materials that used to produce internal curing concrete. According to his study, there is not any research which has yet identified the optimum structure of the pre-wetted particles, pore size and the distribution of particles, water absorption kinetics and the effect of ion concentration in pore solution in order to use it as an effective internal curing material. As a result of the above facts, a requirement for a proper research to an develop effective pore structure for internal curing porous aggregate has emerged.

Numerous investigations have been carried out to evaluate the performance of internal curing concrete but, researchers have not been focused on the development of concrete properties by changing the mix design parameters of internal curing concrete, such as the quantity, distribution, size, type and material of the internal curing agent. Notwithstanding, this study was focused on the development of an effective microstructure for an internal curing aggregate according to the requirement of ICC. Moreover, this investigation aims to define an effective pore structure based on pore size, pore connectivity, pore expansion and strength of pore structure. Firstly, it is mandatory to identify the internal curing concept, requirements of internal curing and how internal curing works with existing materials.

2.3 Internal curing theories

Normally concrete is produced using cement, coarse aggregate, fine aggregate, water and air. Those can be divided into two main components as fillers and binders. The fillers are fine or coarse mixtures while the binders are generally made up of cement and water. Water reacts with chemical compounds of cement, and hydrated cement gets formed as crystals, intertwining themselves while bonding the neighboring components together. This process is known as the hydration of cement. Those chemical compounds are shown in Table 2.1. The hydration process increases the strength of concrete. Internal curing enhances the hydration process while reducing the autogenous shrinkage. But still, chemical shrinkage occurs.

2.3.1 Chemical shrinkage

Chemical shrinkage is the absolute internal volume change of the cement paste that occurs as a result of the hydration of cementitious materials [19]. As hydration continues, the chemical compounds of cement will react and produce hydrated products. Those hydrated products have a lower volume than the reactants. Basically, this happens due to the difference in volume between the initial reactants and final products. Accordingly, Holt and Tazawa [19, 20] have reported that the magnitude of chemical shrinkage can be estimated using the molecular weights and densities of the reactants and products, as listed in Table 2.1[21].

Table 2.1: Chemical shrinkage of different compounds in cement.

Cementitious compound	Density (g/cm^3)	Molar volume ($cm^3/mole$)	Chemical shrinkage (ml/g)
Tricalcium silicate (C_3S)	3.21	71.0	0.0674
Dicalcium silicate (C_2S)	3.28	52.0	0.0672
Tricalcium aluminate (C_3A)	3.03	89.1	0.1745a, 0.1122b,
Tetracalcium aluminoferrite (C_4AF)	3.73	128.0	0.1154a 0.0802b

a Assuming sufficient sulfate to convert all of the aluminate phases to ettringite.
b Assuming total conversion of the aluminate phases to monosulfate.

Thus, chemical shrinkage cannot be eliminated from the cement system. If cement hydration occurs, there will be chemical shrinkage. The coefficients of each major chemical component available in cement are shown in Table 2.1. Altogether, (7 to 9) ml/100 g of chemical shrinkage occurs in Portland cement paste [22]. The measurable external volume shrinkage of the cement system can be different from chemical shrinkage and is defined as the Autogenous shrinkage. In this stage, internal curing plays a major role, because it can eliminate the autogenous shrinkages [15].

2.3.2 Autogenous shrinkage

As hydration occurs, the internal absolute volume of concrete reduces. However, after the initial setting of the concrete , resistance to deform develops with in the concrete systems. Further continuation of the hydration process consumes water available inside the concrete matrix, as self-desiccation occurs due to the absence of extra water. It leaves the pores of the cement matrix, partially filled with vapor rather than with water [23]. Thus, partially filled pores form within the microstructure of the concrete. The meniscus of water remaining in them creates a significant capillary pressure/stress inside the concrete. It is directly related to the radius of the pore, contact angle and the surface tension of the pore solution. Equation 2.1 shows the relationship between internal stress and pore radius [24].

$$\sigma = (-2\gamma cos\theta)/r \tag{2.1}$$

where σ is the internal capillary pressure or stress, γ is the surface tension of water, θ is the contact angle, and r is the pore radius. The capillary pressure will subsequently produce a significant shrinkage of the concrete micro-structure, causing a measurable external shrinkage in the cement system. At one-point, autogenous shrinkage will differ from chemical shrinkage and, shrinkage cracks may form inside the concrete system. This point is called the concrete setting point. Henceforth, concrete cannot shrink without forming shrinkage cracks.

2.3.3 Shrinkage cracks

Shrinkage cracking is defined as the "cracking of a structure or member due to failure in tension, caused by external or internal restraints as moisture content reduction develops, carbonation occurs, or both"[3]. Those cracks reduce the durability of concrete structure. Formation of shrinkage cracks can be simulated according to Figure 2.4. At the first stage, cement grains mix with water and produce a liquid cement paste as shown in Figure 2.4 (a).

Subsequently, those cement grains react with water and, different hydrated products are formed by consuming water available inside the cement paste. Those hydrated products are shown as black colored border around the cement grains in Figure 2.4(b) and Figure 2.4(c). The cement system can collapse continuously upon itself when the system is in a fluid state. Consequently, the system gets smaller as shown in Figure 2.4(b).

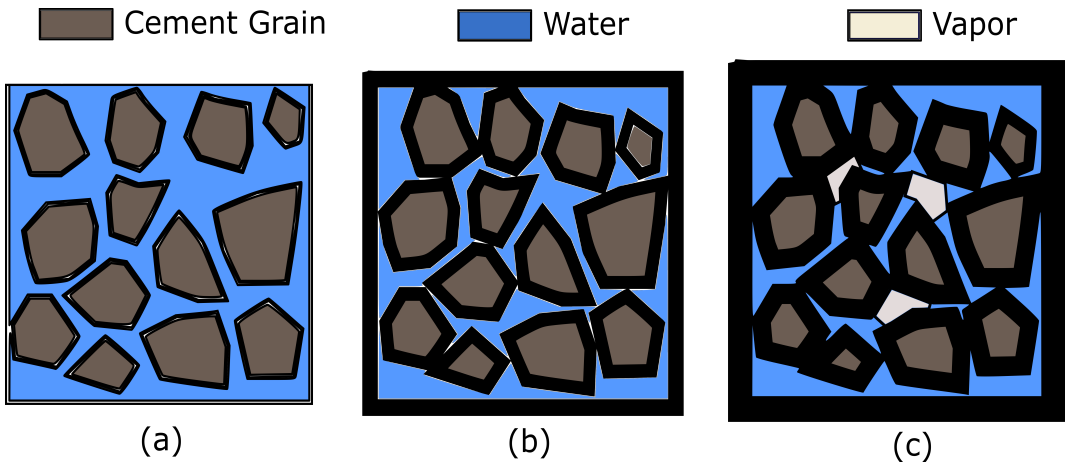


Figure 2.4: Self-desiccation of a concrete system

This is known as the self-desiccation. At this stage, the volume of chemical shrinkage and autogenous shrinkage are equal. At some point, particles can no longer continue to collapse upon itself. This is known as the setting point. Once a mixture has set, the volumes of chemical shrinkage and autogenous shrinkage differ significantly due to the external volume being restrained. External volume cannot change equivalently with the chemical shrinkage [4]. Thus, vapor filled pores form inside the concrete system, as illustrated in Figure 2.4(c). As a result of that, internal stresses are developed inside the concrete system. Those stresses develop inside the cement matrix because of the resistance caused by neighboring materials or connected members. Further increase of the stresses produce a measurable shrinkage in concrete microstructure, inducing micro cracks inside the concrete system. Shrinkage and shrinkage cracks will occur in the drying surface much faster than the core of cement system. Inside the concrete system, moisture is lost only through hydration, but moisture in the concrete surface is lost through evaporation and hydration. Thus, the drying process is much faster in the concrete surface than the core [25].

At an early age, conventional concrete was cured externally, and capillary actions and shrinkage cracks were regarded as negligible. Over the past decade, a significant number of problems, related to early age cracks in high strength concrete, were reported. Researches are pursuing the development of strength and durability of concrete. Thus, researchers want to eliminate the shrinkage cracks of cementitious materials which has a significant influence on the strength and durability of concrete. shrinkage cracks can be eliminated by avoiding humidity drop inside the concrete.

2.3.4 Humidity drop

Humidity level of concrete affects several important properties of the concrete. Shrinkage and shrinkage cracks are the most significant problems related to the humidity drop of concrete. Normally drying and hydration are the two main processes that alter the moisture level inside the concrete. Surrounding humidity can be lower than level of humidity inside the concrete. Therefore, water evaporates from the concrete surface to the surrounding concurrently, cement hydration consumes available moisture to produce hydrated products. As a result of that, humidity level of the concrete reduces causing water filled pores of the cement matrix to begin empty and develop stresses inside the cement system. This can be indicated according to the Kelvin Equation 2.2 [24]. Where, R is the universal gas constant, T is absolute temperature, RH is the relative humidity, and Vm is the molar volume of the pore solution.

$$\sigma = RTln(RH)/V_m \tag{2.2}$$

Zhang Z. B [26] found that the magnitude of shrinkage strain developed inside the cement system is proportional to the humidity drop of the concrete. Bissonnette [27] proved that, the relationship between the shrinkage strain and humidity is approximately a linear one. Humidity of concrete will vary from surface to center of the concrete. Consequently, shrinkage of each location is directly related to the humidity of pores. The humidity level in pores directly affects the strength, thermal characteristics, and rate of cement hydration [27]. This indicates the requirement of a proper curing method to maintain a proper humidity level inside the concrete pore system, and to reduce early age crack forming. The internal curing agent must release absorbed water as the humidity level drops. The potential of water releasing must be very sensitive, as it releases water when there is a small reduction of humidity level. Thus, the requirement of effective aggregates for internal curing can be identified quantitatively based on these theories.

2.3.5 Requirement of the EICA

Generally, the hydration process of ICC depends on the water absorption, water desorption and distribution of internal curing aggregates. Weaker aggregates can reduce the strength of concrete as discussed in section 2.4. The strength of porous aggregate directly related to the density of the aggregate [28]. Based on these factors, Figure 2.5 shows the basic requirement of effective aggregate for internal curing.

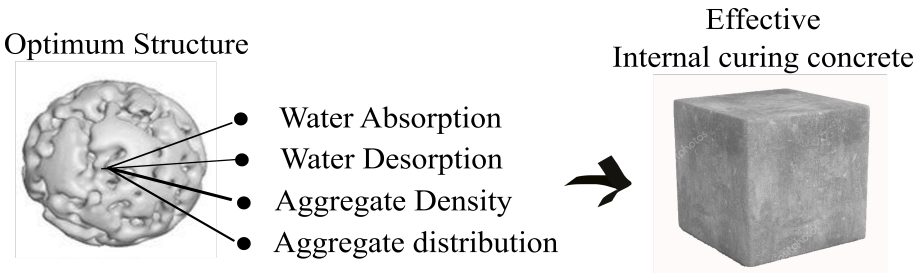


Figure 2.5: Requirement of ICA to produce effective ICC.

If any materials satisfy those requirements, it can be used to produce effective ICC without compensating strength of concrete. Thus, those requirements were studied thoroughly, and limitations were established quantitatively to identify effective internal curing agents.

2.3.5.1 Density of the ICA

The maximum dry loose bulk density of lightweight fine aggregate which used for the structural application is $1120 kg/m^3$. Subsequently, the equilibrium density of the light weight concrete should be lower than $1760 kg/m^3$ [29]. Those LWAs can be used as internal curing lightweight aggregate if it satisfies the ASTM-C1761 standard [30]. This study is focused on developing high strength internal curing aggregate (ICA), thus aggregate strength should be developed. The strength of porous aggregate increases with the aggregate density [28]. Thus, the ICA should achieve higher density value to obtain higher strength. The dry apparent density of normal weight aggregates should be greater than $2.0 g/cm^3$ to use in structural concrete as mentioned in both the European and the Italian standards[31, 32]. The density of conventional concrete exists within the range of 2200 to 2400 kg/m^3. The ICA consists with a pore structure to absorb water, thus those aggregates cannot achieve the same density value as conventional aggregate like sand, but aggregates which have the dry apparent density in the range of (1.4 -3)g/cm^3 can be used in the structural concrete [33]. Thus, the dry apparent density of ICA should be greater than $1.4 g/cm^3$.

2.3.5.2 Aggregate distribution

The ICA should have proper gradation to uniformly provide water throughout concrete. According to the ASTM C33/C33M standard, the fineness modulus (FM) of fine aggregate should be not less than 2.3 and not more than 3.1 to use in the load bearing

structures [34]. On the other hand, fine aggregates which have the fineness modulus in the range of 2.3 or 3.1 protect 99% or 91% of concrete by uniformly distributing water throughout the concrete [1]. Thus, the fineness module ranging from 2.3 to 3.1 is suitable as a grading specification for the ICA. According to those facts, the size of an effective ICA was defined.

2.3.5.3 Water absorption

According to ASTM-C1761 standard, LWA should have a 72-hour water absorption not less than 5% to use in the production of ICC. Conversely, internal curing manufactures have specified that water absorption capacity of lightweight fine aggregate should be greater than 15% to produce effective ICC [35]. Thus, the water absorption capacity of effective ICA should be greater than 15%.

2.3.5.4 Water desorption

According to ASTM C1761/C1761M, aggregate should release at least 85 % of its absorbed water at 94 % relative humidity[30]. Subsequently, the North American lightweight fine aggregates made from expanded shale, clay, slate or slag released 92% to 98% of absorbed water at 93% relative humidity [36]. Thus, the effective ICA should release 92% of absorbed water at 94% relative humidity.

2.3.6 Summary of findings

According to the theories of internal curing concrete, water absorption, water desorption, density and distribution of aggregates were identified as the main requirements of effective ICA. The limitations of those parameters were defined quantitatively based on existing standards, specifications and research findings. Thus, those parameters can be used to identify the effective ICA. Following are the limitations of the parameters of effective ICA. Aggregates should satisfy the requirements of Effective Internal Curing Aggregate (EICA), in order to produce effective ICC.

- Water absorption should be greater than 15% within 48hours
- Water desorption should be greater than 90% at 94% relative humidity
- Density (dry apparent density) should be greater than $1.4 g/cm^3$
- Fineness modulus of aggregate should ranges from 2.3 to 3.1.

2.4 Different methods of internal curing

Generally, internal curing can be divided into two major categories as internal water curing and internal sealing. Internal sealing can be done by using water soluble chemicals. Subsequently, internal water curing can be done by using internal water reservoirs.

Internal water reservoirs are some sort of water containers like cells and gels. Those water reservoirs can be formed either after or before concrete mixing. If reservoirs form after the mixing of concrete, it should form before the setting of concrete. After the concrete sets, those reservoirs should be freely available to supply water as cement hydration occurs. Different internal water reservoirs hold water in different ways. Those are chemically bound water, physically adsorbed water, physically held water and unbound water as shown in Table 2.2.

Table 2.2: Water storing methods of different materials.

Principle of functioning	Example
Chemically bound water	Crystalline water in ettringite
Physically adsorbed water	Water in superabsorbent polymers
Physically held water	Capillary water in fine pores
Unbound water	Encapsulated water

Water absorption and desorption capabilities completely depends on the mechanism of water storing.

2.4.1 Internal curing with materials which can bound water chemically

Many materials contain chemically bound water, and that water is held inside the molecular structure due to the primary chemical bonds. If the chemically bound water content is high enough, and compatible with the cement hydration system, also easily releasing the absorbed water to surrounding as the relative humidity drops, those materials are suitable as internal water reservoirs. Some materials that exist in the cement system have such properties up to some extent. Calcium-aluminates (C_4AH_{19}) and ettringite ($C_3A(SC)_3H_{32}$) are few examples[37]. When the cement system is

subjected to a drying process, its water releases to the surrounding, depending on the energy level in which water binds to the cement system. Firstly, free water evaporates, then physical and capillary water releases. Finally, chemically bound water releases [38]. As the chemically bound water releases, the mechanical properties of the cement paste reduce [39]. However, there is no proper study that would enable the utilization of these techniques without affecting the strength of concrete.

2.4.2 Internal curing with materials which have unbound water

The water is packaged inside the micro level spheres of another material [40]. Technically, this is known as "Micro-encapsulation ". This water cover should deteriorate with time in order to release water as the humidity drops inside the cement system. Conversely, the capsule wall should be strong enough to last until the setting time, while not reacting with cement. Over the past decade, this technology was developed, and many materials were developed for the capsule wall. Interfacial surface polycondensation, is the technique used to encapsulate water drops in polymer form. After releasing water, those capsules will leave empty porous within the cement system, causing a reduction in the compressive strength of concrete.

2.4.3 Internal curing with materials which can absorb water physically

In super absorbent polymers (SAP), there are several polymer chains which are cross-linked and negatively charged, on its molecules. The water molecules are polar, and small charges on them. Consequently, water molecules are attracted to the negative charges on the polymer network and the water molecules are held tightly in the network by Hydrogen-bonding as shown in Figure 2.6 [41, 42].

These polymer networks absorb a larger amount of water from its surrounding, without dissolving in water [43]. According to [44], the theoretical maximum water capacity of SAP is 5000 times as its own weight. SAP is commercially produced with a $50g/g$ capacity. SAP holds water loosely making it freely available for the internal curing process. The effect of SAP on compressive strength depends on mixture proportions. Hasholt and others have studied about different concrete samples which have different levels of SAP [45]. As the percentage of SAP was increased from 0.1% to 0.6%, the compressive strength of the concrete was reduced. This result indicates that the compressive strength of concrete depends on the level of SAP addition. Consequently, there is a limitation in utilization of SAP for concrete mixtures. If water requirement

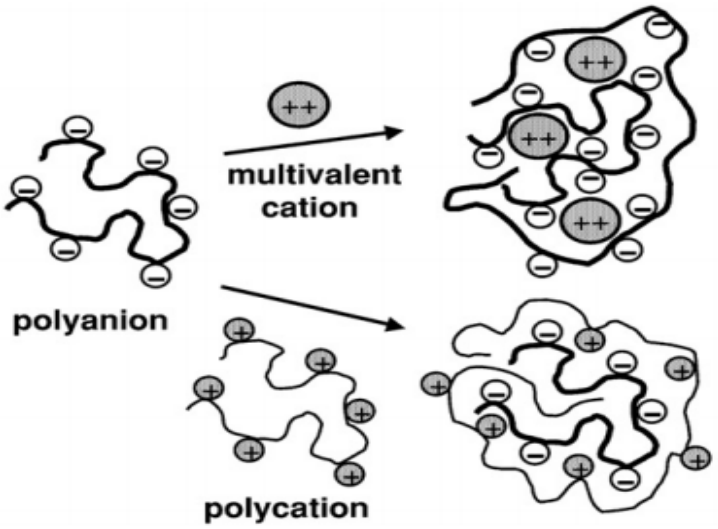


Figure 2.6: Polymer network of SAP.

is high, SAP cannot fulfill the water requirement with a low percentage [46]. As a result of that, SAP cannot be used in high strength concrete which has a lower water to cement ratio.

2.4.4 Internal curing with materials which can held water physically

Cells and pores can store water due to capillary interaction between cell/pore membrane and surface tension of water. The surface tension of water holds water surface intact, and the cell membrane provides a boundary to water as adhesion to the surface material is stronger than the cohesive forces between water molecules [47]. Then capillary forces uptake water to store in cells.

Recycle aggregates consist of pores. Thus, it can hold water physically. Researchers have investigated on recycled aggregates to reuse in the construction process. As a result of that, recycled aggregates have been investigated to identify the potential of internal curing [48]. Those aggregates have relatively higher water absorption than conventional aggregates. Sato had shown a promising result by using recycled aggregates to produce internal curing concrete [49]. Generally, demolishing and recycling process cause fractures in recycled aggregates, thus the compressive strength of the aggregate becomes relatively lower than the conventional aggregate. Those recycled aggregates have an adverse effect on physical and mechanical properties of concrete.

Kim and others, [50] produced ICC using crushed return concrete aggregates and LWA. Those concretes illustrated a considerable reduction in autogenous shrinkage, but it reduced the compressive strength of concrete. The strength reduction was curtailed using an appropriate mix proportion of recycled, lightweight and conventional aggregates. However, recycled aggregates cannot be used along as an internal curing concrete aggregate due to the poor water desorption capability. Those aggregates have an outer shell which is attached to the original concrete or remnants of original concrete [48]. The outer shell consists of tiny porous which hold water tightly and release at relatively high humidity drops. Technically, water travels from large capillaries to small capillaries because capillary forces are high in small capillaries. Thus, water holds inside relatively small pores will not be freely available for the hydration process. For this reason, recycled aggregates are less useful as effective ICA [37].

LWAs consist of a series of pores, thus those aggregates can physically hold water inside the pore structure. Capillary force is the primary mechanism responsible for holding water in these materials. LWAs are popular in the concrete construction industry because of low density. Thus, it decreases dead load while increasing handling capabilities [51]. LWAs are a type of a coarse aggregate, used in the production of lightweight concrete products. The main function of LWAs are the reduction of concrete density. Generally, most manufactured and natural LWAs have a range of particle density between 0.8 and 2.0 gcm^{-3} [52]. While density of the natural aggregates range from 2.4 to 2.8gcm^{-3}. LWAs are defined as an aggregate of low density such as (1) expanded or sintered clay, shale, slate, diatomaceous shale, perlite, vermiculite, or slag; (2) natural pumice, scoria, volcanic cinders, tuff, and diatomite; (3) sintered fly ash or industrial cinders [3].

Materials of lightweight aggregates are generally classified into four groups: natural, manufactured structural, manufactured insulating and by-product as listed in Table 2.3 [53]. These aggregates can be used as internal curing agents if they can hold enough water as internal water reservoirs. Bush, Kovler and Clarke had studied about the behavior of LWA concrete systems [2, 53, 54]. Over the past decades, different research groups studied about the internal curing potential of LWA [55]. Bentz and Weber successfully produced an internal curing concrete using conventional LWA as internal water reservoirs [1, 56]. LWA should be pre-wetted by submersion in order to absorb water. The problem is, sometimes these LWA takes days to completely saturate because, the air inside the pores of LWA hampers water ingress [57].

Thermal insulation, sound insulation and fire resistance are several benefits that as-

Table 2.3: Lightweight aggregates types

Natural	Manufactured		Byproducts
	Structural	Insulation	
pumice	shale	vermiculite	slag
scoria	clay	perlite	organic cinders
tuff	slate		coke breeze
breccia			fly ash
volcanic cinders			bottom ash

sociates with LWA [58]. Natural LWAs are produced by directly extracting from mines, crushing and sieving to required sizes. Pumice, perlite and volcanic cinders are the most popular natural LWAs. Those LWAs are readily available in recent volcanic terrains. Some LWA have an acceptable potential to be utilized as internal water reservoirs. Nonetheless, properties can vary from one aggregate to another one, thus studying each LWA becomes a necessity in order to comprehend their internal curing potential.

Pumice is a porous volcanic rock that can be found in recent volcanic terrains. The porous connectivity may vary from completely closed, to completely open. Consequently, it has a considerable water absorption capacity of $0.27 kg/kg$ [59]. The open porosity of this aggregate has been measured to 40% [37]. Perlite contains 2-6% of combined water. Those combined water vaporizes and creates countless bubbles spontaneously when perlite is rapidly heated around 900°C. Those air bubbles expand up to 4 to 20 times from its original volume. The bulk density and water absorption of the perlite range between 30-400kg/m^3 and 200-600%, respectively. Perlite has been primarily used as a cavity filling insulation material in the construction industry. However, perlite and pumice reduce the compressive strength of concrete. These aggregates have a weaker porous structure that consists of a low amount of solids and a high amount of air voids. As a result of that, these are not used in load bearing concretes.

2.4.4.1 Expansive materials

The expanded clays are raw materials that expand itself when it subjected to a heating process. Expanded clay pellets are manufactured using expansive clays. During the production process, those materials are prepared as pellets. Subsequently, pellets are

subjected to a heating process. Then, hard ceramic pellets are produced. Those pellets consist with a dense outer shell and porous core. The outer shell consists of tiny pores and a core that has relatively larger pores. Porosity of this expanded clay clinkers can be as high as 90%[37]. However, a larger part of the pores is closed, hence most pores are not available to store water. Zhang and Weber conducted studies on two different expanded clay types using mercury intrusion porosimeter. The obtained results showed that the pellets were consisted of pores which had an average pore size of 400μm, and minimum pore size of 100μm [60, 61]. The water absorption of these expanded clay clinkers is around $0.17kg/kg$ [61]. Even though researchers have used these materials to develop ICC [1], those aggregates have not been proved high effectiveness. Moreover, there is no consideration on the development of internal curing properties such as open porosity, pore size and pore strength during the production process of these aggregates. Generally, manufactured LWAs show low density, low compressive strength, high porosity, high water absorption and low elastic modulus [62].

2.4.4.2 Non-expansive materials

Expansive clays are categorized according to the degree of expansion. Bloating coefficient (Kp) expresses the potential of expansion. Clays which have the bloating coefficient lower than 2.5, can be categorized as a non-expansive clay[63]. Various types of non-expansive clays are available in most countries. Pioro L.S [64] produced LWA using non-expansive clays and various additives. Those aggregates have the bulk density within the range of 0.16 and 0.85 g/cm^3, and the cylindrical compressive strength ranges between 0.78 and 14.4MPa. Even though non-expansive clays do not expand much during heating, it may be a sustainable resource to produce effective ICA with required density value.

2.4.5 Internal sealing with water soluble chemicals

Evaporation of water takes place from an exposed surface due to the difference in free energy between the vapor and liquid phases. Water soluble chemicals can be added during the concrete mixing to reduce the water evaporation. Water-soluble chemicals have hydroxyl and ether functional groups. Those groups form hydrogen bonds with water molecules and reduce the free energy of the molecules [65]. As a result of that, vapor pressure reduces. Thus, the rate of water evaporation reduces. Amr and Dieb studied about olyethylene glycol and polyacrylamid as a water-soluble chemicals to

develop internal curing concept. According to the results of this experiment, water retention was higher in the concrete mixes incorporating these chemicals compared to conventional concrete mixes [66]. On the other hand, Tech [67] has shown that, the use of Polyvinyl alcohol in 0.48% by the weight of cement as self curing agent provides higher compressive, tensile and flexural strength than the strengths of conventional mix [67].

According to the aforementioned facts there are different methods for internal curing. In order to find the optimum method for internal curing, those methods should be evaluated as discussed in the next section.

2.4.6 Comparison of internal curing methods

Different materials that used to produce internal curing concrete, have different properties. If those materials satisfy the requirements of effective internal curing aggregate (EICA), it can be used to produce effective ICC. Based on those requirements, those materials were analyzed to study the internal curing potential of each aggregate.

Calcium aluminate and ettringite will release water, only if there is a significant humidity drop inside the concrete. Consequently, it reduces the mechanical properties of the concrete [39]. Superabsorbent polymers and micro encapsulate particles leave empty pores, after releasing absorbed water. Thus, the compressive strength of concrete reduces even though it avoids the early age crack propagation [45]. Recycled aggregates can absorb a satisfactory amount of water but, the water will not be released for cement hydration due to the high capillary energy of relatively tiny pores compared to the cement matrix. Recycled aggregates reduce the compressive strength of concrete [50]. Table 2.4 shows water absorption and open porosity values of some LWA [48].

Table 2.4: Water absorption of different porous materials.

Material	Water content [kg/kg]	Useful porosity
Superabsorbent polymer	15	N. A
Pumice	0.27	40%
Perlite	4.5	90%
Expanded clay (Leca, Liapor)	0.16	40%
Expanded shale (Stalite)	0.06	5%
Diatomaceous earth	1	70%

Pumice and perlite have a considerable water absorption capacity and useful porosity but, reduce the compressive strength of concrete due to low density. Thus, Perlite and pumice cannot be used in the production of structural concrete.

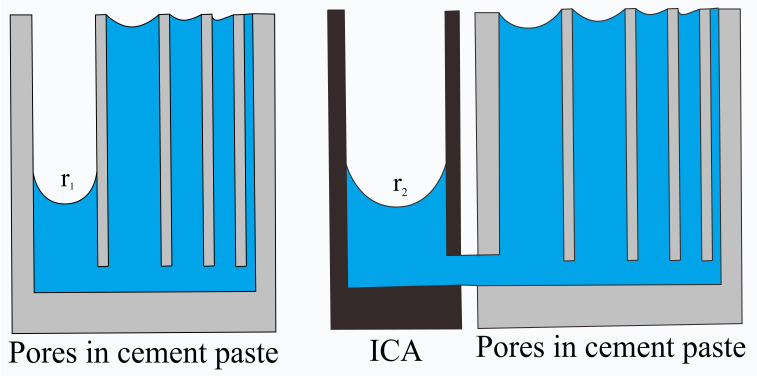
Generally, LWAs are produced as a coarse and fine pellet. Coarse aggregates cannot use as a effective internal curing aggregate (EICA) due to low density. Fine pellets have relatively high strength due to the outer shell. Consequently, the outer shell reduces the water absorption and desorption capacity of the lightweight pellets. Moreover, raw materials are not available in most countries. As a conclusion, there is not any single material which satisfies all the requirement of EICA to produce effective ICC. Thus, the study was focused on the development of effective pore structure for manufactured aggregate to satisfy the requirements of EICA.

2.5 Development of the Pore structure for EICA

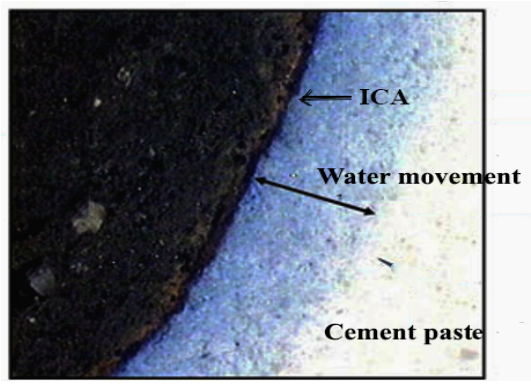
The existing internal curing agents have different properties. Thus, properties of concrete which made using those aggregates exhibit different characteristics. Thus, non-expansive clays were selected to develop EICA as per the research objectives. Generally, Those aggregates hold water as physically held water due to capillary forces. Thus, water absorption and desorption capacities mainly depend on the pore structure of that aggregate. As a result of that, the pore structure of those aggregates should be developed in order to achieve the properties of EICA. The pore structure of those aggregates can be easily controlled during the production process. Firstly, it requires to identify the parameters of pore structure and the effect of heating process on the development of effective pore structure (EPS) for aggregates.

2.5.1 Parameters of pore structure of the EICA

Figure 2.7 visualizes water movement from internal water reservoir to cement paste. The cement paste consists of solids and pores as shown in Figure 2.7(a). These pores and solid parts have a significant influence on the mechanical and physical properties of concrete [68, 69]. Basically, four different pore types exist within the concrete structure. Those are gel pores, air voids, capillary pores and macro pores [69]. The gel pores significantly affect the shrinkage of concrete but, it is not related to the strength of the concrete. Capillary pores, macro pores and air voids are responsible for the reduction in strength of concrete and increment of shrinkage. Li and others [70] identified the



(a) Pore system and water movement ICC



(b) Water movement

Figure 2.7: Visualization of water transport through pore system

distribution of those pores with respect to the age of concrete system as shown in Table 2.5.

A relationship between humidity level and emptying pore size can be derived based on Equation 2.1 and Equation 2.2 [1]. The relationship between humidity level and emptying pore radius is not linear. Large pores are emptied first as relative humidity drops inside the concrete (Figure 2.7(a)). The pores which have radius approximately greater than 100 nm, first began to empty when relative humidity of concrete drops to 99% [1]. Thus, ICA should release water to fill those pores as shown in Figure 2.7(a) and 2.7(b). The main water driven forces are the pressure difference and capillary actions. If the pore radius is small, the difference in pressure required to develop a motion in water will be high. Conversely, if the radius is higher, difference in pressure required to develop water movement will be less [71]. According to that, pore size can be identified as an important parameter in the pore structure.

Figure 2.8(a) shows the capillary forces that act on a Nano tube. The capillary forces originate due to the cohesive and adhesive attraction exerted between molecules [72].

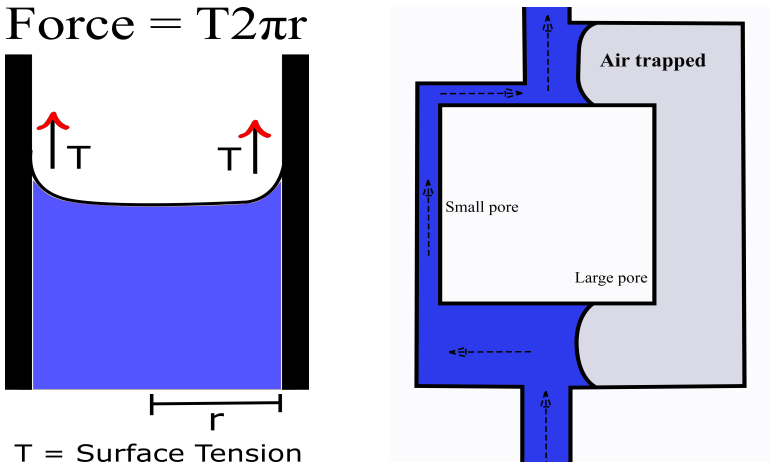
Table 2.5: Volume percentage of three types of pores.

	Pore distribution		
Age	Gel pores (%) (1-10nm)	Capillary pores(%) (10-1000nm)	Macro pores (%) ($> 10,000nm$)
28 Days	18.28	42.29	39.43
56 Days	21.23	40.69	38.08
100 Days	29.50	33.40	36.8

Generally, the most common scenario of the capillary force occurs when the surface of water or liquid contacts with air. The surface energy of water develops due to the unbalance and unsymmetrical bonding forces of water molecules that exist in air-water surface [73]. Perpetually, the water surface tries to minimize the energy level reducing the area of air-water interface. Thus, water molecules always move forward to reduce the radius of the meniscus. At the first stage, water will spread over the surface of boundary material due to adhesive forces. After the initial wetting process of boundary materials, the adhesive forces will no longer be effective in water movement. Finally, adhesive forces hold a thin layer of water firmly in contact with the boundary material of the pore membrane [47]. Then cohesive forces produce the motion of water due to the unbalanced forces of the surface water molecules. Water flows only because of the surface tension, cross sectional area of water flowing and curvature to the pressure [72].

There should be interconnected pores to flow water continuously otherwise water cannot flow into the pore structure due to the capillary forces and reduce the water absorption and desorption capacity of pore structure. The closed pores are not capable of absorbing water thus, closed pores should be minimized. Thus, pore connectivity is an important factor in the pore structure. Moreover, pore isolation can be happened due to the presence of small and large pores. When pore structure absorbed water as shown in Figure 2.8(b), water will travel fast in small pores due to the capillary force and larger pores become isolated as shown in Figure 2.8(b). On the other hand, thick walls of pores may increase strength of the pore structure and the density of internal curing aggregate (ICA). Thus, strength of the pore structure is an important factor because strength of aggregate is a major concern in development of effective internal curing concrete. According to aforementioned facts, Figure 2.9 illustrates the parameters of

effective pore structure (EPS).



(a) Capillary forces on a nanotube

(b) Visualization of pore isolation.

Figure 2.8: Visualization of water transport and pore isolation

2.5.2 Effective pore structure (EPS)

The main objective of this study is to develop EPS for porous aggregate using non-expansive clays. The internal curing properties of porous aggregates mainly depend on the pore structure of that aggregate. Thus, EPS should be developed within the aggregate in order to achieve the requirement of EICA. Afterwards, the parameter of the EPS can be identified quantitatively.

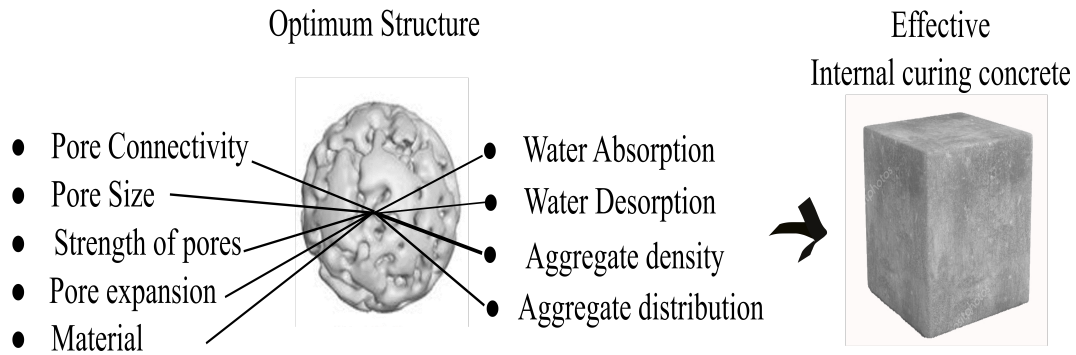


Figure 2.9: Visualization of the parameters of smart aggregate .

In order to establish those parameters quantitatively, different pore structures with different pore sizes, pore connections, pore expansions and pore strengths should be developed within the clay mass. It can be developed within clay mass by heating. Thus,

it requires to study about the effect of heating temperature in the development of pore structures within clay mass.

2.6 Effect of heating process on development of pore structures

Pore structures can be developed within clay mass using a proper heating process. Thus, it is necessary to identify variables of the heating process. Afterwards those variables can be changed effectively to produce different pore structures within clay mass. This section discusses about effects of the heating process in the development of water absorption, desorption and strength of pore structures. Moreover, the type of the clay material is the most important factor to be considered in development of different pore structures. Thus, effect of the raw materials is studied through this section. Finally, variables of the heating process were identified in order to define a proper heating process.

2.6.1 Effect on material type

Generally, clay contains different minerals and chemical compounds such as kaolinite ($Al_2O_3.2SiO_2.2H_2O$), Felspathic ($K_2O.Al_2O_3.6SiO_2$), quartz (SiO_2), ferric oxide (Fe_2O_3) and Lime (CaO) [74]. Those chemical compounds are a combination of basic chemical elements such as silicon, aluminum, iron, calcium, sodium and other elements which are available in very small amounts [75]. Murray and Bennour [76, 77] mentioned that, during the heating process, clays will become a red fired clay, if there is a high amount of hematite greater than 5%. Otherwise it will become white fired clay when there is lower hematite content than 1%.

Basically, clays are divided into different categories depending on their bloating coefficient (K_p) which gives a direct idea about the potential of self-expansion. According to the K_p clays are divided into the following categories; [63, 78].

- $Kp > 7 - 8$ = clays of good bloatability.
- $Kp = 4 - 5$ = medium bloatability.
- $Kp = 4 - 2.5$ = poorly self-bloating.
- $Kp < 2.5$ = not self-bloating clay.

Generally, two conditions necessary to achieve a proper bloating mechanism. Clay mass must produce a plastic clay paste with proper viscosity during the heating process

and at that temperature range, materials present in the clay mass must emit gases. Generally, the chemical compounds that exist in the clay mass emit gases such as water (H_2O), oxygen (O_2), carbon dioxide (CO_2), carbon monoxide (CO), Sulfur dioxide (SO_2), fluorine (F), chlorine (Cl_2) and ammonia (NH_3) during the clay firing [79, 80]. Moreover, clay particles fuse and form plastic clay paste with enough viscosity during the sintering process. Thus, the sintering process plays a major role in pore expansion. Some clays will not bloat but some clays will bloat and expand slightly in between 1 to 2.5. According to the clay categorization, both clay types can be considered as non-expansive clays. Thus, those clays can be named as bloated-non expansive clays (BNEC) and unbloated-non expansive clay (UNEC)

These clay types can be identified according to the method that suggested by Charles M. Riley [81]. Charles M. Riley [81] had observed different non-expansive and expansive clay types and defined the limit of bloating on a composition diagram with silica, alumina, and fluxing compounds as shown in Figure 2.10. Non-bloating clays can be bloated by adding Al_2O_3 and fluxing agents. Therefore, this is a more relevant method to find bloating clay types based on the chemical composition, but it does not give any idea about the level of expansion. Thus, the bloating coefficient test should be conducted to identify the level of expansion.

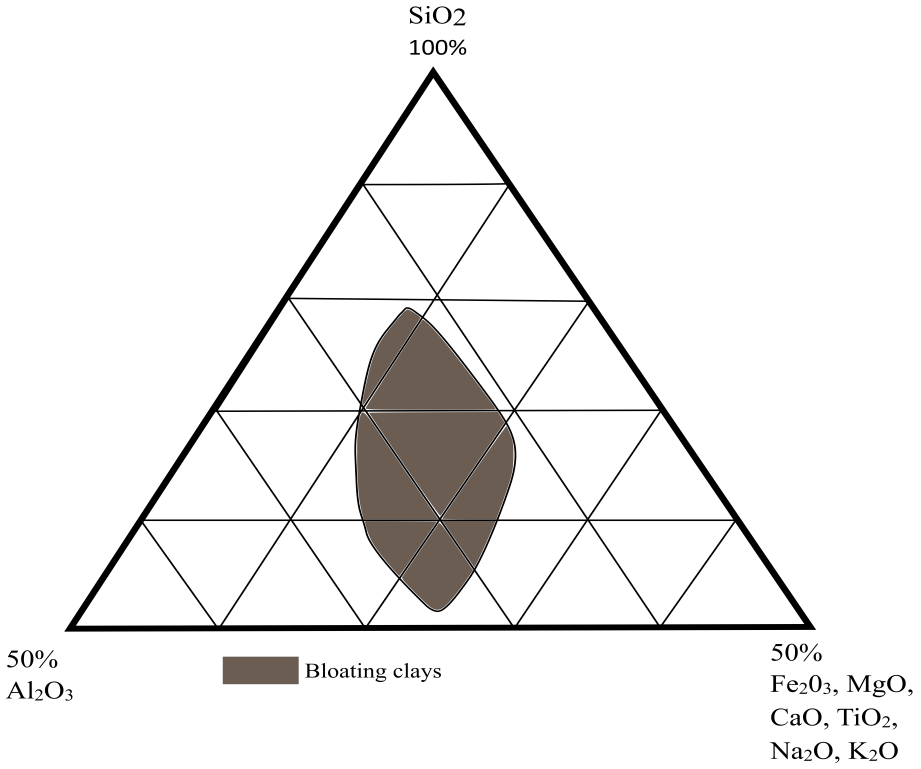


Figure 2.10: Bloating clays

2.6.2 Effect on strength development

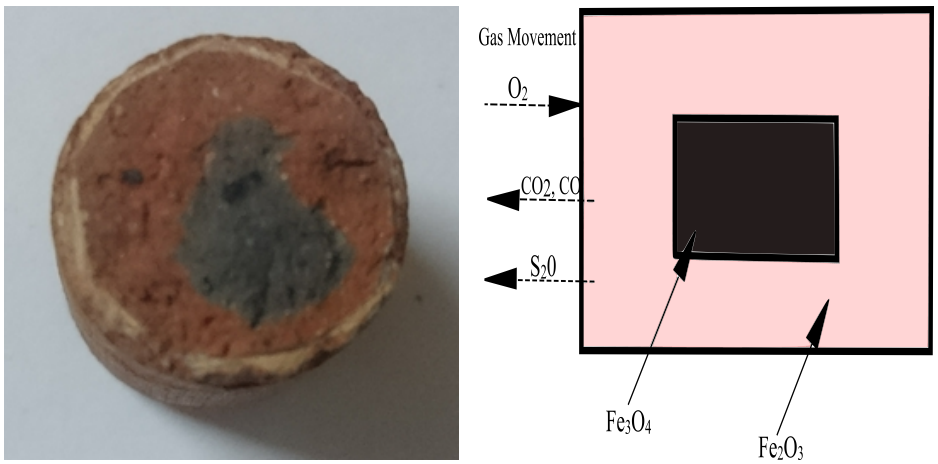
During the production process of internal curing aggregate, strength development is a necessity. Strength of fired clay aggregates mainly depend on the following characteristics [82, 83];

- Defects
- Micro-cracks
- Formed phases
- Pore structure

These factors should be clearly understood to define a heating process.

2.6.2.1 Defects

Defects are the main problem of strength development. Black coring is a major defect of clay firing. During the clay firing process, clay samples can be subjected to different combustion environments. In order to have a complete ignition or a complete oxidation process, oxygen must react with various chemical compounds of clay mass. Therefore, air must have a sufficient path to reach those areas easily [84]. During the clay combustion, surface of the clay mass burns with a relatively high amount of oxygen leading to the formation of a perfectly combusted shell part and a partially combusted black core area in the heated clay sample as shown in Figure 2.11(a).



(a) Black core area of fired clay (b) Visualization of gass transport.

Figure 2.11: Visualization of gases movements

MacKenzie and Cardile [85] found that black coring is not directly related to unoxidized carbon residues. Moreover, black coring occurs due to the conversion of iron oxide from hematite (Fe_2O_3) to magnetite (Fe_3O_4). This happens during the combustion process as shown in Figure 2.11 (b). Carbon monoxide reacts with hematite and form magnetite as shown in Equation 2.3. Generally, Magnetite is a black or brownish-black colored chemical compound originating the black colored core inside the clay body [85, 86]. The formation of magnetite is the root cause for black coring.

$$3Fe_2O_3 + CO \rightarrow 2Fe_3O_4 + CO_2 \tag{2.3}$$

Color is not an indispensable element of an internal curing aggregate. But is an important indicator to measure the ignition level of the core area. As the oxygen content is low inside the core of clay sample, carbonaceous matters will oxidize partially and weakening the fired clay mass [87]. Incomplete ignition will not form new crystalline phases which increase strength of pore structure [82]. Moreover, black core causes excess bloating inside the core area and reduces the strength of pore structure [88]. As a result of that, black color should be removed within the clay body.

The black core can be eliminated by providing an oxidizing environment [89]. As the amount of oxygen increases inside the combustion chamber, the area of black core decreases releasing a comparatively higher $CO_2(g)$ amount than CO (g) [80, 90]. Thus, oxidizing environment will reduce the formation of black core area. The diffusion of oxygen depends on the thickness of the aggregate [91]. If there is higher density in the clay mass, oxygen will not diffuse into the core area due to the lack of interconnected voids. If the aggregate size is smaller the oxygen diffusion path becomes shorter and oxygen will interact with the inner clay mass to complete the oxidation process. Thus, small aggregates reduce the black colored core area [86]. Kadir and Mohajerani [92] mentioned that the intrusion of oxygen may be hindered by water vapor that originates during fast heating rates, because there is not enough time for evolving gases to diffuse into the surrounding. Consequently, oxygen has no time to diffuse into the clay body during fast heating rates. Thus, slow heating rates can avoid the formation of the black colored core area. Arnold and Duncombe mentioned that the black colored core area can be eliminated by extending the firing time because a longer heating time will provide enough time for oxygen to diffuse into the core area [93].

As a conclusion, If there is a high surface area in clay body that exposed to the uniform rate of combustion with excess air in the firing kiln (oxidizing environment), will

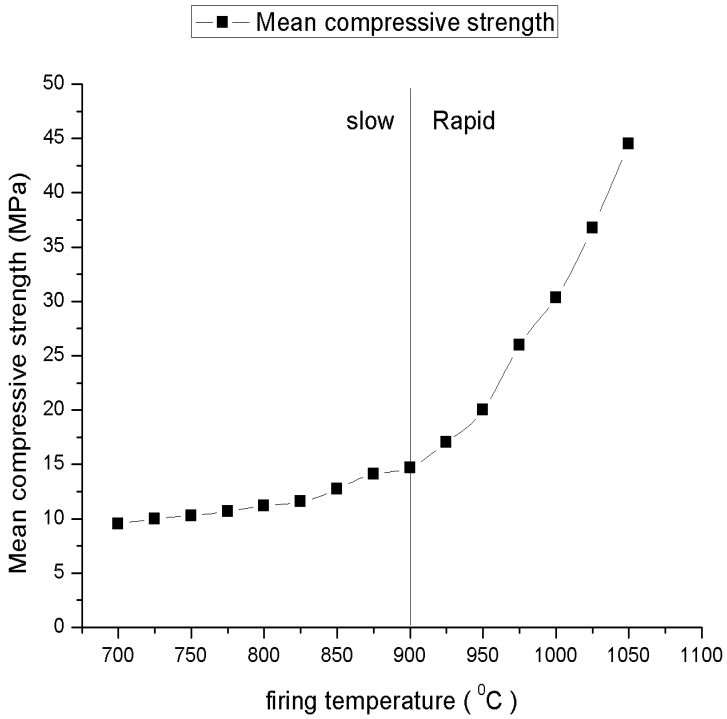
ensure proper combustion of carbon and iron residues exist in core area of clay body and will avoid the formation of black color area within fired clay mass [94].

2.6.2.2 Formed phases

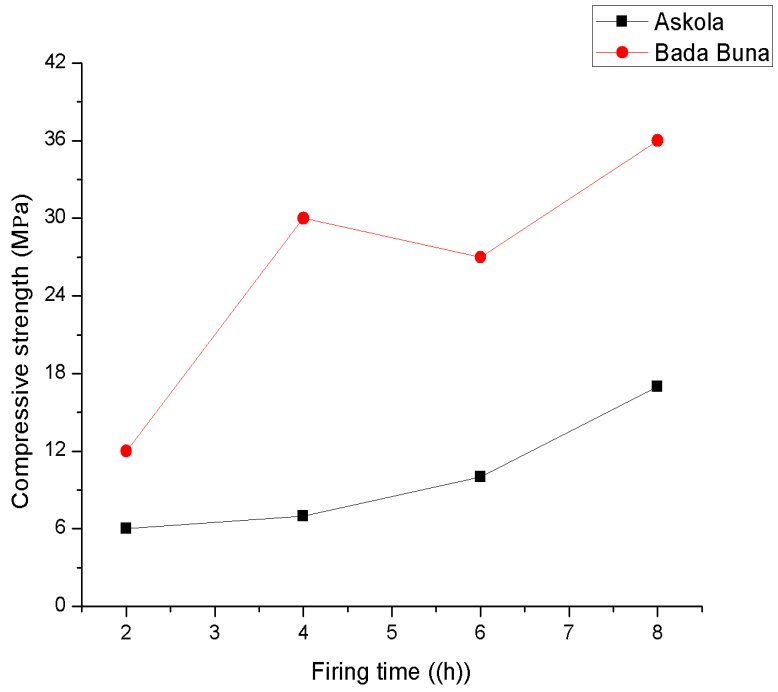
Generally, different phases develop during the clay firing process. Those phases associate with the sintering and vitrification process of the clay mass [95, 96]. It increases durability, strength and other mechanical properties of the fired clay sample [97]. The amorphous phase becomes the dominant phase during the vitrification process. It binds clay particles together. Materials which have a low melting point melts quickly and fills space between more stable particles. As a result, melted materials will compact and strengthen the clay body [77]. At higher temperatures greater than 1100°C, aluminum silicate ($2Al_2O_3SiO_2$, mullite) formes as long needle like crystals and binds the surrounding materials even further. This process enhances strength of the heated clay mass[98]. Thus, strength of the heated clay mass depends on the maximum temperature reached during the vitrification stage. However, excess vitrification deforms the clay sample. Karaman and others [99] studied the variation of the compressive strength respect to the heating temperature as shown in Figure 2.12(a).

According to Figure 2.12(a), the compressive strength of clay mass increased with heating temperature and there was a significant increment in the compressive strength after 900°C which is normally relates to the sintering, vitrification and consolidation of clay mass [100]. These test results stand as proof to show the formed phases can increase the strength of the pore structure.

Higher soaking time provides a proper ignition to residual materials of the clay mass and completes the formation of material phases which occur at each temperature level. Thus, firing time increases the compressive strength of clay materials as shown in Figure 2.12(b)[100].



(a) Compressive strength and firing temperature



(b) Compressive strength and staying time (970^{o}C).

Figure 2.12: Variation of strength with firing temperature and staying time

2.6.2.3 Microcracks

The formation of cracks significantly affects by the rate of heating temperature. During rapid heating process expansion of quartz occurs and creates an unbalance shrinkage around the quartz particles. This causes cracks in heated clay mass. On the other hand, rapid heating process creates an unbalance expansion between the outer shell and inner core area of the clay mass. As a result of that, cracks form and reduce the strength of the fired clay sample. The formation of those micro-cracks can be eliminated by introducing slow firing rates at critical temperatures [101]. Moreover, slow heating prevents disrupted texture forming due to the rapid emission of water vapor [90] and other gases [86]. According to the above facts, slow firing rates are recommended to produce ICA without forming micro-cracks.

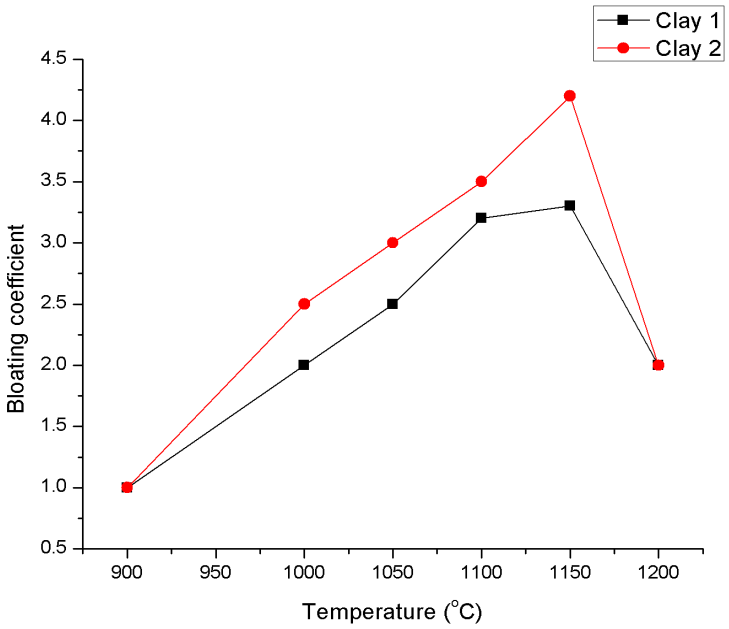
2.6.2.4 Pore structure

Pore expansion is an important factor in the development of different pore structures within clay mass. Bloating coefficient K_p is the indicator of the level of expansion and the formation of porous structure due to the self-expansion. Moreover, density of heated clay samples is inversely proportional to K_p. Thus, high K_p values reduce the density of heated clay mass. Khafaji and others [78] studied about the variation of K_p with respect to heating temperature and staying time. Figure 2.13 shows the obtained results for two clay samples. According to Figure 2.13(a), the bloating coefficient of the clay samples increased with heating temperature and reached the maximum value at a specific temperature. Afterwards, the bloating coefficient was reduced due to the melting and consolidation of clay mass. According to Figure 2.13(b), bloating coefficient increased with staying time to a certain limit because it increases energy input to the firing chamber.

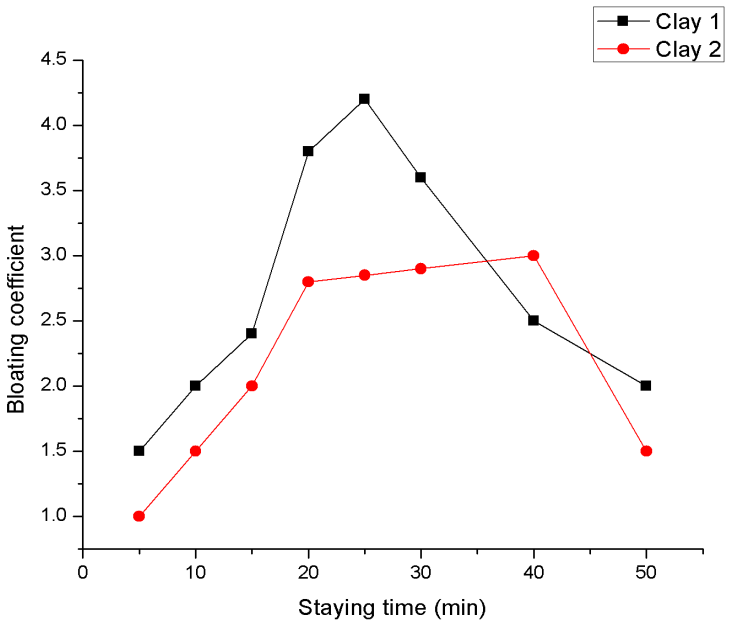
As the staying time was increasing, sintering and vitrification of the clay mass occurred, and density was increased as a result of consolidation. According to this study, it can clearly understand that, increasing the staying time and temperatures decreases the density of the heated clay samples, but after the melting of clay mass, density increases but it deforms the clay mass due to the formation of low viscous melting clay mass.

Heating rate effects the mechanical properties of heated clay samples. Thus, the heating rate becomes an important factor in the development of pore structures. Kadir and Mohajerani [92] mentioned that, higher firing rates reduced the compressive strength

of heated clay samples. This can be observed according to the results of that study as shown in Table 2.6 [92]. The compressive strength values were not changed linearly.



(a) K_p and firing temperature



(b) K_p and staying time

Figure 2.13: Variation of K_p according to firing temperature and staying time

Table 2.6: The compressive strength variation with heating rates.

Heating rate (°C/min)	Compressive strength (MPa)	Density (Kg/m^3)	Water absorption (%)
0.7	25.65	2118	5
2	17.90	2124	7
5	16.34	2134	7
10	N/A	2213	5

Dondi and Marsigli also conducted an experiment to study the effect of slow (24hr) and high (3hr) firing rates in clay bodies. The obtained results of that study are shown in Table 2.7 and Table 2.8. Clay samples were heated up to 1100°C and studied properties of the clay samples [102]. According to the test results as shown in Table 2.7, same density values can be achieved from slow and fast heating rates except for the clay sample J. This clay sample had been melted during the firing process. Moreover, the variation of density and open porosity values according to the heating rates were insignificant. It indicates that strength development of the pore structure by changing the heating rate is insignificant. Higher heating rates save cost and energy.

2.6.3 Effect on water absorption and desorption kinetics

Water absorption and desorption kinetics are directly related to the pore structure of porous aggregate. Pore size, pore expansion and pore connectivity are the main parameters of the pore structure. Mainly, two factors influence the variation of water absorption and desorption kinetics of fired clay bodies. First one is the increase of liquid phase and second factor is the micro-structural heterogeneity [103].

When heating temperature increases, sintering occurs and consolidates the clay mass due to contractions between different micro regions of the clay body. Further increasing the heating temperature produces a liquefying clay mass and vitrification occurs. As a result of that, liquefying clay mass flows under capillary forces and consolidate the clay mass furthermore. As a result of that, smaller pores are gradually eliminated from the clay mass and produce isolated pores which do not support to the water absorption process. Generally, this scenario can be observed at high temperatures that have high levels of sintering or vitrification [101]. The formation of closed pores affect the water absorption and desorption properties of the heated clay sample. According to

Table 2.7: Comparison of fast and slow heating processes

Clay sample	Slow firing		Fast firing	
	Bulk density	open porosity	Bulk density	open porosity
	gcm^3	cm^3g^1	gcm^3	cm^3g^1
A	1.8	0.192	1.8	0.182
B	1.59	0.264	1.46	0.271
C	1.77	0.206	1.77	0.191
D	1.57	0.253	1.66	0.233
E	1.71	0.235	1.56	0.233
F	1.85	0.168	1.8	0.136
G	1.78	0.217	1.77	0.231
H	1.74	0.216	1.62	0.227
I	1.67	0.246	1.66	0.272
J	2.01	0.158	1.75	0.142
K	1.77	0.203	1.76	0.205
L	1.67	0.241	1.64	0.241

the Table 2.8 [102], the obtained results show approximately the same water absorption values at slow and fast firing processes at low temperatures. At that temperature range vitrification does not occur. If vitrification occurs, it will reduce the water absorption capacity of the aggregate. Slow firing at that temperature will provide enough time for liquefying clay mass to flow under capillary forces. Fast firing will not provide enough time to produce liquefied clay mass, thus water absorption values are high in fast firing at high temperatures, but in low temperatures, approximately the same water absorption capacities can be studied in both fast and slow firing processes.

The variation of heating rate is insignificant at a lower temperature which melting does not occur, but heating rates are critical in temperatures in which melting occurs. All the clay samples showed a reduction in water absorption at 1100°C more than the water absorption value at 1000°C. This result indicates that high temperatures reduce the water absorption properties of the pore structure.

Table 2.9 [100] shows variation of the water absorption capacity with staying time. If staying time increases, the energy input to clay mass will be increased and proper

Table 2.8: Effect on heating rate and temperature on water absorption

Temperature	Water absorption (slow firing)			Water absorption (fast firing)		
	900°C	1000°C	1100°C	900°C	1000°C	1100°C
A	16.9	16.7	11.5	16.8	17	14.2
B	27.5	28.7	26	27.5	27.9	26.1
C	21.1	19.2	13.1	20.2	19	15.7
D	21.3	22.5	16.4	23.6	23.4	22.5
E	18.5	20.1	17.5	19.4	20.4	18.8
F	15.1	12.7	2.6	13	10.2	4.2
G	16.2	17.3	1.8	21.7	21.2	16.3
H	20.2	18.3	17	21.1	21.5	20.4
I	19.9	22	23.1	22.8	24.6	25.4
J	11.9	11.6	2.7	20.9	15.2	melting

Table 2.9: Change in water absorption according to heating time and temperature

Raw materials	Temperature °C	Staying time (hr)	Water absorption
Bada Buna	970	2	10.1
		4	7.92
		6	6.57
		8	5.58
Askola	970	2	37.51
		4	26.31
		6	12.23
		8	11.89

sintering process will take place. On the other hand, if staying time increases at vitrification level, it will reduce the viscosity of melting clay mass. Subsequently, consolidation of the clay mass takes place rapidly. Moreover, the clay sample tends to produce closed pores as staying time increases. As a result of that, water absorption reduces with staying time.

2.6.4 Summary

Raw material, size of clay body, heating temperature, heating rate, heating time and heating environment have a significant effect on the development of pore structure within clay body. Thus, those parameters can be identified as the control variables of firing process as shown in Figure 2.14. Those control parameters can be changed during the firing process to control the formation of pore structure within the clay body. According to the literature study, the effect of those parameters was studied in detail. Based on those study, a new firing process was defined to produce different pore structures within heated clay body. The development of this firing process and the production of different pore structures were discussed in next chapter.

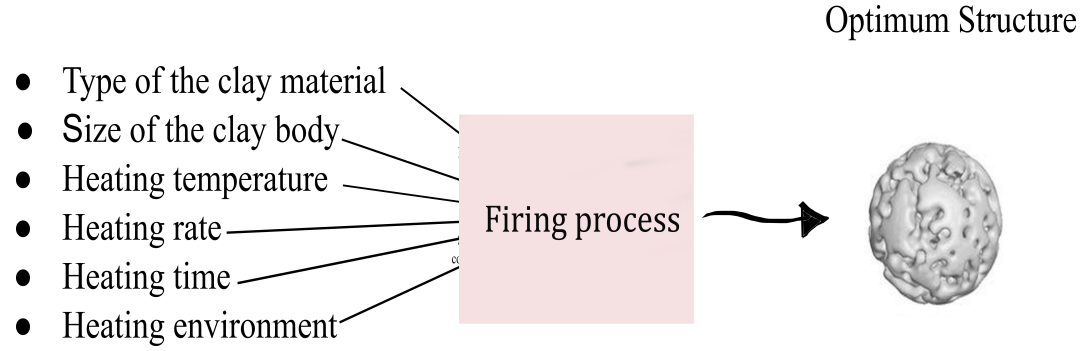


Figure 2.14: Control variables of the heating process

CHAPTER 3

RESEARCH METHODOLOGY

3.1 Introduction

Chapter 2 explains the main parameters of the effective pore structure (EPS) and control variables of heating process. The parameters of EPS should be identified quantitatively in order to define an effective pore structure for internal curing aggregates. So that, different pore structures were produced only by changing the heating temperature and raw material while keeping other control variables fixed throughout the study. The production process of the different pore structures is shown in Figure 3.1. Moreover, this chapter explains how experimental works were carried out to analyze different pore structures which consist of specific pore size, pore expansion, pore connectivity and pore strength.

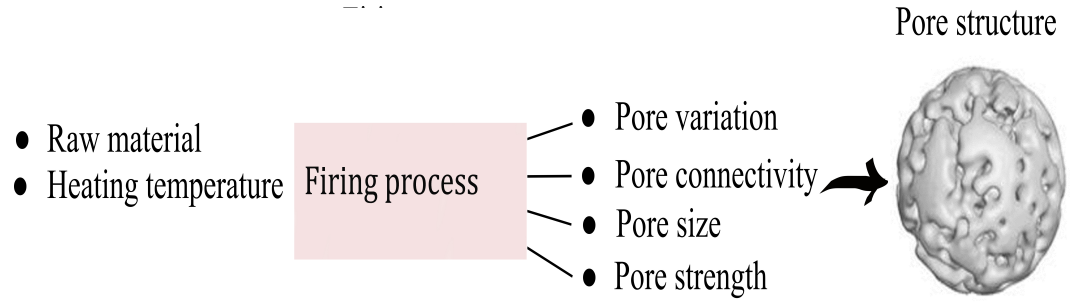


Figure 3.1: Production process of different pore structures

3.2 Raw materials selection

Non-expansive clays were selected as a raw material to develop pore structures as per the research objectives. Thus, the first step was obtaining suitable clay types for

the study. Different clay mines were observed and three clay mines were found from Nachchaduwa, Dankotuwa and Metiagoda area. Another clay sample was imported from China. Figure 3.2 shows the selected clay mines and the imported clay type. Table 3.1 shows the chemical composition of the selected clay materials.



(a) Nachchaduwa Clay

(b) Metiagoda Clay

(c) China Clay

(d) Dankotuwa Clay

Figure 3.2: Selected clay mines.

The potential of bloating was identified according to the Charles M. Riley method as described in section 2.6. The obtained chemical compositions were recalculated as per Charles M. Riley's method and presented in Table 3.2. The points represent the recalculated percentages of the main chemical composition of the selected clay samples were plotted in a triangular graph as shown in Figure 3.3. Nachchaduwa, Dankotuwa, Metiagoda and China clay samples are shown in point N, D, M and C respectively. The points of Nachchaduwa and Dankotuwa clay samples are existing within the boundary of bloating clays.

Thus, those clay types were categorized as bloating clays. Conversely, the points of Metiadoda and China clay samples exist outside the boundary of bloating clays. Thus, those clay types were categorized as unbloating clays. The next step was the identification of the bloating coefficient of those clay samples. In order to identify the bloating coefficient of heated clay specimens, a range of heating temperature should be identified beforehand.

Table 3.1: Chemical composition of the selected clay samples.

Compound	Percentage of compound element (%)			
Element	Nachchaduwa	China	Metiagoda	Dankotuwa
SiO_2	65.00	46.78	45.12	57.72
Al_2O_3	18.99	36.96	36.68	21.38
Fe_2O_3	5.99	0.40	0.34	13.00
MgO	1.49	0.10	0.02	1.72
CaO	1.80	0.20	0.11	0.97
TiO_2	1.18	0.03	0.51	1.46
Na_2O	1.13	0.28	0.57	0.32
K_2O	3.18	1.19	0.15	2.44

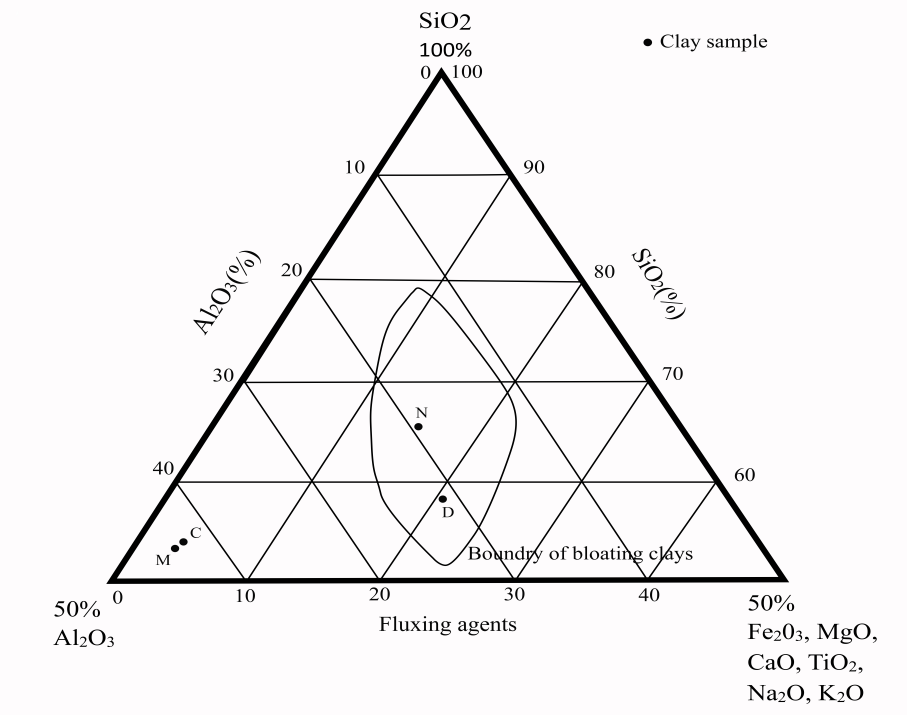


Figure 3.3: Percentage chemical composition of bloating clays.

Table 3.2: Re-calculated chemical composition of the selected clay samples.

Compound	Percentage of compound elements (%)			
Element	Nachchaduwa	China	Metiagoda	Dankotuwa
SiO_2	65.8	54.4	54	58.3
Al_2O_3	19.2	43	43.9	21.6
Total fluxing agents	15	2.6	2	20.1

3.3 Selection of heating temperature

In order to identify the effective range of temperature, the simultaneous thermal analysis (STA) were conducted for each clay type. STA was conducted with differential scanning calorimetry (DSC) and thermogravimetry analysis (TGA). It was carried out on SDT Q600 V20.9 instrument using a heating rate of 10 °C/min. The temperature ranged from 30 °C to 1300°C under a normal atmosphere (100.0 ml/min). The ceramic sample handlers and crucibles were used in the sample preparation. The test results are shown in section 4. According to the TGA analysis that explained in section 4, a temperature ranges from 800°C to 1300°C was selected for Nachchaduwa and Dankotuwa clay samples. A temperature range from 800°C to 1200°C was selected for China and Metiagoda samples.

3.4 Preparation of clay specimens

Raw clay materials were crushed and mixed with water to achieve plastic clay paste as shown in Figure 3.4(a). Subsequently, the clay paste was sifted through 5 mm and 2mm sieves to remove debris, and to mix further as shown in Figure 3.4(b). After that, the clay mass was left in a desiccator for 2 hours to distribute humidity within the clay mass. Meanwhile, a cylindrical mold was prepared using a PVC pipe of 14mm in diameter and steel piston with rubber bushes as shown in Figure 3.4(c). Subsequently, clay sticks, 14 mm in diameter, were formed with a laboratory piston press and cut into specimens, 80 mm long, in the frame with two tensed wires as shown in Figure 3.4(d). The prepared clay specimens were kept in open space for 72 hours for hardening.



(a) Prepared clay paste



(b) Clay paste sifting through sieve



(c) Cylindrical piston



(d) Prepared clay specimen

Figure 3.4: preparation of clay specimens.

3.5 Heating process

Prepared clay specimens were heated at 200°C for two hours to remove free moisture otherwise, it causes explosive expansion within the clay mass at high temperature due to the sudden expansion of available moisture. Subsequently, heated clay specimens were immediately transferred to a laboratory furnace which operated at higher temperature as shown in Figure 3.5(a). In the same way, all the specimens were heated to a different temperatures ranging from 800°C to 1300°C in steps of 100°C. The soaking time was fixed as 20 minutes. Finally, the heated clay specimens were taken out and cooled in ambient temperature as shown in Figure 3.5(b).

3.6 Measurement of the level of expansion (Kp)

After the pre-heating process of the clay specimens, length and diameter were measured using Vernier caliper. For diameter, three measurements were taken at the top, middle and bottom of the clay specimens. Subsequently, three measurements were recorded for the length of samples. According to the obtained measurements, the volume of each specimen was calculated before heating. After the heating process, the specimens were measured with Vernier caliper and volume was calculated. Afterwards



(a) High temperature furnace (b) Heated clay sample.

Figure 3.5: Heating process

the bloating coefficient was calculated by using Equation 3.1 where, K_p represents the bloating coefficient, V_1 represents the volume of clay sample after firing and V_2 represents the volume of clay sample before firing. In the same way, bloating coefficient of all the clay samples was calculated at each temperature.

$$K_p = V_1/V_2 \tag{3.1}$$

3.7 Produced aggregates with different pore structures

Aggregate produced from four different clays types: Nacchaduwa, Dankotuwa, Metiagoda and China clay are shown in Figure 3.6 Figure 3.9. There were 6 different aggregates produced from each clay type extracted from Nacchaduwa and Dankotuwa in the range of 800°C,to 1300°C as shown in Figure 3.6 and Figure 3.7 respectively. In addition, there were 5 different aggregates produced from each clay type extracted from Metiagoda and China in the range of 800°C,to 1200°C as shown in Figure 3.8 and Figure 3.9 respectively. Altogether, 22 different aggregate specimens were prepared from four clay types by heating from 800°C to 1300°C. The next step was the identification of the pore structure based on pore connectivity, pore size, pore expansion and the compressive strength of the pore structure.

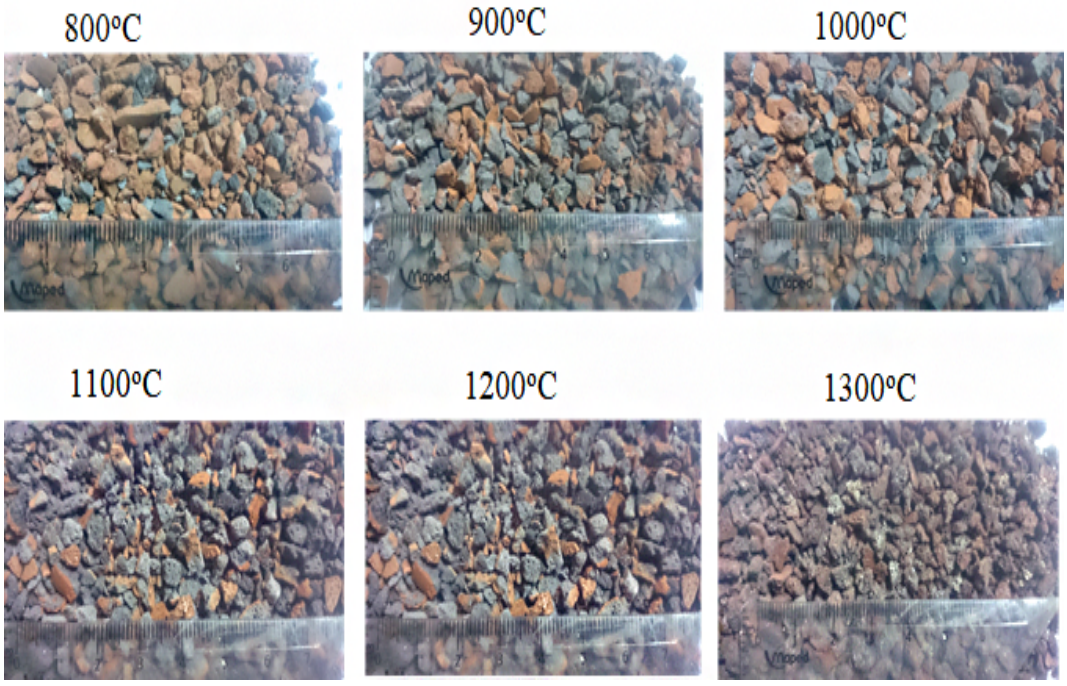


Figure 3.6: Prepared aggregate from Nachchaduwa clay.

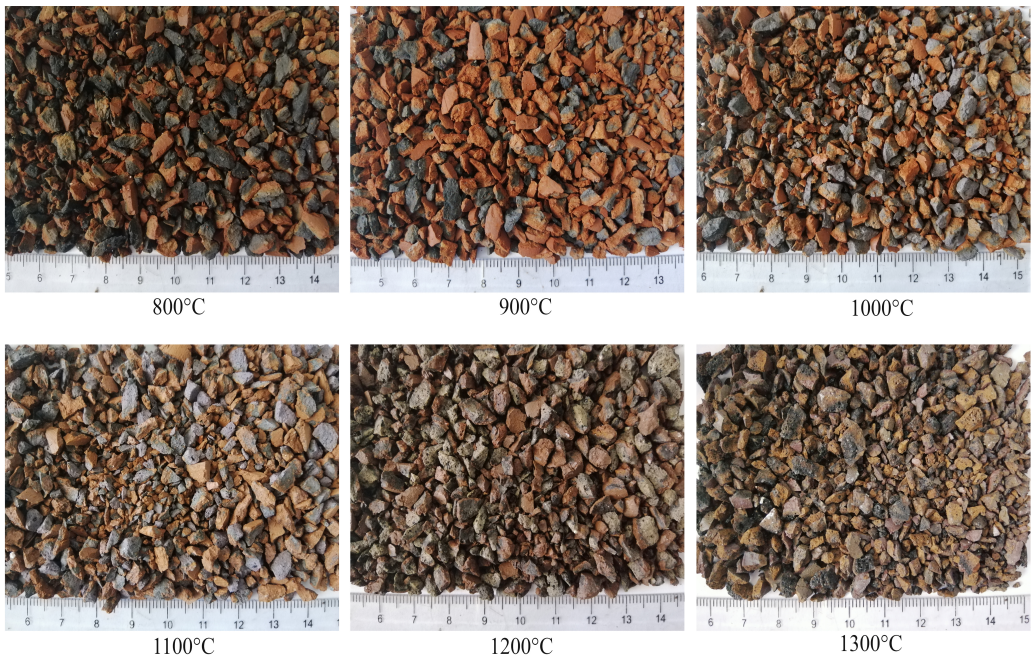


Figure 3.7: Prepared aggregate from Dankotuwa clay.

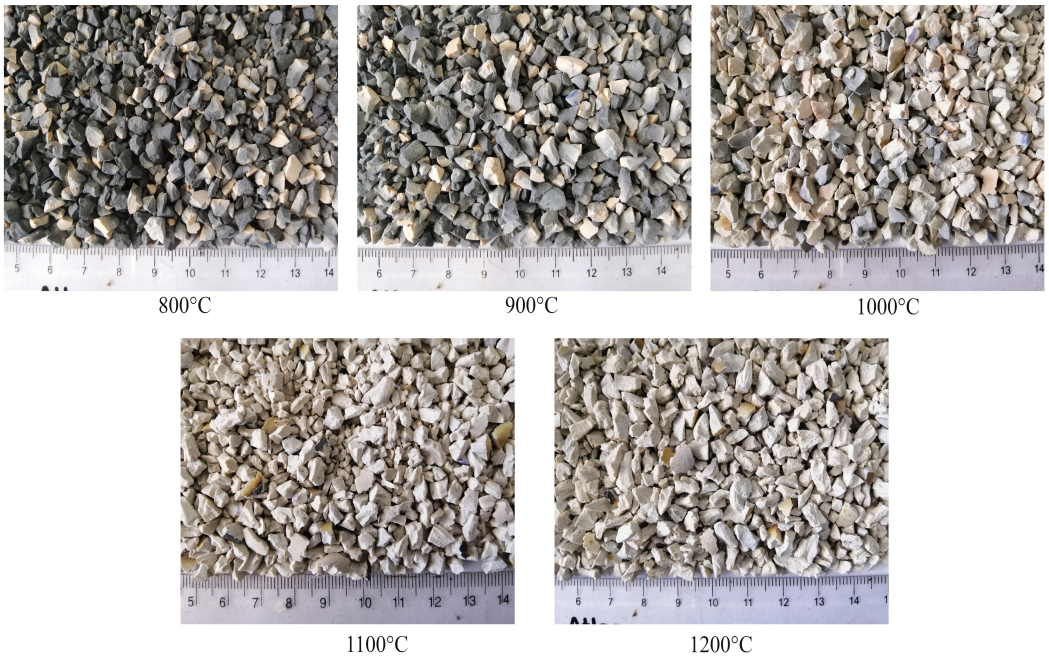


Figure 3.8: Prepared aggregate from Metiagoda clay.

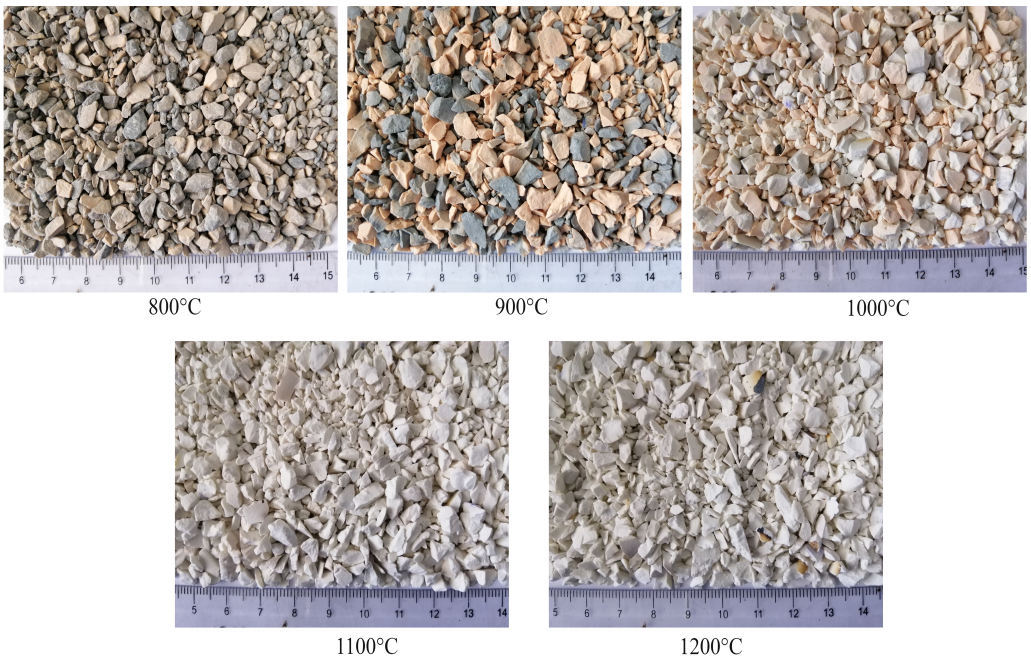


Figure 3.9: Prepared aggregate from China clay.

3.8 Identification of the pore structure of the aggregates.

3.8.1 Measurement of the pore connectivity

In order to measure open porosity, the aggregates were submerged for 72 hours to saturate completely. Afterwards aggregates were taken out and wiped with a moist cloth to achieve SSD condition. Subsequently, the mass of each sample was recorded, and the samples were submerged in water and weighted. Figure 3.10 shows the equipment which was used to measure the submerged weight. After that, aggregates were oven dried at 120°C for 24 hours and measured the dry aggregate weight. Finally, open porosity (AP) was calculated by using Equation 3.2 as specified in the UNE-EN-7724, 1999 standard [104, 101]. In order to measure the open porosity of each aggregate type, three replications were used.



Figure 3.10: Measurement of submerged weight of aggregates

$$AP(\%) = \frac{(W_{SA} - W_D) \times 100}{(W_{SA} - W_{SW})} \tag{3.2}$$

- AP = apparent porosity.
- W_D = mass of aggregate specimen in oven-dry condition, g.
- W_{SA} = mass of aggregate specimen in SSD, g
- W_{SW} = mass of saturated specimen submerged in water, g

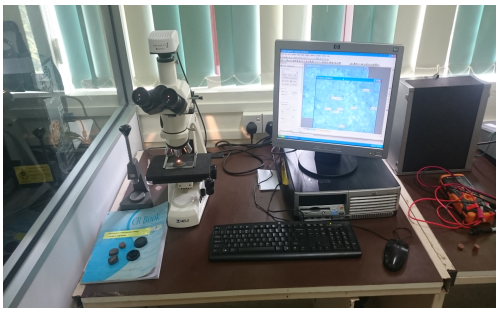
3.8.2 Measurements of Pore sizes and pore distribution

Cross-sections of each aggregate samples were studied using the Scanning electron microscope (SEM) (Carl Zeiss Evo 18 Research equipment) and optical microscope as shown in Figure 3.11(a) and Figure 3.11(b) respectively. Subsequently, images of the pore structures of each aggregate were obtained using SEM. Those images are shown in appendix A. Afterwards, the boundaries of each pore were marked manually to minimize the errors in identification of the pore boundary through image analysis software. During the pore area calculation, an elliptical areas for each pore boundary

was marked and area of each pore was calculated by using image analysis software. Finally, the radius of each pore was calculated by assuming all the pores were circular.



(a) Scanning electron microscope



(b) Optical microscope

Figure 3.11: Pore structure analysis

3.8.3 Measurements of the Compressive Strength

In order to measure the compressive strength of sintered clay samples, ASTM C1424 15 standard [105] was referred. Figure 3.12 shows the apparatus that used to measure the compressive strength of clay samples.



$$C_u = \frac{P_{max}}{A} \tag{3.3}$$

- C_u = compressive strength, MPa,
- P_{max} = maximum force, N, and
- A = original cross-sectional area, mm^2.

$$A = \frac{\pi d^2}{4} \tag{3.4}$$

- A = cross-sectional area
- d = cross-sectional diameter

Figure 3.12: Loading machine

The cylindrical clay samples which prepared through the heating process, were cut into specimens of 2cm in height as specified in the standard. The diameter of those specimens was approximately 15mm. The bottom and top surfaces were flattened and the tolerance for the level difference was maintained at or below 0.005mm. The upper and lower surfaces of the specimens were parallel to each other within 0.01mm and perpendicular to the load plate of the test machine within 0.01mm . The diameter

of the surface was measured by using Vernier caliper and the area was calculated. The prepared specimens were kept in a loading machine as shown in Figure 3.12. Subsequently, the test machine was operated at a speed of 1.27 mm/min speed, and the maximum loading was recorded. Three cylindrical specimens were used to measure the compressive strength of each pore structure. After that, the mean compressive strength was calculated according to Equation 3.3 and Equation 3.4.

3.9 Internal curing Properties of the pore structures

3.9.1 Measurements of the water absorption

The experiment was performed at room temperature (∼27 °C). An electronic balance, 0.01 g sensitivity, was used to measure the weight. During the laboratory test, approximately 15g of aggregate sample, particle size of 1.18 - 4.75 mm was used to avoid the loss of aggregate in testing. Three replications were used during the testing. Figure 3.13 shows the prepared aggregates for soaking for 24, 48 and 72 hours. Subsequently, soaked samples were taken out, wiped and weighted in SSD condition. Weighted samples were heated for 24hr at 105 °C to obtain dry weight. Equation 3.5 was used to measure the water absorption capacity of each aggregate samples according to the ASTM- C1761/C1761M 17 standard [30].



$$W_A = \frac{(M_{SD} - M_{OD}) \times 100}{M_{OD}} \tag{3.5}$$

- W_A = Water absorption
- M_{OD} = mass of aggregate (oven-dry), g.
- M_{SD} = mass of aggregate in SSD, g.

Figure 3.13: Aggregate soaking process

3.9.2 Measurements of the water desorption

Water desorption capacity of the aggregates was determined according to ASTM-C1761 / C1761M 17 standards [30]. According to the standard, the amount of absorbed water released when the aggregates stored in a chamber at 94 % relative humidity were measured. A humidity chamber was created as shown in Figure 3.14

using a sealed container and humidity meter. A supersaturated solution of potassium nitrate was used to maintain the relative humidity of container approximately equal to 94 % as specified in the standard. The test was conducted under controlled temperature of 24°C. Approximately 15g of aggregates were obtained from each aggregate type. Afterwards, samples were soaked 72 hours and taken out and wiped to achieve SSD condition. Subsequently, the weight of each sample was measured, and samples were stored inside the humidity chamber. Then, samples were taken out and weighted continuously for 30 days. Afterwards, all the samples were oven dried for 24 hours and calculated the water desorption capacity according to the Equation 3.6.



$$D = \frac{W_{AGG} \times 100\%}{A_{72}/100\%} \tag{3.6}$$

- A_{72} = The 72-h absorption, expressed as a percentage of the oven-dry mass.
- W_{AGG} = mass of water released by lightweight aggregate in going from the wetted surface-dry condition to the equilibrium mass at a relative humidity of 94 %, expressed as a fraction of the oven-dry mass.

Figure 3.14: Humidity chamber

3.9.3 Measurements of the density

Prepared aggregate samples were soaked for three days to achieve saturate conditions. Afterwards, the samples were taken out and wiped to achieve surface saturated dry (SSD) condition, and weighted. Subsequently, the SSD samples were filled to a container with water and weighted. After that, the container filled only with water and weight of the samples was measured. Finally, samples were oven dried and the weight of the samples was measured. According to the obtained results, the theoretical maximum density was calculated by using Equation 3.7 as mentioned in the ASTM C1761/C1761M17 standard [30]. Figure 3.15 shows the scale and the container used to measure the density of prepared aggregates.



$$G_{OD} = \frac{M_{OD}}{(M_{SD} + M_{PW} - M_{PS})} \tag{3.7}$$

- G_{OD} = Relative density of aggregate (oven-dry).
- M_{OD} = Mass of aggregate(oven-dry), g.
- M_{PW} = Mass of pycnometer filled with water, g.
- M_{SD} = Mass of aggregate specimen in SSD, g
- M_{PS} = Mass of pycnometer containing aggregate and water, g

Figure 3.15: Measuring aggregate weight in Phynometer

3.9.4 Summary

According to this chapter, different aggregates were produced by using four different clay types. Afterwards, characteristics of different pore structures were identified using SEM analysis of the heated clay samples. Moreover, the internal curing properties of each aggregate was obtained based on water absorption, water desorption and density. Analysis and the results are presented in the next chapter.

CHAPTER 4

RESULTS AND ANALYSIS

Throughout this chapter, the obtained results were analyzed in order to develop an effective pore structure (EPS) for porous aggregates. The heat reactions of the selected clay samples were studied based on STA results. Then, different pore structures were analyzed and categorized based on the characteristics of pore structure and internal curing properties of aggregates. According to that, the efficiency of different pore structures as an internal water reservoir was identified and parameters of EPS were quantitatively defined.

4.1 Development of the heating process

The new heating process was defined only by changing firing temperature and material type. Thus, the limits of heating temperature should be identified properly. It can be done according to STA analysis and the bloating coefficient.

4.1.1 Simultaneous thermal analysis (STA)

Different chemical reactions and changes occur at different temperatures during clay heating. Those changes basically depend on their chemical composition. STA analysis can be done to identify those reactions. Exothermic reactions, endothermic reactions, weight reductions, heat flow variation and temperature variation are the corresponding attributes of STA. These attributes are used to identify various effects of the selected clay masses that exhibit during the heating process.

4.1.1.1 Nachchaduwa clay sample

The STA was conducted using 25.0120mg of Nachchaduwa clay sample. Figure 4.1 shows the obtained results of the STA analysis. An endothermic peak which ranged from 30°C to 150°C was observed at 66°C. Moreover, it was related to considerable weight loss of 5.5%. Thus, it was identified as the temperature of free water evaporation [106, 107, 108]. As the temperature was increased, an exothermic reaction was observed with a peak at 334.5°C and was related to approximately 1% of weight reduction.

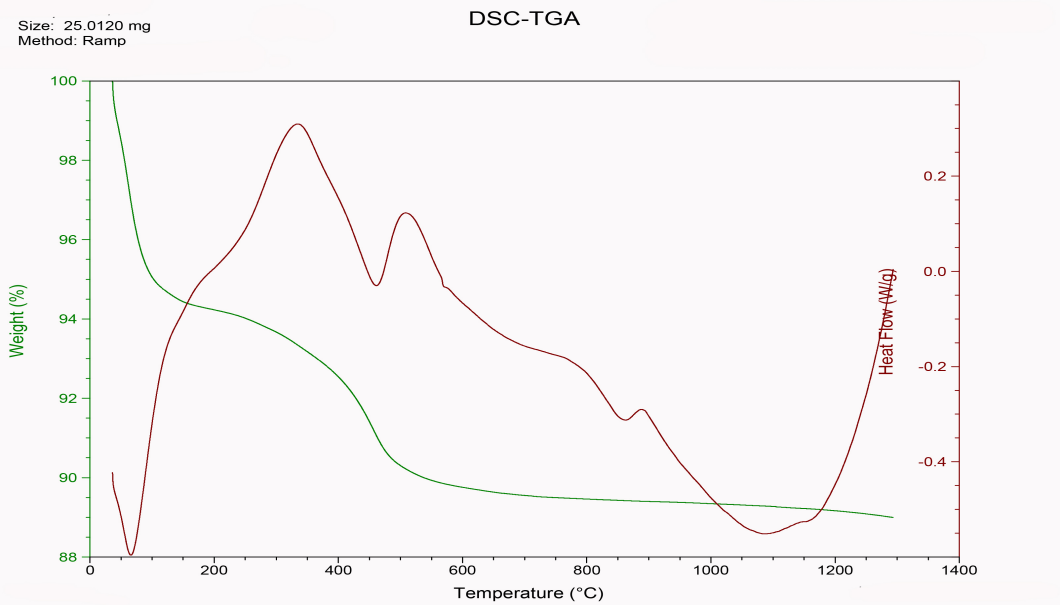


Figure 4.1: STA of Nachchaduwa clay sample

Thus, it was identified as decompositions of organic matters [109, 83]. A sharp endothermic reaction which was related to the considerable weight loss of 2% was recorded with a peak at 461.38°C. It occurred due to the dehydration process [110, 111]. The quartz inversion occurred at 561°C with a small endothermic reaction [83, 108, 112, 113]. As temperature was increasing, an endothermic reaction which was related to the decarbonatization was observed at 865°C [114, 77]. Moreover, it is not associate with visible weight reduction because of their small amount in observed clay mass. An exothermic reaction was observed at 884.8°C which was not related to a weight loss. Thus, it was identified as the crystallization process of existing substances [109, 115, 116]. It can be related to the formation of hematite or to the phase transformation from Meta-kaolinite to spinel. A small exothermic reaction can be observed at 1147°C that related to the formation of the mullite crystallization phase [117, 83]. A peak of a wider endothermic reaction was observed at 1087°C and it was not associated

with significant weight loss. Consequently, it was identified as the fluidization of clay mass.

4.1.1.2 Dankotuwa clay sample

The weight of Dankotuwa clay sample was recorded as 24.9110 mg. As shown in Figure 4.2, an endothermic peak was observed at 61.5°C which was related with considerable weight loss of 3%. Thus, it was identified as the free water evaporation [106, 107, 108].

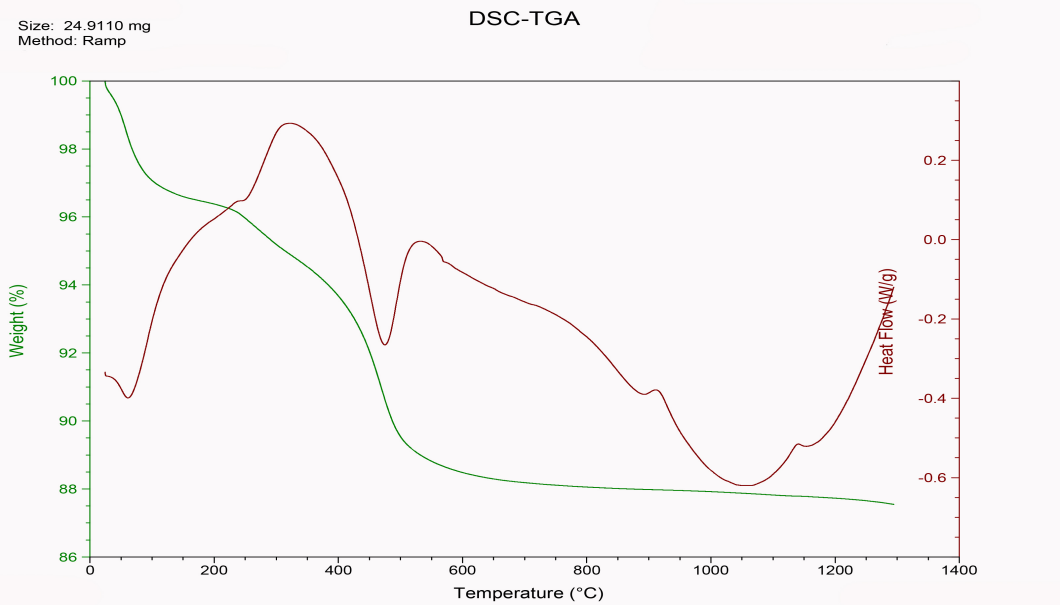


Figure 4.2: STA of Dankotuwa clay sample

After that, an exothermic reaction, related to an approximately 3% of weight reduction was observed with a peak at 322°C. Thus, this was identified as decompositions of organic matters [109, 83]. As temperature increased, a sharp endothermic reaction was recorded with a peak at 474.8°C. It was related with 3% of weight loss thus, it was identified as the removal of chemically combined water [110, 111]. A small endothermic reaction which was related to the quartz inversion was observed at 569°C [83, 108, 112, 113]. An endothermic reaction which was related to the decarbonization was observed at 891°C [114, 77]. Furthermore, it was not associated with visible weight reduction because of their small amount in observed clay mass. Another exothermic reaction, unrelated with a weight loss was observed at 910.7°C. Thus, it was identified as the crystallization process of existing substances [109, 115, 116]. It was related to the formation of hematite or to the phase transformation from Meta-

kaolinite to spinel. After that, a small exothermic reaction was observed at 1145°C that related to the formation of the mullite crystallization phase. A peak of a wider endothermic reaction was observed at 1064°C and it was not associated to significant weight loss. Thus, it was identified as the melting temperature of Dankotuwa clay sample.

4.1.1.3 Metiagoda clay sample

The weight of the prepared clay sample was 24.57mg. According to Figure 4.3, an endothermic peak was observed at 54°C. Furthermore, it was related to a weight loss of 0.5%. Thus, this was identified as the free water evaporation [106, 107, 108]. As temperature was increased, an exothermic reaction was observed with a peak at 342.6°C. On the other hand, it was related with approximately 1% of weight reduction thus, it was identified as decompositions of organic matters [94, 109, 83].

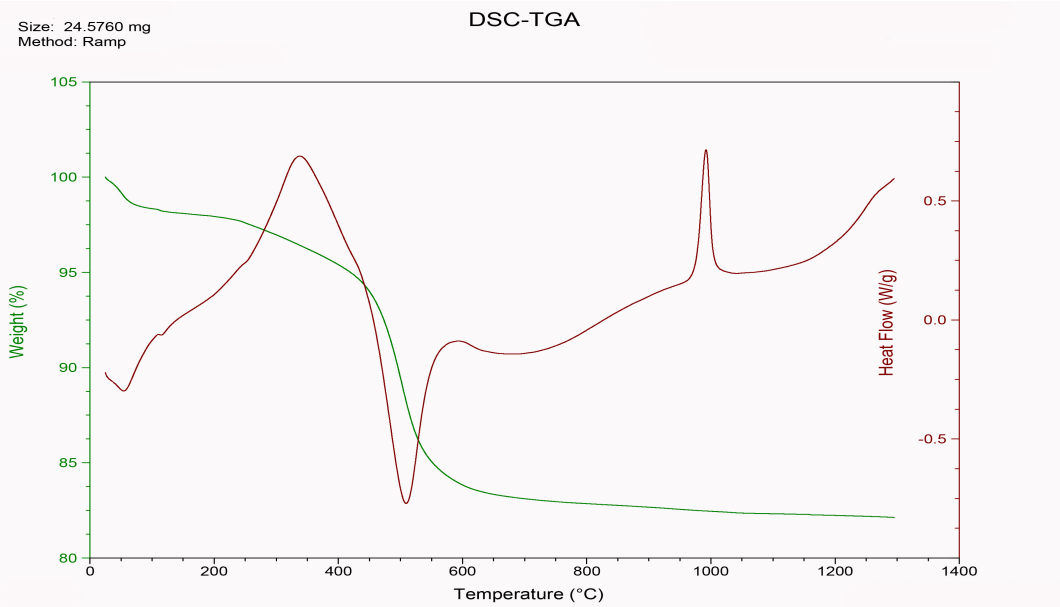


Figure 4.3: Metiagoda clay sample

A sharp endothermic reaction was recorded with a peak at 509.2°C and was related to 9% of weight loss. Thus, it was identified as the removal of chemically combined water [110, 111]. A small endothermic reaction, which is related to the quartz inversion should occur around 570°C temperature but it could not be identified due to the overlapping of a large endothermic reaction of chemically combined water driven off. A sharp exothermic reaction was observed at 992°C and was unrelated to weight loss. Thus, it was related to the crystallization of Spinel [115, 116]. This material did not

exhibit a melting stage throughout the STA.

4.1.1.4 China clay sample

The weight of the China clay sample was 19.4810 mg. According to Figure 4.4, an endothermic peak which was related to a weight loss of 0.5% can be observed at 48°C. Thus, this was identified as the temperature of free water evaporation[106, 107, 108]. As temperature was increased, a considerably small exothermic reaction which was related to a negligible weight reduction was observed with a peak at 326.4°C. It was identified as decompositions of organic matters [94, 109, 83]. The small exothermic reaction occurred due to the presence of a considerably low amount of organic matters in clay mass. A sharp endothermic reaction was recorded again with a peak at 509.2°C. It was related to 11% of weight loss thus, this exothermic reaction can be identified as the removal of chemically combined water[110, 111]. When clay sample was heating, a small endothermic reaction, which is related to the quartz inversion should occurred around 570°C but it could not be identified due to overlapping of larger endothermic reaction of the chemically combined water driven off. When the clay was heating, sharp exothermic reaction was observed at 993.8°C which was not related to a weight loss. Thus, it was identified as the crystallization of Spinel [115, 116]. This material also did not exhibit any melting stage throughout the STA.

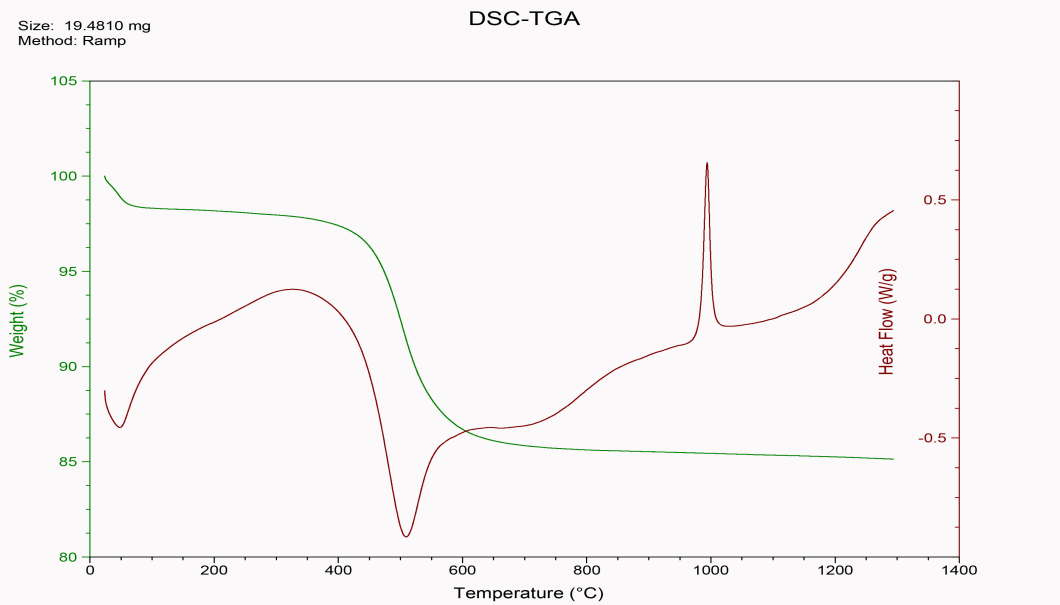


Figure 4.4: STA of China clay sample

4.1.2 Level of Self-expansion

4.1.2.1 Nachchaduwa clay sample

Figure 4.5(a) shows the heated clay specimens at different temperature thus, the level of expansion at each temperature can be compared visually. Moreover, the variation of self-expansion with respect to the heating temperature was quantitatively identified and illustrated in Figure 4.5(b). There was a slow increment in bloating coefficient in between 800°C to 1000°C. After 1000°C, the bloating coefficient increased suddenly until it reached to 1200°C. According to the STA analysis, the melting point of the clay sample was identified as 1087 °C. Thus, the specimen prepared at 1100°C was related to a considerable expansion. As further increased of temperature, less viscous clay mass formed and flowed into the voids of the clay structure under capillary action. Consequently, clay specimen was deformed and deviated from the rapid increment of self-expansion around 1300°C. According to that, the maximum bloating coefficient of 2.2 was observed in Nachchaduwa clay sample at 1300°C.

4.1.2.2 Dankotuwa clay sample

Heated clay specimens of Dankotuwa clay sample are shown in Figure 4.6(a). It illustrates the level of expansion with respect to the heating temperature. Variation of the self-expansion was identified according to the bloating coefficient values which are shown in Figure 4.6(b). The clay samples did not exhibit considerable expansion in between 800°C to 1000°C, but there was a sudden increment in bloating coefficient after 1000°C. According to the STA analysis, the melting temperature of Dankotuwa clay sample was identified as 1064°C. After the melting temperature, the clay sample expanded rapidly due to the formation of plastic clay mass. When clay sample achieved the melting point, it achieved comparatively a high expansion, but further increasing the heating temperature up to 1300°C caused a deformation in the clay body. As a result of this, the specimens heated at 1300°C illustrated a small deviation from the increment of self-expansion that observed from 1000°C to 1200°C. According to the above result, the maximum bloating coefficient of 1.57 was observed in Dankotuwa clay sample at 1300°C. Thus, it can be categorized as non-expansive clays.

4.1.2.3 Metiagoda clay sample

According to Figure 4.7, the level of expansion of Metiagoda clay specimens was identified. The heated clay specimens did not exhibit any expansion throughout the heating process. There was a small shrinkage in the clay specimen after 800°C. STA analysis did not illustrate any melting characteristics, but it shows crystallization process around 1000°C. According to the above result, the maximum bloating coefficient of 1.0 was observed in Metiagoda clay sample. Thus, it was categorized as non-expansive clays.

4.1.2.4 China clay sample

Clay sample obtained from China exhibited the same behavior as Metiagoda clay sample. The clay specimens did not exhibit any expansion with respect to the heating temperature as shown in Figure 4.8. On the other hand, STA analysis did not illustrate any melting characteristics with an endothermic peak, but it shows a crystallization process around 1000°C. According to the above result, the maximum bloating coefficient of 1 was observed in Metiagoda clay sample. Thus, it was categorized as non-expansive clays.

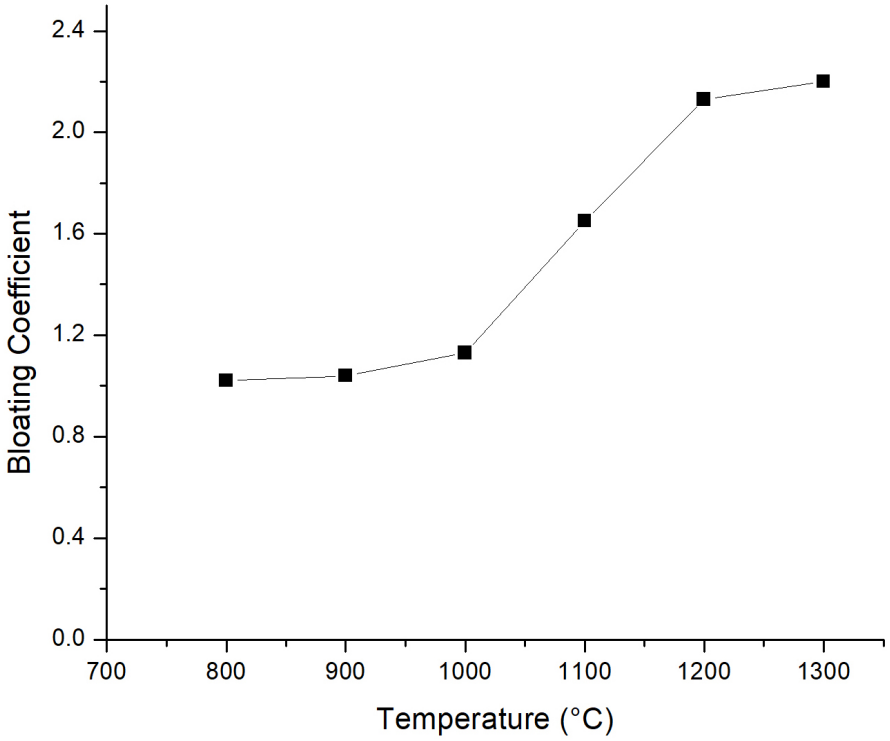
4.1.3 Summary

According to the obtained results of the bloating coefficient, Nachchaduwa and Dankotuwa clay samples exhibited a bloating mechanism but China and Metiagoda clay samples did not exhibit any bloating during the heating process. Moreover, all the samples achieved a bloating coefficient value lower than 2.5. Thus, selected clay types can be categorized as non-expansive clays and those materials represent all the types of non-expansive clays.

According to the STA analysis of each sample, 800°C to 1300°C range of temperature was selected for Nachchaduwa and Dankotuwa clay samples. China and Metiadoda clay samples did not exhibit any melting characteristics up to 1300°C. Thus, 800°C to 1200°C range of temperature was selected for these clay samples. Afterwards, different pore structures were produced changing the heating temperature and material type. Then, the pore structure of those aggregates should be identified.



(a) Heated clay specimens

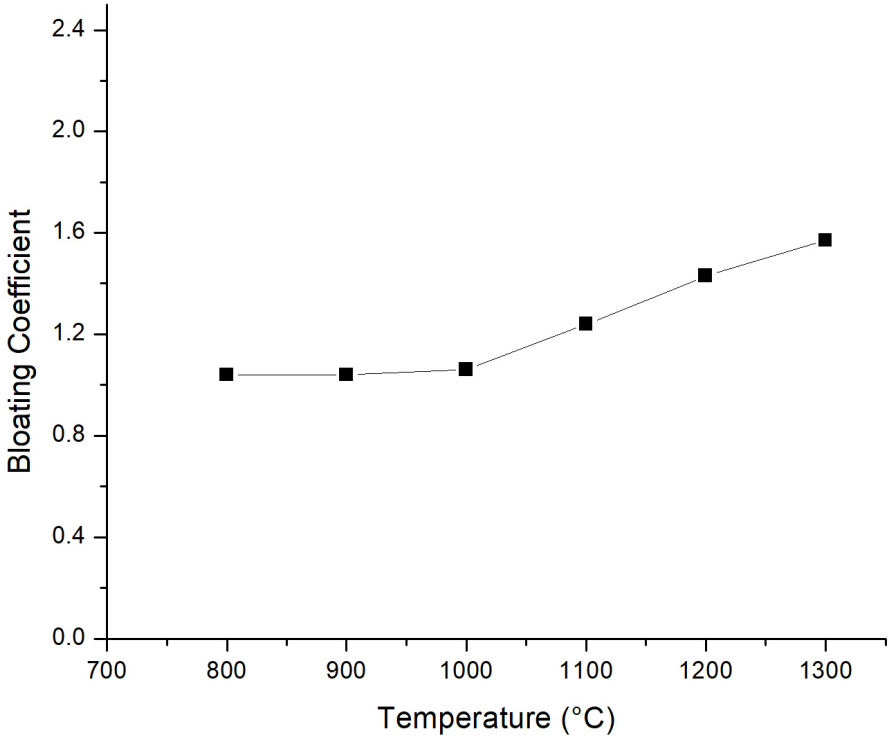


(b) Variation of the K_p

Figure 4.5: level of Self expansion in Nachchaduwa clay



(a) Heated clay specimens

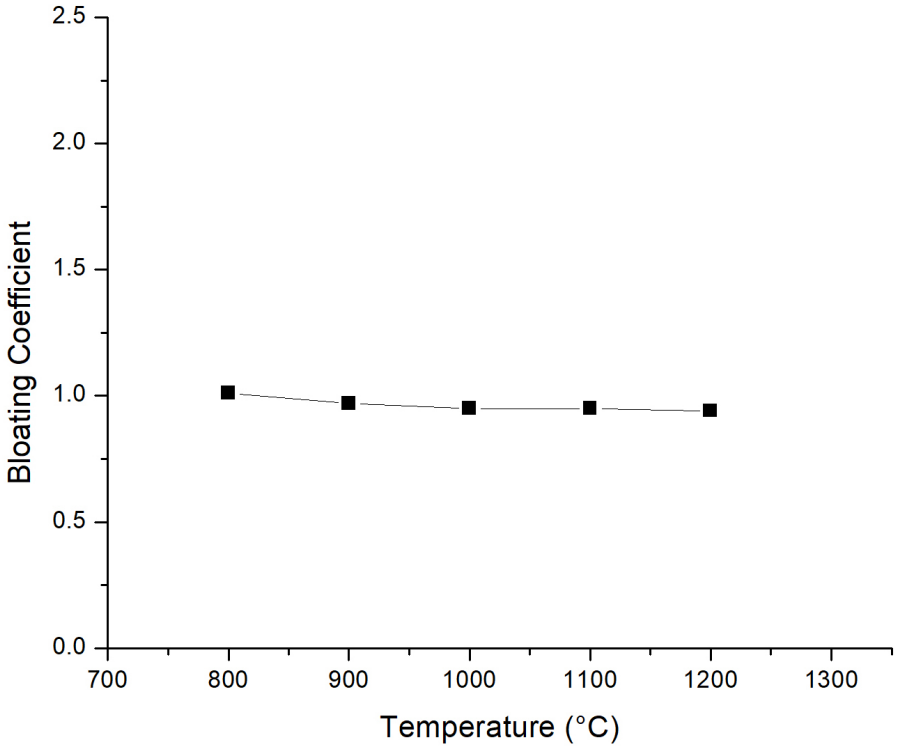


(b) Variation of the K_p

Figure 4.6: level of Self expansion in Dankotuwa clay

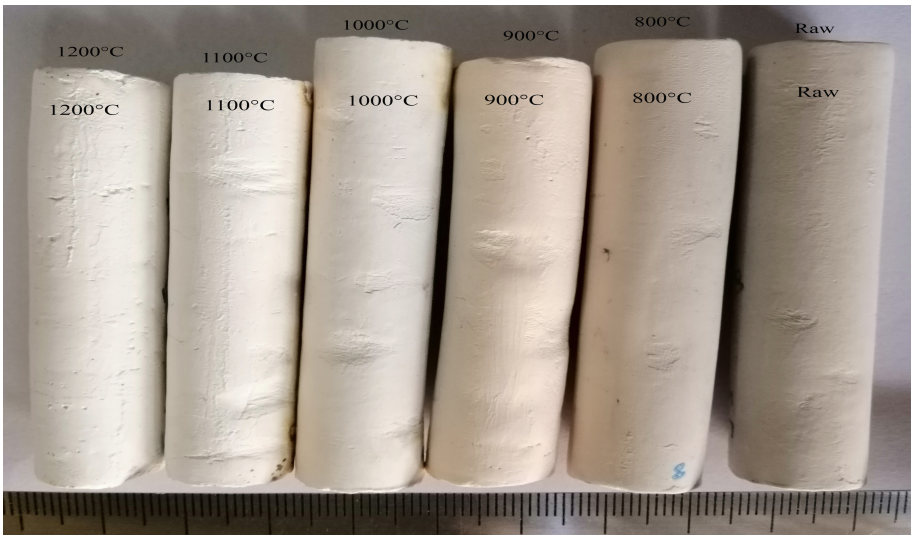


(a) Heated clay specimens

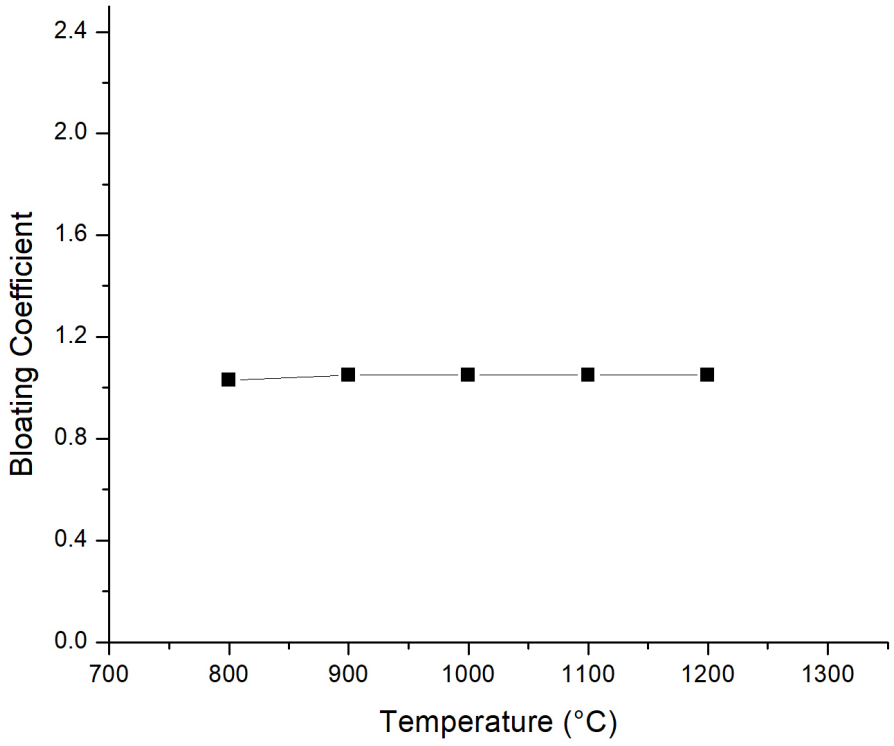


(b) Variation of the K_p

Figure 4.7: level of Self expansion in Metiagoda clay



(a) Heated clay specimens



(b) Variation of the K_p

Figure 4.8: level of Self expansion in China clay

4.2 Identification of different pore structures

During the production process, different pore structures were produced. Thus, it is necessary to identify characteristics of each aggregate based on pore size, pore connectivity, pore strength and pore distribution. In order to compare the pore structures, obtained SEM images are shown as a group in Figure 4.9, Figure 4.11, Figure 4.14, Figure 4.16, but high-quality enlarged images are provided in Appendix A. During the image taking, some pores which exist near to the image border were not captured completely. Thus, those pores were eliminated during the pore boundary identification. Finally, all the pore structures were analyzed according to the pore size, pore connectivity, pore strength and pore expansion.

4.2.1 Variation of pore size and pore distribution

4.2.1.1 Nachchaduwa clay sample

Figure 4.9 shows SEM images of different pore structures at various temperatures produced from Nachchaduwa clay boundaries of pores are shown in Figure 4.10. Table 4.1 shows the summary of the analyzed data. According to that, pore sizes were increased with heating temperature, but there was no any linear relationship between pore size and heating temperature. The mean pore size was increased slowly from 800°C to 1000°C and the standard deviation of pore size obtained a lower value than 1μm. Thus, a uniform pore distribution was observed in temperatures between 800°C to 1000°C. This range of temperature was not associated with the fluidization of clay mass, but it associates with the first stage of sintering process. There was a rapid increment in pore size after 1000°C. Moreover, the mean pore size and the standard deviation increased significantly and clay specimens produced a melted clay mass as described in STA. Thus, comparatively, large pores were observed in this range of temperature. Even though there was not much difference in standard deviation value of the clay specimens produced at 1100°C and 1200°C, the clay specimen produced at 1300°C had approximately 4 times greater value than the 1200°C specimen. According to Figure 4.9, at 1300°C clay mass tends to produce perfectly smooth closed pores with less viscous melted clay mass. The characteristics of produced pore structures were presented in Table 4.1.

Table 4.1: Pore size variation of the pore structures of Nachchaduwa clay.

Nachchaduwa	800°C	900°C	1000°C	1100°C	1200°C	1300°C
Maximum (μm)	1.67	2.29	1.75	194	144.4	701.8
Minimum (μm)	0.10	0.11	0.03	2	1.5	2.9
Mean (μm)	0.32	0.3	0.51	22.4	23.7	26.6
Standard deviation	0.21	0.38	0.43	22.4	23	88

4.2.1.2 Dankotuwa clay sample

SEM images of different pore structures which produced by using Dankotuwa clay sample are shown in Figure 4.11. The obtained pore boundaries through image analysis software were shown in Figure 4.12. Subsequently, the obtained images were analyzed, and the results were presented in Table 4.2. According to Table 4.2, mean pore size was increased with heating temperature in a non-linear way. A small variation can be observed from 800°C to 1000°C. Dankotuwa clay sample did not illustrate a significant increment in pore size at 1100°C as Nachchaduwa sample, but after 1000°C the increment has deviated to a rapid increment. Standard deviation values presented in Table 4.2, shows a uniform pore distribution in between 800°C to 1000°C. This range of temperature was associated with first stages of the sintering process as explained under STA analysis but, after the 1000°C clay melted, and pore structure expanded. As temperature was increased furthermore, the mean pore size was increased more rapidly due to the expansion of pore structure. As a result of this, 1300°C specimen had a greater maximum and mean pore size compare to 1200°C specimen. According to the results of Table 4.2, the clay sample obtained from Dankotuwa illustrates a more similar pattern to Nachchaduwa clay.

Table 4.2: Pore size variation of the pore structures of Dankotuwa clay.

Dankotuwa	800°C	900°C	1000°C	1100°C	1200°C	1300°C
Maximum (μm)	1.3	3.61	5.7	11.05	72.69	128.43
Minimum (μm)	0.15	0.21	0.28	0.59	1.49	4.1
Mean (μm)	0.42	1.04	1.06	2.87	7.06	19.59
Standard deviation	0.25	0.68	0.6	1.26	6.6	18.19

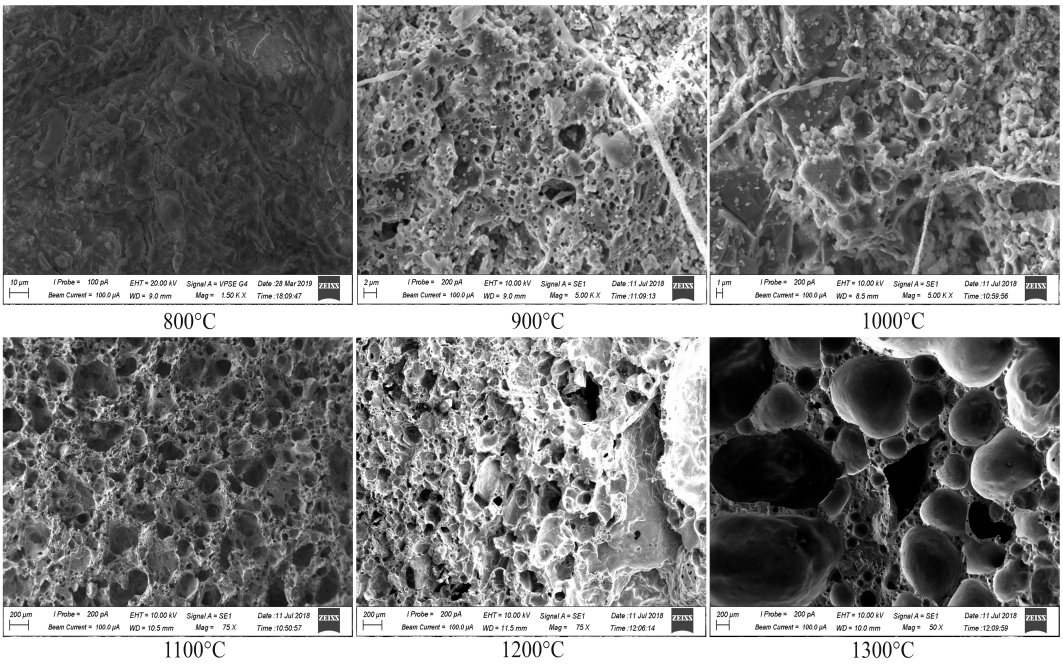


Figure 4.9: SEM images of the different pore structure (Nachchaduwa clay)

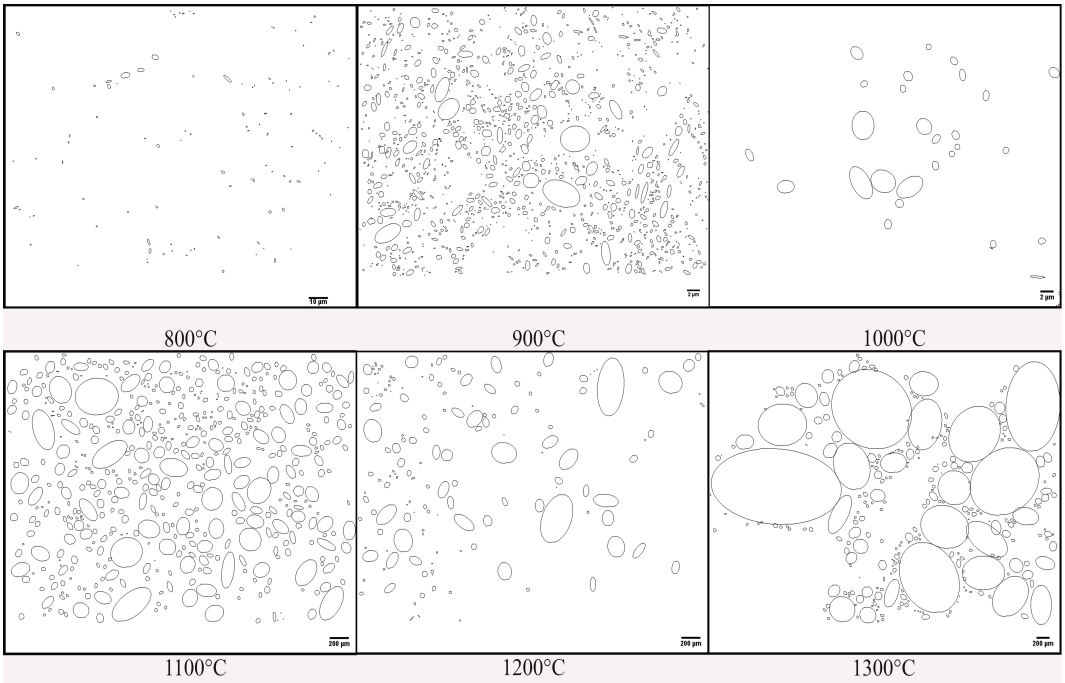


Figure 4.10: Identified boundaries of pores in SEM images (Nachchaduwa clay)

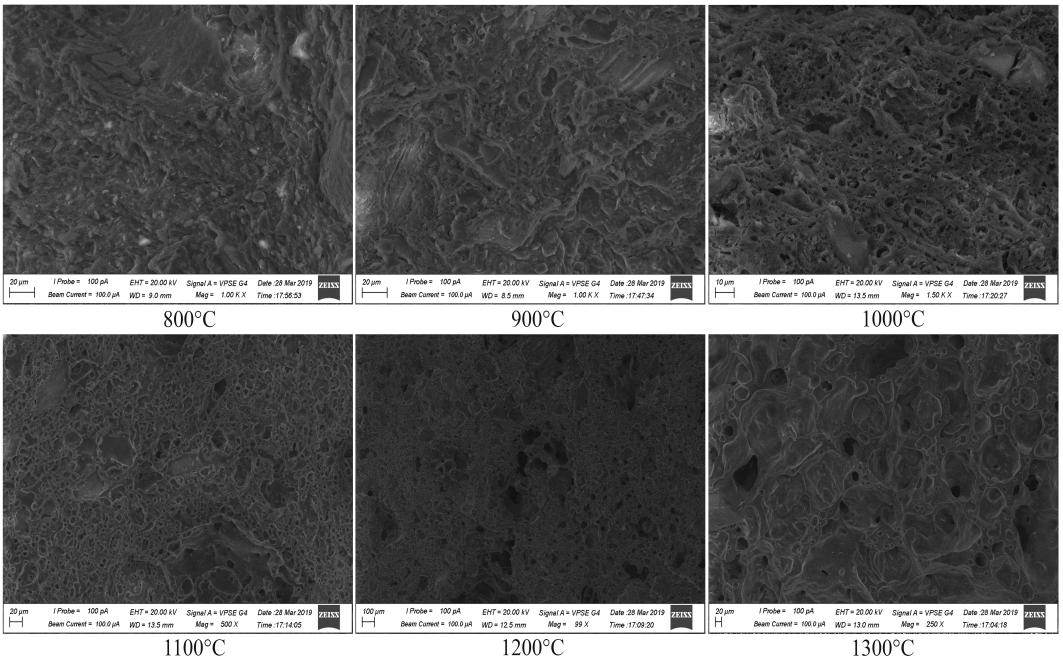


Figure 4.11: SEM images of the different pore structure (Dankotuwa clay)

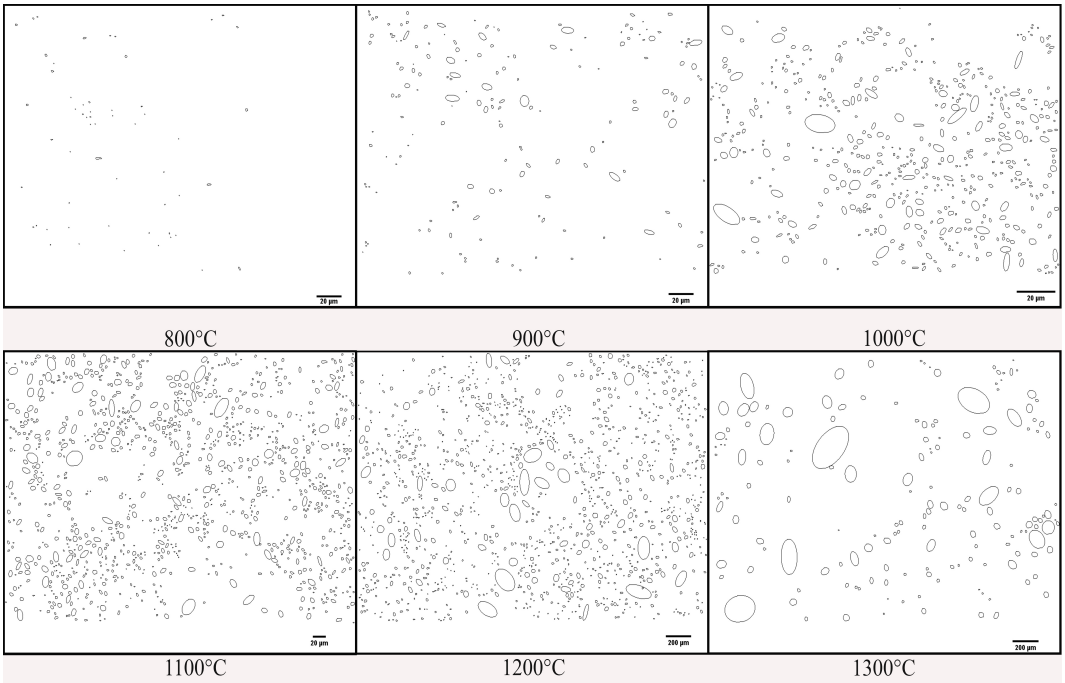


Figure 4.12: Identified boundaries of pores in SEM images (Dankotuwa clay)

4.2.1.3 Metiagoda clay sample

The clay sample obtained from Metiagoda showed totally different behavior from the clay sample obtains from Nachchaduwa and Dankotuwa. Figure 4.13 shows an enlarged SEM image of the pore structure of the clay specimen prepared at 1200°C. Crystallization of spinel was observed around 1000°C as described in STA analysis, but it was not associated with the development of proper bloating mechanism inside the clay body. Crystalline structures were observed all over the pore structure as needles and there was a different type of pores among those structures. Figure 4.14 shows the obtained images of different pore structure of Metiagoda clay sample.

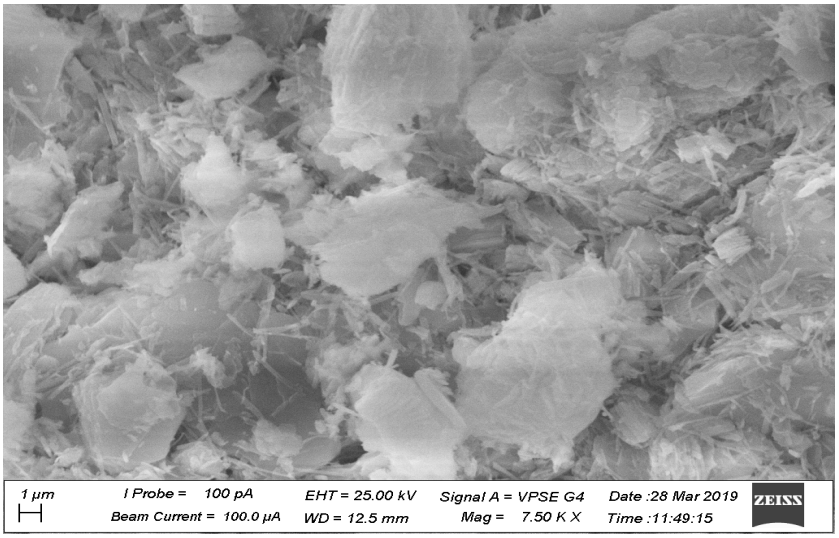


Figure 4.13: SEM image of the pore structure of the aggregate (Metiagoda)

Those clay specimens did not illustrate any melting point according to the STA analysis. Thus, the formation of pores or rapid increment in pore sizes was not observed in any specimen.The size of those pores may range from nanometers to micrometers. Figure 4.15 illustrates the identified boundaries of pores.

According to Table 4.3, the mean pore size decreased with heating temperature in a non-linear way. The variation was very small. Moreover, there was no much variation in standard deviation, but all the standard deviation values were lower than 1. Thus, those pore structures have more uniform pore variation. Table 4.3 shows a summary of the identified pore. All the pore structures consisted with complex tiny pores as shown in Figure 4.13. Thus, not only the larger pores but also the complex tiny pores absorbed water. As a result of that, high water absorption and low water desorption can be observed in these pore structures.

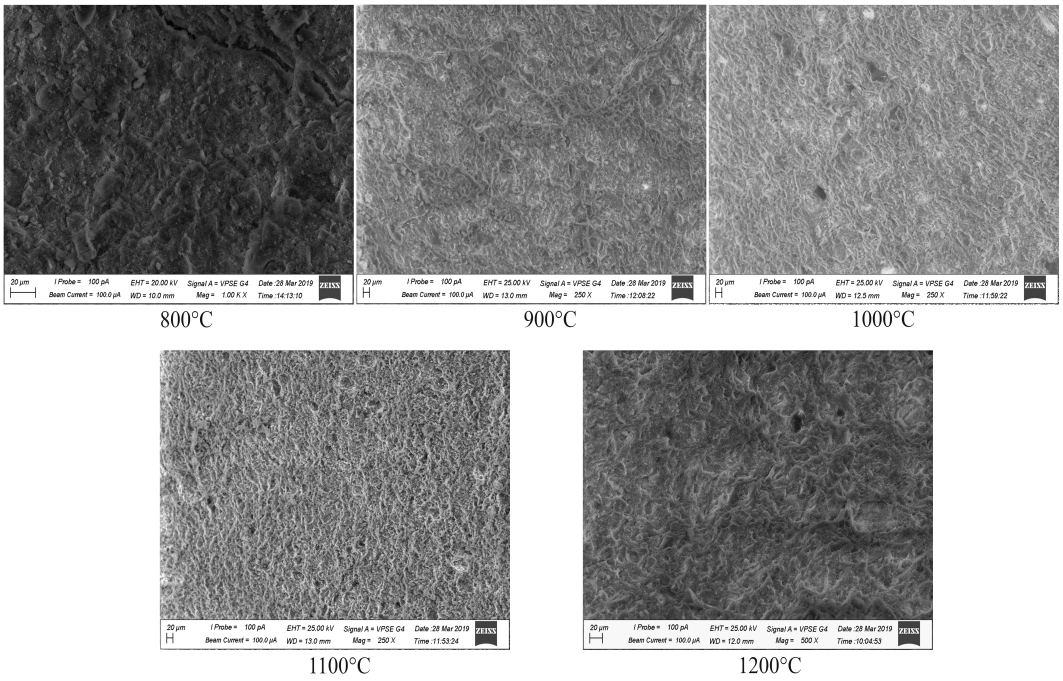


Figure 4.14: SEM images of the different pore structure (Metiagoda clay)

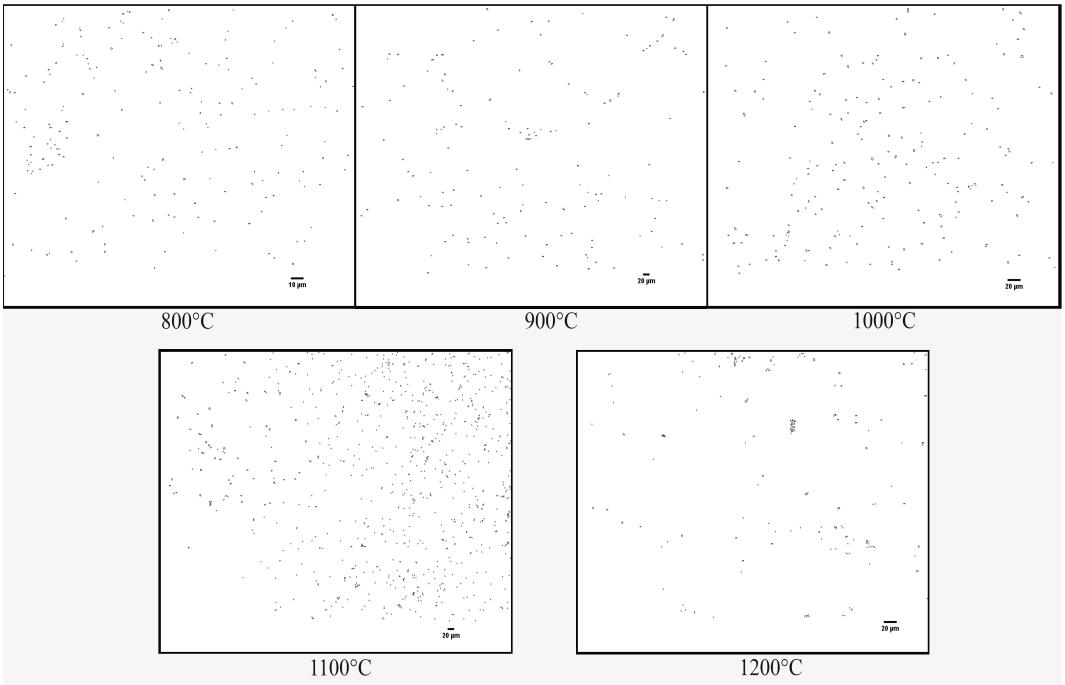


Figure 4.15: Identified boundaries of pores in SEM images (Metiagoda clay)

Table 4.3: Pore size variation of the pore structures of Metiagoda clay.

Metiagoda	800°C	900°C	1000°C	1100°C	1200°C
Maximum (μm)	0.76	2.71	1.99	2.75	1.77
Minimum (μm)	0.15	0.57	0.29	0.57	0.29
Mean (μm)	0.87	0.8	0.77	0.74	0.6
Standard deviation	0.44	0.58	0.35	0.4	0.36

4.2.1.4 China clay sample

Images of different pore structures which produced using China clay sample are shown in Figure 4.16. China clay had the same behavior as Metiagoda clay sample. The clay specimens prepared using China clay did not illustrate any melting point according to the STA analysis. As a result of that, a perfectly formed pore structures were not observed within clay mass. Crystallization of Spinel was observed around 1000°C as described in STA analysis, but a properly formed pore structure cannot be observed at this temperature also. Figure 4.18 shows the enlarged image of the pore structure of clay specimens prepared at 1200°C. According to that, a complex pore structure was observed within the clay mass. There were different types of tiny pores. Those pores will absorb and store water. The size of those pores may range from nanometers to micrometers. The size of those pores was identified as shown in Figure 4.17 using image analysis software.

The clay sample obtained from China shows the same behavior of the clay sample obtained from Metiagoda. According to Table 4.4, the mean pore size decreased with heating temperature, but it was a negligible change. Furthermore, there was no much variation in standard deviation as shown in Table 4.4. All the standard deviation values were lower than 0.2. Thus, those pore structures have more uniform pore variation than the Metiagoda clay sample. According to the results of Table 4.4, clay sample obtain from China illustrates a more similar pattern to Metiagoda clay, but it differs from Nachchaduwa and Dankotuwa clay samples.

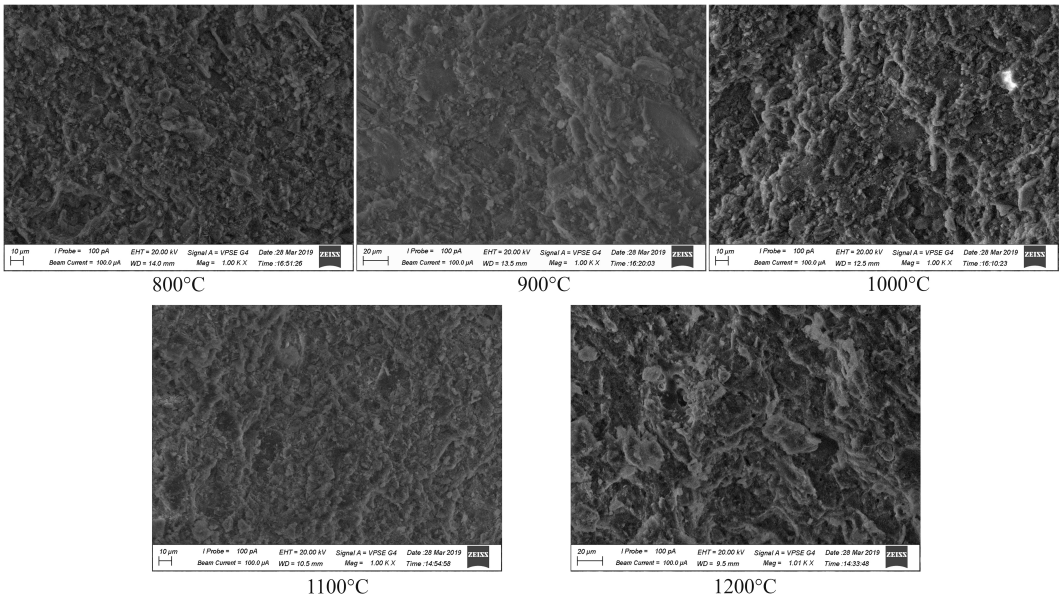


Figure 4.16: SEM images of the different pore structure (China clay)

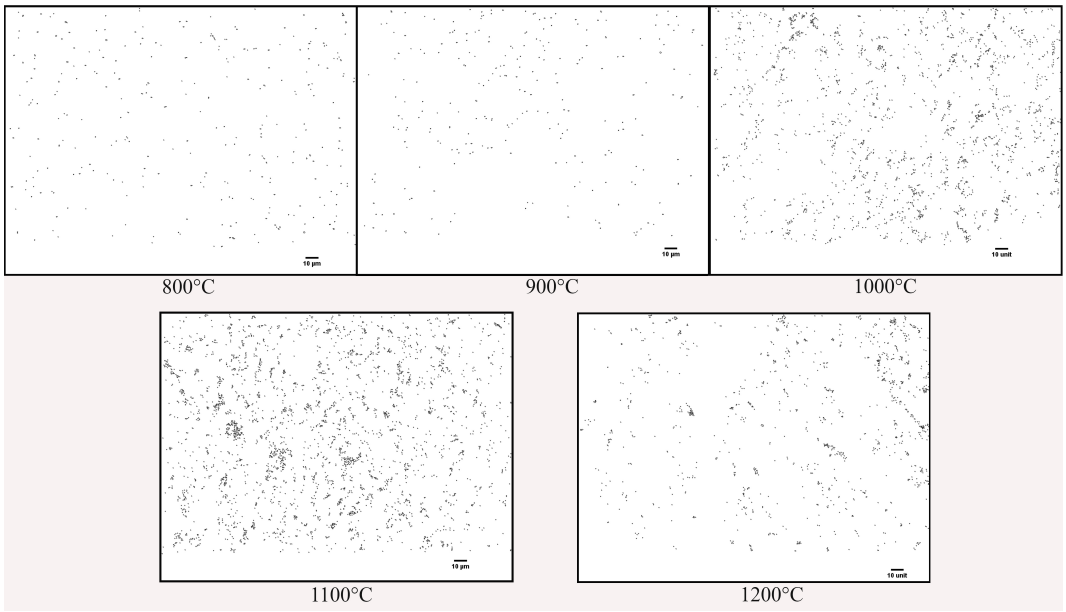


Figure 4.17: Identified boundaries of pores in SEM images (China clay)

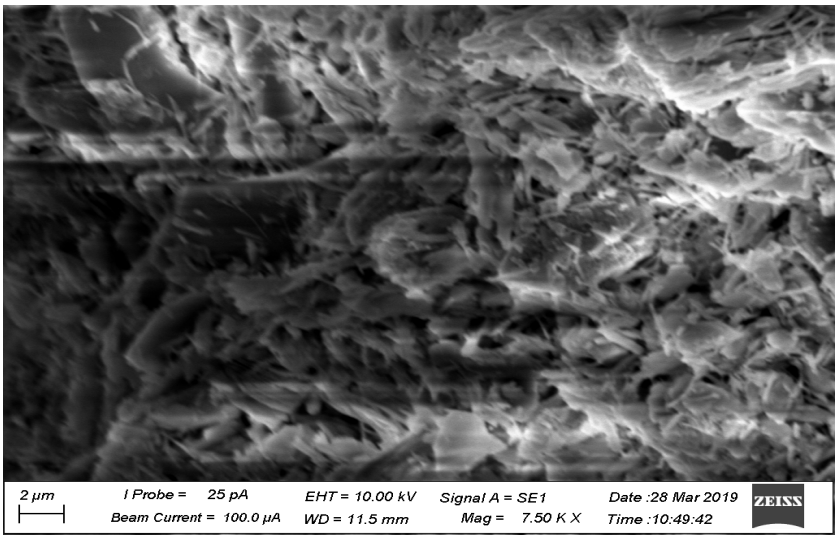


Figure 4.18: SEM image of the pore structure of the aggregate (China)

Table 4.4: Pore size variation of the pore structures of China clay.

China	800°C	900°C	1000°C	1100°C	1200°C
Maximum (μm)	0.6	0.66	0.75	1.04	1.12
Minimum (μm)	0.1	0.21	0.14	0.14	0.15
Mean (μm)	0.28	0.3	0.19	0.18	0.17
Standard deviation	0.12	0.06	0.05	0.08	0.07

4.2.2 Variation of pore connectivity

4.2.2.1 Nachchaduwa clay sample

According to Figure 4.19, open porosity increased with heating temperature and decreases after 1100°C thus, the maximum interconnected open pores of 36% was observed in the clay specimen heated at 1100°C. Open porosity increased from 800°C to 900°C due to the formation of pores. As the temperature was increasing from 1000°C to 1100°C, open porosity significantly increased due to the expansion of the pore structure. Moreover, melting of clay mass occurred at that range of temperature and clay mass expanded more rapidly forming interconnected pores. As a result of that higher open porosity was observed in the clay sample heated at 1100°C. After 1100°C, open porosity significantly reduced. At this range of temperature, the melted clay mass

formed less viscous clay mass and flowed into pores under capillary action and filled up the pores in clay body. As a result of that, more closed pores were observed in the clay samples heated at 1200°C and 1300°C as shown in Figure 4.19. Thus, open porosity reduced after 1100°C

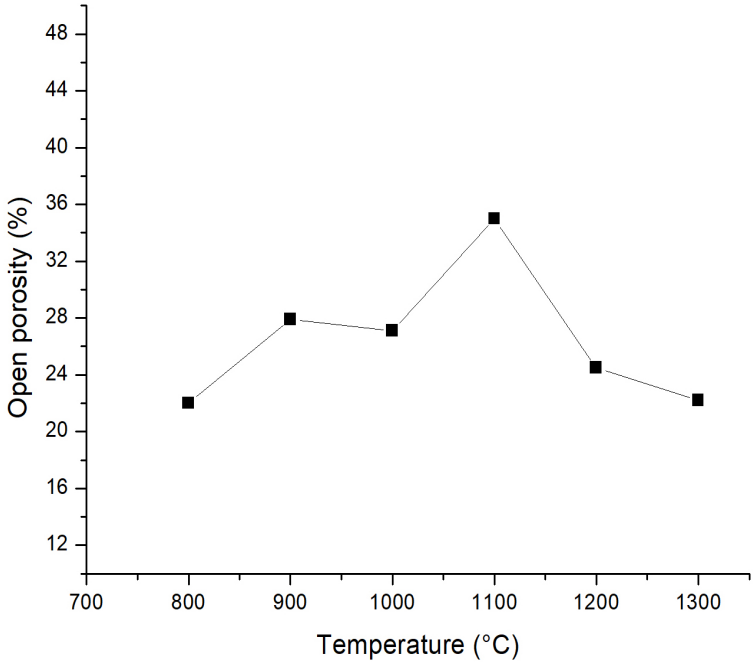


Figure 4.19: Open porosity variation of Nachchaduwa clay

4.2.2.2 Dankotuwa clay sample

Figure 4.20 shows the variation of open porosity of clay specimens. Accordingly, the maximum open porosity of 36.5% was observed at 800°C. The open porosity reduced with heating temperature and increased after 1200°C due to the expansion of pore structure. There was a reduction of open porosity between 800°C to 1200°C. Moreover, clay samples prepared at 800°C, 900 °C and 1000 °C were not associated with considerable expansion due to formation of large pores as shown in Table 4.2. On the other hand, the sintering process was observed in this range of temperature as explained in STA analysis. As a result of that, clay particles combined each other and filled smaller voids in clay mass and partially blocked the pre-existing pore network. Thus, open porosity reduced between 800°C to 1100°C. The melting point of Dankotuwa clay sample was 1064°C as explained in STA. The clay sample produced at 1100°C associated with melting, but did not exhibit much expansion. Thus, open porosity was significantly reduced as melted clay mass formed a less viscous mass,

flowed into the pores under capillary action and fills up the pores in the clay body. The clay samples heated at 1200°C and 1300°C deviated from the rapid reduction of open porosity and increased the open porosity. The mean pore size increased at this range of temperature as shown in Table 4.2. Thus, expansion of the pore structure was observed due to evolving of some gases. As a result of that, open porosity was increased after 1200°C.

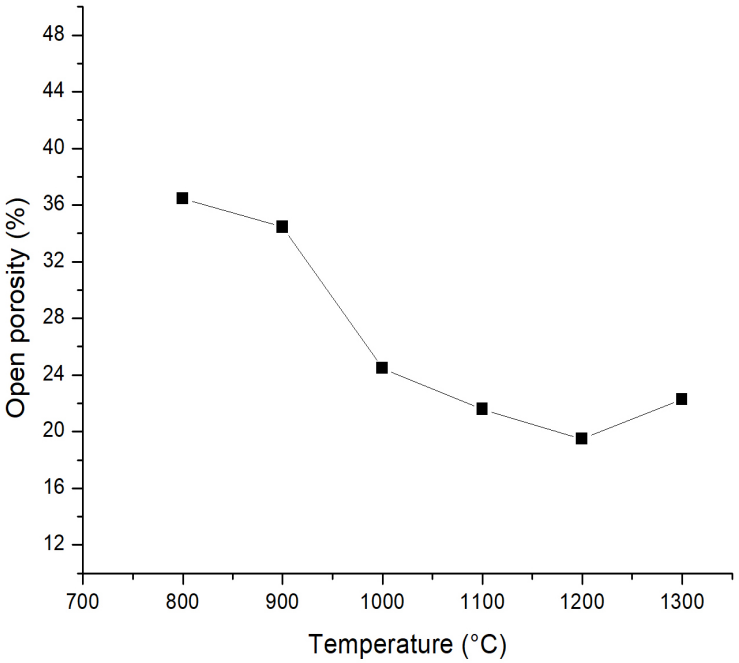


Figure 4.20: Open porosity variation of Dankotuwa clay.

4.2.2.3 Metiagoda clay sample

Figure 4.21 shows the variation of open porosity with heating temperature. The open porosity was gradually decreased with heating temperature. The maximum interconnected open pores of 47.6% was observed at 800°C. According to the STA, this clay type was not associated with the fluidization process but, micro regions of the clay body have different contractions. As a result of that, the smaller pores are gradually eliminated from the clay mass and clay mass gets consolidated without melting. As a result of that, open porosity reduced.

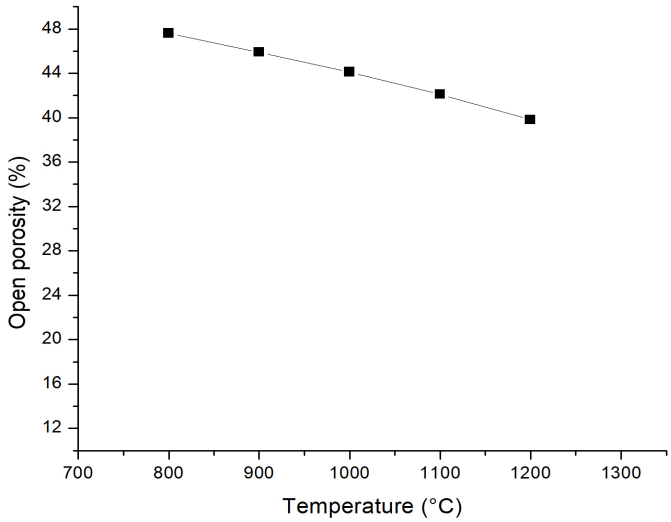


Figure 4.21: Open porosity variation of Metiagoda clay

4.2.2.4 China clay sample

The variation of open porosity is shown in Figure 4.22. There was a small reduction in open porosity but, the reduction was not significant. The obtained pattern for the variation of open porosity was much similar to the pattern of Metiagoda clay. Even though, the clay specimens were not associated with fluidization process as described in STA analysis, consolidation of clay mass occurred and gradually reduce the open porosity.

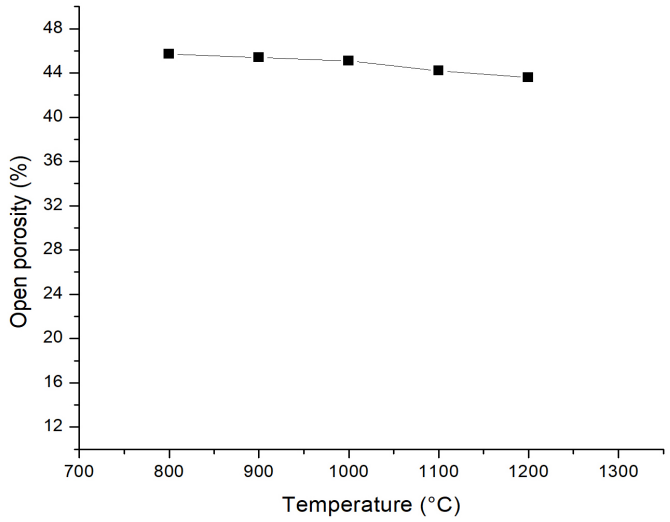


Figure 4.22: Open porosity variation of China clay

4.2.3 Variation of the compressive strength

4.2.3.1 Nachchaduwa clay sample

Nachchaduwa clay sample obtained the maximum compressive strength of 16.5 N/mm^2 at 900°C as shown in Figure 4.23. A minimum of 1.7 N/mm^2 was observed at 1300°C. The compressive strength increased from 800°C to 900°C due to the sintering process. According to the STA analysis, 900°C associated with proper sintering process more than 800°C. As a result of that, clay particles bound each other and increased the strength of pore structure. After 900°C, compressive strength continuously reduced due to the expansion of pore structure. There was a rapid increment in the bloating coefficient in between 1000°C to 1200°C, thus the compressive strength was significantly reduced between that range of temperature. After 1200°C, the rate of strength reduction was reduced due to a proper vitrification process. As a result of the vitrification process, proper consolidation occurred and increased the strength of the pore structure.

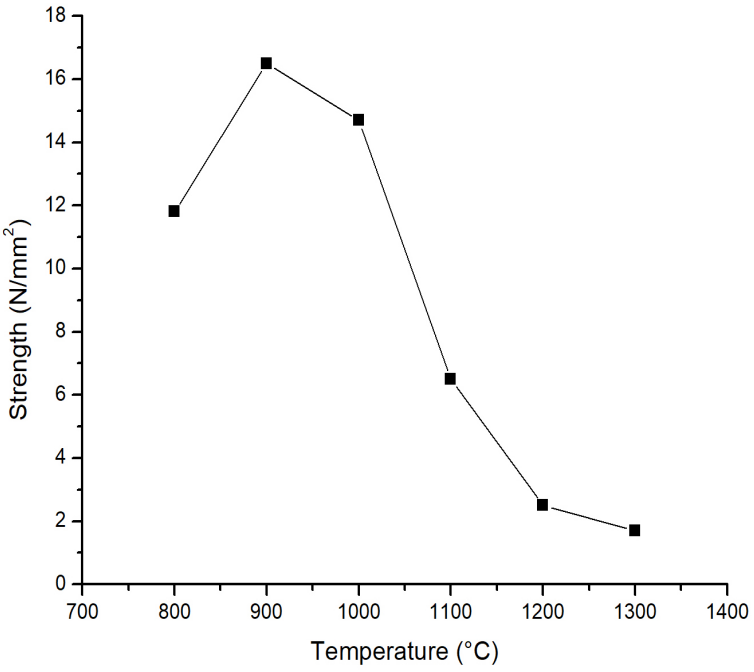


Figure 4.23: Variation of the compressive strength in Nachchaduwa clay

4.2.3.2 Dankotuwa clay sample

Dankotuwa clay specimens obtained the maximum strength of $16N/mm^2$ at 1100°C as shown in Figure 4.24. There was a continuous increment in compressive strength from 800°C to 1100°C. Furthermore, there was a rapid increment in the compressive strength between 1000°C to 1100°C. It happened due to the consolidation of clay mass as a result of a proper sintering process. Moreover, clay samples did not exhibit much expansion in pore structure and the mean pore size did not change significantly between this range of temperature. After 1100°C, clay sample was subjected to a considerable expansion in pore structure due to the formation of low viscous fluid. It can be identified according to the variation of mean pore size as shown in Table 4.2. As a result of that, the compressive strength was significantly reduced after 1100°C and reached the minimum of $7.8N/mm^2$.

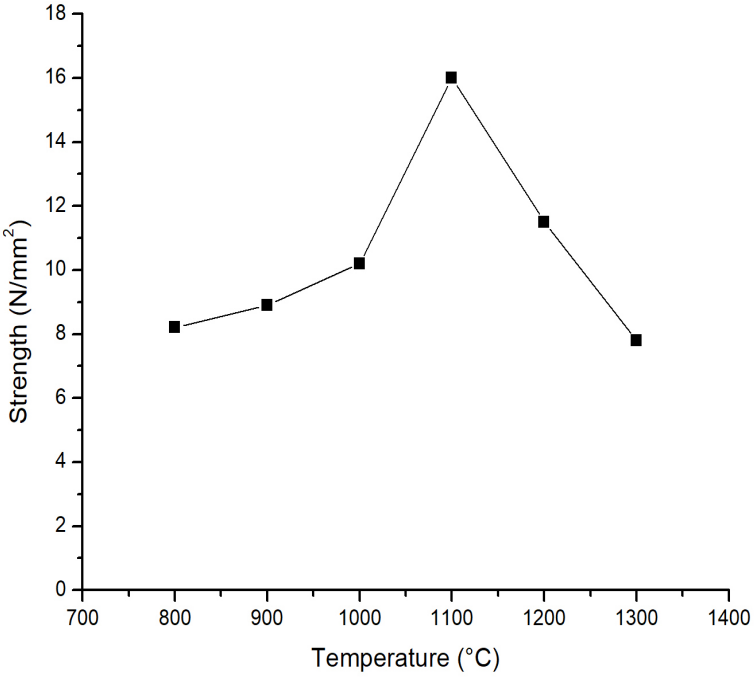


Figure 4.24: Variation of the compressive strength in Dankotuwa clay

4.2.3.3 Metiagoda clay sample

Meatiagoda clay obtained a gradual increment in compressive strength between 800°C to 1000°C as shown in Figure 4.25. After 1000°C, a slightly higher rate of strength increment was observed. According to the STA analysis, crystallization of Spinel was observed around 1000°C. Those crystalline phases increased the strength of pore struc-

ture. Furthermore, clay samples sintered and consolidated around these higher temperatures. As a result of that, a small increment was observed after 1000°C.

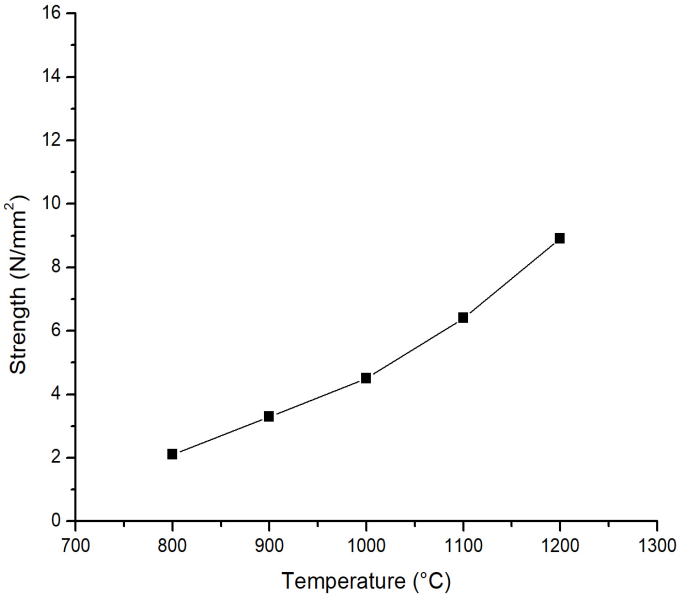


Figure 4.25: Variation of the compressive strength in Metiagoda clay

4.2.3.4 China clay sample

China clay sample achieved its maximum compressive strength of $8.4 N/mm^2$ at 1200°C as shown in Figure 4.26. The behavior of China clay sample was almost same to Metiagoda clay sample. China clay sample did not exhibit any expansion throughout the heating process. Thus, density increased gradually.

As a result of that, strength of the clay specimen was increased continuously. After 1000°C the rate of increment of compressive strength was slightly increased due to the formation of crystalline structures as described in STA analysis.

4.3 Summary of the identified pore structures

Different characteristics of different pore structures were observed throughout this section. Nachchaduwa and Dankotuwa; Metiagoda and China clay samples illustrate a similar behavior. Those clay samples were identified as bloated non-expansive clay (BNEC) and bloated non-expansive clay (UNEC). The behavior of those two clay types was quietly different.

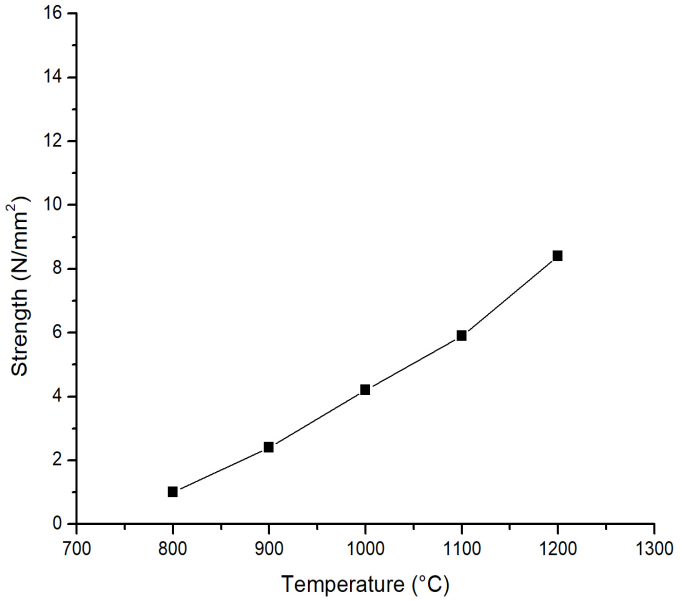


Figure 4.26: Variation of the compressive strength in China clay

According to Indian Standard: IS 1077: 1992 [118], the compressive strength of sintered clay materials should be greater than 3.5 N/mm^2 to prepare load bearing clay bricks. The strength of the sintered clay specimen directly related to the strength of the pore structure. Thus, this value can be taken as a rough guide to measure the quality of pore structure. In sintered material strength of the pore structure directly related to the density and the phase changes in clay mass. Water absorption and desorption capacities mainly depend on the pore structure of the heated clay mass. The pore structures were identified quantitatively based on parameters of the effective pore structure (EPS) and presented in Table 4.5. Afterwards, the internal curing requirements were analyzed in next chapter to evaluate the effectiveness of those pore structures.

Table 4.5: Parameters of different pore structures

Aggregate Type	Mean pore size (μm)	Standard deviation	Comprssive strength(N/mm^2)	Open porosity	Bloating Coefficient
N8	0.32	0.21	11.8	22	1.02
N9	0.3	0.38	16.5	27.9	1.04
N10	0.51	0.43	14.7	27.1	1.13
N11	22.4	22.4	6.5	35	1.65

Aggregate Type	Mean pore size (μm)	Standard deviation	Comprssive strength(N/mm^2)	Open porosity	Bloating Coefficient
N12	23.7	23	2.5	24.5	2.13
N13	26.6	88	1.7	22.2	2.2
D8	0.42	0.25	8.2	36.45	1.04
D9	1.04	0.68	8.9	34.44	1.04
D10	1.06	0.6	10.2	24.48	1.06
D11	2.87	1.26	16	21.57	1.24
D12	7.06	6.6	11.5	19.48	1.43
D13	19.59	18.19	7.8	22.27	1.57
M8	0.87	0.44	7 2.1	47.6	1.01
M9	0.8	0.58	3.3	45.9	0.97
M10	0.77	0.35	4.5	44.1	0.95
M11	0.74	0.4	6.4	42.1	0.95
M12	0.6	0.36	8.9	39.8	0.94
C8	0.28	0.12	1	45.7	1.03
C9	0.3	0.06	2.4	45.4	1.05
C10	0.19	0.05	4.2	45.3	1.05
C11	0.18	0.08	5.9	44.2	1.05
C12	0.17	0.07	8.4	43.6	1.05

4.4 Measurements of internal curing properties of pore structures

4.4.1 Variation of density

4.4.1.1 Nachchaduwa clay sample

Figure 4.27 illustrates the variation of density with respect to the heating temperature. Density of the aggregates reduced with heating temperature, but there was no any linear reduction in density. There was a considerable reduction in density from 800°C to 900°C and from 1000°C to 1100°C.

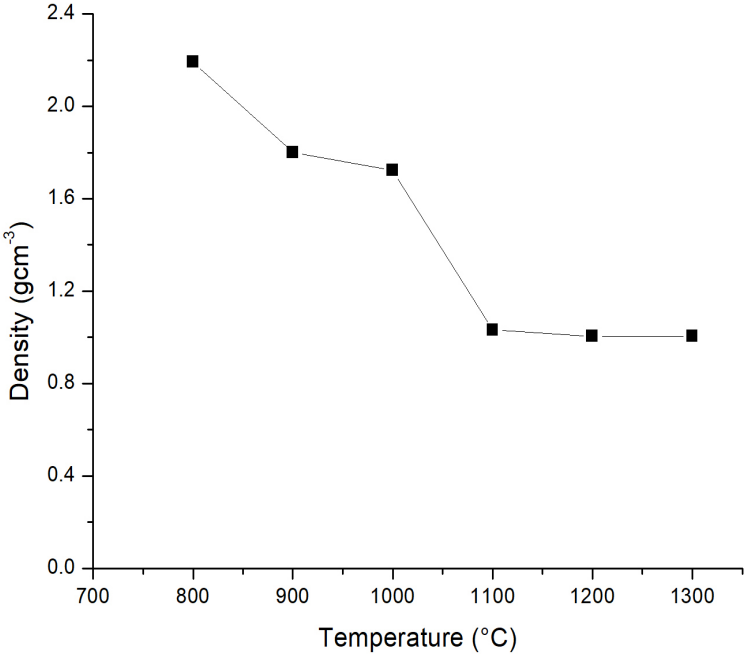


Figure 4.27: Variation of density in Nachchaduwa clay

According to the pore structure analysis, an increment in the number of pores was observed within the clay specimen around this temperature. Thus, 900°C associated with the formation of pore structure. Consequently, density of the aggregates reduced. As the temperature increased, a significant reduction in density was observed between 1000°C and 1100°C. According to STA analysis, 1100°C associated with the formation of viscous clay mass. Thus, the pore structure expanded between 1000°C and 1100°C. This causes the reduction of density at that temperature range. After 1100°C the rate of temperature reduction declined due to the fluidization process. Melted clay mass filled the smaller pores and began to consolidate thus, it reduced the rate of density reduction from 1100°C to 1300°C.

4.4.1.2 Dankotuwa clay sample

Variation of density with respect to the heating temperature is shown in Figure 4.28. Even though, the variation is not significantly visible as Nachchaduwa clay sample, it is much similar to the pattern of Nachchaduwa clay sample.

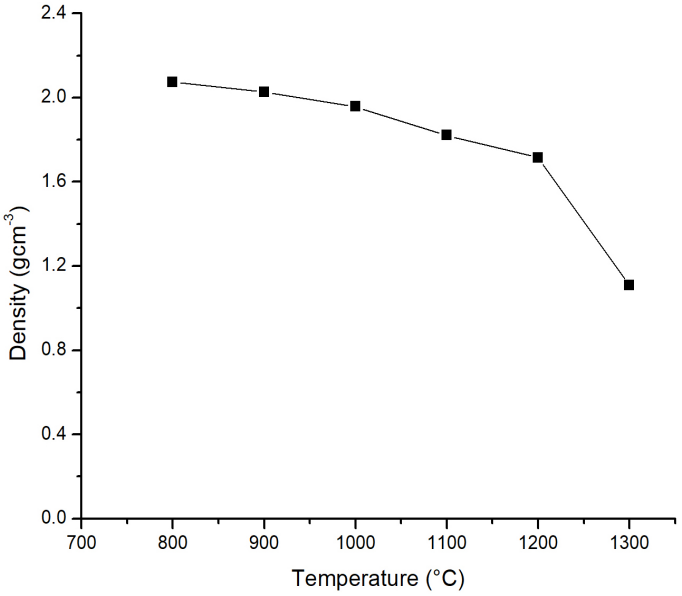


Figure 4.28: Variation of density in Dankotuwa clay

There was a gradual reduction in density from 800°C to 1200°C as shown in Figure 4.28. It happened due to the increment in the bloating coefficient and mean pore size. Moreover, there was a considerable reduction in density between 1200°C and 1300°C. It can be observed according to the variation of the bloating coefficient. As discussed in the simultaneous thermal analysis, 1300°C associated with the formation of viscous clay mass, thus pore structure was expanded rapidly and caused a significant reduction in density at 1300°C.

4.4.1.3 Metiagoda clay sample

The clay sample obtained from Metiagoda showed a completely different variation in density compared to Nachchaduwa and Dankotuwa clay samples. Figure 4.29 illustrates the variation of density with respect to the heating temperature. Density increased with the heating temperature of clay specimens. After 900°C density increased more rapidly, but clay mass was not associated with any vitrification process. The clay particles fused at that temperature and solid-state sintering occurred. As a result of

this process, density of the clay specimens was increased. According to STA analysis, around 1000°C crystallization of spinel occurred but there is not significant affect in the density of heated clay specimens.

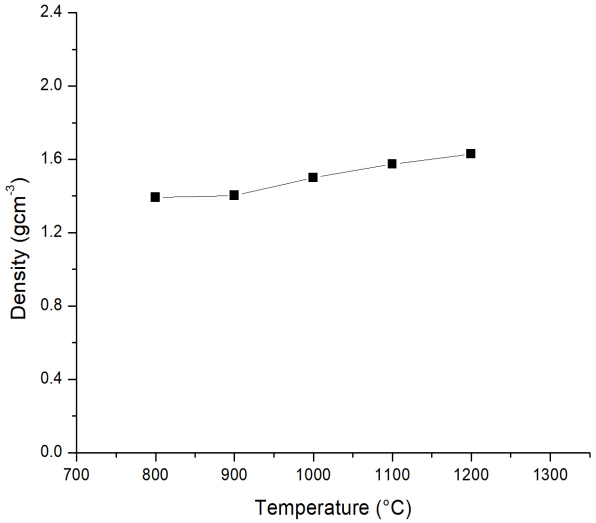


Figure 4.29: Variation of density in Metiagoda clay

4.4.1.4 China clay sample

The clay sample obtained from China showed a similar pattern compared to Metiagoda clay sample. Figure 4.30 illustrates the variation of density with respect to the heating temperature.

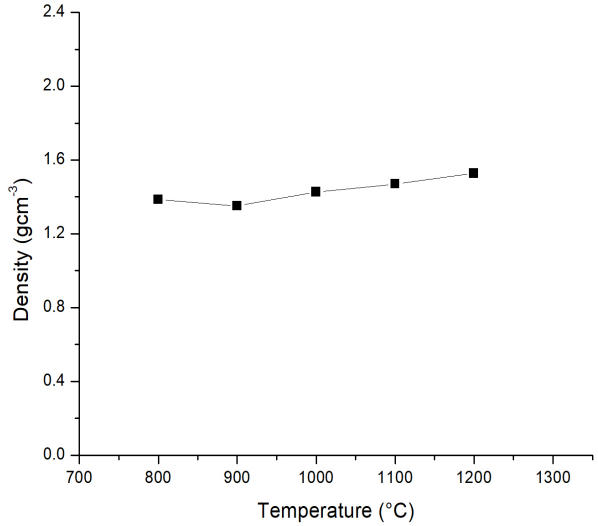


Figure 4.30: Variation of density in China clay

Density increased with the heating temperature. After 900°C the density increased more rapidly, but the clay mass was not associated with any fluidization process. Thus, solid-state sintering occurred, and the density of the clay specimens was increased. According to STA analysis, around 1000°C crystallization of spinel occurred, but it was not significantly affected to the density of heated clay specimens.

4.4.2 Variation of water absorption

4.4.2.1 Nachchaduwa clay sample

Nachchaduwa clay sample obtained the maximum water absorption(48 hours) of 35.2% at 1100°C. The water absorption capacity of Nachchaduwa clay specimens was increased with heating temperature and decreased after 1100°C as shown in Figure 4.31. There was a sudden increment in water absorption capacity at 1100°C. According to the STA analysis, that temperature clearly associated with the vitrification process, thus pore structure expanded rapidly. As a result of that, large pores were produced. Moreover, there was a rapid increment in open porosity. The water absorption capacity reduced after 1100°C due to the reduction of open porosity, because water absorption capacities are directly related to the open porosity of the heated clay samples. The clay samples heated at 1200°C and 1300°C has more closed pores. These types of closed pores cannot store water, thus the water absorption reduced even though it has a high expansion level.

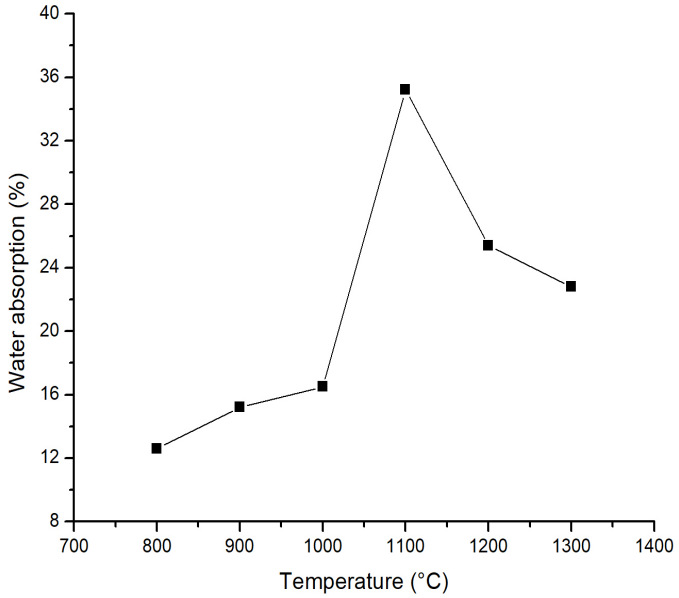


Figure 4.31: Variation of water absorption in Nachchaduwa clay

4.4.2.2 Dankotuwa clay sample

Dankotuwa clay samples exhibit quite different water absorption pattern as shown in Figure 4.32. It obtained a maximum of 19.8% water absorption capacity at 900°C. After 900°C, the water absorption capacity was reduced significantly. This happened due to the sintering process of the clay sample. The clay specimens did not show much expansion between 800°C and 1200°C. Thus, consolidation of clay mass continuously occurred and reduced the pore connectivity. Subsequently, it reduced the water absorption capacity. The mean pore sizes were increased slightly between 800°C and 1100°C due to the pore expansion within the clay mass. As a result of that, water absorption was significantly reduced. After 1200°C a significant increment in pore size and open porosity was observed. Thus, water absorption was increased rapidly after 1200°C.

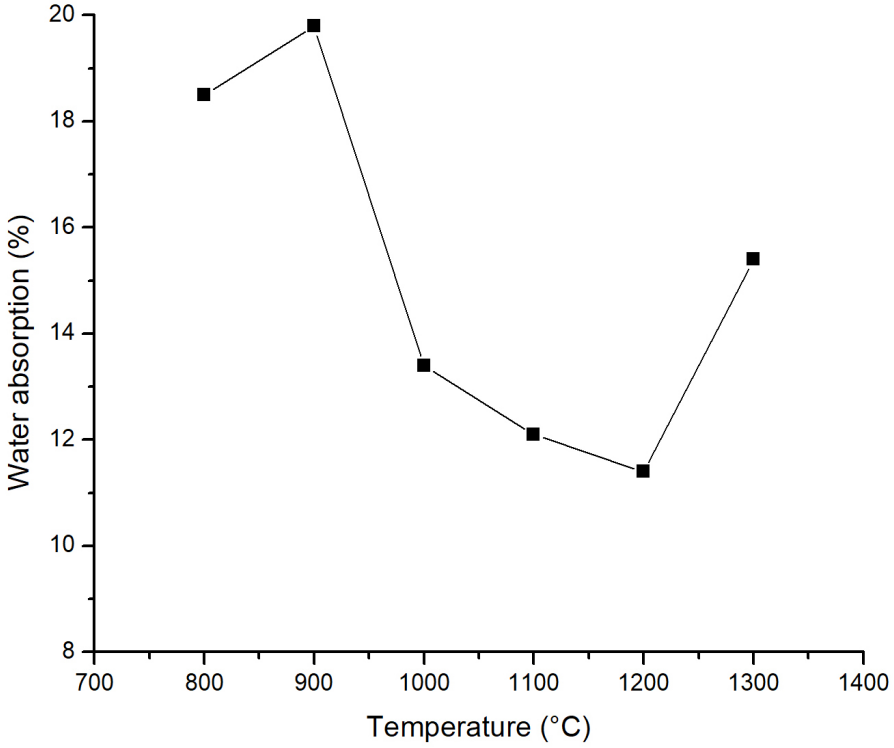


Figure 4.32: Variation of water absorption in Dankotuwa clay

4.4.2.3 Metiagoda clay sample

The variation of water absorption with respect to heating temperature of Metiagoda clay specimens is shown in Figure 4.33. According to that, Meatiagoda clay samples exhibited comparatively higher water absorption capacity with Dankotuwa and

Nachchaduwa clay samples. It achieved a maximum of 35.1% water absorption and a minimum of 24% water absorption as shown in Figure 4.33. There was an approximately equal water absorption capacity at 800°C and 900°C. After 900°C, the water absorption capacity was reduced continuously as a result of the consolidation of the clay mass.

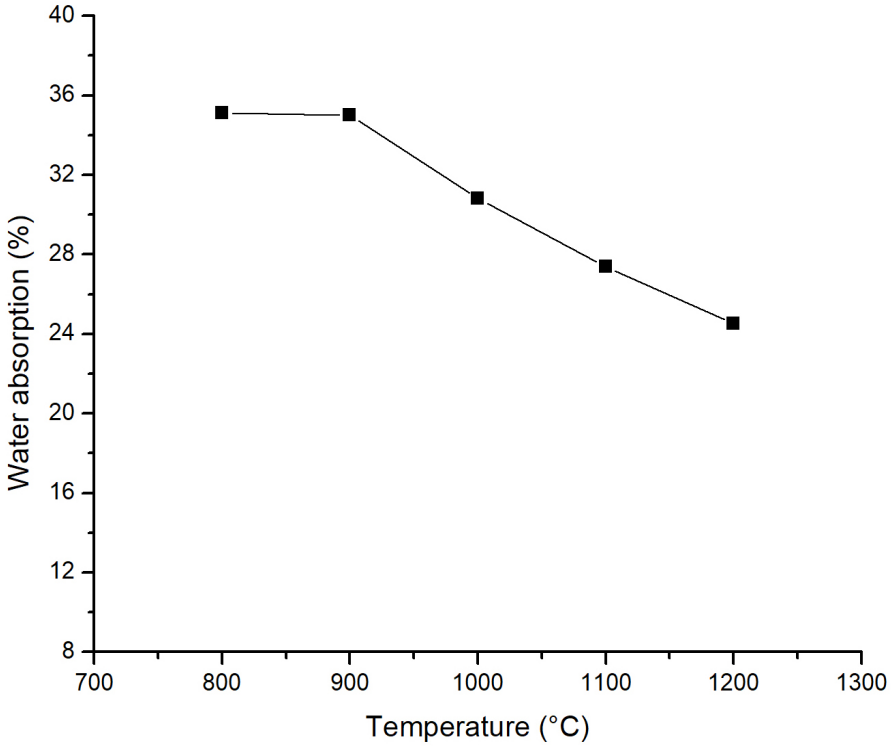


Figure 4.33: Variation of water absorption in Metiagoda clay

4.4.2.4 China clay sample

China clay samples exhibit a similar pattern to Metiagoda clay sample. The variation of water absorption with respect to heating temperature of China clay specimens is shown in Figure 4.34. China clay samples did not exhibit any expansion in porous structure. Moreover, the open porosity was reduced with the heating temperature as a result of the consolidation process. China clay sample also achieved a maximum of 34.4% and a minimum of 28.5% water absorption.

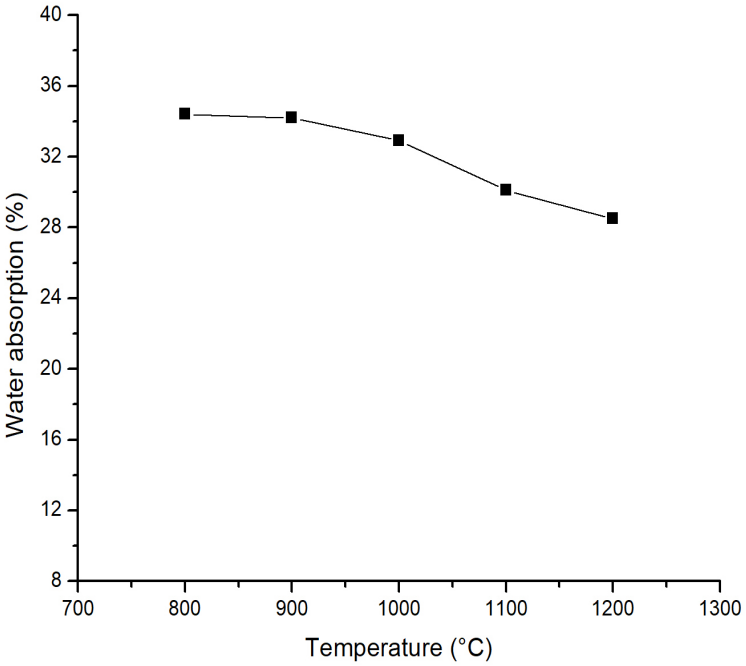


Figure 4.34: Variation of water absorption in China clay

4.4.3 Variation of water desorption

4.4.3.1 Nachchaduwa clay sample

Figure 4.35 shows the water desorption behavior of Nachchaduwa clay sample. The sample prepared at 800°C released 74% of absorbed water at 94% relative humidity. Moreover, the desorption rate of that sample was reduced significantly after 14 days. The sample produce at 800°C did not associate with a perfectly formed pore structure. The pore structure contains larger pores, tiny pores and inter layer spaces. Water that exists within those tiny spaces will not be released at 94% relative humidity. All other clay sample have a perfectly developed pore structure due to the proper sintering and vitrification process. As a result of that, small spaces eliminated from the clay mass, and the clay mass gets consolidated. Consequently, those samples, exhibited higher water desorption more than 95% at 94% relative humidity due to the existence of proper pore structure.

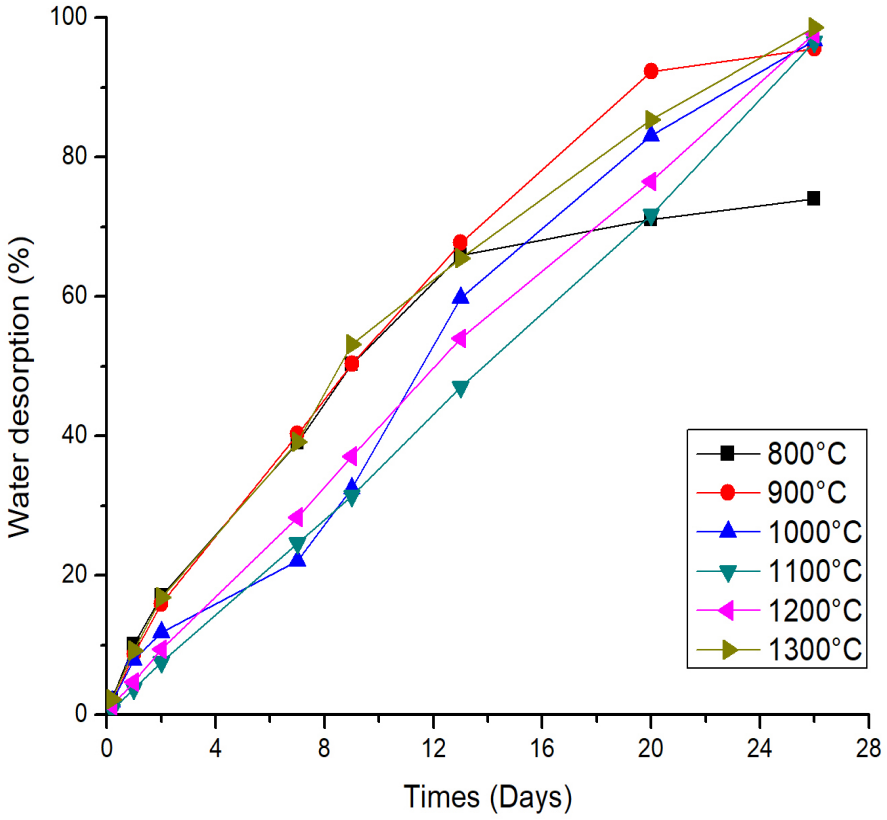


Figure 4.35: Variation of water desorption in Nachchaduwa clay samples

4.4.3.2 Dankotuwa clay sample

Variation of the water desorption in Dankotuwa clay samples with respect to heating temperature is shown in Figure 4.36. Dankotuwa clay samples also exhibit the same pattern of Nachchaduwa clay sample. The clay sample heated at 800°C and 900°C did not associate with proper sintering and vitrification process as discussed in STA. Thus, those clay samples contain small pores and interlayer spaces. Those tiny spaces and pores will absorb water, but the tiny spaces will not release absorbed water. In clay specimen prepared at 1000°C had large pores but, still it was not associated with proper sintering process. Thus, some tiny pores can be remained within the pore structure. As a result of that, it exhibits 90% of water desorption at 94% relative humidity. All other samples exhibit a proper sintering process. Consequently, those samples were associated with a perfectly formed pore structure. Moreover, it consists of large pores compares to 800°C and 900°C samples. Thus, all the aggregates except to 800°C and 900°C samples show higher water desorption capacity.

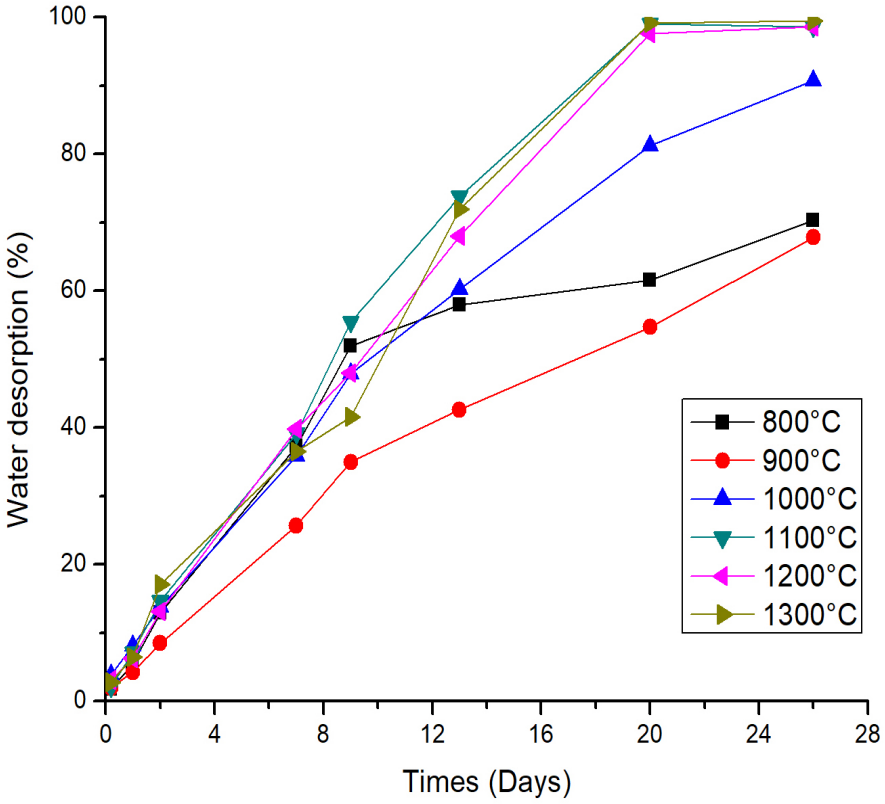


Figure 4.36: Variation of water desorption in Dankotuwa clay samples

4.4.3.3 Metiagoda clay sample

Metiagoda clay sample differs from Nachchaduwa and Dankotuwa clay samples. There was no properly formed pore structure within the heated clay samples. Moreover, clay specimens did not exhibit any expansion or variation in mean pore size with respect to the heating temperature. Those samples absorbed water due to the existence of interlayer spaces and tiny pores. Those spaces will hold water tightly and will not release. According to Figure 4.37, the water desorption rate was gradually increased with heating temperature due to the gradual decrement in smaller pores which hold water tightly. Clay samples continuously released a considerable amount of water for 28 days as shown in Figure 4.37, but the quantity of released water was comparatively low according to the absorbed water content. Thus, there is not single aggregate which has the water desorption capacity greater than 80%. The ICC samples should achieve the design strength within 28 days, thus absorbed water should be available within 28 days to produce EICA.

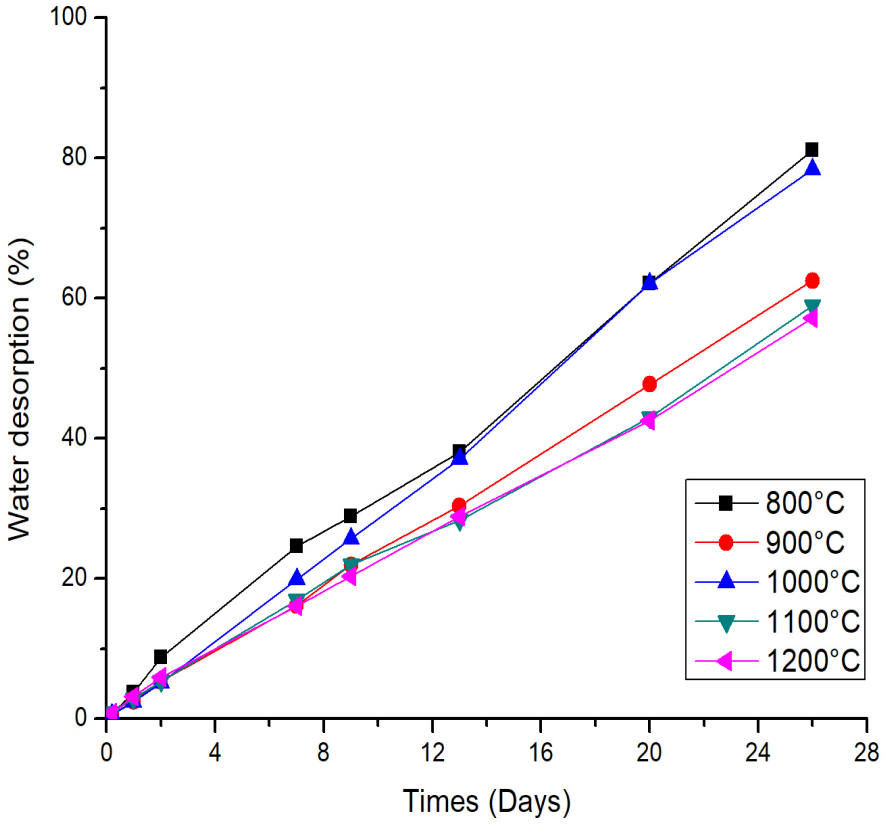


Figure 4.37: Variation of water desorption in Metiagoda clay samples

4.4.3.4 China clay sample

China clay also exhibits a similar pattern to Metiagoda clay sample. Those aggregates release less amount of absorbed water within 28 days as shown in Figure 4.38. In China clay sample a continuous reduction in mean pore size was observed. As a result of that water releasing capacity also reduced with heating temperature. Maximum of 81.13% was observed in 800°C sample and minimum of 57% was observed in 1200°C sample.

4.5 Summary of the internal curing properties of the pore structures

According to the experiments on water absorption, water desorption and density of the produced aggregates, the internal curing properties of different pore structures were identified and presented in the Table 4.6. According to the obtained results, relationships between internal curing properties of the aggregates and the characteristics of the pore structure of the aggregates can be developed to identify the limits of the ef-

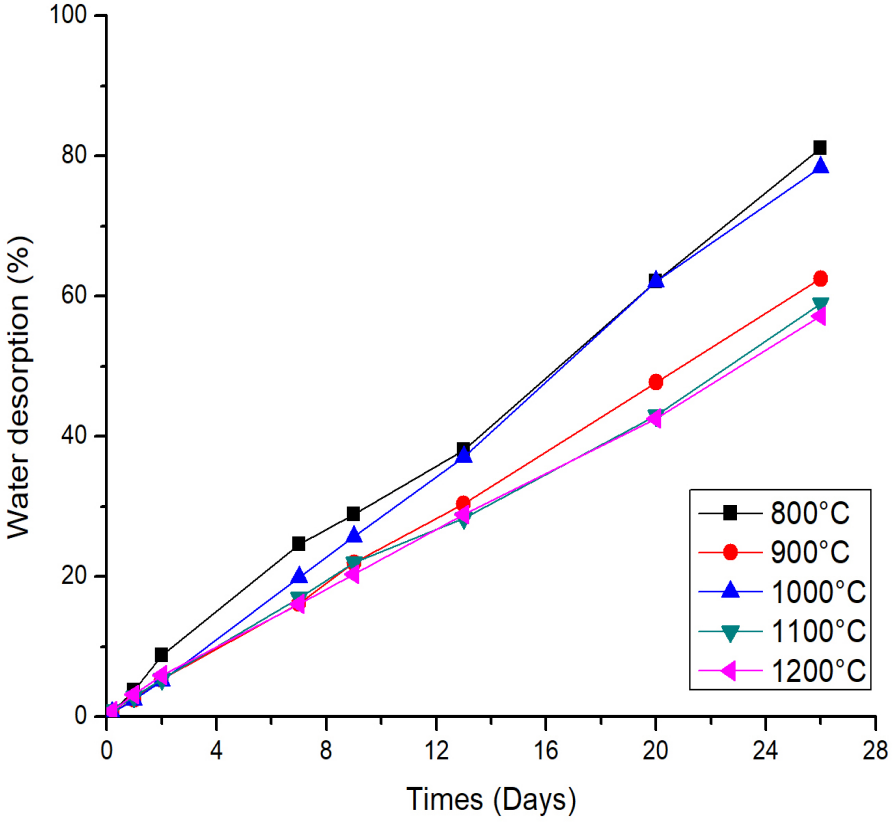


Figure 4.38: Variation of water desorption in China clay samples

fective pore structure. Thus, section 4.6 discussed about the development of different relationships between those parameters.

Table 4.6: Internal curing properties of the pore structures

Aggregate Type	Water absorption %	Density gcm^{-3}	Water desorption %
N8	12.6	2.192	74
N9	15.2	1.8	95.55
N10	16.5	1.724	96.75
N11	35.2	1.031	96.52
N12	25.4	1.005	97.73

Aggregate Type	Water absorption %	Density gcm^{-3}	Water desorption %
N13	22.8	1.004	99.44
D8	18.5	2.074	70.3
D9	19.8	2.026	67.81
D10	13.4	1.957	90.74
D11	12.1	1.82	98.58
D12	11.4	1.715	98.57
D13	15.4	1.109	99.44
M8	35.1	1.3916	53.04
M9	35	1.403	49.85
M10	30.8	1.5	60.13
M11	27.4	1.579	59.24
M12	24.5	1.629	69.82
C8	34.4	1.385	81.13
C9	34.2	1.351	62.52
C10	32.9	1.426	78.4
C11	30.1	1.47	58.89
C12	28.5	1.528	57.18

4.6 Identification of the effective pore structure (EPS) for internal curing aggregate

Throughout this section, the limits of the EPS were defined based on the properties of different pore structures. The limits of the pore connectivity, pore size, pore expansion and pore strength were defined based on water absorption, water desorption, density and phase changes of sintered aggregate. Finally, the limits of the EPS were established quantitatively. Firstly, it is necessary to analyze about the relationship between density and compressive strength of aggregates.

4.6.1 Relationship among density, expansion and compressive strength

The compressive strength of the pore structure mainly depends on density and phase change of clay mass (Formation of glass phase) as discussed in section 2.6.2. Moreover, it can be verified according to Figure 4.39. D13 and N11 samples achieved higher compressive strength due to the formation of melted glass phase even though it had low density value. Thus, the limits of density and sintering process should be identified beforehand the establishment of the compressive strength of pore structure. The compressive strength of sintered clay materials should be greater than 3.5 N/mm^{2}to ensure the proper sintering process. According to the properties of EICA, the density of the aggregates should be greater than 1.4 g/cm^3. Based on those requirements the compressive strength of EPS was defined.

Generally, pore expansion can be observed in BNEC materials, thus the density of those materials mainly depends on the level of pore expansion. Figure 4.39 shows the variation of density with respect to the bloating coefficient of the sintered clay aggregates. According to that, the clay samples which have a higher Kp value than 1.5 produced low density aggregates. Those aggregates cannot utilize in the production of load bearing structures. Thus, N10, N11, N12 and D13 are not suitable in ICA production.

The clay samples produced by using UNEC did not expand during the heating process. Thus, whatever the density was, the bloating coefficient of those aggregates was lower than 1.5. As a result of that, whatever the clay type is, the bloating coefficient should be lower than 1.5 to achieve the required density value as shown in Figure 4.39.

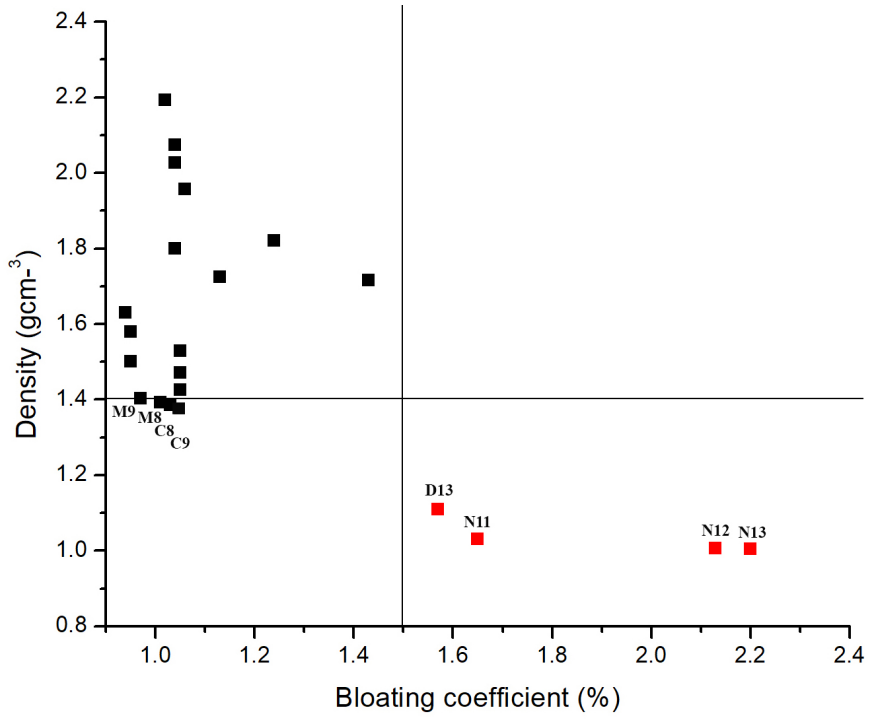


Figure 4.39: Relationship between density and K_p

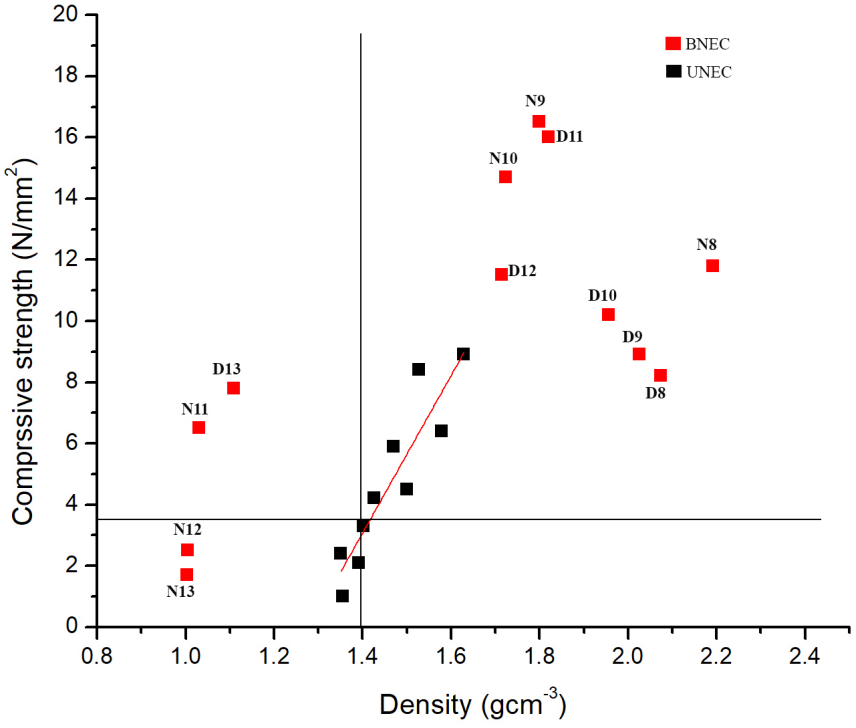


Figure 4.40: Relationship between density and Strength

Figure 4.40 shows the variation of compressive strength of the pore structure with respect to the density. The pore structures which produced by using UNEC were not associate with pore expansion or the formation of the glass phase. Generally, those materials show proper sintering process above 1200°C [119]. Thus, all the pore structures produced from UNEC fitted into a linear relationship of density and compressive strength as shown in Figure 4.40. The equation of the line is presented in Equation 4.1. The R-square value ranges from 0 to 1 statically indicates the strongness of any relationship between selected parameters. The R-Square value for this relationship is 0.821 thus, it indicates a statically strong relationship.

$$Y = -32.91985 + 25.71645x \tag{4.1}$$

where;

- Y = Compressive strength,
- x = Density,

According to the relationship, all the aggregates produced using UNEC should achieve at least 3.15 N/mm^2 compressive strength to obtain higher density value greater than 1.4 g/cm^3. On the other hand, all the aggregates should achieve at least 3.5 N/mm^2 compressive strength to ensure the proper sintering process as mentioned in section 4.3.5. Furthermore, when the bloating coefficient is lower than 1.5, all the aggregates produced by using UNEC obtained higher density value more than 1.4 g/cm^3, As a conclusion, whatever the clay material type, the compressive strength of EPS should be greater than 3.5 N/mm^2 and the bloating coefficient should be lower than 1.5 to achieve the required density of EICA.

4.6.2 Relationship between water absorption and open porosity

Water absorption is directly related to the open porosity of the pore structure. Thus, the limit of open porosity can be defined based on the water absorption capacity of effective aggregate for internal curing as discussed in section 2.6.3. Figure 4.41 shows the relationship between open porosity and water absorption capacity of pore structures. The obtained relationship shows R-square value of 0.9815. Thus, there is a strong relationship between all the data points except to N11, N12, N13, D13 data points. Those samples were subjected to comparatively higher expansion (1.5,(Kp) $\geq$) and not suitable in the production of aggregate for internal curing. Thus, when clay samples have a low Kp value than 1.5, it exhibits a strong relationship between open porosity and

water absorption capacity as shown in Figure 4.41. The equation of the polynomial is shown in Equation 4.2. According to that, there should be at least 27.5% of open porosity to achieve 15% of water absorption. When the sample shows a higher bloating coefficient than 1.5, it absorbs a high amount of water with less open pores. It means that, those pore structures consist of perfectly interconnected pores which water can access easily, but those aggregates cannot achieve the required density of EICA. As a conclusion, sintered clay materials which have the Kp lower than 1.5, should have at least 27.34 percentage of open porosity.

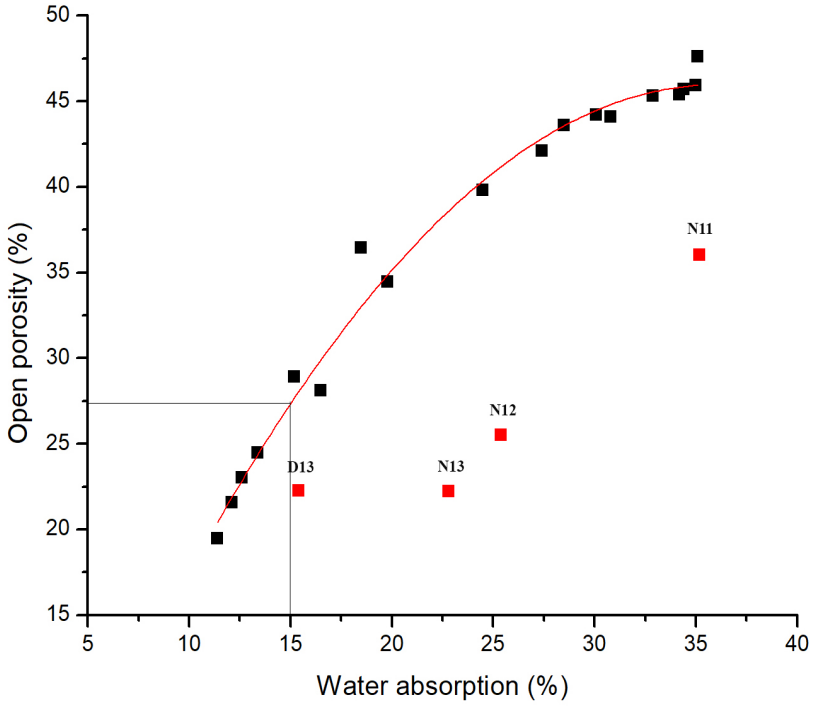


Figure 4.41: China clay sample

$$Y = -8.67575 + 3.03235x - 0.04207x^2 \tag{4.2}$$

where;

- Y = Open porosity,
- x = water absorption,

4.6.3 Relationship between mean pore size and water desorption

Water desorption capacity of the pore structures mainly depends on the size of pores as discussed in the section 2.6. Figure 4.42 shows the relationship between mean pore

size and water desorption capacity of the produced pore structures.

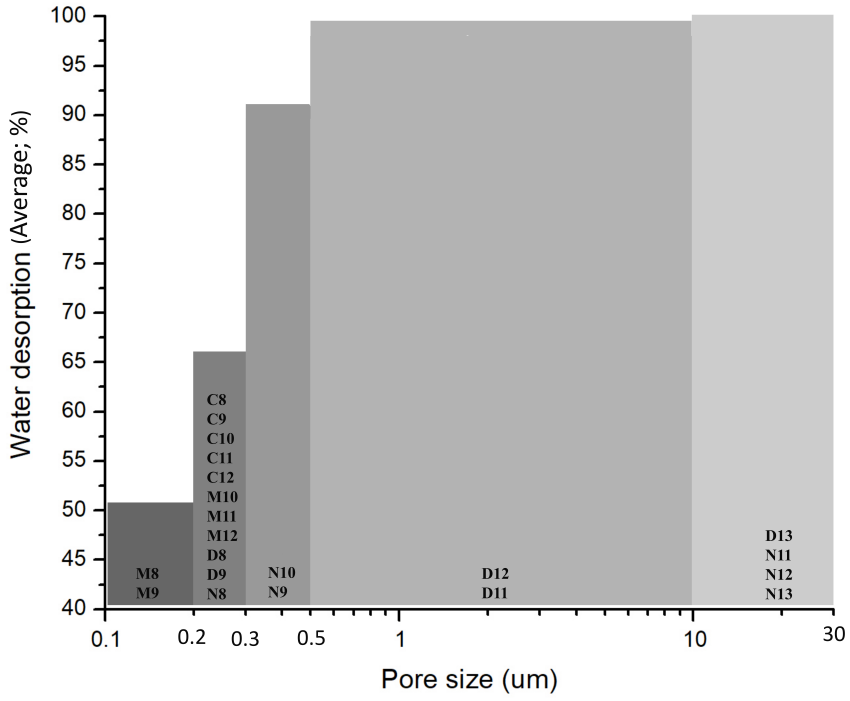


Figure 4.42: Relationship between pore size and water desorption

Water desorption capacity increases with pore size. The pore structures that the mean pore size range from 0.1 to 0.2μm and 0.2 to 0.3μm released only a 50% and 65% of absorbed water. Those desorption capacities are much low according to the requirement of EICA,. When the mean pore size ranges between 0.1 and 0.3, it contains a higher number of tiny pores inside the pore structure. Those pores will not release water at 94% relative humidity. when mean pore size exists between 0.3 to 0.5, it releases 90% of absorbed water, and the pore structures which have the mean pore size greater than 0.5 released considerable amount of water greater than 95%. Thus, the aggregates which have the mean pore size greater than 0.3 are suitable to produce EICA in the sense of water desorption, but the aggregates which has mean pore size greater than 10μm had subjected to a higher bloating coefficient value more than 1.5 as shown in Figure 4.39. Thus, the mean pore size should be within the range of 0.3 to 10μm . All the aggregates produced using UNEC had lower mean pore size than 0.3μm thus, UNEC is not suitable in the production of EICA. Figure 4.43 shows the variation of pore size and the bloating coefficient of the aggregates.

The mean pore size of the pore structures which have the bloating coefficient lower than 1.1, ranges between 0.1 and 0.3μm. On the other hand, when bloating coefficient is greater than 1.1, the mean pore size ranges from 0.3 to 0.5μm. Thus, bloating

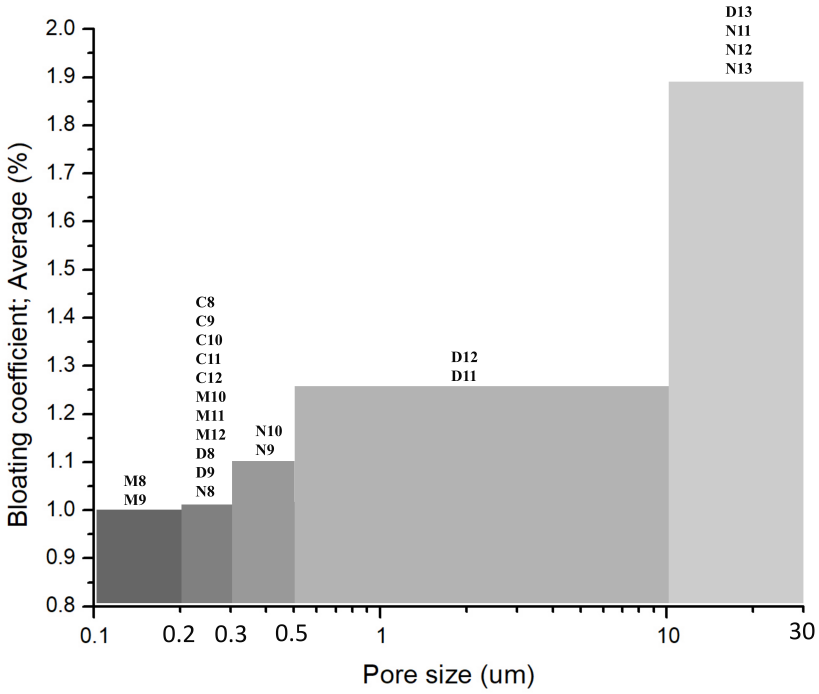


Figure 4.43: Relationship between pore size and K_p

coefficient should be greater than 1.1. as a conclusion, the mean pore size of the pore structure should range from 0.3 to 10μm, and the bloating coefficient should be greater than 1.1.

4.6.4 The effective pore structure.

According to the obtained results of this section, bloating non expansive clays (BNEC) should be selected. Afterwards, it should be heated to an appropriate temperature as the bloating coefficient achieve a higher value than 1.1 to ensure the formation of the pore structure. Furthermore, the bloating coefficient should be lower than 1.5 to ensure proper aggregate density to use in structural concrete. Moreover, it should achieve higher compressive strength than 3.5 N/mm^2 to ensure proper sintering process, and it should achieve higher open porosity than 27.5% to achieve enough water absorption capacity. Finally, the mean pore size of the pore structure should be greater than 0.3 to ensure proper water desorption capacity. If the bloating coefficient of BNEC ranges from 1.1 to 1.5, the mean pore size exists between 0.3 and 10μm and it achieves required density. Thus, as a conclusion, in order to produce EICA, the pore structure of those aggregates must satisfy followings;

1. Selected clay type should be BNEC
2. The bloating coefficient should range from 1.1 to 1.5
3. The open porosity of EPS should be greater than 27.5%

According to the selection criteria 1, all the C and M type aggregates are not suitable to produce EICA. According to the second criteria, N11, N12, N13 and D13 are not suitable from the remaining aggregates due to the low density. Furthermore, D8, D9, D10 and N8 are not suitable due to the loss of proper pore structure to archive required water desorption capacity. According to the third criterion, D11 is not suitable due to the insufficient water absorption capacity. Finally, N9 and N10 aggregates can be selected as the aggregates which have the EPS.

This can be verified according to the internal curing properties of porous aggregates. Figure 4.44 shows the main requirement of effective internal curing concrete in 3 axis graphs.

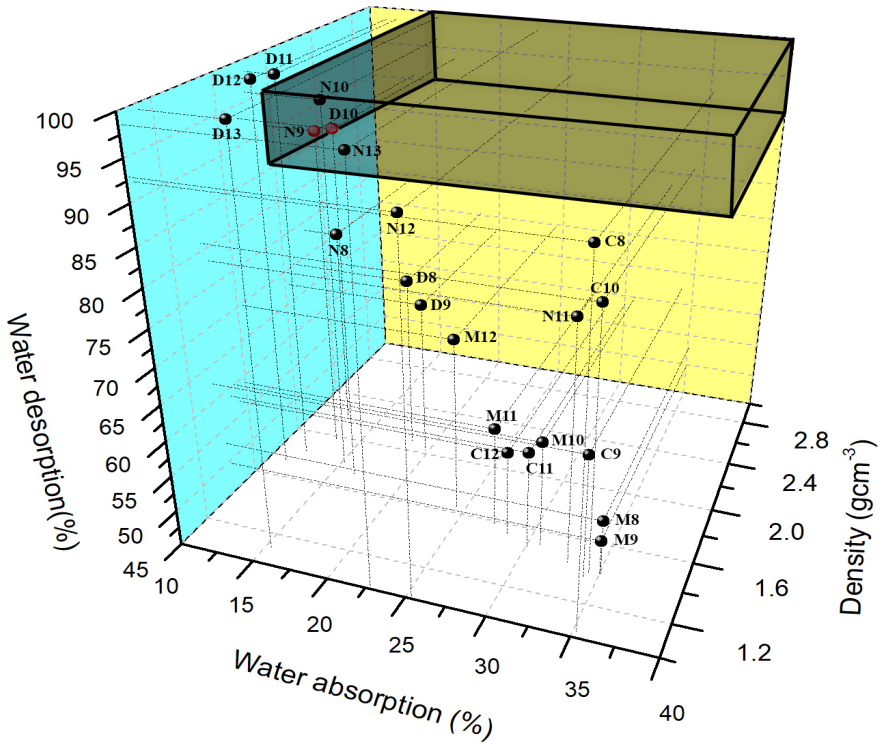


Figure 4.44: Aggregates which satisfy the main requirement of EICC

The limits of those requirements are presented as a black box in Figure 4.44. Aggregates that exist within this box will fulfill all the requirements of effective internal curing concrete. According to that, N9 and N10 samples fulfill all the requirements of EPS. Thus, those aggregates can be identified as an effective aggregate to produce ICC.

On the other hand, the pore structure of those aggregates satisfies all the requirements of EPS. This can be verified by producing concrete samples as discussed in the next chapter.

CHAPTER 5

VALIDATION OF FINDINGS

5.1 Validation of the test results

5.1.1 Introduction

If a Effective Pore Structure (EPS) is developed within any aggregate, it will perform as an effective aggregate for internal curing concrete (ICC) production. Thus, those types of aggregates can be used in the production of ICC without compensating the compressive strength of concrete. Two aggregate types were selected and ICC was produced to verify the effectiveness of the EPS. The aggregate, N9 was selected as the aggregate which satisfies the requirement of EPS. On the other hand, the aggregate C12 was selected as the second aggregate which did not satisfy the requirement of EPS. The properties of those aggregates are mentioned in Table 4.5 and 4.6.

Those aggregates were produced in a larger scale using industrial facilities of Rajarata tile and Midaya ceramic factories. Subsequently, concrete samples were produced including those aggregates and measure the properties of concrete. This chapter explains the production process and the behavior of those concretes based on the compressive strength, workability and drying shrinkage to verify the EPS.

5.1.2 Aggregate production in industrial facilities

Clay samples obtained from Nachchaduwa and China were selected for the verification process. Clay was extracted from the Nachchaduwa clay mine and extracted clay was kept in open air for several months (5 to 6 months) to complete the seasoning process. Figure 3.2 shows the extracted clay. During the seasoning process clay was homogenized and moistened. After the seasoning process, clay lumps were crushed using

a jaw crusher as shown in Figure 5.1(a). Subsequently, crushed samples were mixed with some water and were sifted through 5mm and 2mm rolling mills as shown in Figure 5.1(b) and Figure 5.1(c) respectively. During the sieving process, unwanted debris were removed and clay materials were mixed further. The preparation of the cylindrical sample in the industrial scale is not practicable with stationary heating furnace. Thus, after the sieving process, clay samples were passed through a press and prepared clay blocks which have same thickness of cylindrical specimens. Figure 5.1(d) shows the prepared clay plates for firing (150mm x 250 mm x 14mm).



(a) Jaw crusher (b) 5mm rolling mill

(c) 2mm rolling mill (d) Prepared clay specimen

Figure 5.1: Prepared aggregate from Dankotuwa clay.

Prepared clay samples were kept in a dryer for 4 hours at 160°C in order to remove moist otherwise, it will cause an exploding reaction due to the sudden temperature increase. Then, Pre-heated clay blocks were conveyed to the stationary heating furnace. Figure 5.2 shows the furnace that used for the heat treatment process. It was a stationary furnace which operates through a step heating process. During the heating process slow firing rate was used to avoid black core formation as described in section 2.6. The soaking time under 900°C was 30min and the total time for the heating process was approximately 5 hours. After the heating process, samples were cooled at ambient temperature. Then the heated clay samples were prepared for the crushing process. Clay samples were crushed using a mechanical crusher and collected the aggregates



Figure 5.2: Stationary furnace



Figure 5.3: Crushing and sieving process

that pass through the 4.75mm sieve. Another aggregate was produced using China clay. The heating temperature for China clay was 1200°C and the firing time was 5.5 hours with 30 min soaking time. Figure 5.3 shows the crushing and sieving process of heated clay specimen made from China clay.

Production cost of the internal curing aggregate is one of the important parameters to validate the suitability of the new aggregate for concrete application. Literature on cost estimation for internal curing aggregate (ICA) were not available since the proposed methodology has not been used for ICA production. Thus, it is necessary to discuss with local industries to use their available facilities to produce the aggregate. According to the available facilities and equipment, a production process was developed, and cost estimation was carried out. A detailed description about the cost estimation and the production process were mentioned in Appendix B.

5.1.3 Mix design

The required amount of internal curing aggregate (ICA) for internal curing was determined through Equation 5.1. The equation basically worked on the amount of moisture in the aggregate, the type and amount of cementitious materials in the mixture and the water to cement ratio at the time of mixing [6]. Bentz and Snyder developed Equation 5.1 equating the water demand of the hydrating mixture and the mass of water provided by internal reservoirs [23, 22]. The aggregates were pre-soaked over 48 hours to absorb water and kept in an open space to achieve SSD condition. Subsequently, a grade 30 concrete mix design was prepared. Table 5.1 shows the concrete compositions and materials used to prepare $1m^3$ of concrete.

Table 5.1: Mix design calculation for grade 30 concrete

Ingredients for G30 concrete		Concrete types		
		ECC	ICC(N9)	ICC(C12)
Cement	(kg/m^3)	373	373	373
Water	(kg/m^3)	205	205	205
Fine aggregate	(kg/m^3)	677	493	529
Coarse aggregate	(kg/m^3)	1105	1105	1105
ICA	(kg/m^3)	-	174	148

$$C_f C_s \alpha_{max} = S\phi M_{agg} \tag{5.1}$$

- M_{max} = mass of fine aggregate needed per unit volume of concrete (kg/m^3).
- C_f = cement factor (content) for concrete mixture (kg/m^3) =1.
- C_s = chemical shrinkage of cement (g of water/g of) = 0.07.
- α_{max} = maximum expected degree of hydration of cement 1.
- S = degree of saturation of aggregate = 1.
- ϕ = absorption of aggregate.

5.1.4 Compressive strength and workability

Mix designs were prepared according to the BS 1881-116:1983 standard. Afterward the calculated amount of internal curing aggregate was replaced with a conventional fine aggregate of the grade 30 concrete mix design. Three different concrete specimens of 15cm x 15cm x 15cm were cast as shown in Figure 5.4 and Figure 5.5. External curing concrete (ECC) specimens were kept submerged for curing. Non-curing concrete (NCC) specimens and Internal curing concrete (ICC) specimens were kept in an open space without subjected external curing. During the preparation of concrete specimens, workability of the samples was measured. Afterwards, three concrete specimens were tested to obtain the mean compressive strength values at the end of 7,14, and 28 days. Moreover, grade 25, 30 and 35 concrete were prepared to study the variation of compressive strength and workability with respect to the grade of the concrete.



Figure 5.4: Prepared concrete specimens



Figure 5.5: Tested concrete specimen

5.1.5 Drying shrinkage

Generally, ICC reduces the drying shrinkage and improve the durability of concrete. Thus, effective internal curing aggregates enhance not only the concrete strength but also the drying shrinkage. As a result of that, evaluation of the drying shrinkage property is a mandatory thing in ICC. Thus, three different concrete types were casted to evaluate the performance of EPS in mitigation of drying shrinkage. The drying shrinkage of these concretes was observed using ASTM C157 test method. The prepared concrete types were ECC, ICC/N9 and ICC/C12. Three prismatic concrete specimens which had a height of 75mm, a length of 285mm and a width of 75mm were cast for each concrete type as shown in Figure 5.6. After, 23hours the specimens were demolded. ICC/N9 specimens and ICC/C12 specimens were kept in a humidity chamber as specified in the standard. Meanwhile, concrete specimens were tested to obtain the drying shrinkage values at the end of 5, 9, 14, 21, 28 and 35 days as shown in Figure 5.7.

5.2 Validation of the test results

5.2.1 Water absorption

Figure 5.8 and Figure 5.9 showed the water absorption capacity of C12 and N9 aggregates. According to the laboratory experiments, the mean water absorption capacity

of N9 and C12 samples were 15.2 and 28.5 percentage. N9 and C12 aggregates which produced in industrial scale, obtained 15.5 and 27.9 percentage of water absorption within 2 days. On that account, there was not much difference in water absorption capacity in laboratory production and industrial production. Figure 5.10 and Figure 5.11 show the pore structure of C12 and N9 aggregates respectively. In accordance

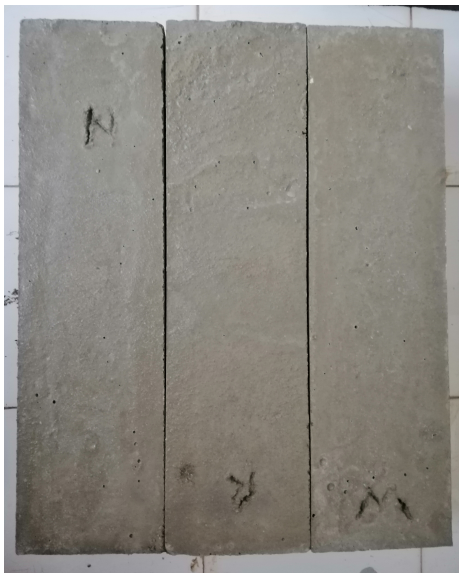


Figure 5.6: Prismatic concrete specimens



Figure 5.7: Drying shrinkage apparatus

with figures, the same behavior can be observed in larger production. Afterwards, ICC mix design was prepared using obtained water absorption capacity. The compressive strength is also an important factor of any concrete type, but in ICC concrete drying shrinkage is the most important one. As a result of that, the compressive strength and the drying shrinkage of the ICC samples were measured. Thus, the acceptable compressive strength and drying shrinkage illustrated the effectiveness of the aggregate to produce internal curing concrete.

5.2.2 Drying shrinkage

The average drying shrinkage of prepared concrete specimens are presented in Figure 5.12. According to the results, ICC/C12 concrete specimen exhibits higher drying shrinkage than other samples at the end of 35 days. ICC/C12 concrete specimens were produced including C12 aggregates as an internal curing agent. C12 aggregate released only 57% of stored water at 94% of relative humidity, thus higher drying shrinkage was observed in this sample due to the formation of internal stresses. In ECC concrete specimens, there was a lower drying shrinkage compared to ICC/C12 sample, but it was greater than the drying shrinkage of ICC/N9 sample. In ECC sample, there was not any internal curing agent to release water as hydration consumes available water but there was no moisture evaporation during the first fourteen days due to the external curing process. As a result of that, lower drying shrinkage was observed in ECC sample than ICC/C12 sample. After 14 days, external curing process of ECC specimens was

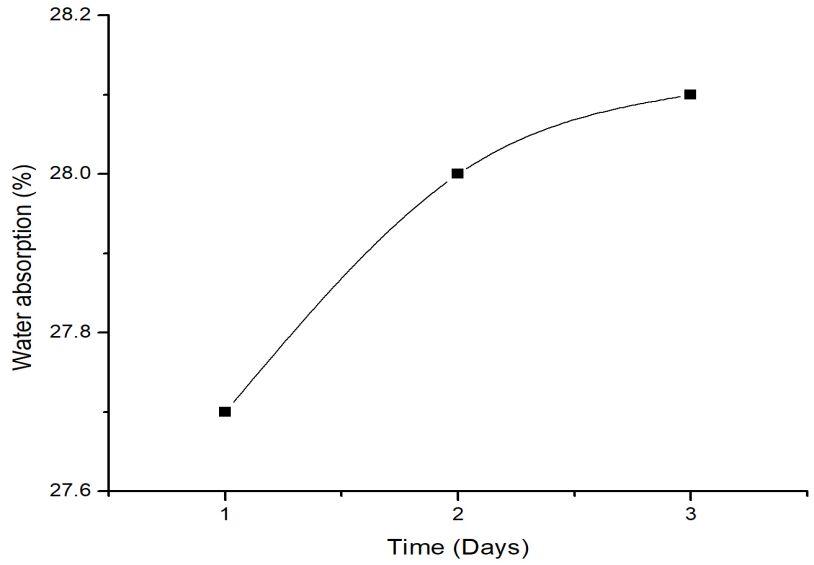


Figure 5.8: Water absorption rate of C12 aggregate

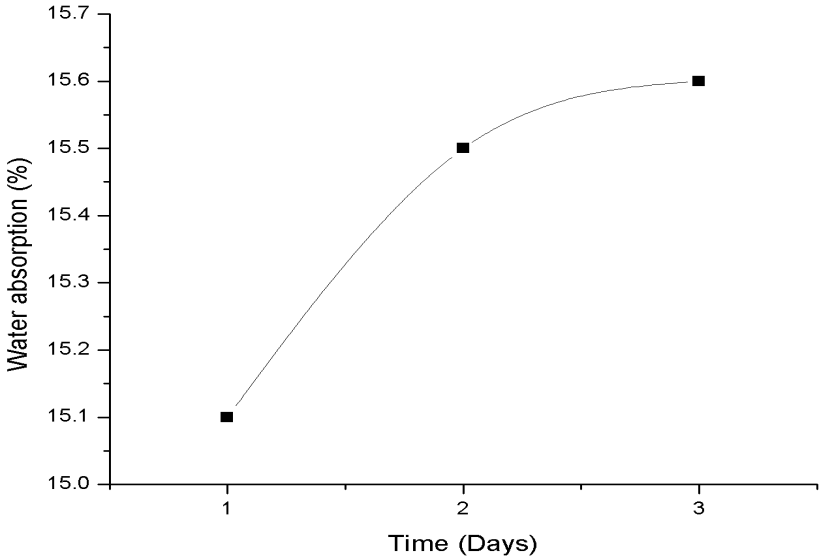


Figure 5.9: Water absorption rate of N9 aggregate

stopped to simulate the practical curing conditions. Thus, available moisture loss not only due to hydration process, but also due to evaporation. Subsequently, the rate of moisture loss increased in ECC specimens after 14 days. Thus, higher drying shrinkage was observed after 14 days. In ICC/N9 specimens, N9 aggregates released 95% of absorbed water within 28 days, thus level of moisture was not reduced in ICC/N9 sample. As a result of that, lower drying shrinkage was observed in ICC/N9 samples

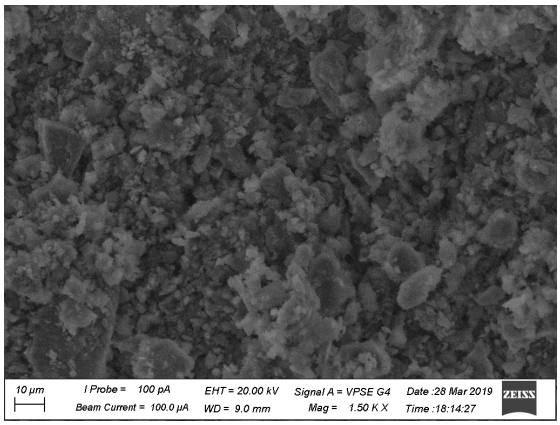


Figure 5.10: Pore structure of C12 aggregate

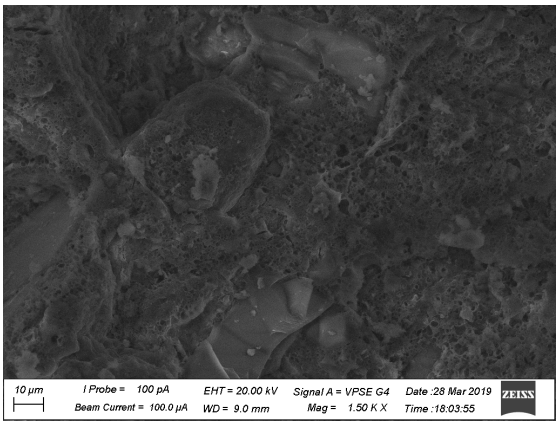


Figure 5.11: Pore structure of N9 aggregate

than other concrete samples. The effectiveness of N9 aggregate over C12 aggregate could be verified based on obtained results.

5.2.3 Compressive strength and workability

The compressive strength of the concrete mixtures produced using N9 aggregates are shown in Figure 5.13. According to Figure 5.13, ECC and ICC/N9 samples achieved almost the same compressive strength during 7, 14 and 28 days. Moreover, ICC/N9 achieved higher strength than ECC at 28 days. NCC and ICC/N9 specimens were kept in open space without any external curing process that avoids moisture loss in concrete. As a result of that, NCC specimens did not achieve the designed compressive strength. It may be due to the ineffective hydration process and early age crack formation of NCC specimens.

ICC/N9 specimens achieved a higher compressive strength. It was almost equal to the compressive strength of ECC. In this case, internal curing aggregates play a major role by providing excess water to continue the hydration process. Thus, ICC/N9 specimens gained strength for a longer period without any restriction due to the moisture loss using internal water storages. The mean density and the slump of ECC concrete mix were 2402kg/m^{3}and 164mm respectively. Subsequently, ICC/N9 concrete achieved 2395 kg/m^3 density value and a 187mm slump value. According to those results, it can be proved that the produced aggregates functioned as an effective internal curing aggregates. Furthermore, those aggregates did not reduce the weight of concrete. Thus, these aggregates are not another type of LWA, but it is an effective internal curing aggregate.

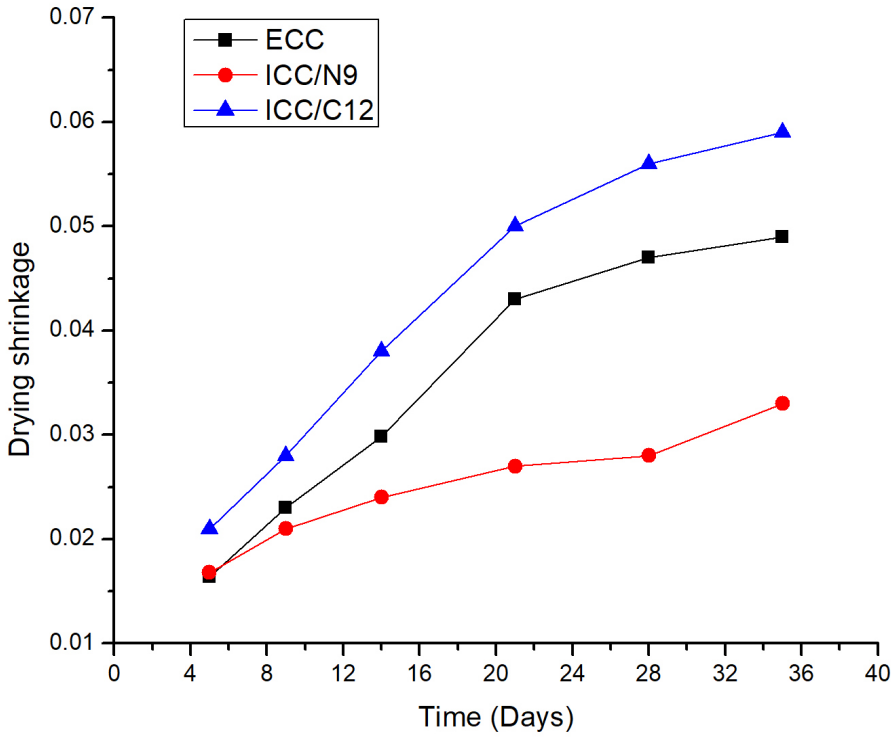


Figure 5.12: The average drying shrinkage of prepared concrete specimens.

Figure 5.14 shows the obtained results of concrete mixtures that prepared by using C12 aggregate. ICC/3EC/C12 specimens were prepared to study the combined effect of internal curing and external curing. The mean density and the slump of ECC concrete were 2398 kg/m^3 and 160mm respectively. ICC/C12 concrete achieved 2393 kg/m^3 density and a 182mm slump. According to Figure 5.14, ECC sample achieved higher compressive strength than ICC/C12 and ICC/3EC/C12 concrete samples within 28 days.

After mixing, all the concrete specimens were saturated with enough moisture to continue the hydration process. Available moisture reduced with time due to the evaporation and hydration process. On the other hand, external water could not penetrate the concrete system and relative humidity of the concrete reduced. As a result of that, ICC/C12 concrete samples exhibited higher drying shrinkage than conventional concrete as shown in Figure 5.12. Consequently, the strength gaining of ICC/C12 and ICC/3EC/C12 specimens were restricted and achieved lower compressive strength than ECC sample after 28 days. Moreover, there was a considerable reduction in compressive strength of ICC/C12 and ICC/3EC/C12 concrete samples at 7 and14 days but it was greater than NCC sample.

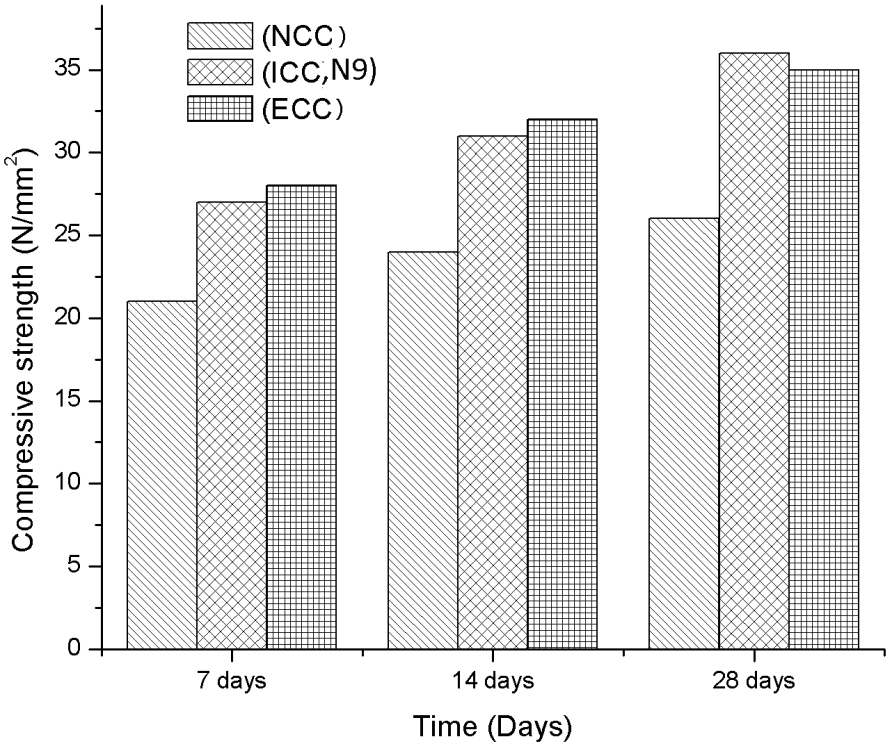


Figure 5.13: The compressive strength of ICC/N9.

As relative humidity decreases, water stored inside relatively tiny pores of C12 aggregate released due to higher capillary force. The strength gaining of ICC/C12 and ICC/3EC/C12 were increased between 14 and 28 days. Even though, ICC/C12 and ICC/3EC/C12 samples achieved the design compressive strength at 28 days, it is lower than the ECC sample. Moreover, the drying shrinkage values were much high in those samples compared to ECC samples. As a result of that, C12 aggregate failed to perform as an effective internal curing aggregate.

In ICC/N9 concrete specimen N9 aggregate provided excess water to continue the hydration process, enabling the strength gaining of ICC specimens for a long period. Moreover, it achieved its maximum strength for a longer period, using the internal water storage. As a result of that, ICC/N9 sample achieved slightly, higher compressive strength than the ECC/N9 sample. In ICC/C12 concrete specimen C12 aggregate failed to provide required amount of water at early stage due to the low water desorption properties.

According to Figure 5.14, the development of the compressive strength can be verified by comparing the results of NCC and ICC/N9 samples. NCC samples had comparatively much lower compressive strength value due to poor hydration process but,

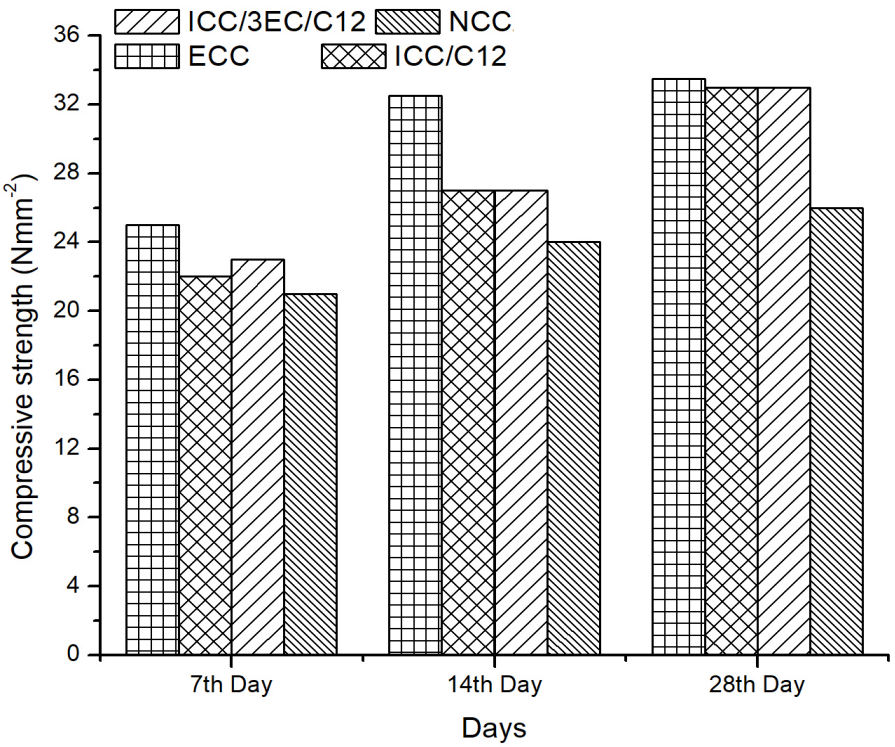


Figure 5.14: The compressive strength of ICC/C12

ICC/N9 samples achieved comparatively high strength as a result of adding N9 aggregate. Thus, the aggregate will enhance the cement hydration process and increase the compressive strength of concrete. According to those results, it can be proved that N9 aggregate functioned as effective internal curing aggregates meanwhile C12 aggregate failed to function as an effective ICA.

Table 5.3 shows variation of the compressive strength and workability according to the grade of concrete. According to Table 5.3, ECC and ICC samples achieved almost the same compressive strength during 7,14 and 28 days.

Furthermore, concrete with ICC aggregate achieved higher slump resulting high workability of the concrete without affecting to the concrete strength. It proved that water/ cement ratio can be reduced with ICC aggregates and higher grade of concrete can be produced without increasing the cement content. On the other hand, Internal curing concrete have higher rate of strength gaining after 14 days. Thus, ICC will achieve higher strength more than the conventional concrete in the later stage. It can be verified according to the test results of Table 5.3.

Table 5.3: The variation of the compressive strength and workability according to the grade of concrete.

Concrete Grade	Concrete type	Compressive strength (N/mm^2)			Slump
		7^{th} day	14^{th} day	28^{th} day	mm
Grade 25	ECC	22.46	26.7	27.88	195
	ICC	19.97	22.91	28.18	225
Grade 30	ECC	23.26	29.89	36.47	175
	ICC	22.08	26.44	35.22	195
Grade 35	ECC	29.78	35.96	36.43	160
	ICC	28.39	33.8	36.37	180

5.3 Summary

According to the obtained results, the effectiveness of the N9 aggregate over C12 aggregate in the production of internal curing concrete can be proved. The concrete mixtures which consist of C12 and N9 aggregates achieved the design compressive strength at 28 days. Moreover, C12 aggregate absorbed more water than the N9 aggregate, but C12 released less amount of water compared to the N9 aggregate. Thus, C12 aggregates increased the drying shrinkage of the internal curing concretes compare to the conventional concrete, but N9 aggregates reduced the drying shrinkage of concrete. As a result of that, C12 aggregates failed to act as an effective internal curing aggregate due to higher drying shrinkage, but N9 aggregates acted as an effective internal curing aggregate due to lower drying shrinkage and higher compressive strength at 28 days. The test results obtained from different grades of internal curing concrete shows that whatever the concrete grade is, internal curing concrete increased the workability of concrete without affecting the concrete strength. Based on these results and the findings of the research, recommendations were provided to develop internal curing aggregate in chapter 6.

CHAPTER 6

CONCLUSIONS AND RECOMMENDATIONS

Internal curing requires internal water reservoirs to produce ICC. As a result of that, researchers have been investigating on different materials to produce ICC since Roman time. Some researchers developed internal curing mix-designs using different porous aggregates. Those types of natural aggregates are not available in most countries. As a result of that, different researchers produced ICC using manufactured porous aggregates but still, there are drawbacks of using those materials for ICC production. Thus, an effective pore structure was developed throughout this study based on pore size, pore connectivity, pore expansion and the compressive strength of pore structure.

Following are the major conclusions derived from the study.

- Water absorption, water desorption, density and distribution are the main requirements of a internal curing aggregate (ICA). Water absorption of ICA should be greater than 15% within 48hours, water desorption should be greater than 90% at 94% relative humidity, density (dry apparent density) should be greater than 1.4g/cm3.
- According to the ASTM C33/C33M standard, the fineness modulus of fine aggregate should be not less than 2.3 nor more than 3.1 to use in load bearing structures. Moreover, fine aggregates which have the fineness modulus of 2.3 or 3.1 protect 99% or 91% of concrete uniformly distributed water throughout the concrete. Thus, the fineness module ranging from 2.3 to 3.1 is suitable as a grading specification for the ICA.
- Material type, heating rate, heating temperature, sample size, heating environment are the main parameters of the clay firing process. Different pore structures can be developed within clay mass by changing those parameters.

- All the types of non-expansive clays are not suitable to produce the effective pore structure. Clay materials which Kp ranges from 1.1 to 1.5, are the most suitable material to produce optimum pore structure. Thus, unbloated non-expansive materials are not suitable to produce internal curing aggregate.
- Pore connectivity, pore size, pore expansion and the compressive strength are the main parameters of any pore structure. In order to produce effective ICA, open porosity should be greater than 27.5%, the mean pore size should range from 0.3 to 10μm, the pore expansion (Kp) should exist between 1.1 to 1.5 and the compressive strength of pore structure should be greater than 3.5 N/mm2. When any porous material satisfies those limits of the pore structure as shown in Figure 6.1, it can be used as an effective ICA.



Figure 6.1: Parameters of Effective pore structure.

6.1 Recommendations and future work

This study has enclosed a new area to understand the behavior of porous structure in the development of internal curing properties. This is important in the production of ICA to produce ICC. The pore structure of heated clay mass can be controlled as required, during the firing process. Through this study, the effect of firing temperature and the material type was observed. Future development can be focused on the development

of pore structure controlling other parameters of the firing process and to develop an optimum heating process. Furthermore, the potential of bloating in non-expansive clay can be improved using additives. Thus, it enclosed another area for researchers to optimize the heating process using different additives.

References

[1] D. P. Bentz and W. J. Weiss, *Internal curing: a 2010 state-of-the-art review*. US Department of Commerce, National Institute of Standards and Technology , 2011.

[2] K. Kovler, "Smart additives for self-curing concrete," *MRS Online Proceedings Library Archive*, vol. 1488, 2012.

[3] ACI, "American concrete institute," *ACI Concrete Terminology, Farmington Hills, MI*, vol. 1, pp. Pg;58–59, 2013.

[4] R. Henkensiefken, D. Bentz, T. Nantung, and J. Weiss, "Volume change and cracking in internally cured mixtures made with saturated lightweight aggregate under sealed and unsealed conditions," *Cement and Concrete Composites*, vol. 31, no. 7, pp. 427–437, 2009.

[5] T. C. Powers, L. E. Copeland, and H. Mann, "Capillary continuity or discontinuity in cement pastes," tech. rep., 1959.

[6] A. Babcock and P. Taylor, "Impacts of internal curing on concrete properties: Literature review," report, 2015.

[7] A. M. Neville *et al.*, *Properties of concrete*, vol. 4. Longman London, 1995.

[8] K. W. Meeks and N. J. Carino, *Curing of high-performance concrete: Report of the state-of-the-art*. Citeseer, 1999.

[9] C. Rao and M. Darter, "Evaluation of internally cured concrete for paving applications," *Applied Research Associates, Champaign, IL*, 2013.

[10] K. Raoufi, J. Schlitter, D. Bentz, and J. Weiss, "Parametric assessment of stress development and cracking in internally cured restrained mortars experiencing autogenous deformations and thermal loading," *Advances in Civil Engineering*, vol. 2011, 2011.

[11] M. Golias, J. Castro, and J. Weiss, "The influence of the initial moisture content of lightweight aggregate on internal curing," *Construction and Building Materials*, vol. 35, pp. 52–62, 2012.

[12] S. Ahmad, "Reinforcement corrosion in concrete structures, its monitoring and service life predictiona review," *Cement and Concrete Composites*, vol. 25, no. 4-5, pp. 459–471, 2003.

[13] N. Delatte *et al.*, "Evaluation of high absorptive materials to improve internal curing of low permeability concrete:[executive summary]," tech. rep., Ohio. Dept. of Transportation. Office of Research and Development, 2007.

[14] R. Henkensiefken, P. Briatka, D. Bentz, T. Nantung, and J. Weiss, "Plastic shrinkage cracking in internally cured mixtures made with pre-wetted lightweight aggregate," *Concrete international*, vol. 32, no. 2, pp. 49–54, 2010.

[15] M. R. Geiker, D. P. Bentz, and O. M. Jensen, "Mitigating autogenous shrinkage by internal curing," *ACI Special Publications*, pp. 143–154, 2004.

[16] B. Persson and G. Fagerlund, "3 rd international research seminar on self-desiccation and its importance in concrete technology," 2002.

[17] T. Friggle and D. Reeves, "Internal curing of concrete paving: laboratory and field experience," *Special Publication*, vol. 256, pp. 71–80, 2008.

[18] C. Ozyildirim, "Evaluation of ultra-high-performance fiber-reinforced concrete, final report vctir 12-r1," *Virginia Center for Transportation Innovation and Research, Charlottesville, VA, USA*, 2011.

[19] E. E. Holt, *Early age autogenous shrinkage of concrete*, vol. 446. Technical Research Centre of Finland Espoo, Finland, 2001.

[20] E.-i. Tazawa, S. Miyazawa, and T. Kasai, "Chemical shrinkage and autogenous shrinkage of hydrating cement paste," *Cement and concrete research*, vol. 25, no. 2, pp. 288–292, 1995.

[21] T. Zhang, P. Gao, R. Luo, Y. Guo, J. Wei, and Q. Yu, "Measurement of chemical shrinkage of cement paste: Comparison study of astm c 1608 and an improved method," *Construction and Building Materials*, vol. 48, pp. 662–669, 2013.

[22] D. P. Bentz, P. Lura, and J. W. Roberts, "Mixture proportioning for internal curing," *Concrete international*, vol. 27, no. 02, pp. 35–40, 2005.

[23] D. P. Bentz and K. A. Snyder, "Protected paste volume in concrete: Extension to internal curing using saturated lightweight fine aggregate," *Cement and concrete research*, vol. 29, no. 11, pp. 1863–1867, 1999.

[24] D. F. Alberty R, *Physical Chemistry*. John Wiley & Sons, 1980.

[25] T. Ayano and F. H. Wittmann, "Drying, moisture distribution, and shrinkage of cement-based materials," *Materials and Structures*, vol. 35, no. 3, pp. 134–140, 2002.

[26] Z.-B. Zhang and J. Zhang, "Experimental study on relationship between shrinkage strain and environmental humidity of concrete.," *Jianzhu Cailiao Xuebao(Journal of Building Materials)*, vol. 9, no. 6, pp. 720–723, 2006.

[27] B. Bissonnette, P. Pierre, and M. Pigeon, "Influence of key parameters on drying shrinkage of cementitious materials," *Cement and Concrete Research*, vol. 29, no. 10, pp. 1655–1662, 1999.

[28] T. Y. Lo, W. C. Tang, and H. Z. Cui, "The effects of aggregate properties on lightweight concrete," *Building and Environment*, vol. 42, no. 8, pp. 3025–3029, 2007.

[29] ASTM-C330/C330M, "Standard specification for lightweight aggregates for structural concrete," 2009.

[30] ASTM-C1761/C1761M, "Standard specification for lightweight aggregate for internal curing of concrete," 2017.

[31] ENV12620, "European standard for aggregates for concrete," p. 136, 2000.

[32] UNI-8520/2, "Italian standard for concrete aggregates," p. 12, 1997.

[33] J. L.Clarke, *Structural Lightweight Aggregate Concrete*. British Cement Association, 2006.

[34] ASTM-C33, "Standard specification for concrete aggregates," 2002.

[35] NortheastSoliteCorporation, "Internal curing specifications," 2017. "http://nesolite.com/internal-curing-specifications/,[Online;accessed12-May-2019]".

[36] W. J. Weiss and L. Montanari, "Guide specification for internally curing concrete," report, 2017.

[37] *Report 41: internal curing of concrete-state-of-the-art report of RILEM Technical Committee 196-ICC*, vol. 41. RILEM publications, 2007.

[38] P. Procho and T. Piotrowski, "Bound water content measurement in cement pastes by stoichiometric and gravimetric analyses," *Journal of Building Chemistry*, vol. 1, no. 1, pp. 18–25, 2016.

[39] I. Hager, "Behaviour of cement concrete at high temperature," *Bulletin of the Polish Academy of Sciences: Technical Sciences*, vol. 61, no. 1, pp. 145–154, 2013.

[40] J. Franjione and N. Vasishtha, "The art and science of microencapsulation," *Technology Today*, vol. 2, pp. 1–6, 1995.

[41] A. S. Hoffman, "Hydrogels for biomedical applications," *Advanced drug delivery reviews*, vol. 64, pp. 18–23, 2012.

[42] P. D. Drumheller and J. A. Hubbell, "Densely crosslinked polymer networks of poly (ethylene glycol) in trimethylolpropane triacrylate for cell-adhesion-resistant surfaces," *Journal of biomedical materials research*, vol. 29, no. 2, pp. 207–215, 1995.

[43] F. Buchhlz and T. Graham, "Modern superabsorbent polymer technology," *Tew York: Wiley-VCH*, 1998.

[44] O. M. Jensen and P. F. Hansen, "Water-entrained cement-based materials: Ii. experimental observations," *Cement and Concrete Research*, vol. 32, no. 6, pp. 973–978, 2002.

[45] M. T. Hasholt, M. H. S. Jespersen, and O. M. Jensen, "Mechanical properties of concrete with sap part i: Development of compressive strength," in *International RILEM conference on use of superabsorbent polymers and other new additives in concrete*, p. 10, RILEM Publications SARL, 2010.

[46] B. E. Byard, A. K. Schindler, R. W. Barnes, and A. Rao, "Cracking tendency of bridge deck concrete," *Transportation Research Record*, vol. 2164, no. 1, pp. 122–131, 2010.

[47] J.-P. Wang, E. Gallo, B. Franois, F. Gabrieli, and P. Lambert, "Capillary force and rupture of funicular liquid bridges between three spherical bodies," *Powder Technology*, vol. 305, pp. 89–98, 2017.

[48] T. C. Hansen and H. Narud, "Strength of recycled concrete made from crushed concrete coarse aggregate," *Concrete International*, vol. 5, no. 01, pp. 79–83, 1983.

[49] S. T. Yildirim, C. Meyer, and S. Herfellner, "Effects of internal curing on the strength, drying shrinkage and freeze–thaw resistance of concrete containing recycled concrete aggregates," *Construction and Building Materials*, vol. 91, pp. 288–296, 2015.

[50] H. Kim and D. Bentz, "Internal curing with crushed returned concrete aggregates for high performance concrete," in *NRMCA Concrete Technology Forum: Focus on Sustainable Development*, pp. 20–22, Citeseer, 2008.

[51] R. De Gennaro, P. Cappelletti, G. Cerri, M. De'Gennaro, M. Dondi, S. Graziano, and A. Langella, "Campanian ignimbrite as raw material for lightweight aggregates," *Applied clay science*, vol. 37, no. 1-2, pp. 115–126, 2007.

[52] C. Cheeseman and G. Virdi, "Properties and microstructure of lightweight aggregate produced from sintered sewage sludge ash," *Resources, Conservation and Recycling*, vol. 45, no. 1, pp. 18–30, 2005.

[53] A. L. Bush, D. P. Bryan, and D. R. Hack, "Lightweight aggregates," *Industrial Minerals and Rocks: Commodities, Markets, and Uses*, pp. 181–194, 2006.

[54] J. L. Clarke, *Structural lightweight aggregate concrete*. CRC Press, 1993.

[55] K. Kovler and O. Jensen, "Internal curing of concrete, state-of-the-art report of rilem technical committee 196-icc," *RILEM Report*, vol. 41, 2007.

[56] S. Weber and H. W. Reinhardt, "A new generation of high performance concrete: concrete with autogenous curing," *Advanced cement based materials*, vol. 6, no. 2, pp. 59–68, 1997.

[57] P. Lura, "Autogenous deformation and internal curing of concrete," 2003.

[58] E. Fakhfakh, W. Hajjaji, M. Medhioub, F. Rocha, A. López-Galindo, M. Setti, F. Kooli, F. Zargouni, and F. Jamoussi, "Effects of sand addition on production of lightweight aggregates from tunisian smectite-rich clayey rocks," *Applied Clay Science*, vol. 35, no. 3-4, pp. 228–237, 2007.

[59] S. Zhutovsky, K. Kovler, and A. Bentur, "Autogenous curing of high-strength concrete using pre-soaked pumice and perlite sand," in *Self-desiccation and*

its importance in concrete technology, Proceedings 3rd International Research Seminar, Lund, Sweden, pp. 161–173, 2002.

[60] M. H. Zhang and O. E. Gjvorv, "Mechanical properties of high-strength lightweight concrete," *Materials Journal*, vol. 88, no. 3, pp. 240–247, 1991.

[61] S. Weber and H. Reinhardt, "Manipulating the water content and microstructure of high performance concrete using autogeneous curing," in *Modern concrete materials: binders, additions and admixtures*, pp. 567–577, Thomas Telford Publishing, 1999.

[62] S.-C. Huang, F.-C. Chang, S.-L. Lo, M.-Y. Lee, C.-F. Wang, and J.-D. Lin, "Production of lightweight aggregates from mining residues, heavy metal sludge, and incinerator fly ash," *Journal of hazardous materials*, vol. 144, no. 1, pp. 52–58, 2007.

[63] K. A. V. D. Vaickelionis, Giedrius, "Production of expanded clay pellets by using non-selfbloating clay, lakes sapropel and glycerol," *Materials Science*, vol. 17, no. 3, pp. 314–321, 2011.

[64] L. Pioro and I. Pioro, "Production of expanded-clay aggregate for lightweight concrete from non-selfbloating clays," *Cement and concrete composites*, vol. 26, no. 6, pp. 639–643, 2004.

[65] O. M. Jensen, *Report 41: internal curing of concrete-state-of-the-art report of RILEM Technical Committee 196-ICC*, vol. 41. RILEM publications, 2007.

[66] A. S. El-Dieb, T. A. El-Maaddawy, and A. A. Mahmoud, "Water-soluble polymers as self-curing agents in cement mixes," *Advances in cement research*, vol. 24, no. 5, pp. 291–299, 2012.

[67] S. Evangeline, "Self curing concrete and its inherent properties," *International Journal of Engineering Research and Applications*, vol. 4, no. 8, 2014.

[68] C. Gallé, "Effect of drying on cement-based materials pore structure as identified by mercury intrusion porosimetry: a comparative study between oven-, vacuum-, and freeze-drying," *Cement and Concrete Research*, vol. 31, no. 10, pp. 1467–1477, 2001.

[69] S. Diamond, "Mercury porosimetry: an inappropriate method for the measurement of pore size distributions in cement-based materials," *Cement and concrete research*, vol. 30, no. 10, pp. 1517–1525, 2000.

[70] B. Li, J. Mao, J. Lv, and L. Zhou, "Effects of micropore structure on hydration degree and mechanical properties of concrete in later curing age," *European Journal of Environmental and Civil Engineering*, vol. 20, no. 5, pp. 544–559, 2015.

[71] Y. Tsunazawa, T. Yokoyama, and N. Nishiyama, "An experimental study on the rate and mechanism of capillary rise in sandstone," *Progress in Earth and Planetary Science*, vol. 3, no. 1, p. 8, 2016.

[72] L. A. Richards, "Capillary conduction of liquids through porous mediums," *physics*, vol. 1, no. 5, pp. 318–333, 1931.

[73] D. M. Mattox, "Chapter 2-substrate (real) surfaces and surface modification," *Handbook of Physical Vapor Deposition (PVD) Processing*, vol. 2, 2010.

[74] O. Akinshipe and G. Kornelius, "Chemical and thermodynamic processes in clay brick firing technologies and associated atmospheric emissions metrics-a review," *J Pollut Eff Cont*, vol. 5, no. 190, p. 2, 2017.

[75] D. M. Moore and R. C. Reynolds, *X-ray Diffraction and the Identification and Analysis of Clay Minerals*, vol. 322. Oxford university press Oxford, 1989.

[76] H. Murray, "Applied clay mineralogy. developments in clay science, vol. 2," 2007.

[77] A. Bennour, S. Mahmoudi, E. Srasra, S. Boussen, and N. Htira, "Composition, firing behavior and ceramic properties of the sejnne clays (northwest tunisia)," *Applied Clay Science*, vol. 115, pp. 30–38, 2015.

[78] S. K. T. Khafaji and E. A. Al-Majed, "Synthesis of light expanded clay aggregates from iraqi raw materials," 2016.

[79] D. Morgan, "Thermal analysisincluding evolved gas analysisof clay raw materials," *Applied clay science*, vol. 8, no. 2-3, pp. 81–89, 1993.

[80] D. Dos Santos, R. Toledo, R. Faria Jr, J. Carri, M. Da Silva, L. Auler, and H. Vargas, "Evolved gas analysis of clay materials," *Review of scientific instruments*, vol. 74, no. 1, pp. 663–666, 2003.

[81] C. M. Riley, "Relation of chemical properties to the bloating of clays," *Journal of the American Ceramic Society*, vol. 34, no. 4, pp. 121–128, 1951.

[82] C. Vieira, P. Da Silva, F. Da Silva, J. Capitaneo, and S. Monteiro, "Microstructural evaluation and properties of a ceramic body for extruded floor tiles," *Revista Matéria*, vol. 10, no. 4, pp. 526–536, 2005.

[83] I. tuba, T. Hlan, T. Kaljuvee, and L. Vozr, "Investigation of dynamic mechanical properties of estonian clay arumetsa during firing," *Applied Clay Science*, vol. 153, pp. 23–28, 2018.

[84] J. Pacini, "Bloating and black coring," *Laguna Clay Co*, 1999.

[85] K. MacKenzie and C. Cardile, "A 57 fe mössbauer study of black coring phenomena in clay-based ceramic materials," *Journal of Materials Science*, vol. 25, no. 6, pp. 2937–2942, 1990.

[86] L. Gredmaier, C. Banks, and R. Pearce, "Calcium and sulphur distribution in fired clay brick in the presence of a black reduction core using micro x-ray fluorescence mapping," *Construction and Building Materials*, vol. 25, no. 12, pp. 4477–4486, 2011.

[87] C. Rathossi and Y. Pontikes, "Effect of firing temperature and atmosphere on ceramics made of nw peloponnese clay sediments. part i: Reaction paths, crystalline phases, microstructure and colour," *Journal of the European Ceramic Society*, vol. 30, no. 9, pp. 1841–1851, 2010.

[88] B. Butterworth and D. Honeyborne, "Bricks and clays of the hastings beds," *Transactions of the British Ceramic Society*, vol. 51, pp. 211–259, 1952.

[89] F. Negre, A. Barba, J. Amoros, and A. Escardino, "Oxidation of black core during the firing of ceramic ware-2. process kinetics," *British Ceramic Transactions*, pp. 5–11, 1992.

[90] R. Toledo, D. Dos Santos, R. Faria Jr, J. Carrió, L. Auler, and H. Vargas, "Gas release during clay firing and evolution of ceramic properties," *Applied Clay Science*, vol. 27, no. 3-4, pp. 151–157, 2004.

[91] A. Barba, F. Negre, M. Ortis, and A. Escardino, "Oxidation of black core during the firing of ceramic ware-3. influence of the thickness of the piece and the composition of the black core," *British Ceramic Transactions*, vol. 91, pp. 36–46, 1992.

[92] A. A. Kadir and A. Mohajerani, "Effect of heating rate on gas emissions and properties of fired clay bricks and fired clay bricks incorporated with cigarette butts," *Applied Clay Science*, vol. 104, pp. 269–276, 2015.

[93] R. Arnold and G. H. Duncombe Jr, "Clay sewerpipe manufacture1 vi. heatbalance determinations," *Journal of the American Ceramic Society*, vol. 12, no. 6, pp. 410–422, 1929.

[94] E. Rowden, *The firing of Bricks*. Brick Development Association, 1964.

[95] B. Cicel, I. Novák, and I. Horváth, "Mineralogy and crystallochemistry of clays," *SAV, Bratislava*, 1981.

[96] J. Hlavác, "Technology of silicates," *SNTL, Praha*, 1981.

[97] A. A. Kadir and A. Mohajerani, "Effect of heating rate on gas emissions and properties of fired clay bricks and fired clay bricks incorporated with cigarette butts," *Applied Clay Science*, vol. 104, pp. 269–276, 2015.

[98] W. Lee, G. Souza, C. McConville, T. Tarvornpanich, and Y. Iqbal, "Mullite formation in clays and clay-derived vitreous ceramics," *Journal of the European Ceramic Society*, vol. 28, no. 2, pp. 465–471, 2008.

[99] S. Karaman, S. Ersahin, and H. Gunal, "Firing temperature and firing time influence on mechanical and physical properties of clay bricks," 2006.

[100] E. Tsega, A. Mosisa, and F. Fufa, "Effects of firing time and temperature on physical properties of fired clay bricks," *American Journal of Civil Engineering*, vol. 5, no. 1, pp. 21–26, 2017.

[101] P. M. Velasco, M. P. M. Ortiz, M. A. M. Gir, D. M. Melia, and J. H. Rehbein, "Development of sustainable fired clay bricks by adding kindling from vine shoot: Study of thermal and mechanical properties," *Applied Clay Science*, vol. 107, pp. 156–164, 2015.

[102] M. Dondi, M. Marsigli, and I. Venturi, "Microstructure and mechanical properties of clay bricks: comparison between fast firing and traditional firing," *British Ceramic Transactions*, vol. 98, no. 1, pp. 12–18, 1999.

[103] L. Lorici and A. Brusa, "Porous and vitrified single-fired tiles," *Materials & Equipment/Whitewares: Ceramic Engineering and Science Proceedings*, pp. 183–184, 1991.

[104] "Methods of test for masonry units-part 4: determination of real and bulk density and of total and open porosity for natural stone masonry units.," *UNE-EN 7724*, 1999.

[105] A. C1424-10, "standard test method for monotonic compressive strength of advanced ceramics at ambient temperature," no. Code No: 81.060.30., 2012.

[106] S. Ahmari and L. Zhang, "Production of eco-friendly bricks from copper mine tailings through geopolymerization," *Construction and building materials*, vol. 29, pp. 323–331, 2012.

[107] J. Boulingui, C. Nkoumbou, D. Njoya, F. Thomas, and J. Yvon, "Characterization of clays from mezafe and mengono (ne-libreville, gabon) for potential uses in fired products," *Applied Clay Science*, vol. 115, pp. 132–144, 2015.

[108] P. Pialy, C. Nkoumbou, F. Villiras, A. Razafitianamaharavo, O. Barres, M. Pelletier, G. Ollivier, I. Bihannic, D. Njopwouo, and J. Yvon, "Characterization for industrial applications of clays from lembo deposit, mount bana (cameroon)," *Clay Minerals*, vol. 43, no. 3, pp. 415–435, 2008.

[109] S. Mahmoudi, A. Bennour, E. Srasra, and F. Zargouni, "Characterization, firing behavior and ceramic application of clays from the gabes region in south tunisia," *Applied Clay Science*, vol. 135, pp. 215–225, 2017.

[110] I. Waclawska, "Dehydratation and dehydroxylation of smectites. i: Dehydration and dehydroxylation kinetics," *Mineralogia polonica*, vol. 15, no. 1-2, pp. 91–107, 1984.

[111] H. Fan, B. Song, and Q. Li, "Thermal behavior of goethite during transformation to hematite," *Materials Chemistry and Physics*, vol. 98, no. 1, pp. 148–153, 2006.

[112] G. Brown, *Crystal structures of clay minerals and their X-ray identification*, vol. 5. The Mineralogical Society of Great Britain and Ireland, 1982.

[113] M. F. Serra, M. S. Conconi, G. Suarez, E. Agietti, and N. Rendtorff, "Firing transformations of an argentinean calcareous commercial clay," *Cermica*, vol. 59, no. 350, pp. 254–261, 2013.

[114] F. Pardo, M. Jordan, and M. Montero, "Ceramic behaviour of clays in central chile," *Applied Clay Science*, vol. 157, pp. 158–164, 2018.

[115] S. Mahmoudi, A. Bennour, A. Meguebli, E. Srasra, and F. Zargouni, "Characterization and traditional ceramic application of clays from the douiret region in south tunisia," *Applied Clay Science*, vol. 127, pp. 78–87, 2016.

[116] H. Azzouz, R. Alouani, and S. Tlig, "Mineralogical characterization of ceramic tiles prepared by a mixture of cretaceous and mio-pliocene clays from tunisia: factory and laboratory products," *Journal of the Ceramic Society of Japan*, vol. 119, no. 1386, pp. 93–100, 2011.

[117] K. Heide and M. Fldvari, "High temperature mass spectrometric gas-release studies of kaolinite al2 [si2o5 (oh) 4] decomposition," *Thermochimica Acta*, vol. 446, no. 1-2, pp. 106–112, 2006.

[118] A. C1424-10, "Common burnt clay building bricks specifications," *Indian Standard*, vol. fifth revision, no. IS 1077: 1992, 1992.

[119] J. Martín-Márquez, J. M. Rincón, and M. Romero, "Effect of firing temperature on sintering of porcelain stoneware tiles," *Ceramics International*, vol. 34, no. 8, pp. 1867–1873, 2008.

APPENDIX A

SEM images and identified pores

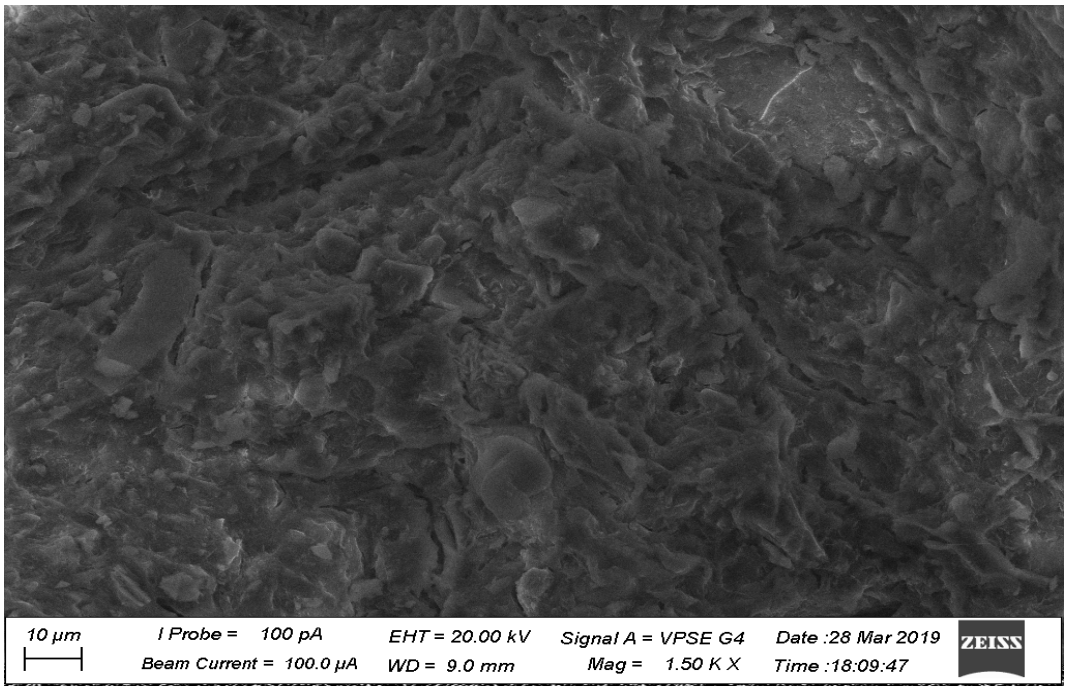


Figure A.1: Pore structure of the aggregate prepared at 800°C (Nachchaduwa clay)

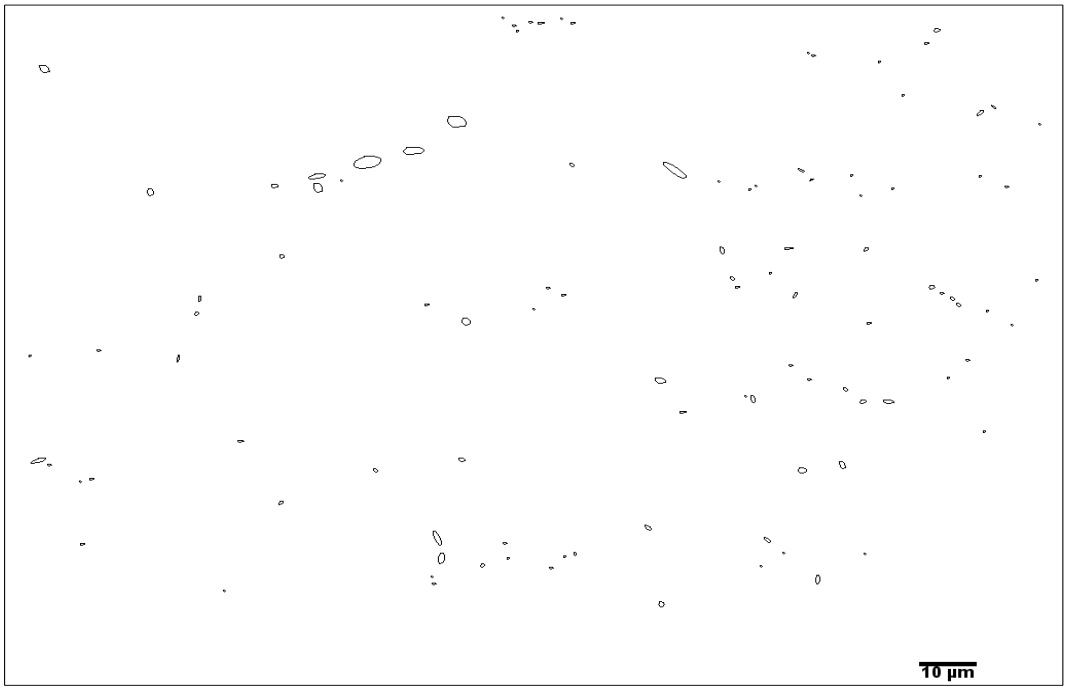


Figure A.2: Identified pore boundaries of the aggregate prepared at 800°C (Nachchaduwa clay)

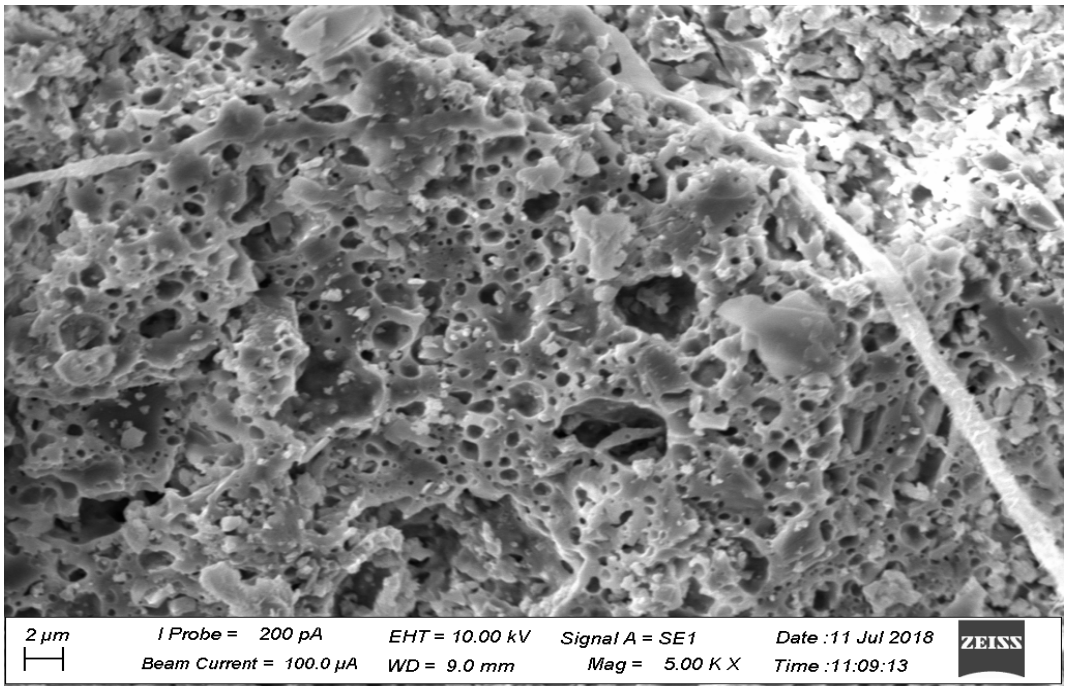


Figure A.3: Pore structure of the aggregate prepared at 900°C (Nachchaduwa clay)

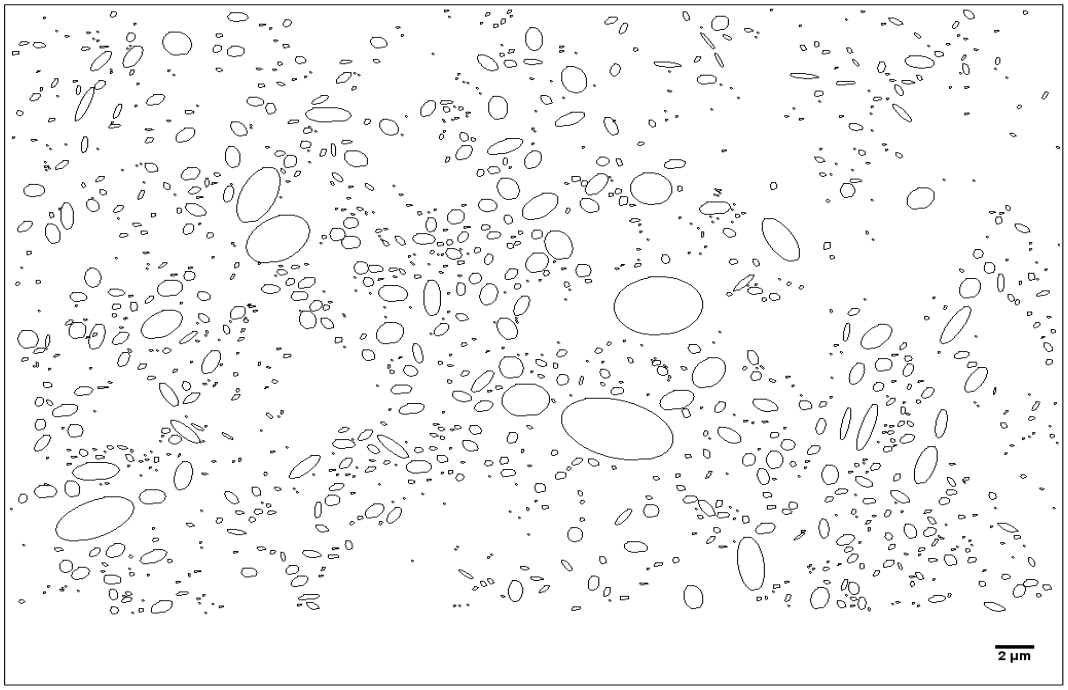


Figure A.4: Identified pore boundaries of the aggregate prepared at 900°C (Nachchaduwa clay)

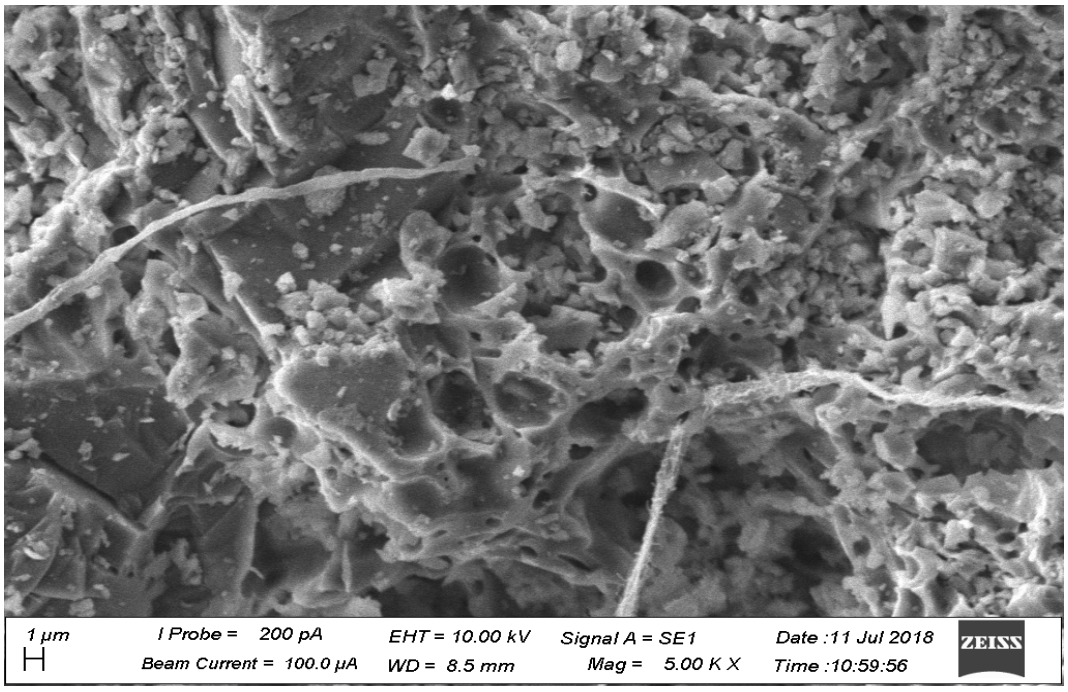


Figure A.5: Pore structure of the aggregate prepared at 1000°C (Nachchaduwa clay)

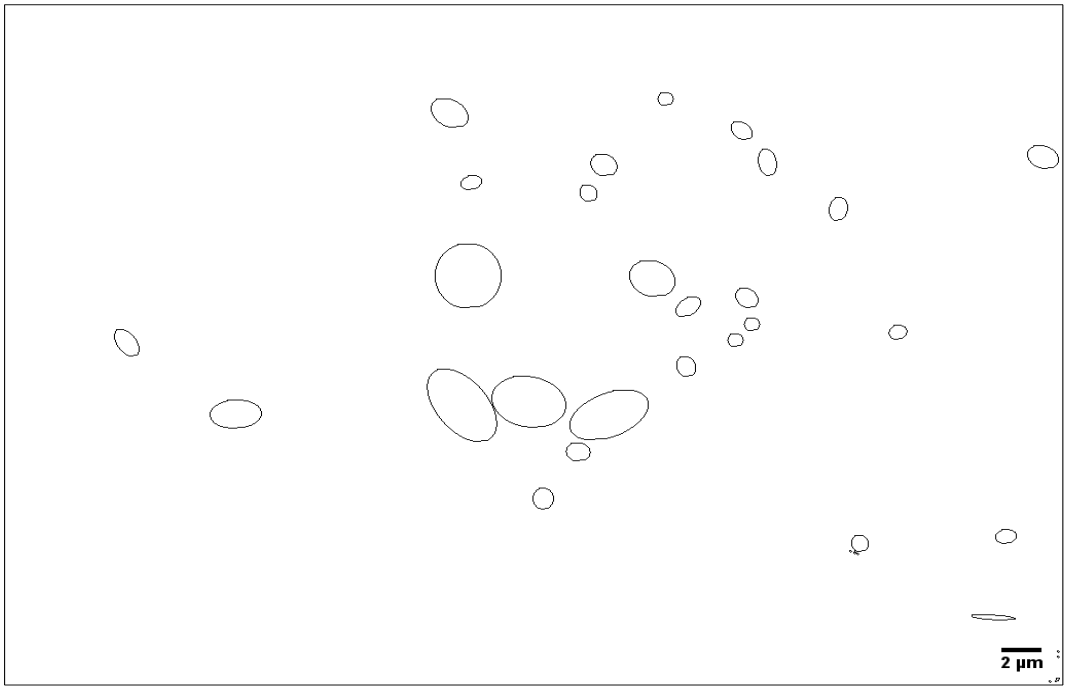


Figure A.6: Identified pore boundaries of the aggregate prepared at 1000°C (Nachchaduwa clay)

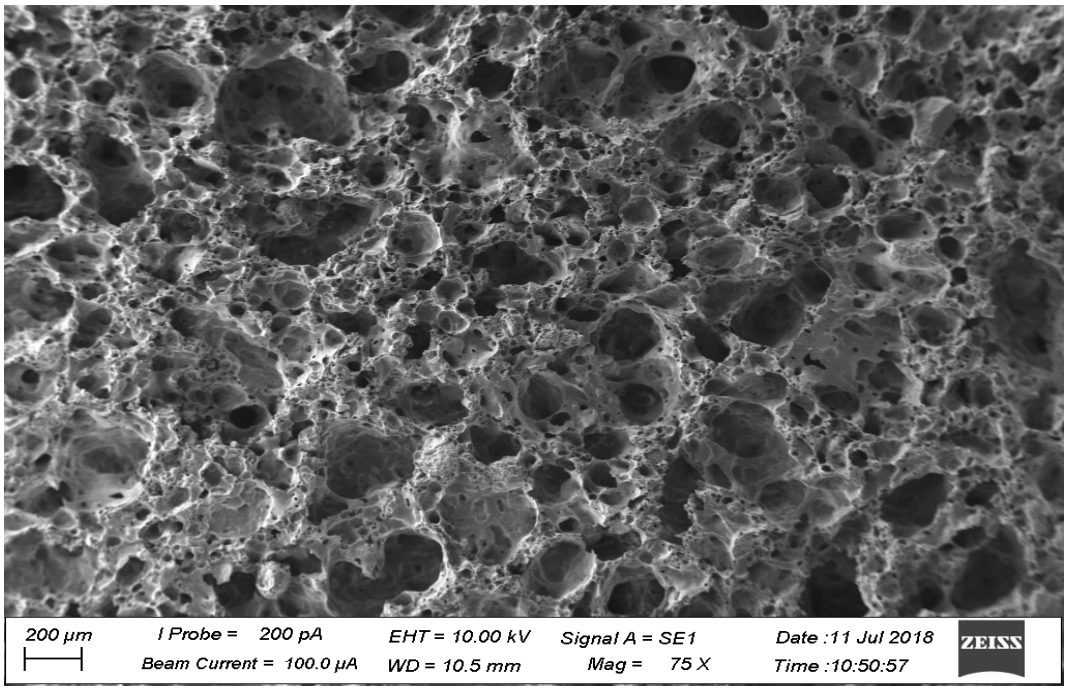


Figure A.7: Pore structure of the aggregate prepared at 1100°C (Nachchaduwa clay)

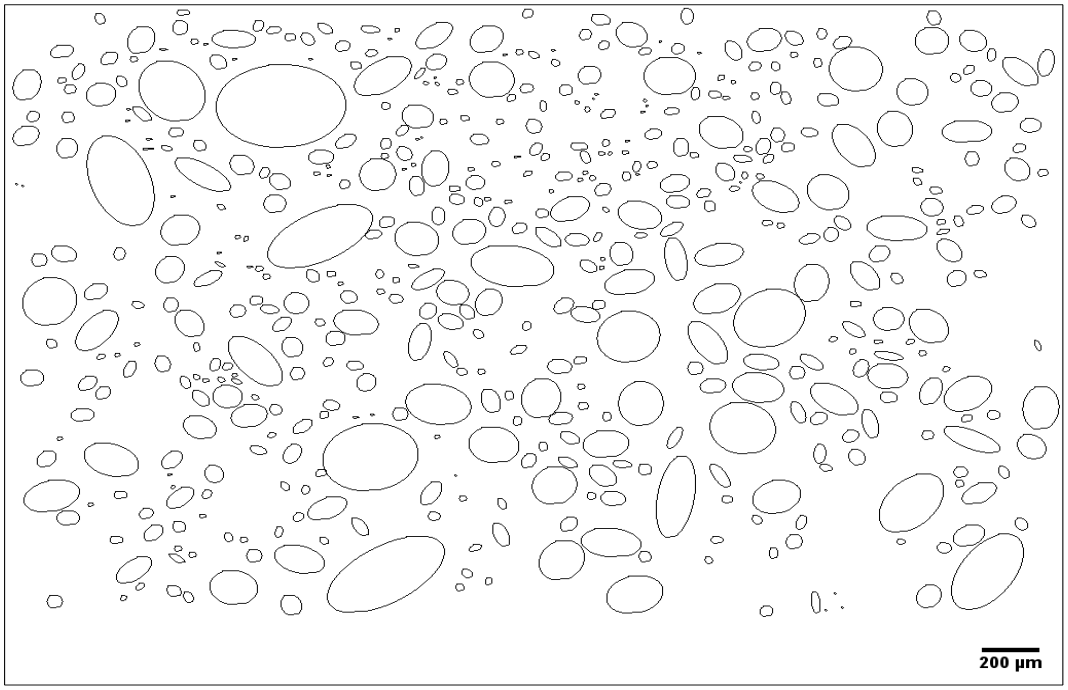


Figure A.8: Identified pore boundaries of the aggregate prepared at 1100°C (Nachchaduwa clay)

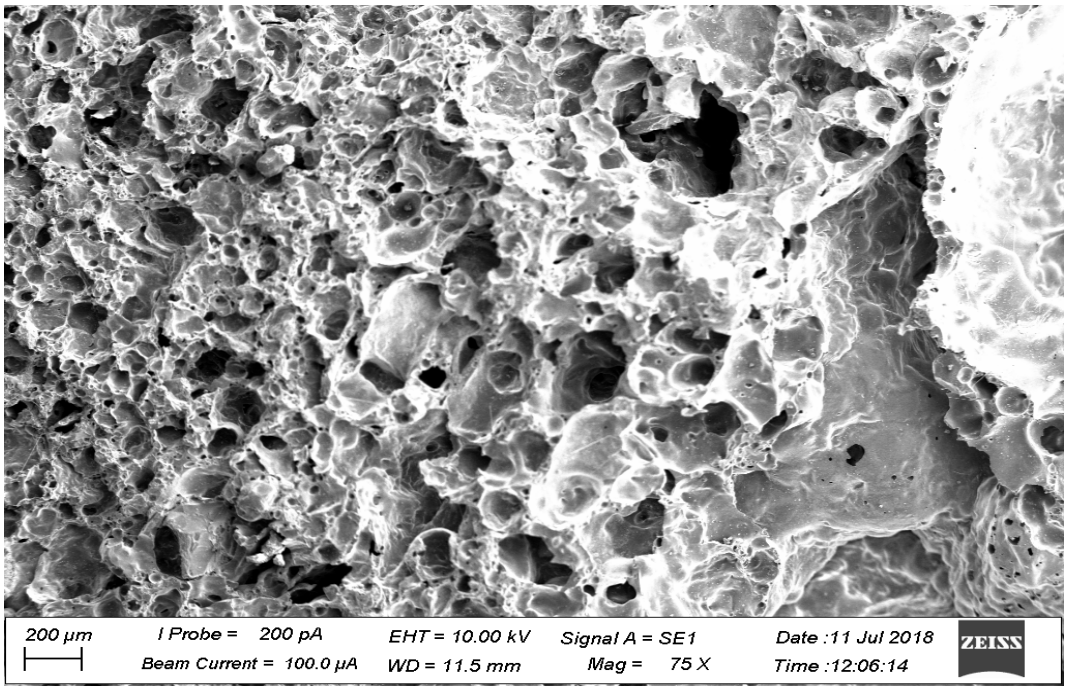


Figure A.9: Pore structure of the aggregate prepared at 1200°C (Nachchaduwa clay)

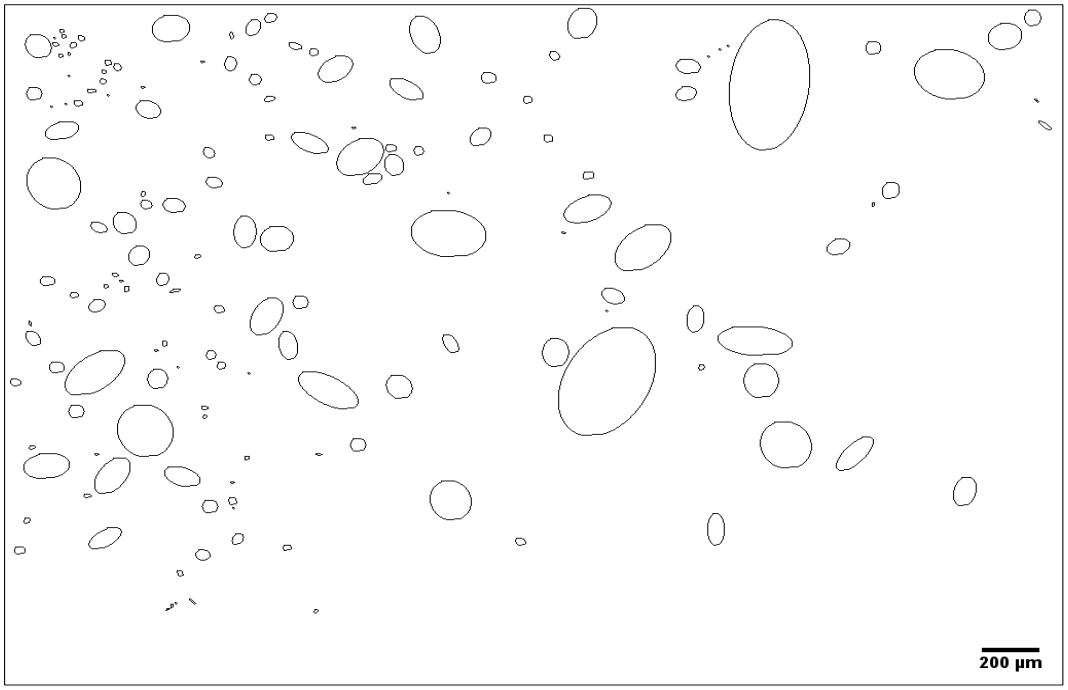


Figure A.10: Identified pore boundaries of the aggregate prepared at 1200°C (Nachchaduwa clay)

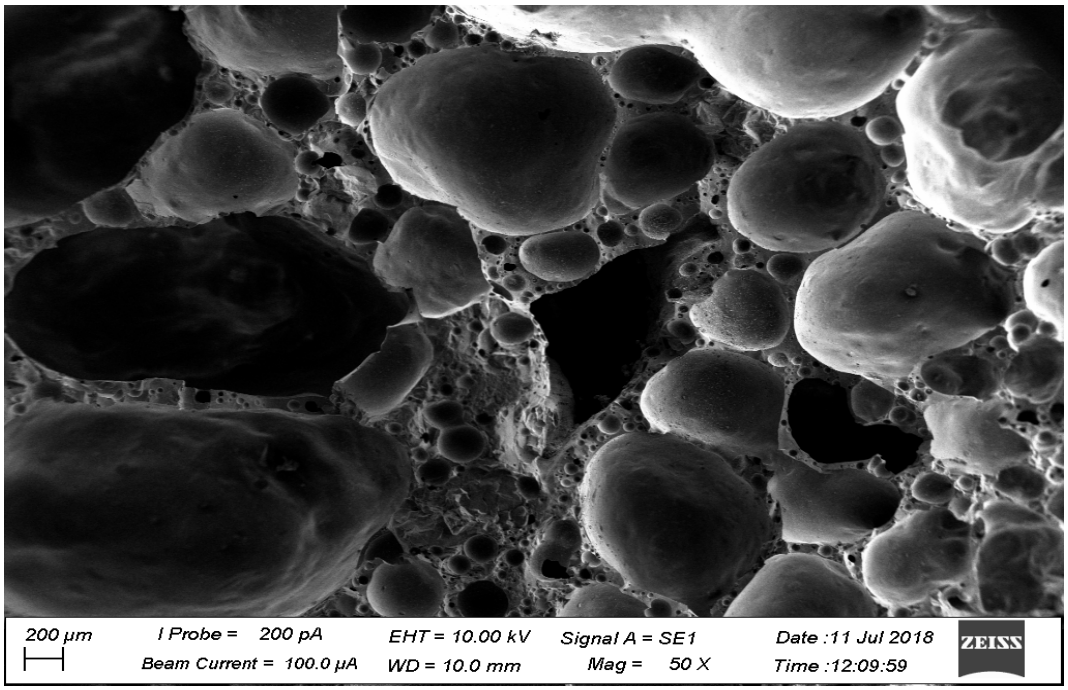


Figure A.11: Pore structure of the aggregate prepared at 1300°C (Nachchaduwa clay)

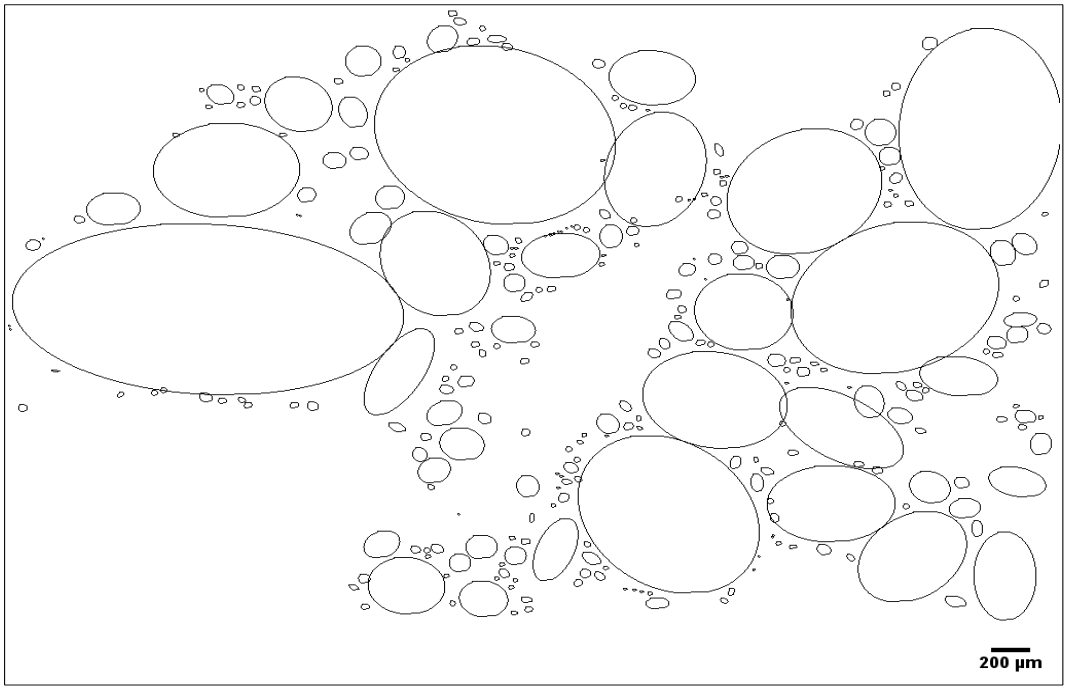


Figure A.12: Identified pore boundaries of the aggregate prepared at 1300°C (Nachchaduwa clay)

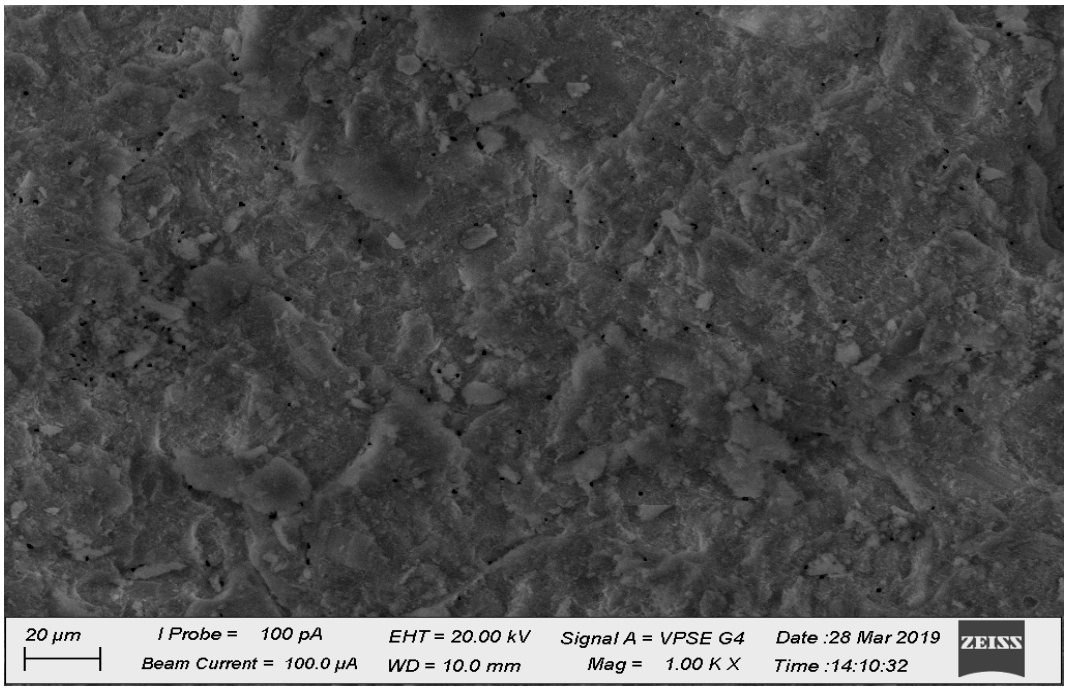


Figure A.13: Pore structure of the aggregate prepared at 800°C (Metiagoda clay)

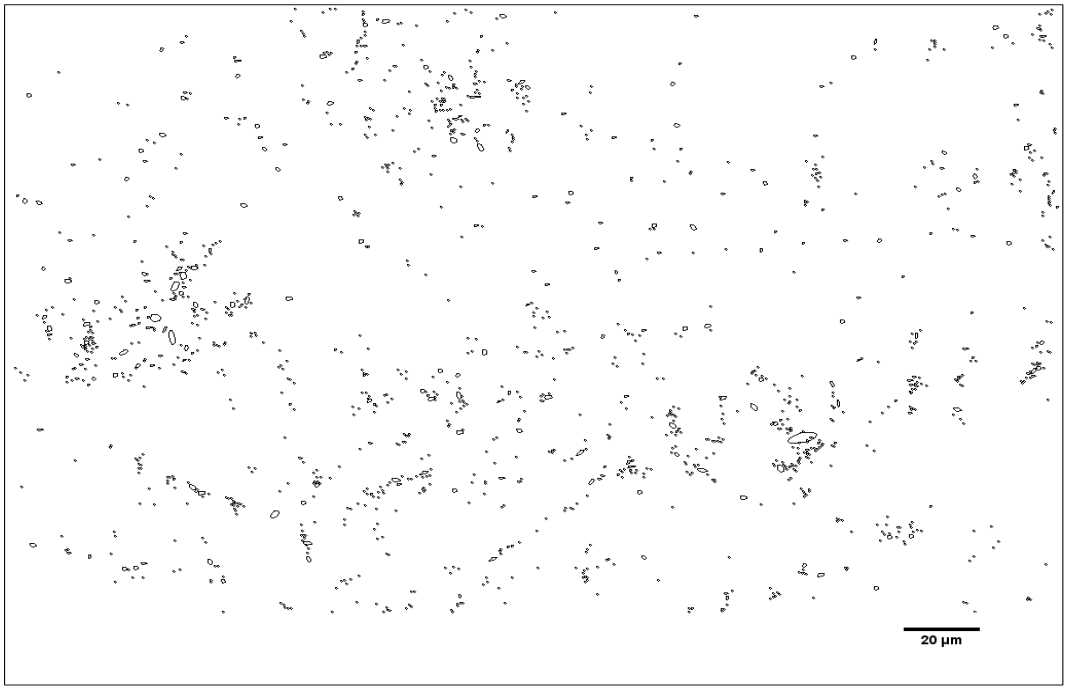


Figure A.14: Identified pore boundaries of the aggregate prepared at 800°C (Metiagoda clay)

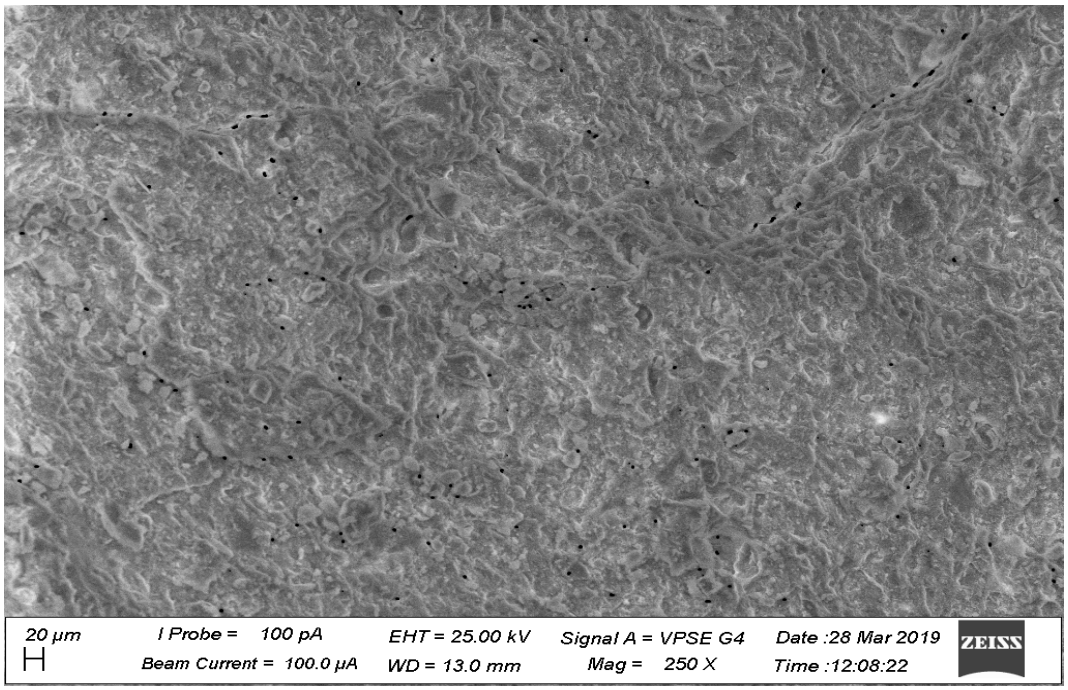


Figure A.15: Pore structure of the aggregate prepared at 900°C (Metiagoda clay)

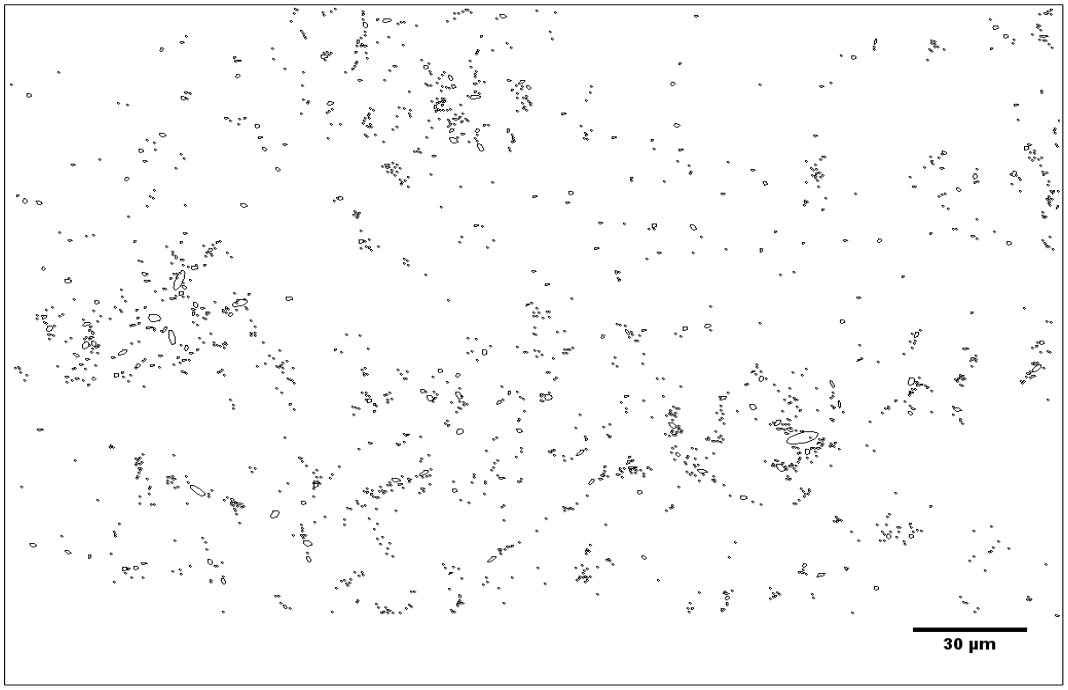


Figure A.16: Identified pore boundaries of the aggregate prepared at 900°C (Metiagoda clay)

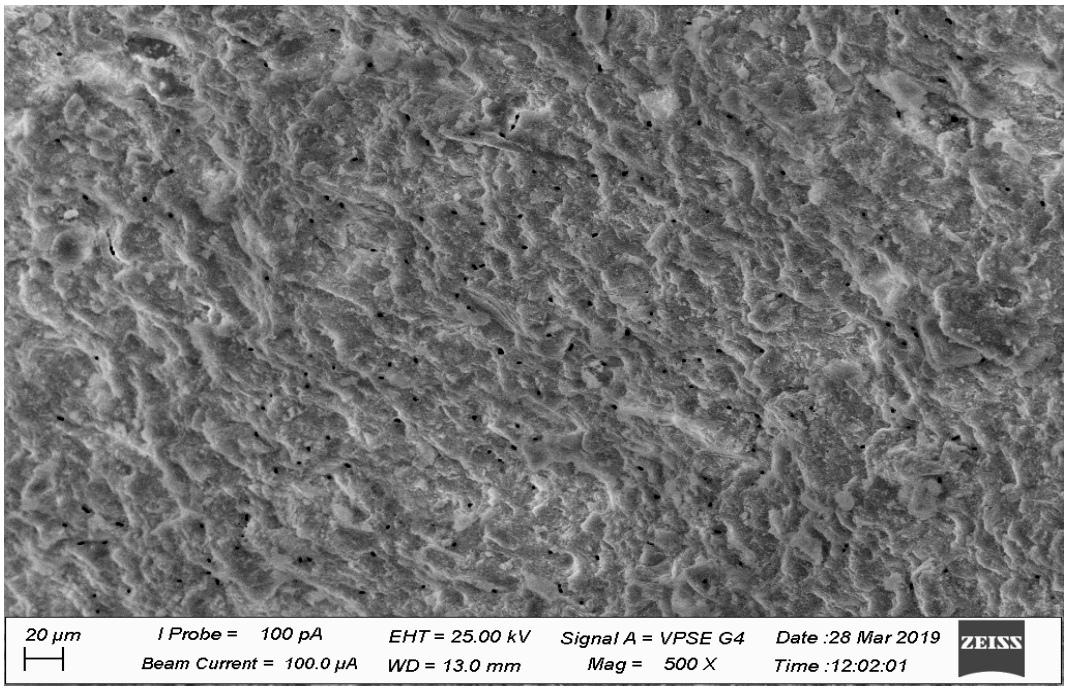


Figure A.17: Pore structure of the aggregate prepared at 1000°C (Metiagoda clay)

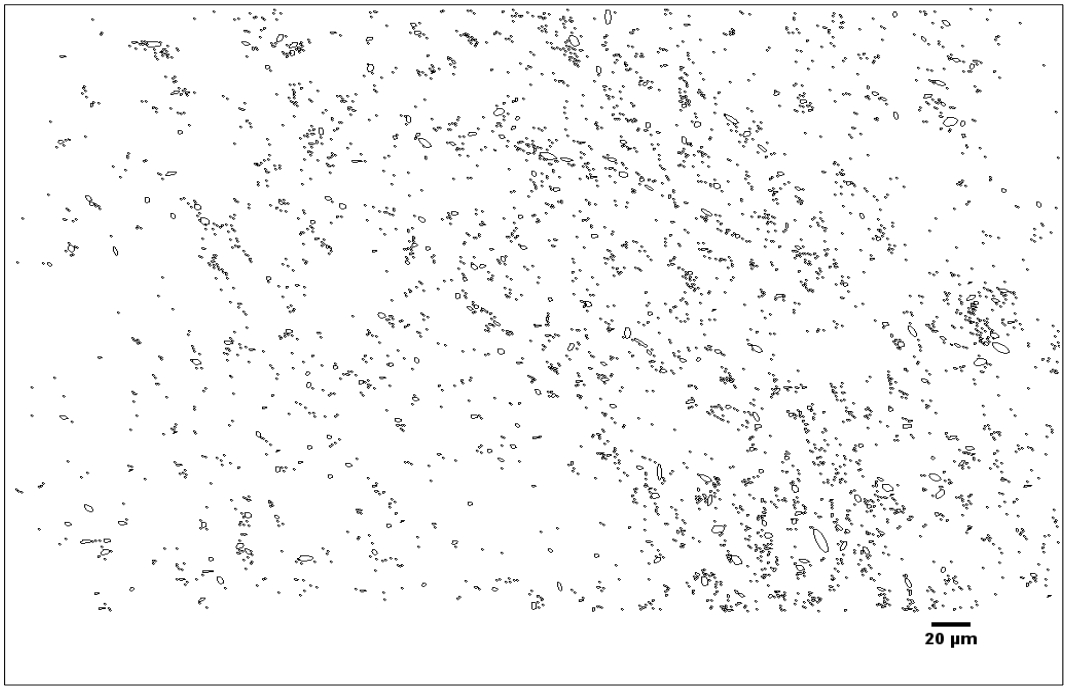


Figure A.18: Identified pore boundaries of the aggregate prepared at 1000°C (Metiagoda clay)

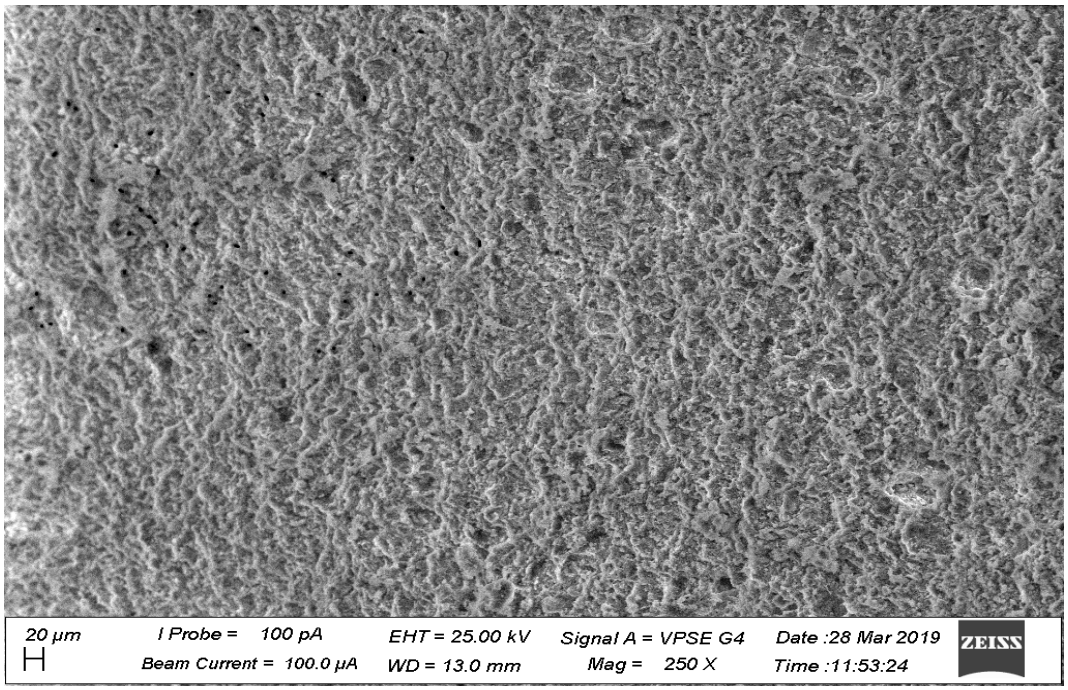


Figure A.19: Pore structure of the aggregate prepared at 1100°C (Metiagoda clay)

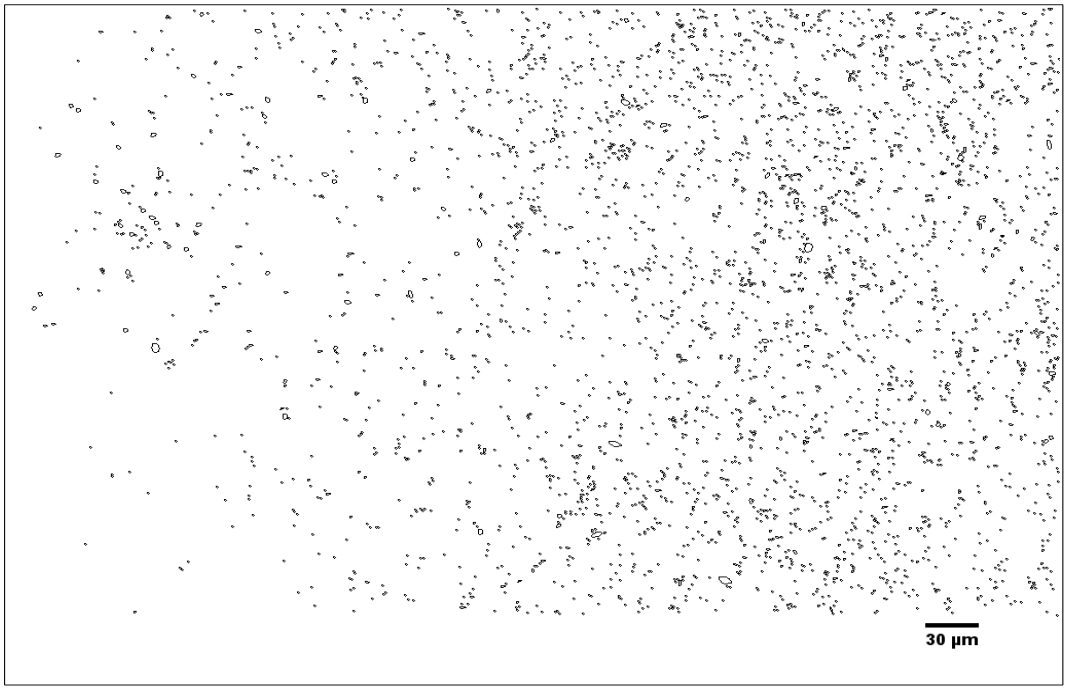


Figure A.20: Identified pore boundaries of the aggregate prepared at 1100°C (Metiagoda clay)

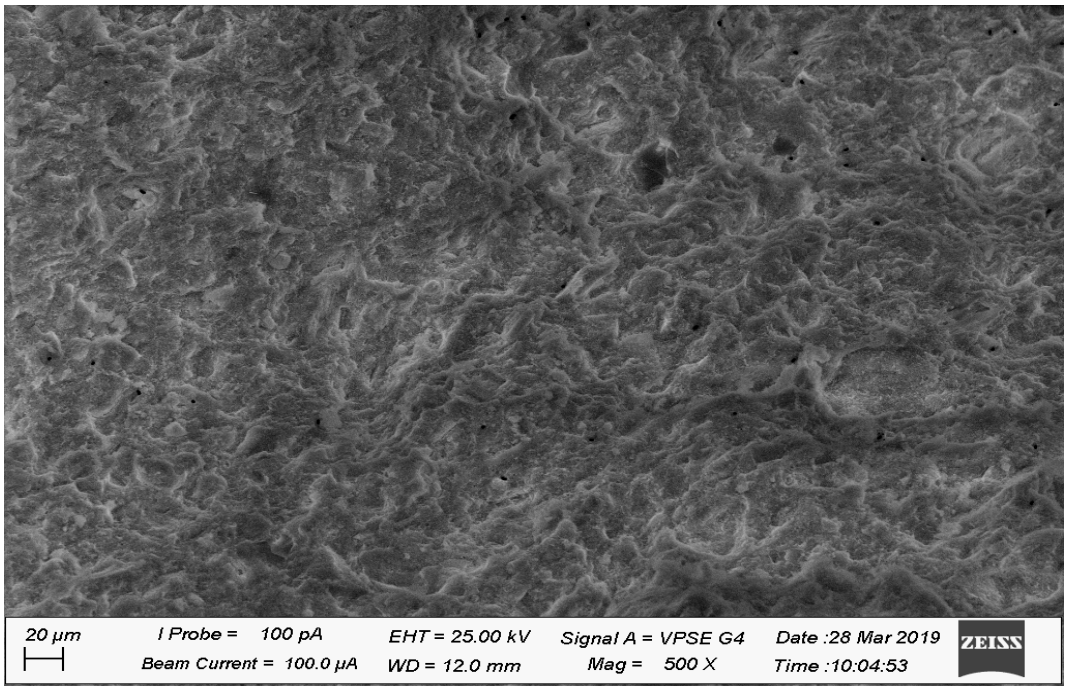


Figure A.21: Pore structure of the aggregate prepared at 1200°C (Metiagoda clay)

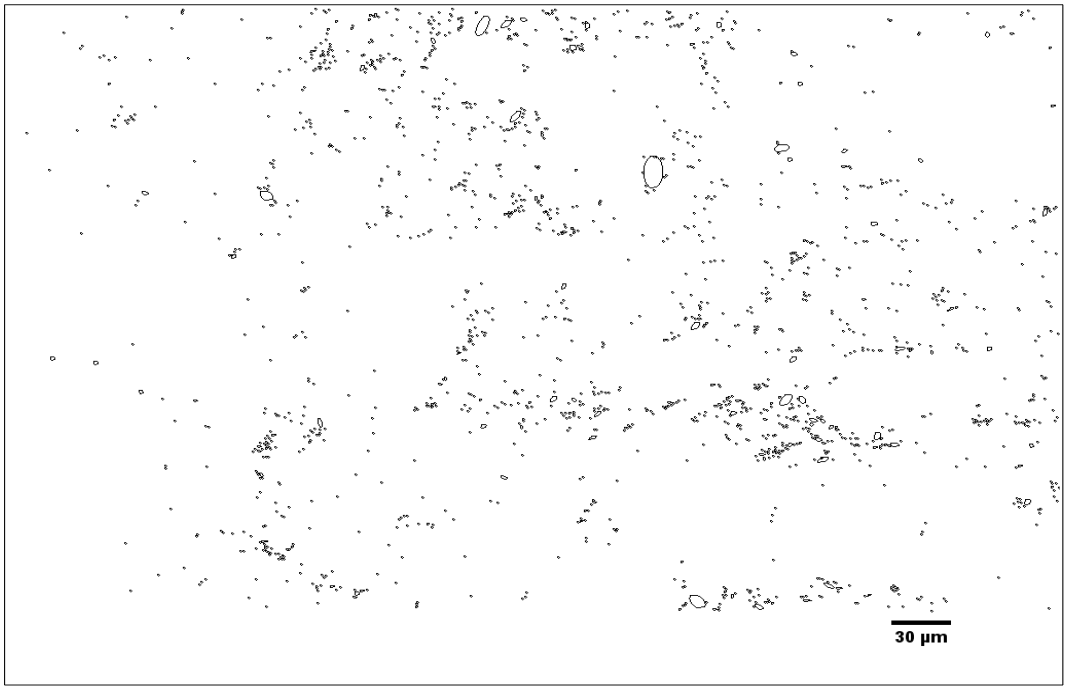


Figure A.22: Identified pore boundaries of the aggregate prepared at 1200°C (Metiagoda clay)

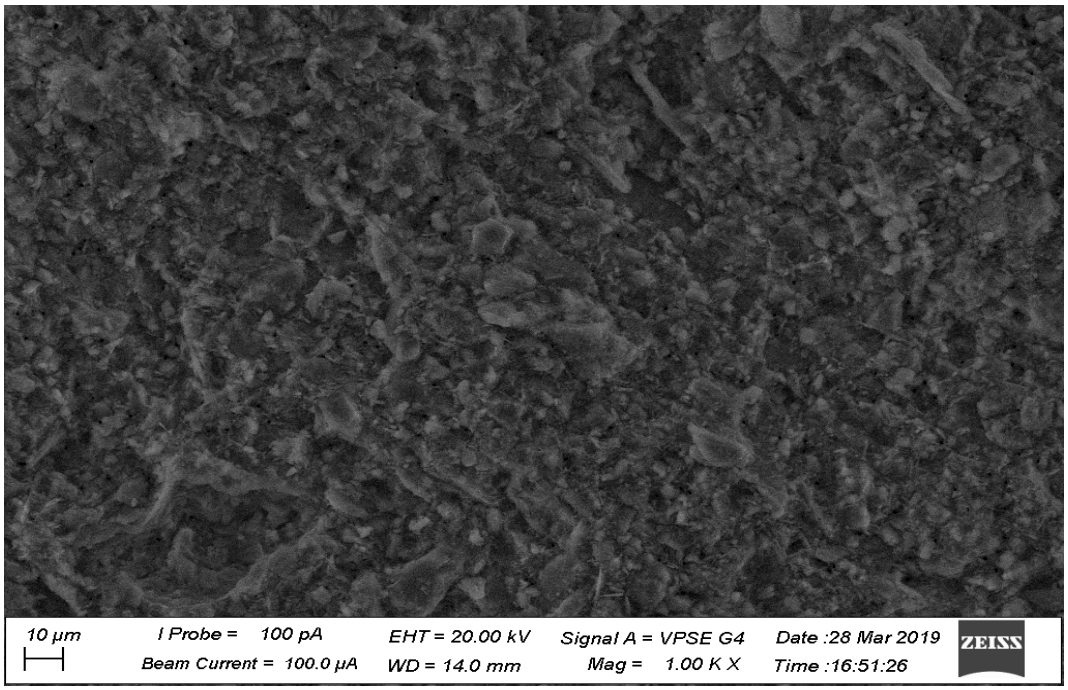


Figure A.23: Pore structure of the aggregate prepared at 800°C (China clay)

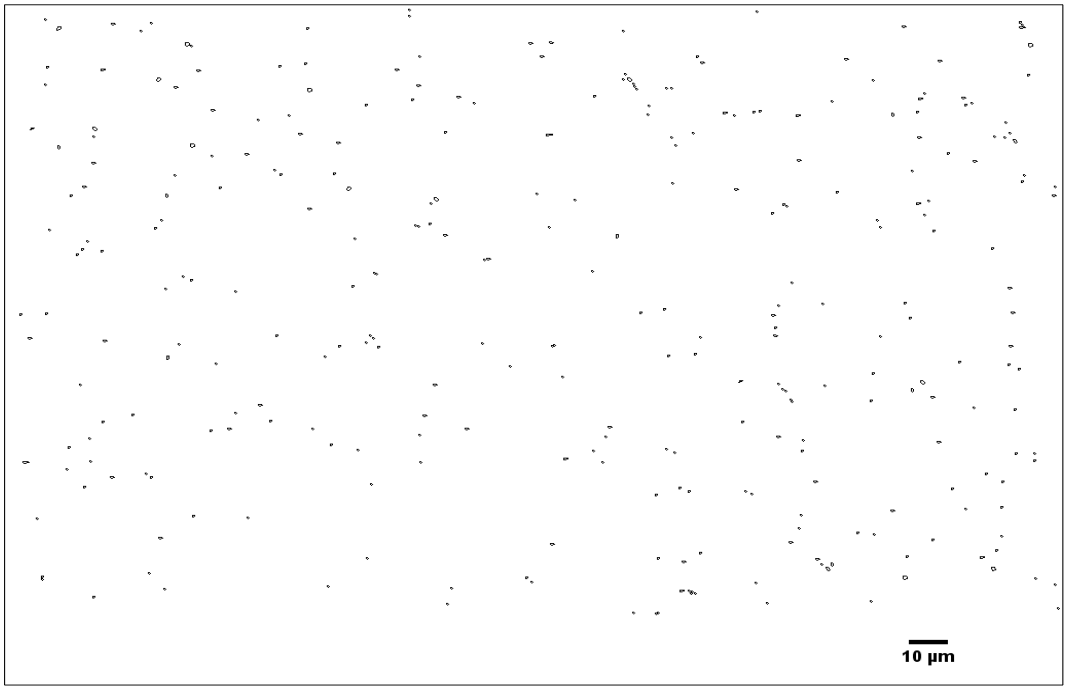


Figure A.24: Identified pore boundaries of the aggregate prepared at 800°C (China clay)

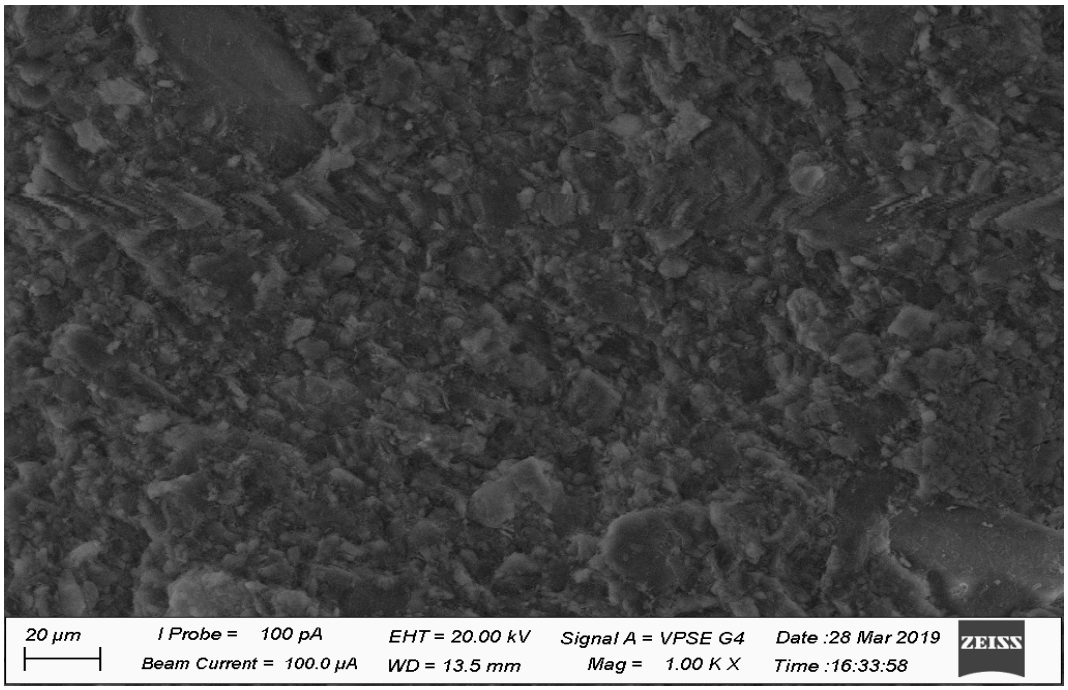


Figure A.25: Pore structure of the aggregate prepared at 900°C (China clay)

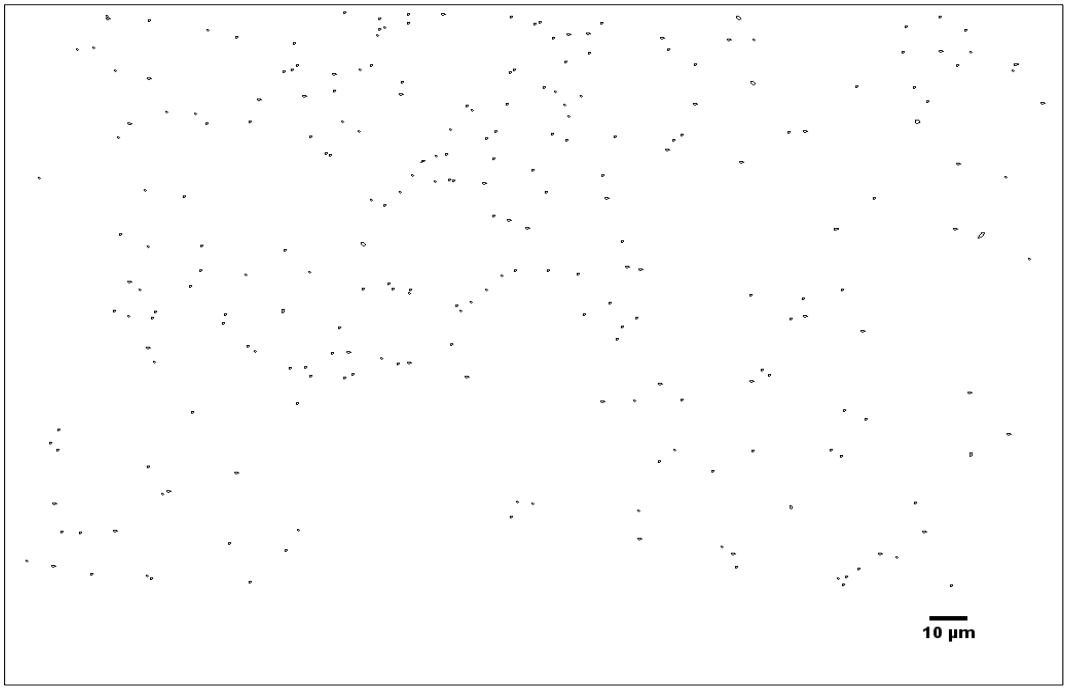


Figure A.26: Identified pore boundaries of the aggregate prepared at 900°C (China clay)

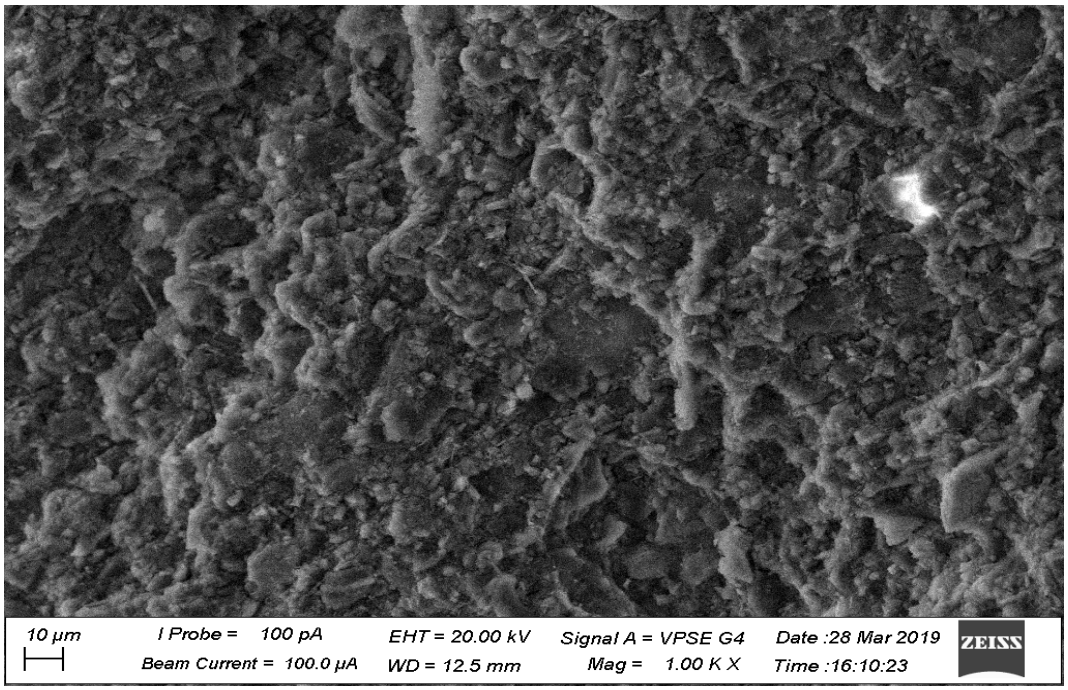


Figure A.27: Pore structure of the aggregate prepared at 1000°C (China clay)

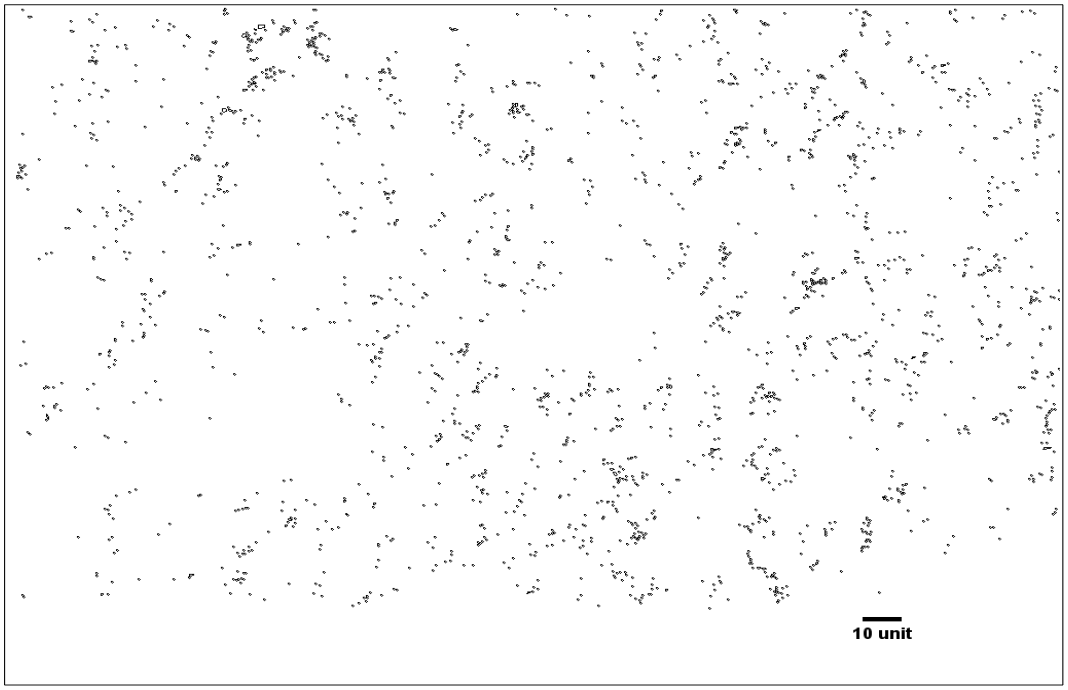


Figure A.28: Identified pore boundaries of the aggregate prepared at 1000°C (China clay)

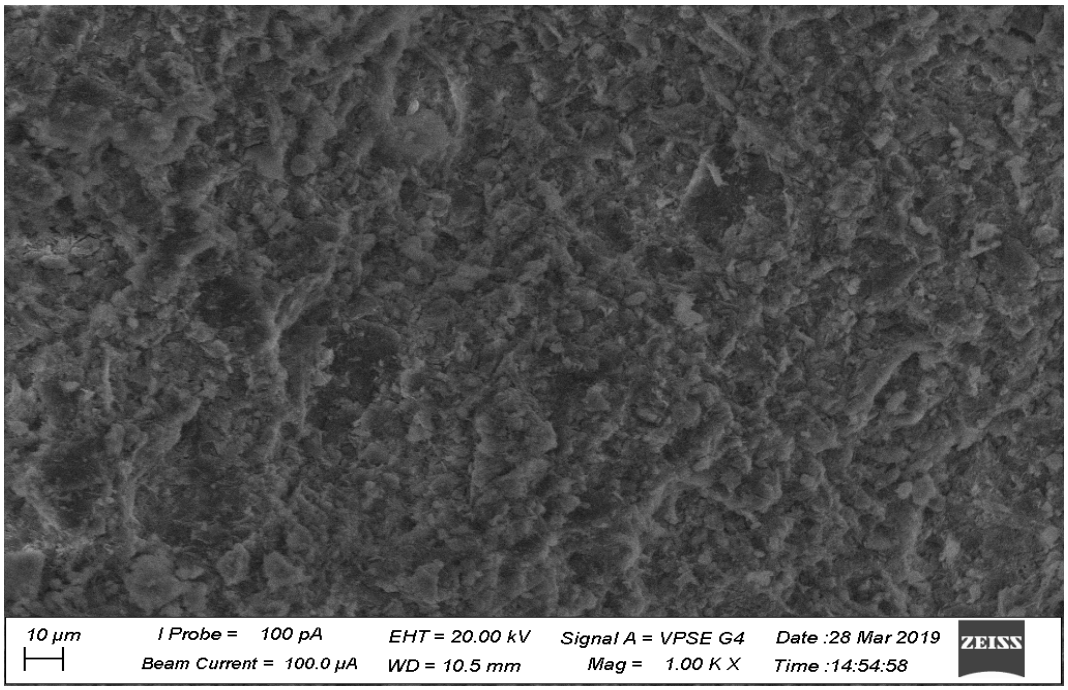


Figure A.29: Pore structure of the aggregate prepared at 1100°C (China clay)

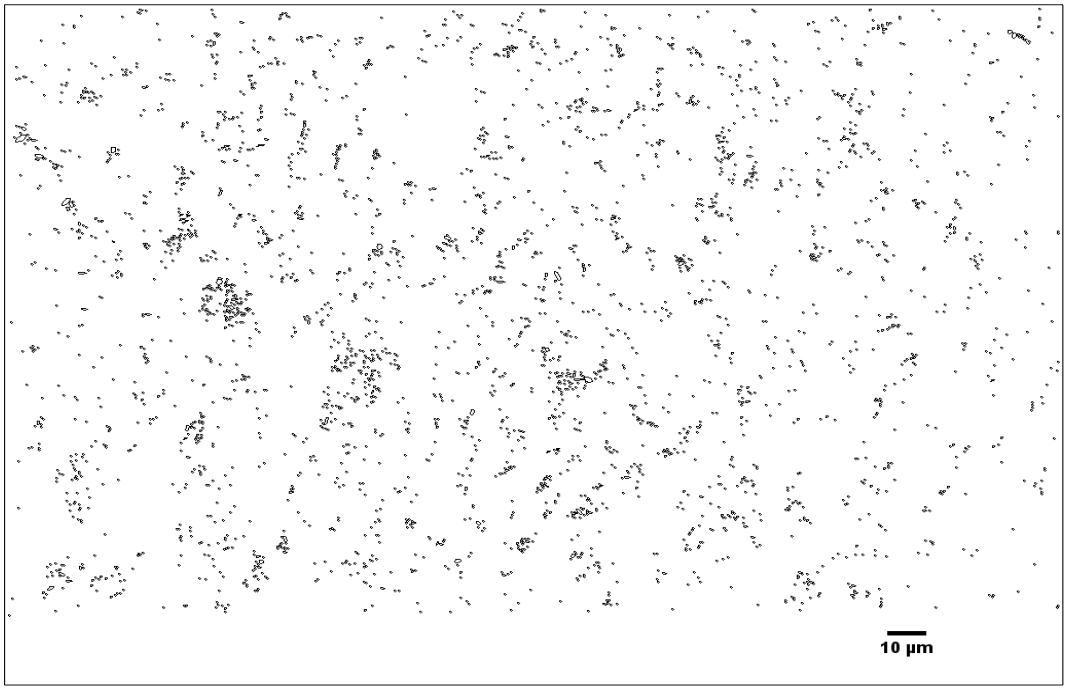


Figure A.30: Identified pore boundaries of the aggregate prepared at 1100°C (China clay)

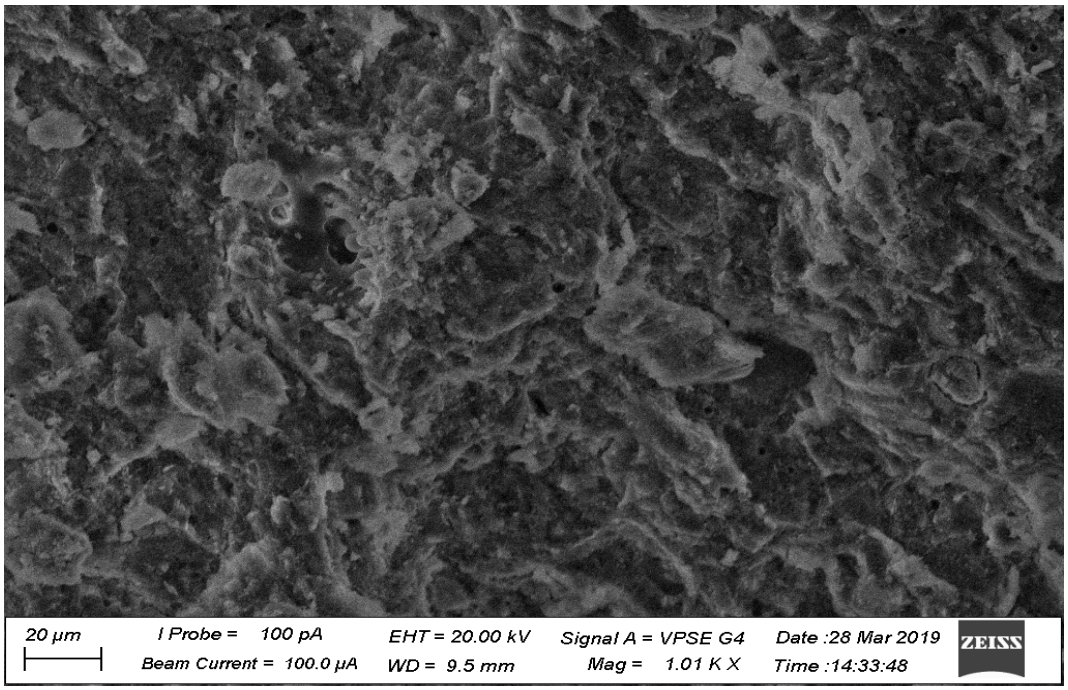


Figure A.31: Pore structure of the aggregate prepared at 1200°C (China clay)

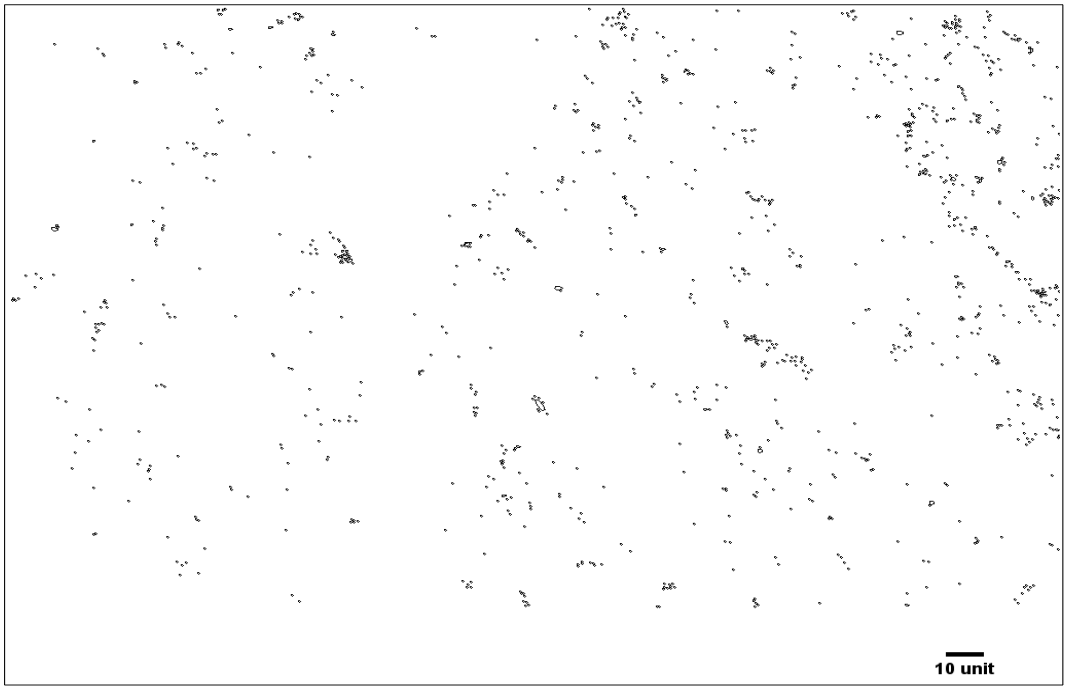


Figure A.32: Identified pore boundaries of the aggregate prepared at 1200°C (China clay)

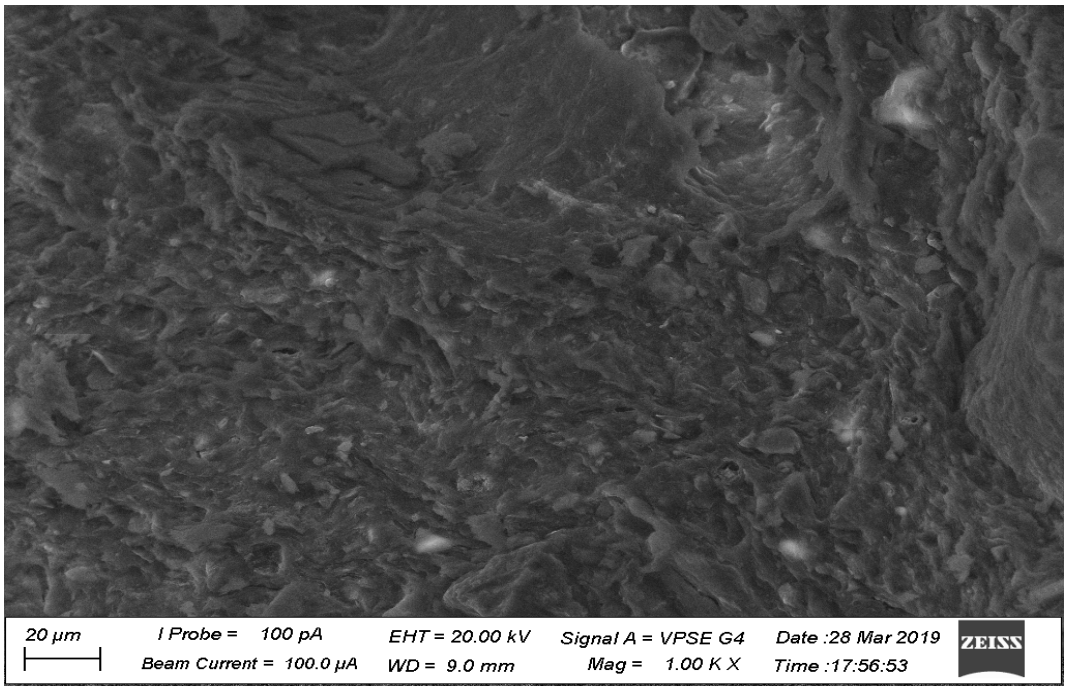


Figure A.33: Pore structure of the aggregate prepared at 800°C (Dankotuwa clay)

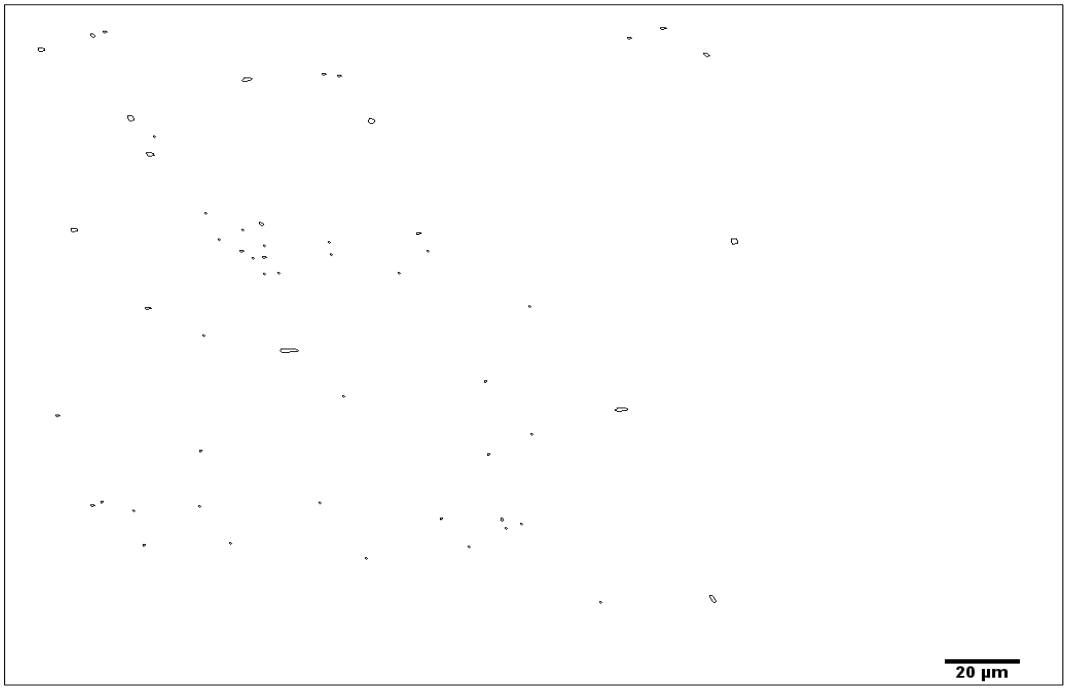


Figure A.34: Identified pore boundaries of the aggregate prepared at 800°C (Dankotuwa clay)

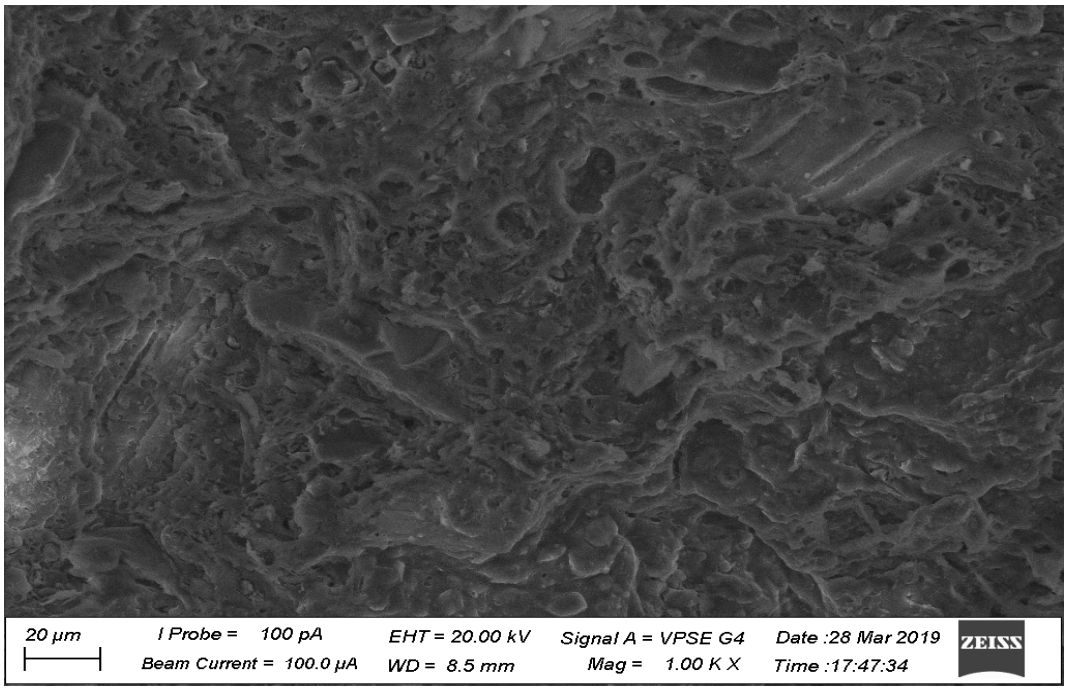


Figure A.35: Pore structure of the aggregate prepared at 900°C (Dankotuwa clay)

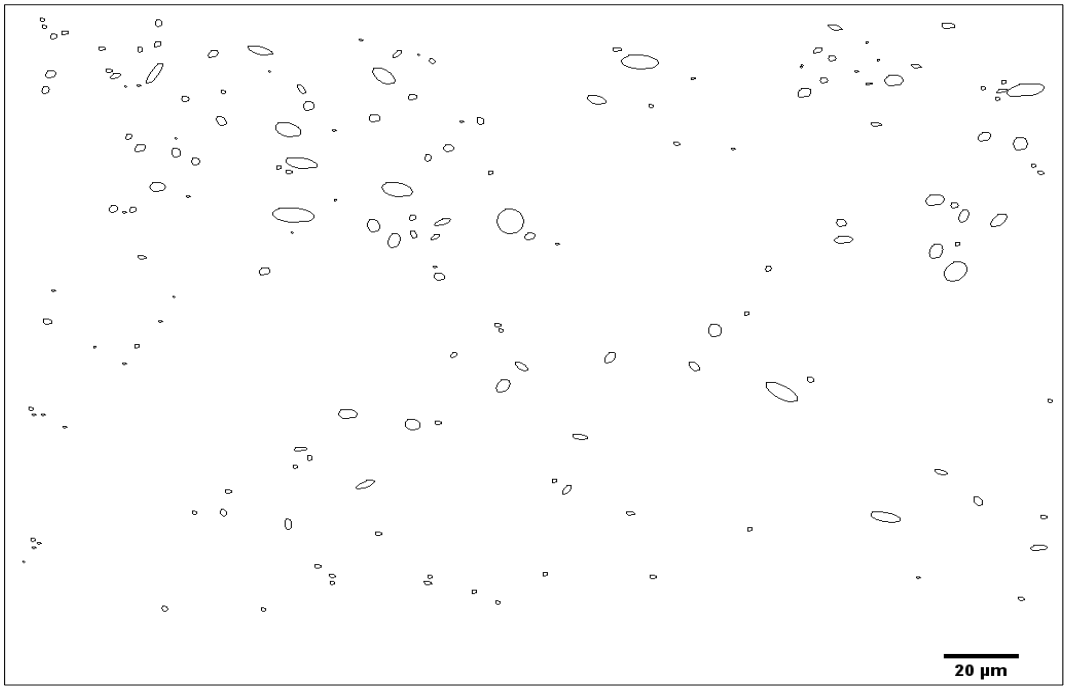


Figure A.36: Identified pore boundaries of the aggregate prepared at 900°C (Dankotuwa clay)

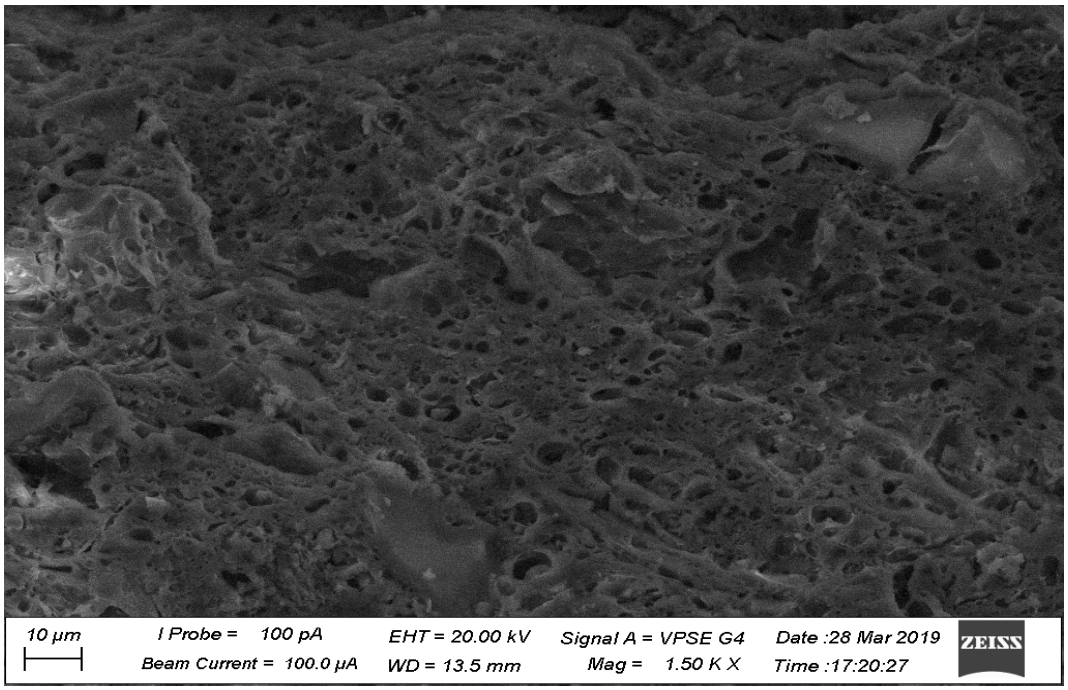


Figure A.37: Pore structure of the aggregate prepared at 1000°C (Dankotuwa clay)

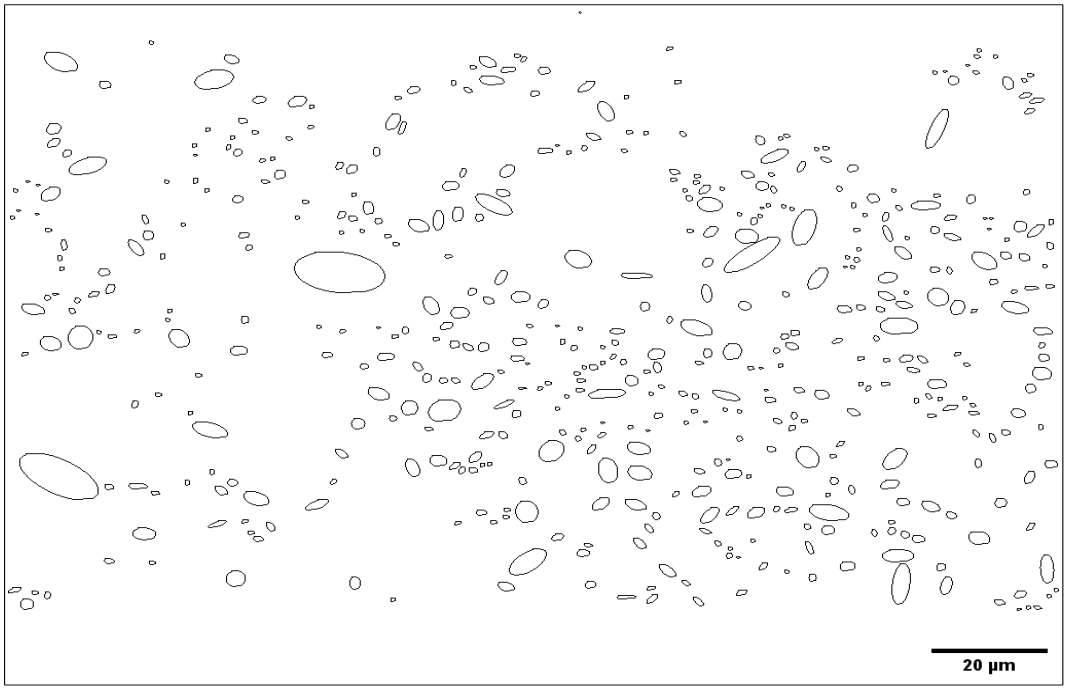


Figure A.38: Identified pore boundaries of the aggregate prepared at 1000°C (Dankotuwa clay)

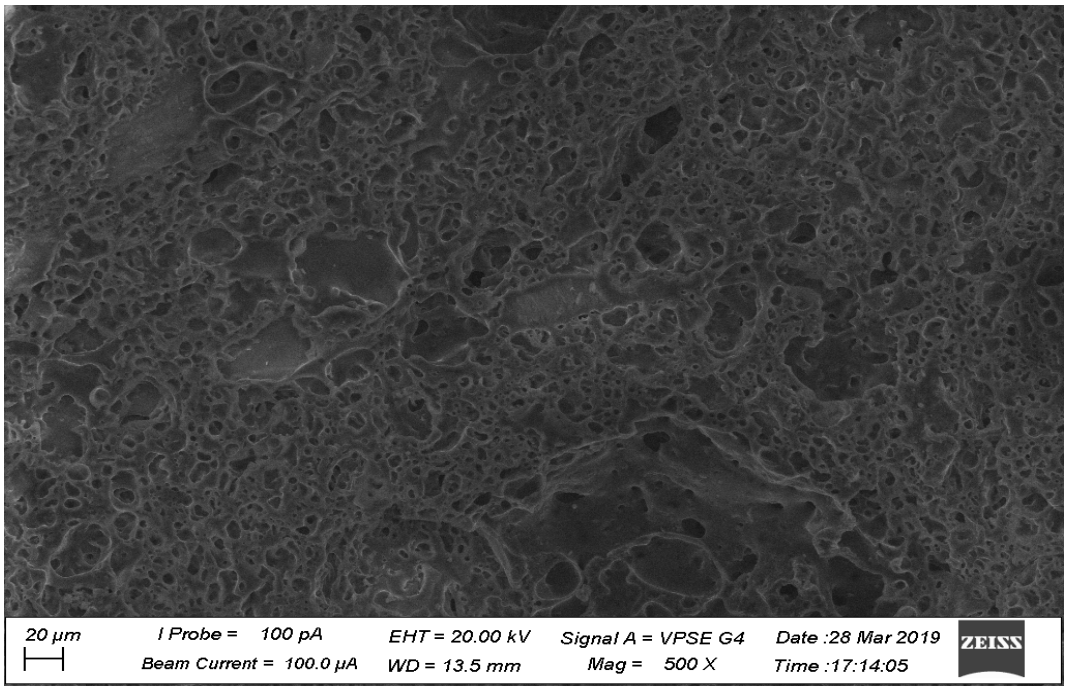


Figure A.39: Pore structure of the aggregate prepared at 1100°C (Dankotuwa clay)

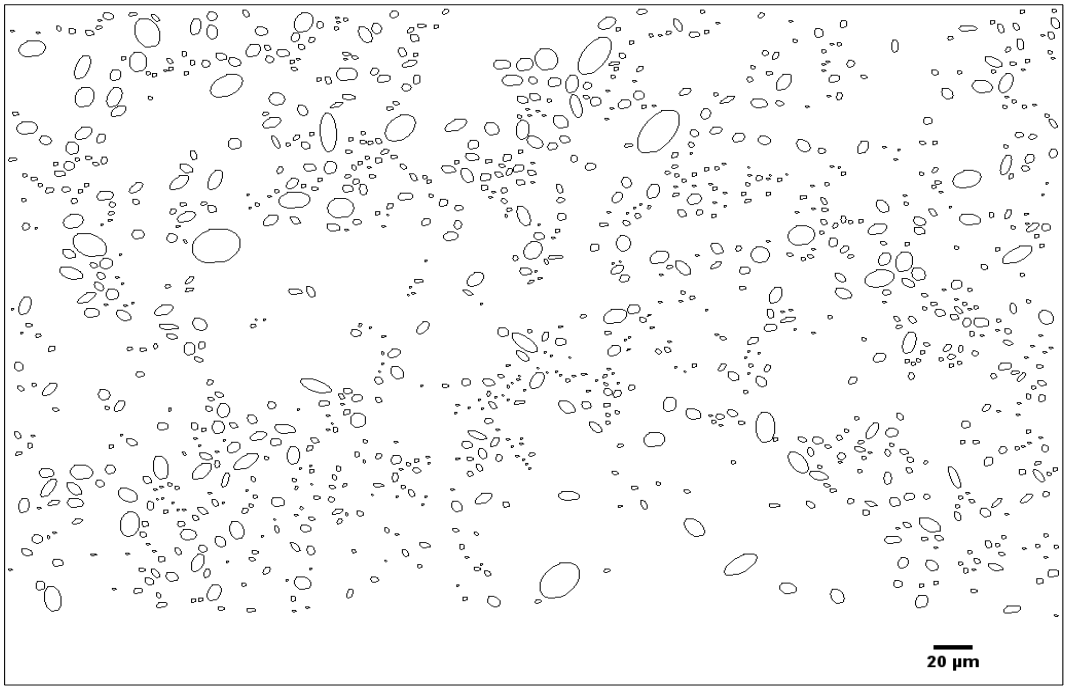


Figure A.40: Identified pore boundaries of the aggregate prepared at 1100°C (Dankotuwa clay)

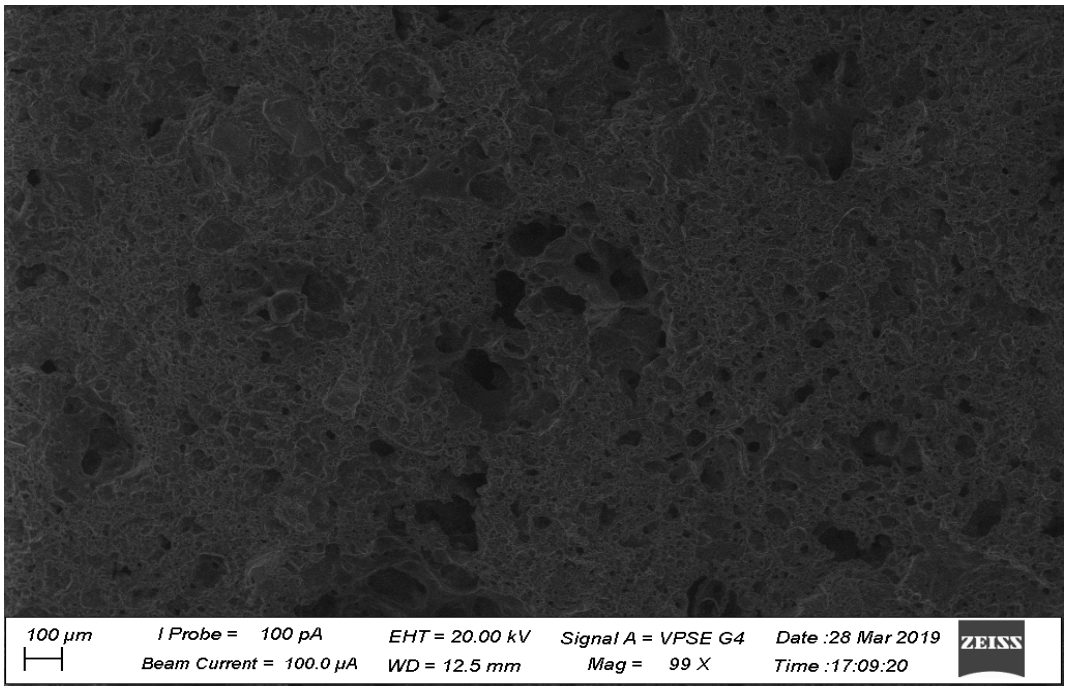


Figure A.41: Pore structure of the aggregate prepared at 1200°C (Dankotuwa clay)

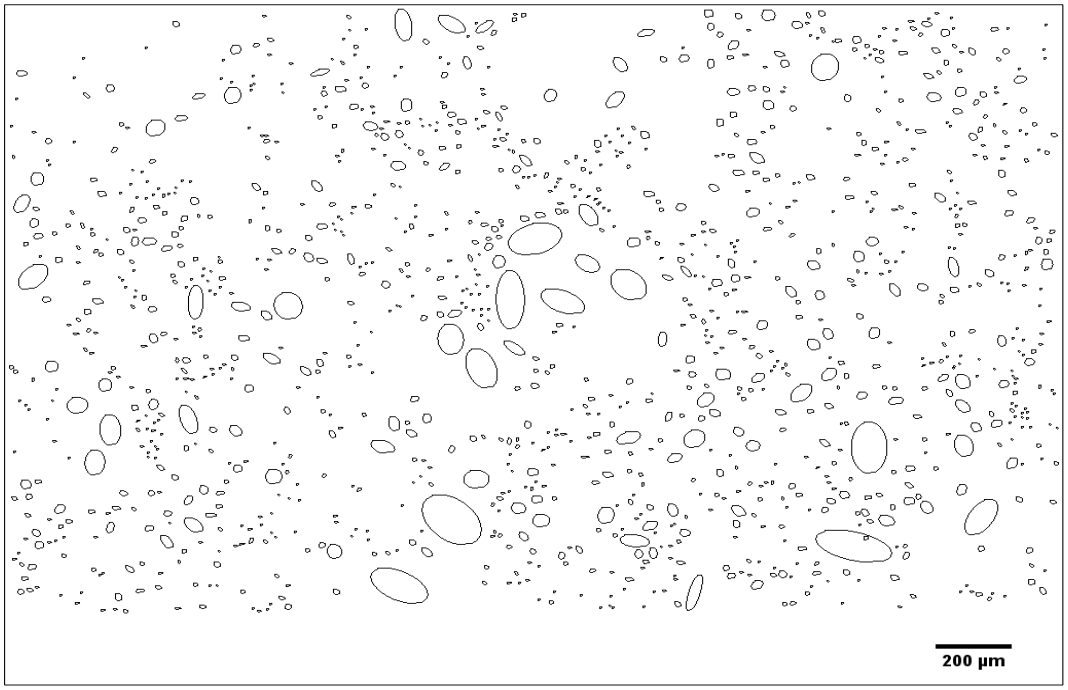


Figure A.42: Identified pore boundaries of the aggregate prepared at 1200°C (Dankotuwa clay)

APPENDIX B

Real scale work study of calculating the unit cost of internal curing concrete aggregate

---

Cost of the aggregate production is an important factor to validate the suitability of the new aggregate. Many industries did not have detailed cost data of aggregate production, but similar procedure is used in the production of clay tiles and porcelain production. In reference to that, Rajarata tiles (PVT) Ltd are processing a similar raw material to produce roof tiles in their plants. Based on their details and collected information, a real scale aggregate production was defined to calculate the unit cost of 1kg internal curing concrete aggregate.

The production process includes raw materials extraction, transportation, preparation, firing and aggregate preparation process. Figure B.1 shows the proposed manufacturing framework of the aggregates. According to this framework, the aggregate production cost was estimated.

Fixed overheads on depreciation of machines and interest on capital investments will be greatly affected for the production cost. Thus, firing kilns must be operated continuously except for maintenance to achieve maximum operating efficiency. According to that, firing process was identified as the critical process in the aggregate production. Thus, all other processes were adjusted to achieve the maximum output of the firing process. Size of the clay bat was 14mm in thickness, 250mm in length and 150mm in width. The maximum output of the firing process was estimated as 70000 bats per day. Normally, it requires to process approximately 50m^3 of raw clay materials.

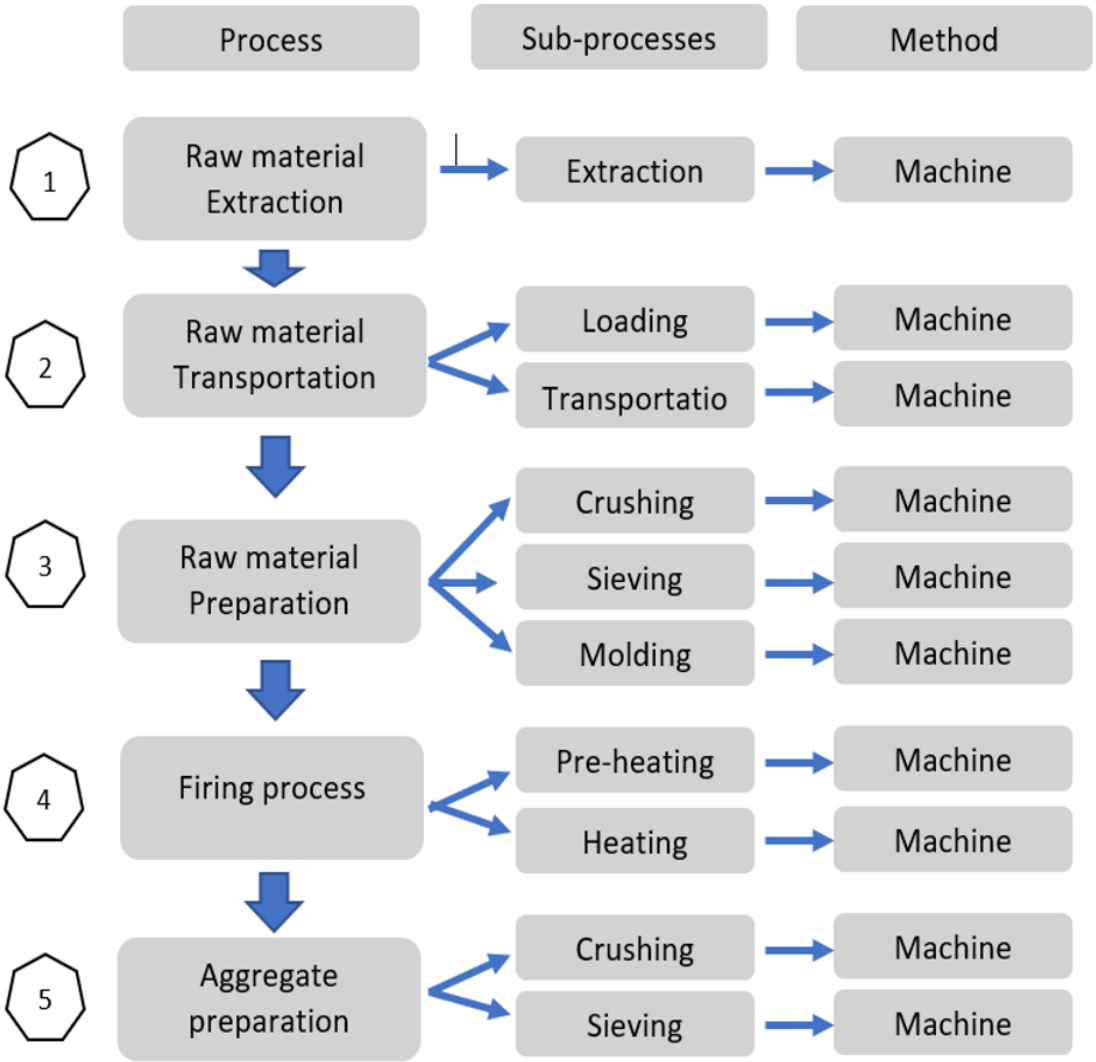


Figure B.1: The manufacturing framework of the aggregates

B.1 Raw materials extraction

Raw materials can be extracted from a suitable mine or buy from outside suppliers. According to the case study referred here; the Rajarata tile factory has a suitable clay mine to collect the raw materials needed. Thus, it was considered, the raw clay materials were extracted from site by using excavator. Excavators were not available in Rajarata tile plant. Thus, it was hired from outside suppliers. Subsequently, a skilled labor was appointed to operate the machine. The model and the specifications of the hired excavator are given in Table B.1. The extracted raw clay materials are shown in

Figure B.2. Cost for raw material extraction process was estimated and presented in Table B.2. The estimation was given for raw material requirement of 50m^3 per day. Raw material extraction can be completed within one hour, but extraction is continuing for 8 hours per day to cover the target of extracting needed raw materials per year.

Table B.1: Specification of the excavator

EXCAVATOR	
Bucket type	0.9m^3 Bucket
Bucket volume	0.9m^3
Cycle Time in Plant	50 Sec.
Efficiency	80%
CAPACITY (0.9 X 60 X 0.8X 60) /50	50m^3/hr.



Figure B.2: Extracted raw clay materials

According to the Production framework, Materials were excavated from the site. In order to excavate materials, government permissions should be obtained. According to the discussions held with Rajarata tiles Pvt. Ltd, government grants permissions to excavate clay in year basis. Thus, 5000LKR per day was added as the cost of materials to account the cost involved in the government approval process.

Table B.2: Cost for the raw material extraction

Equipment	Capacity	Number of equipment	Working hours ($50m^3$)	Cost per hour	Cost per day
Excavator	$50m^3$/hr	1	1 hour	4000	4000
	Total (LKR)				4000
Labors	Working Shift (8hr)			Cost per Each	Cost per Day
	Shift 1	Shift 2	Shift 3		
Skilled	1(hour)	0	0	375	375
Unskilled					
	Total (LKR)				375
	Material cost (LKR)/day				5000
	Grand Total (LKR)				9375

B.2 Raw materials transportation

This process includes transportation and loading processes. Extracted clay materials were transported for four kilometer distance to reach Rajarata tile plant. Those materials were transported by using tippers. One loader was used to load the tippers. In order to operate the machines, there were three (03) skilled labors assigned for each equipment. All the required equipment was outsourced, and the hiring cost of each equipment was added. The model and the specifications of the hired loader and tippers are given in Table B.3 and Table B.4 respectively. Total cost per day is shown in the Table B.5.

Table B.3: Specifications of the loader

LOADER	
Bucket	$1.7m^3$
Cycle Time in Plant	4 Minute
Efficiency	80%
CAPACITY = (1.7 X 0.8 X 60) /4	$20m^3$ / hr.

Table B.4: Specifications of the tipper

TIPPERS	capacity = $3m^3$
Average Lead	4 Km (4 Km Both way)
Loading Time and Turning On	4 Minute
Leading Average Speed (20 Km / hr.)	18 Minute
Unloading and Turning On	6 Minute
Total Cycle Time	28 Minute
CAPACITY(3x60/35)	$5m^3$ / hour

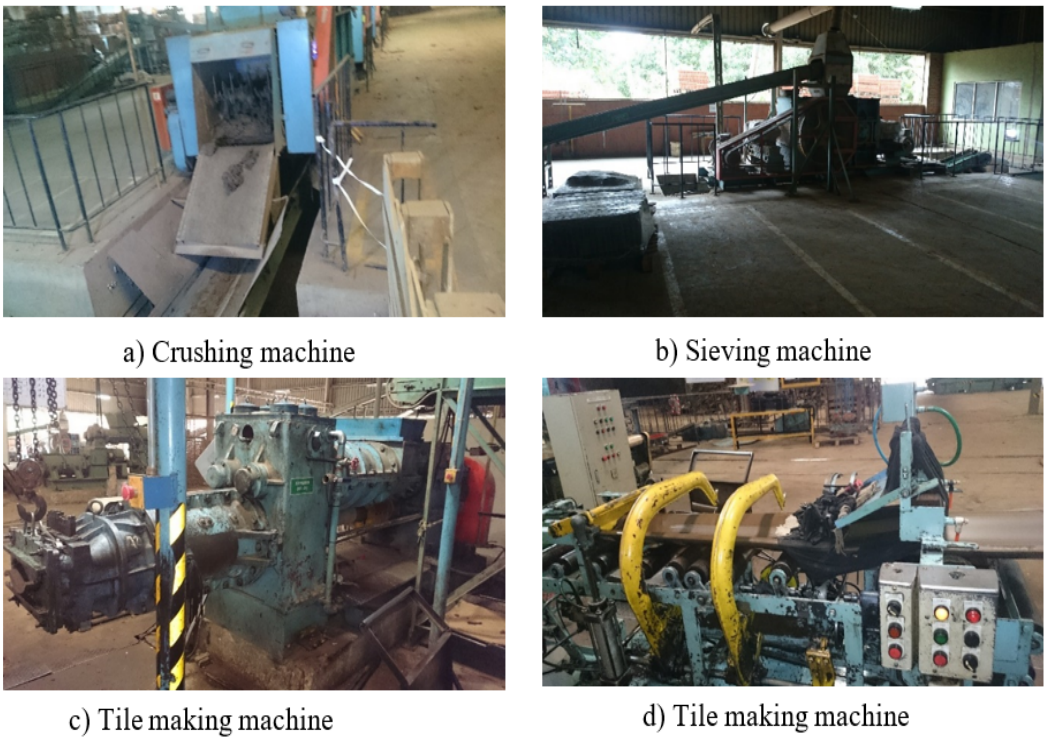
Table B.5: Cost for the raw material transportation

Equipment	Capacity	Number of equipment	Working hours ($50m^3$)	Cost/ hour	Cost/ day
Tripper	$5m^3$/hr.	2	8 hours	10000	20000
Loader	$20m^3$/hr.	1	8 hours	12000	12000
	Total (LKR)				32000
Labors	Working Shift (8hr)			Cost per Each	Cost per Day
	Shift 1	Shift 2	Shift 3		
Skilled	3	0	0	3000	9000
Unskilled				1500	
	5% Overhead/day = 2000 LKR			Total (LKR)	9000
	Grand Total (LKR)				43000

B.3 Raw materials preparation

Raw material preparation includes crushing sieving and molding processes. Materials preparation process and the firing process are developed as a production line in order to get the maximum output and to reduce the production cost. Thus, the materials preparation cost was calculated by assuming all the required machines would be hired from Rajarata tile plant. Figure B.3(a) and Figure B.3(b) show the crusher machine

and sieving machine respectively. Figure B.3(c) and Figure B.3(d) show the clay bats making machine. Unskilled labor will be assigned for each machine to monitor the process while a supervisor will monitor the overall process. Cost for the management are shown in Table B.9.



a) Crushing machine

b) Sieving machine

c) Tile making machine

d) Tile making machine

Figure B.3: Available equipment at Rajarata tile plant

All the machine in the production line will work continuously for 24 hours to achieve the maximum output of the firing process. The process will be stopped only in a break-down of machines. According to that, cost for the raw material preparation process was calculated and are presented in Table B.6.

Table B.6: Cost for the raw material preparation

Equipment	Capacity	Number of equipment	Working hours ($50m^3$)	Cost per hour	Cost per day
Jaw crusher	3.5m3/hr.	1	24 hours	10000	10000
Rolling mills	3.5m3/hr.	1	24 hours	15000	15000
Clay block press	20,000 bats/hr.	2	24 hours	8000	16000
	Total (LKR)				41000
Labors	Working Shift (8hr)			Cost/ Each	Cost/ Day
	Shift 1	Shift 2	Shift 3		
Skilled	0	0	0	3000	0
Unskilled	4	4	4	1500	18000
	5% Overhead/day		= 3000 LKR	Total (LKR)	18000
	Grand Total (LKR)				62000

B.4 Firing cost

Decoration (Onglaze) electrical furnace was used for the heating process shown in Figure B.4. It operates around 900°C. The heating time is considered as 2.5hr per lot. Generally, the output of this furnace is one bat car per 4minutes. Each bat car contains 200 bats. The maximum output of the furnace will be 350 clay bats cars per day. Table B.7 shows the cost for 24 hours continuous operation of the furnace. In order to achieve this output, enough skilled labors and machineries should be provided. The total cost related to firing process according to the data given by Rajarata tile Pvt. Ltd is shown in Table B.7.

Table B.7: Details of Furnace and firing cost

Furnace	Firing Cost per car (LKR)			Firing cost/per car (LKR)	Number of cars per day	Firing cost per day (LKR)
	Labor	Fuel	plant			
	72.06	105.26	84.46	261.78	350	91623



Figure B.4: Decoration (Onglaze) electrical furnace

B.5 Aggregate preparation cost

After completing the heating process, clay bats should be crushed to obtain the required size of aggregates. The crushing and sieving machine were outsourced to complete the process and that rental cost was added to the aggregate preparation cost as shown in Table B.8. The efficiency of aggregate production is considered as 90%.

Table B.8: Cost for aggregate preparation

Equipment	Capacity	Number of equipment	Working hours ($50m^3$)	Cost/ hour	Cost/ day
Loader	2000 bats/hr.	2	24 hours	10000	20000
Crusher	1500 bat /hr.	2	24 hours	12000	24000
Sieving plant	$2m^3$/hr.	1	24 hours	15000	15000
	Total (LKR)				39000
Labors	Working Shift (8hr)			Cost/	Cost/
	Shift 1	Shift 2	Shift 3	Each	Day
Skilled	2	2	2	3000	18000
Unskilled	3	3	3	1500	13500
	5% Overhead/day		= 3500 LKR	Total (LKR)	31500
	Grand Total (LKR)				74000
	Output = 2800kg x 0.9 = 2550kg/hr			61.2 tons	

B.6 Overall supervision cost

A continuous production requires a skilled person supervision of the production line to get maximum output in the production process. Thus, Table B.9 shows the supervision cost per day.

Table B.9: Cost for management

Furnace	Working Shift (8hr)			Cost/ person (LKR)	Cost/ day (LKR)
	shift 1	shift 2	shift 3		
Supervisor	1	1	1	4000	12000
Forman	2	2	2	3500	21000
	Grand Total (LKR)				33000

B.7 Calculation of the unit cost for aggregate

Estimation of unit cost for production of ICA aggregate requires to study a real scale work study. The cost involved in the production can be divided into various parts as Machinery cost (X_a), labor cost (X_l), Material cost (X_m) and Firing plant cost. Firing plant cost can be divided into fuel cost (X_{pf}), labor cost (X_{pl}) and plant overhead (X_{po}). In order to count the unseen cost of production, a overhead of 5% was assign to each process (X_o). Labor cost of the firing plant can be added with overall labor cost. Afterwards, those items can be evaluated separately to estimate the production cost of aggregate.

$$Production\ cost = X_m + X_l + X_a + X_o + X_{pf} + X_{pl} + X_{po} \tag{B.1}$$

Production cost = 5000+91000+116000+9000+25000+36000+30000 = 312,000.00 LKR

Total aggregate production cost per day can be obtained from Equation B.1. According to the Equation B.1, daily cost for the aggregate production is 312,000.00 LKR. The aggregate output per day is 61.2 tons. Thus, production cost per 1Kg of aggregate is 5.1 LKR. This is the approximated production cost in a larger aggregate production line.

According to Equation B.1, larger portion of the cost allocated for the machinery hiring. This can be reduced by investing on purchasing machineries and recovering the cost from profit and the life cycle cost analysis of machineries. On the other hand, heating process also consumed a significant portion of the cost. This can be further reduced by using traditional firing method. Moreover, heating temperature can be reduced by using various additives to the clay mixtures. Further studies should be conducted to optimize the production cost.

A few possible variations for the unit cost calculation as per the Equation B.1 can be given as follows:

- additional transportation cost would be added to the cost with raw material transported to the site
- some saving from machinery cost with the use of purchased machineries or hiring on rental basis
- Changes in government levies for granting permission for clay extraction.
- Use of different heating methods